Hydrological Performance Evolution of Extensive Green Roof Systems

Simon De-Ville MEng. (Hons.)

Supervised by:
Dr Virginia Stovin
Dr Manoj Menon

A thesis submitted in part fulfilment of the requirements

for the degree of Doctor of Philosophy in Civil Engineering

Department of Civil & Structural Engineering

The University of Sheffield

June 2017

Declaration

I declare that no portion of the work contained in this thesis has been submitted in support of an application for another degree or qualification of this or any other university or other institute of learning. The work has been my own except where indicated. All quotations have been distinguished by quotation marks and the sources acknowledged.

Acknowledgements

1. Primarily I would like to thank Dr Virginia Stovin for inspiring my interest in research even before I began undertaking this PhD programme. I would also like to extend my thanks to Dr Manoj Menon who, alongside Virginia, provided encouragement, guidance, and support at every step of the way.

2. This project would not have been possible without the hard work and dedication of Dr Simon Poë and Dr Christian Berretta who ensured the collection of green roof monitoring data prior to the commencement of this PhD programme.

3. I would also like to acknowledge the valuable input from various people outside of the University of Sheffield. Firstly, to Dr Craig Sturrock and Prof Sacha Mooney for the use of their X-Ray Microtomography facilities at the Hounsfield Facility for Rhizosphere Research at the University of Nottingham. Secondly, to Dr Xiaodong Jia of the University of Leeds' School of Chemical and Process Engineering for providing the DigiPac software and technical guidance.

4. Finally, I would like to thank my family and friends for their support throughout the course of this work.

Abstract

Global urbanisation has resulted in a reduction of urban green spaces, replacing moisture permeable landscapes with impermeable surfaces that quickly convey rainfall to receiving drainage systems. Sustainable drainage systems (SuDS) are a selection of devices that can be used to complement and/or replace existing urban drainage structures to meet future demands. SuDS can control rainfall at source, infiltrating it into the ground, thereby replicating the natural hydrological processes of a pre-developed urban site. Green roofs are one example of a source control SuDS device, capable of restoring green spaces to urban environments without requiring land space.

As green roof systems age, there are several temporal processes than can lead to changes in their hydrological performance. Current knowledge of hydrological performance evolution is conflicting; this study presents a coupled non-invasive imaging and long-term monitoring study to provide the missing knowledge required to better inform the long-term maintenance, future development, and modelling of green roof systems.

A 6-year long-term record of rainfall, runoff, climate and substrate moisture data for a field research site in Sheffield has been analysed to identify temporal trends in green roof hydrological performance. This monitoring study is coupled to two green roof microcosm studies which non-invasively characterise differently aged substrate properties and identify the impacts on long-term hydrological performance. Both methods of investigation identify that for conventional green roof system configurations, a crushed brick substrate with Sedum vegetation, there are small improvements to potential hydrological performance year-on-year. These performance improvements arise from a rearrangement of the substrates pore spaces, with smaller pore sizes in aged substrates. However, seasonal variations in substrate properties were identified to be more significant than year-on-year increases. Stormwater practitioners may be encouraged by no evidence of any decline in performance with time for conventional green roof configurations.

Contents

List of Figures

List of Tables

List of Nomenclature

Acronyms

ADWP	Antecedent Dry Weather Period
AIE	Dataset of All Identified Events
ATB	Dataset of All 9 Test Beds being operational
BBS	Brick-based substrate
BBS$_A$	Aged Brick-based Substrate
BBS$_V$	Virgin Brick-based Substrate
CAM	Crassulacean Acid Metabolism
CFD	Computational Fluid Dynamics
CIRIA	construction industry research and information association
CSO	Combined Sewer Overflow
CT	Computed Tomography
ET	Evapotranspiration
HLS	Heather with Lavender Substrate
LBM	Lattice Boltzmann Method
LECA	Lightweight Expended Clay Aggregate
LECA$_A$	Aged LECA Substrate
LECA$_V$	Virgin LECA Substrate
MWHC	Maximum water holding capacity
PAW	Plant Available Water
PET	Potential Evapotranspiration
PRC	Potential Retention Capacity
PRP	Potential Retention Performance
PWP	Permanent Wilting Point
SCS	Sedum Carpet Substrate
SuDS	Sustainable Drainage Systems
TB	Test Bed
VIE	Dataset of Valid Identified Events
WSUD	Water Sensitive Urban Design
XMT	X-Ray Microtomography

Symbols

β	Ratio of Physical to Simulated length scales
d_{50}	Median particle size
D_E	Exponent parameter of reservoir routing
D_S	Scale parameter of reservoir routing
$\Delta\tau$	Discretisation time step
h	Temporary storage depth
k	Scale parameter of reservoir routing
K_{sat}	Saturated Hydraulic Conductivity
K_{XMT}	XMT-derived Saturated Hydraulic Conductivity
L_{lat}	Corresponding simulation dimension of the Characteristic Physical Dimension
L_{phys}	Characteristic Physical Dimension
n	Exponent parameter of reservoir routing
P	Precipitation depth
P_{corr}	Corrected moisture probe period
P_{uncorr}	Raw moisture probe period
ϕ_E	Effective Porosity
ϕ_I	In-effective Porosity
ϕ_T	Total Porosity
θ_{FC}	Field Capacity
Q_{in}	Flow rate into substrate
Q_{out}	Flow rate out of substrate
R	Runoff depth
Re_{lat}	LBM Reynolds number
Re_{phys}	Physical Reynolds number
S	Storage level
S_{max}	Maximum Storage level
T	Temperature
U_{lat}	Superficial Flow Velocity over all fluid sites
V_E	Inter-particle Void volume
V_I	Intra-particle Void volume
v_{lat}	Simulated Kinematic Viscosity
V_T	Total Volume
ψ_m	Matric Pressure
$\Theta_{0,FC}$	Observed Field Capacity
θ_{PWP}	Permanent Wilting Point
v_{phys}	Physical Kinematic Viscosity
τ	Simulation Relaxation Factor

1.

Introduction, Aim & Objectives

1.1 Background

Global urbanisation has resulted in a reduction of urban green spaces, replacing moisture permeable landscapes with impermeable surfaces that quickly convey rainfall to receiving drainage systems. The predicted negative impacts of climate change suggest an increased frequency of extreme rainfall events, alongside more general increases in winter rainfall. Existing urban drainage networks fail to sufficiently manage current stormwater loads during extreme rainfall events. When under pressure, the combined sewerage systems of the UK discharge stormwater and diluted effluent into open water courses. These discharges can create potential health risks, as well as aesthetic pollution and environmental damage. A shift in urban stormwater management strategy is required to ensure future infrastructure resilience against urbanisation and climate change.

Sustainable drainage systems (SuDS) are a selection of devices that can be used to complement and/or replace existing urban drainage structures to meet future demands. SuDS can control rainfall at source, infiltrating it into the ground, thereby replicating the natural hydrological processes of a pre-developed urban site. As well as stormwater quantity controls, SuDS are designed to provide amenity and biodiversity benefits, restoring green spaces to urban environments. Some SuDS

devices can also provide significant water quality benefits, heavily reducing pollutant loads in contaminated road runoff. Currently, within the UK only Scotland requires the provision of SuDS on new developments. However, UK government consultation on the future requirement of SuDS for urban developments is ongoing, with the aim of providing a regulatory framework as well as removing the barriers to wider SuDS adoption.

Green roofs are one example of a source control SuDS device, capable of restoring green spaces to urban environments without requiring land space. Green roofs replicate pre-development hydrology via retention and detention processes. Retention provides volumetric stormwater reduction, returning incident rainfall to the atmosphere via evaporation and transpiration. Detention provides temporal changes in runoff response, reducing peak flow rates and slowing the travel time of runoff to receiving systems. The exact retention and detention performance of a green roof system is dependent upon by its configuration. Green roof vegetation types, substrate compositions, roof slope, and drainage area will all influence a system's performance. Rainfall characteristics and climatic conditions will also significantly affect the performance of the green roof.

Mature green roofs are complex ecosystems that experience temporal changes in vegetation growth and rainfall patterns. As green roof systems age, there are several temporal processes than can lead to changes in their hydrological performance. At a small temporal scale the daily and seasonal changes in evapotranspiration are known to influence the retention performance of a green roof system. However, at larger temporal scales annual root system development, organic matter turnover, weathering and substrate consolidation, are less well understood in the context of green roof hydrological performance. Current knowledge of hydrological performance evolution is conflicting, with some large-scale monitoring studies indicating no changes with time, whilst other fundamental laboratory analyses suggest significant physical changes that may result in observable differences to hydrological performance over time.

This thesis addresses the conflicting evidence presented in the literature by providing new knowledge of green roof substrate physical property evolution on multiple temporal scales and relating these observations to the resultant evolution of hydrological performance. A coupled non-invasive imaging and long-term monitoring study inform the future development and modelling of green roof systems.

1.2 Aims & Objectives

The overall aim of this thesis is to quantify the evolution of hydrological performance in extensive green roofs at multiple temporal scales, and to understand how this is driven by the underlying changes in substrate physical properties. This will aid in the reduction of uncertainty surrounding long-term green roof hydrological performance. The thesis has four primary objectives:

A. Undertake a review of current literature to establish identified trends in green roof hydrological performance over time and to identify the physical properties that control green roof hydrological performance.

B. Develop investigative techniques for characterising substrate physical properties and long term-hydrological performance. Specifically:
   a. Develop methods of detecting changes in the underlying physical characteristics of green roof systems from monitored rainfall, runoff, and substrate moisture data.
   b. Develop a non-invasive imaging methodology and associated image processing protocol to observe substrate properties in-situ.

C. Observe and quantify:
   a. The hydrological performance of extensive green roof test beds using a 6-year rainfall, runoff, climate and moisture content data set, coupled with existing hydrological modelling tools.
   b. The changes in substrate physical properties between virgin and aged, 5-year-old, substrate samples from two green roof test beds of differing configuration, and predict hydrological response using appropriate hydrological modelling tools.
   c. The changes in substrate physical properties and hydrological performance repeatedly over time for specific microcosms across a full year of vegetation growth.

D. Interpret and understand the impacts of any substrate physical property changes and their significance for long-term hydrological performance.

1.3 Thesis Structure & Content

This thesis comprises 9 chapters. Chapter 1 delivers a short introduction to the background highlights the lack of consensus on green roof ageing. It presents objectives aimed at realising the overall aim of the research.

Chapter 2 contains a review of relevant recent literature. Urban drainage practices are outlined before a more in-depth introduction to SuDS philosophy and green roofs is presented. A detailed review of green roof substrate properties, methods of evaluation and controls on hydrological performance is undertaken alongside a review of green roof vegetation and root systems. The current state of knowledge surrounding green roof hydrological performance and its affecting factors is then set out, before the implications of green roof system age are explored.

Chapter 3 outlines all materials and methods used to undertake the necessary research to satisfy the three primary objectives of this study. The chapter is broadly divided into two sections, the first covers the interpretation of long-term monitoring study data, whilst the second is concerned with the non-invasive X-ray imaging used in the cored microcosm study and the longitudinal microcosm study.

Chapters 4, 5, 6 and 7 present the results of the relevant aspects of the research, before a short discussion of the implications of the findings.

Chapter 4 details the results from the identification of long-term hydrological performance evolution for 6 years of rainfall, runoff, climate and moisture content data from 9 green roof test bed configurations located in Sheffield, UK. The responses of all 9 configurations for up to 198 rainfall events were analysed to isolate the changes in retention and detention performance over time. The implications of identified changes are presented for a design storm example.

Chapter 5 presents the results of the cored microcosm study, the first phase of non-invasive X-ray imaging. Extensive image analysis output is presented for two substrate types at two different ages, 0 and 5 years, and used to quantify several key properties known to control hydrological performance. The results of accompanying physical testing are presented before a comparative discussion of the two techniques is delivered.

Chapter 6 presents the substrate property characterisations from the longitudinal microcosm study. As for chapter 5, extensive image analysis is presented for the 6

treatment groups, 2 substrate compositions and 3 vegetation covers. The physical characterisations of substrate properties are compared to non-invasive determinations and the hydrological performance implications of trends over time are discussed.

Chapter 7 presents the hydrological performance characterisations from the longitudinal microcosm study. Predictions of hydrological performance based on conceptual and mechanistic modelling approaches are validated against laboratory detention test results. Links between the substrate characterisations presented in chapter 6 and hydrological performance are then explored before a comparative discussion of the modelling techniques is undertaken.

Chapter 8 is the synthesis and discussion, bringing together the findings from the three areas of investigation. The commonalities as well as the differences are drawn from the data before a summary of the overall findings is presented. Suggested modifications to the methods used in this study are provided, together with thoughts on how they may facilitate future research.

Chapter 9 concludes the thesis, relating summarised findings to the initial primary objectives and overall study aim. Future research questions highlighted by this study are discussed.

1.4 Publications

As of March 2017, there are three published journal papers, 6 published conference papers, and a further submitted conference paper that have resulted from work presented in, or related to, this thesis.

1.4.1 Journal Papers

Chapter 4

Stovin, V., Poë, S., **De-Ville, S.**, Berretta, C., 2015. 'The influence of substrate and vegetation configuration on green roof hydrological performance'. *Ecological Engineering*, 85, 159–172.

Stovin, V., Vesuviano, G., **De-Ville, S.**, 2015. 'Defining green roof detention performance', *Urban Water Journal*, pp. 1–15.

Chapter 5

De-Ville, S., Menon, M., Jai, X., Reed, G., Stovin, V., 2017. 'The impact of green roof ageing on substrate characteristics and hydrological performance'. *Journal of Hydrology*, 547, 332–344.

1.4.2   Conference Papers

Chapter 4

De-Ville, S., Stovin, V., 2014, 'Application of a conceptual hydrological model to identify the impacts of green roof substrate ageing on detention performance'. *The University of Sheffield Engineering Symposium Conference Proceedings Vol. 1.* Sheffield, UK, 24 June 2014.

De-Ville, S., Stovin, V., 2015, 'Temporal trends in green roof detention performance as determined through reservoir routing parameters'. *The 10th International Conference on Urban Drainage Modelling.* Québec City, Canada, 20-23 September 2015.

De-Ville, S., Stovin, V., Menon, M., 2015. 'Temporal trends in green roof hydrological performance'. *SUDSnet International Conference 2015.* Coventry, UK, 3-4 September 2015.

Chapter 5

De-Ville, S., Menon, M., Stovin, V., 2015. 'Using X-Ray Microtomography to identify physical changes in green roof substrates as a result of ageing'. *The Annual Postgraduate Research Student Conference - 2015,* Sheffield, UK, 15 April 2015.

De-Ville, S., Menon, M., Jai, X., Stovin, V., 2016. 'Using X-Ray Microtomography to explain observed detention characteristics of green roofs'. *9th International Conference Novatech,* Lyon, France, 28 June-1 July 2016.

Chapter 7

De-Ville, S., Stovin, V., Menon, M., Submitted. 'Hydrological performance evolution of extensive green roof systems'. *14th IWA/IAHR International Conference on Urban Drainage.* Prague, Czech Republic, 10-15 September 2017.

Other

Kasmin, H., Stovin, V., **De-Ville, S.**, 2014. 'Evaluation of green roof hydrological performance in a Malaysian context'. *13th IWA/IAHR International Conference on Urban Drainage.* Sarawak, Malaysia, 7-12 September 2014.

2. *Literature Review*

2.1 Chapter Overview

This chapter comprises a comprehensive review of recent relevant green roof literature. The following sections explore the wider context of the Sustainable Drainage Systems (SuDS) philosophy and the role that green roofs play. Whilst acknowledging the multiple benefits that green roofs can provide, this review is primarily concerned with the hydrological performance of extensive green roof systems. The factors affecting green roof hydrological performance are evaluated based on existing monitoring, laboratory, and modelling studies. Specific knowledge related to the role of green roof substrates and vegetation in influencing hydrological performance is presented, before green roof hydrological modelling techniques and system ageing are discussed. The chapter concludes with a summary of the limitations of the current body of knowledge, highlighting the opportunities for further work that this thesis builds upon.

2.2 Urban Stormwater Management

2.2.1   Historical Practices & Applications

For millennia, civilised populations have sought to control the natural environment around them. Access to safe drinking water, sanitation and protection from flooding were considered essential by many ancient civilisations, just as they are today. To provide their populaces with such amenities, many ancient civilisations incorporated artificial drainage structures into their cities. By 2500 BC the Indus civilisation had developed extensive urban drainage networks that allowed for individual property connections to central drainage channels in adjoining streets (Gray, 1940). It was not until 1700 BC that such systems were seen again in the Minoan civilisation of Crete. The Minoan's system also provided for roof drainage alongside sewage and general drainage.

The Roman Empire constructed grand aqueducts to bring fresh water into their cities which provided them with a safe source of drinking water. However in cases where supply was greater than consumption a new problem was created, public baths and street fountains would overflow (Hodge, 2002). To combat this, underground networks of sewers or *cloacae* were constructed, the largest of these is the *Cloaca Maxima* in Rome, which has subsequently been incorporated into the city's modern urban drainage system (Butler and Davies, 2010). Whilst it was not their initial intention, Roman engineers had combined urban water supply and urban drainage to establish an urban water cycle.

2.2.2 Modern Practices & Applications

Advancement in urban water management was slow between the fall of the Roman Empire and the onset of the industrial revolution. In early 19th Century London, drainage was still provided by streams and ditches in the streets which ultimately led to the River Thames. In 1847 all cesspits were required by law to be connected to the sewers, resulting in greater volumes of sewage entering the Thames. It was at this time that Edwin Chadwick suggested a separate sewerage system for both stormwater and sewage, *"Rain to the River and the Sewage to the Soil"* (Butler and Davies, 2010). However such a system was deemed too expensive and complex. Thus, when Bazelgette's sewers were opened in 1865, they operated as a combined system. This new network of sewers was the first to be designed to accommodate the anticipated flows within them.

In the remainder of the UK, similar combined underground sewerage systems were established and after World War 2 there was significant pollution of water courses in wet weather as a consequence of discharges from combined sewer overflows (CSOs). To prevent upstream pluvial flooding, flows in excess of the designed sewer capacity are discharged into a natural water course. Whilst this is an effective method of protecting people and properties upstream, insufficient dilution of the effluent can lead to chemical and aesthetic pollution problems downstream of the CSO. Legislation introduced in 1990 by the then National Rivers Authority (now Environment Agency) and the European Union (EU) led to a clean-up of the UK's rivers. This was achieved across the country through 'hard engineering' solutions such as the installation of large offline storage tanks to store excess flows instead of discharging them to water courses. Moving into the 21st Century, the EU's Water Framework Directive became the impetus for further removal of pollution from water courses and bathing areas.

2.2.3 Philosophy & Basic Principles of Sustainable Drainage Systems & Water Sensitive Urban Design

Sustainable Drainage Systems, contracted to SuDS, are stormwater drainage systems that are developed to meet three key objectives of sustainable design. A reduction in the quantity of surface water runoff, an increase in the quality of surface water runoff and an increase in amenity and biodiversity value (see **Figure 2.1**). Such systems also offer environmental enhancement through the management of environmental risks associated with surface runoff. Note: in the updated SuDS Manual (CIRIA C753, Woods-Ballard et al. 2015) that amenity and biodiversity benefits have been separated to create 4 pillars of SuDS design. However many pillars it is defined by, the over-arching philosophy of SuDS is to replicate the natural drainage from a site prior to development.

SuDS are intended to be different from, often large, 'hard engineering' options in that they should be small, discrete, units. SuDS devices are intended to reduce the volumes of stormwater runoff at source as opposed to providing large downstream flow attenuation or control. To manage stormwater runoff at source some SuDS devices infiltrate the rainfall directly into the ground beneath them. This may not occur instantaneously and many devices also provide a storage element to allow the maximum volume of stormwater to be infiltrated into the soil. Typical SuDS infiltration devices include: soakaways, rain gardens, bio-infiltration areas, infiltration trenches, infiltration basins and pervious pavements (Woods-Ballard et al., 2007).
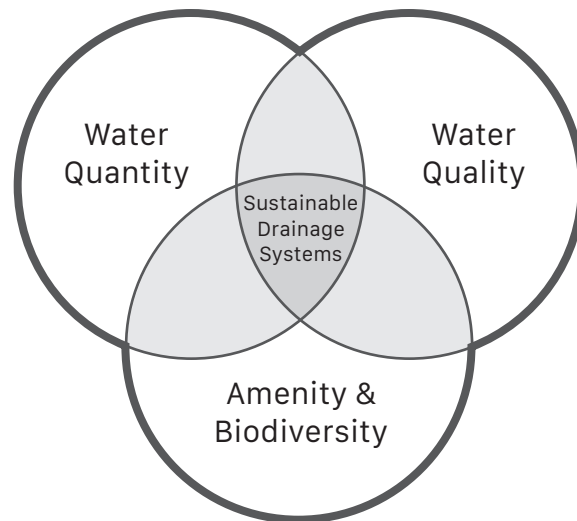
Figure 2.1 The three connected objectives of sustainable drainage (Adapted from Woods-Ballard et al., 2007)

The connection of various SUDS devices to form a treatment or management train is often practiced. The combination of various SUDS allows for the advantages of each to be present in the overall design. Typically a management train design will begin with identifying methods of preventing stormwater runoff, thus reducing overall drainage demands in the remainder of the system. Stormwater runoff can be prevented in numerous ways, for example rainwater harvesting has the ability to prevent a significant level of stormwater runoff as the water is diverted for grey water applications such as toilet flushing or irrigation uses. The disconnection of roof downpipes also prevents stormwater runoff from entering receiving systems, by allowing stormwater to infiltrate into the ground. The management train will generally include several source control devices that feed into a site control which may ultimately feed into a regional control structure. These structures differ in their spatial scale and in their proximity to the source of runoff; any runoff not dealt with by the source control will be conveyed to the site control. Swales are capable of conveying excess runoff whilst at the same time allowing further infiltration to occur. Additional flows from the site control may be directed to a regional control that takes the form of a larger SUDS component such as a wetland. The source, site and regional controls are divided into 7 categories by Woods-Ballard et al. (2015) with some SUDS devices falling into more than 1 category. The 7 categories are: source controls, conveyance channels, filtration devices, infiltration devices, retention and detention structures, wetlands and control structures. The latest CIRIA SuDS Manual (C753) provides several case study examples for all of the above SuDS devices.

Water Sensitive Urban Design (WSUD) is a much broader ideology than SUDS. However, SUDS play a key role in achieving WSUD objectives (**Figure 2.2**). A true WSUD scheme aims to create an integrated water management cycle, which is achievable by following two guiding principles. The first is consideration of all components of the water cycle, along with their various interconnections, to provide an outcome that meets human needs whilst continually supporting a healthy natural environment. Secondly this consideration must always be at the forefront throughout the entire design and planning process (CIRIA, 2013).
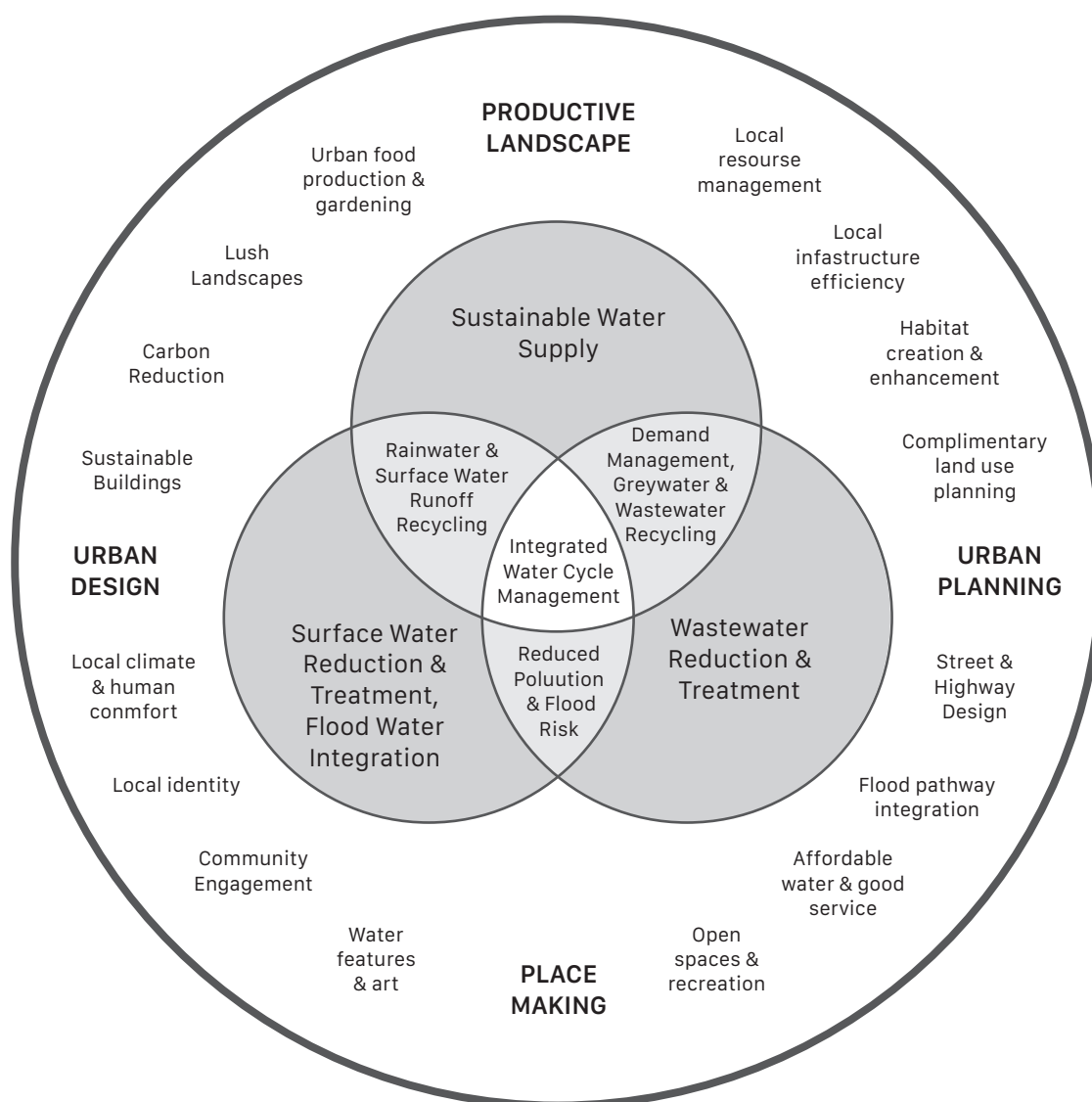
Figure 2.2 The broad ideology of water sensitive urban design (Adapted from CIRIA, 2013)

2.2.4 Drivers for Sustainable Urban Drainage Systems & Water Sensitive Urban Design

 The awareness and implementation of WSUD and SuDS has increased due to various drivers. Cities across the world are continuing to increase in size and since 2008 more

than half of the global population live in urban areas (UN, 2010). Within England and Wales more than 81% of the population are 'usually resident' (live) in an urban area (ONS, 2013); this represents a growth in urban population of around 7% compared to 2001. Continuing urbanisation is leading to reductions in the surface permeability of developed areas by replacing naturally draining ground with roads, roofs and other paved areas. Undeveloped natural areas have the ability to limit the runoff volume and slow the travel time of rainfall into a receiving water course. Plant leaves and other surfaces intercept rainfall before it reaches the ground, root systems help channel rainfall into groundwater and plants ultimately return the water to the atmosphere through evapotranspiration (ET). Clearing of these areas to make way for urban developments reduces the amounts of water that can infiltrate into the ground and, as a direct result, the volume and rate of surface runoff during a rainfall event increases.

The conventional drainage systems in urban areas are designed to convey excess storm water away from areas of development through a network of underground pipes to a receiving system. For combined sewerage systems this is often a treatment works or for separate systems it may be a natural water course. In the past such systems have helped in the prevention of urban flooding. However, in areas with combined sewerage systems the receiving water treatment works can often be overwhelmed in periods of heavy and/or persistent rainfall. To prevent such inundation of the water treatment works, combined sewer overflows (CSOs) have been incorporated into the upstream network. A CSO is designed to allow excess stormwater flows to be diverted into receiving water courses. Whilst this is an effective means of dealing with excess flows within the sewerage network a 'CSO spill', as such an event is called, results in significant chemical and aesthetic pollution of the receiving water course.

Current climate change predictions published by 'UK Climate Projections' estimate that by the 2080s significant alterations to the UK's climate will occur (Jenkins et al., 2009; Murphy et al., 2009). When compared to baseline climate values from 1961–1990, high emissions climate change scenarios (90% probability, indicating potential maximums) include:

- Warmer temperatures throughout the year, with mean summer increases of 8.4°C and mean winter increases of 5.8°C
- Wetter winters that experience up to 30% more rainfall
- Drier summers that experience up to 40% less rainfall

- Annual increases in cloud cover by more than 10% and increases in annual relative humidity of 5%.

The theorised increases in winter rainfall are expected to lead to more frequent or larger CSO spill incidents unless pressure on the UK's network of treatment plants is relieved.

Large scale flooding in the UK is not a new phenomenon. However, the frequency of both pluvial and fluvial flooding events is increasing. For over 50 years the 1947 snow melt flooding was considered the benchmark for the greatest nationwide flooding event (NERC, 2000). It took more than 50 years for a subsequent event to exceed that of 1947, but from the Autumn of 2000 and through to early 2001 the UK saw widespread floodplain inundation as a result of sustained frontal rainfall on essentially saturated catchments (NERC, 2000). Then, in 2007, southern Britain experienced record rainfall through late spring and early summer, which caused frequent localised flash flooding along with extensive floodplain inundation. In those areas that were most affected, flooding was more extreme than that seen in the 1947 benchmark event (Marsh and Hannaford, 2007). Both Sheffield and Hull were also widely affected by flooding in 2007. 2009 experienced more record-breaking floods, this time in the north-west of the country; prolonged rainfall over just 2 days in November caused a flood peak with a return period of more than 2100 years. Some 900 properties were inundated with floodwaters with all river crossings across the Derwent in Workington being either seriously damaged or destroyed (Miller et al., 2013). Flooding events in 2012 occurred in many locations across the UK with Tewkesbury in Gloucestershire, Keswick in Cumbria and York all experiencing substantial flooding events (Stephenson and D'Ayala, 2014). The winter of 2013/14 brought a series of exceptional winter storms which caused severe coastal damage along with persistent widespread flooding. December and January experienced 372.2 mm of rainfall in the south-east of England, which is the wettest 2-month period since 1910 (MET Office, 2014).

Given the increasing levels of urbanisation and loss of green spaces, mounting pressures on existing urban drainage systems, forecasted negative climate impacts, and historical examples of flooding, a shift in urban stormwater strategy is required to provide future infrastructure resilience. SuDS and WSUD approaches provide a selection of tools that can be utilised to reduce the levels of urban stormwater runoff to alleviate pressure on existing drainage networks, whilst also reintroducing green

spaces to urban areas. CIRIA provides considerable guidance on the feasibility of SuDS for both new developments, in C753 — The SuDS Manual (Woods-Ballard et al., 2015), and for the retrofit of SUDS to existing developments, in C713 — Retrofitting for surface water management (Digman et al., 2012). Both of these resources provide the necessary knowledge for the, now cancelled, implementation of Schedule 3 of the Flood and Water Management Act which was to set out new national standards for SuDS. These draft national SuDS standards would have reduced the acceptable rate of runoff from a development to 2 l/s/ha from the current 5 l/s/ha. UK government consultation on the future requirement of SuDS for urban developments is ongoing, but may prove to be the controlling factor in further SuDS adoption in the UK.

2.3 Green Roofs

2.3.1 Green Roofs throughout History

Green roofs have been used for millennia, mainly in the form of roof gardens (Köhler et al., 2002; Osmundson, 1999). The Hanging Gardens of Babylon, one of the Seven Wonders of the World, is perhaps the finest example of an ancient green roof system, although several other ancient civilisations also utilised green roofs (Dunnett and Kingsbury, 2004; Osmundson, 1999). The Vikings made extensive use of turf roofs across much of northern Europe, particularly in Iceland where building resources were scarce (Noble, 2007). The contemporary extensive green roof has its origins in the early 20th century; German apartment blocks were roofed with tar boards and sand as a method of fire protection but over time mosses, sedums and other vegetation colonised the roofs (Werthmann, 2007).

As cities became more urbanised during the 20th Century roof gardens became important amenity spaces. The grass roofs of history developed into landscaped spaces and experienced increased levels of biodiversity. However, they were only a preserve of the rich and were seen as a luxury. Many American theatres incorporated a roof garden into their design and this heritage lives on in names such as Madison Square Garden and the Winter Garden in New York (Osmundson, 1999). The resemblance of these roof gardens to natural catchments through the interception and retention of rainfall led them to be developed and refined into engineered stormwater management systems.

2.3.2 Modern Approach to Green Roof Systems & Design

There are two distinct types of green roof system, intensive and extensive. An intensive green roof is much like a typical garden with deep soil layers and can be planted with grasses, flowering plants, shrubs and in some instances trees (Oberndorfer et al., 2007). These intensive green roofs are highly attractive from an aesthetic and biodiversity point of view. However, the additional load means that the structural cost of such systems can be extreme. In addition, intensive green roofs require a regime of regular irrigation and maintenance, thus raising the cost of their upkeep.

Alternatively, extensive green roofs consist of a considerably thinner soil layer and are vegetated with smaller plants that are more tolerant of climatic extremes (Dunnett and Kingsbury, 2004; Oberndorfer et al., 2007). This allows the roof to have a very low maintenance requirement and no need for irrigation. A typical extensive green roof system consists of four main layers (**Figure 2.3**). The top surface is the vegetated layer (1), which overlies the main body of the roof, the soil substrate (2). Under this substrate is a filter membrane (3), which prevents the washing away of the soil into the drainage layer (4). During a storm event rainfall is first intercepted by the vegetation, then the rainfall infiltrates into the soil substrate. The soil retains this moisture where it will be returned to the atmosphere through a combination of evaporation and transpiration, or evapotranspiration (ET), as these processes are collectively termed. Once the field capacity — the available rainfall storage — is reached, then runoff will occur through the drainage layer and away from the roof.
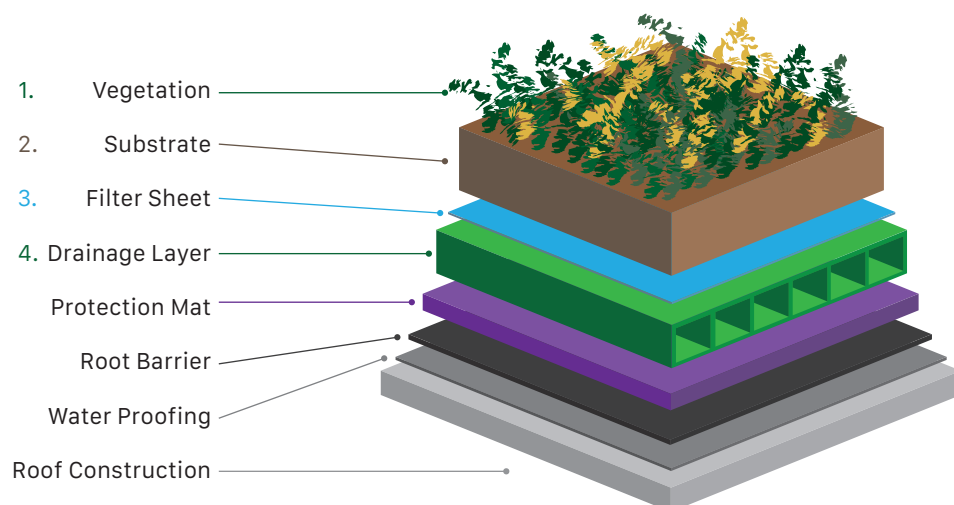
Figure 2.3 Typical extensive green roof construction, the main 4 layers are indicated (Authors own).

2.3.3 Recognised Benefits & Disadvantages of Modern Green Roof Systems

For a modern green roof the key objective is often the reduction in stormwater runoff, a detailed review of green roof hydrological performance is undertaken in section 2.4, yet there are also many other benefits. Green roofs were used on buildings throughout history for the main purpose of providing insulation. Modern systems are also thought of as effective insulating systems (Palomo Del Barrio, 1998), acting as a thermal buffer reducing both heating and cooling needs. However, this is disputed by Anderson (2006) and (Castleton et al., 2010) who recommend for the purposes of design that the substrate and vegetation of a green roof are assumed to provide no insulation properties. The ability to mitigate the urban heat island effect is associated with building insulation benefits, as a result of evaporative cooling (Rizwan et al., 2008; Speak et al., 2013; Takebayashi and Moriyama, 2007). All green roofs are capable of boosting biodiversity by providing new habitats for both plant and animal species (Benvenuti, 2014; Lundholm et al., 2010; Rumble and Gange, 2013). Intensive green roofs are also capable of supporting small scale agriculture projects (Roehr and Laurenz, 2008; Rowe, 2011), which can boost local vegetable production. The continual development of vegetation gives the roof a limited carbon sequestration ability as organic matter builds up in the substrate (Getter et al., 2009, 2007; Li et al., 2010). The layers within the green roof also provide sound insulation (Miller, 2003; Van Renterghem and Botteldooren, 2008) and prevent the deterioration of the underlying roof membranes caused by UV light (Charlie Miller, 2003; Porsche and Köhler, 2003). Building developers are beginning to incorporate green roofs into their developments due to the added financial and reputational value that they can provide (Dunnett and Kingsbury, 2004; Ichihara and Cohen, 2010).

To be compliant with the 3 objectives of SuDS, green roofs should also provide a water quality benefit. It is thought that filtration of rainwaters provided by the roof substrate and uptake through plant roots provide this ability. However, there is some contention surrounding this view. There is evidence to support a water quality benefit (Köhler et al., 2002) yet other published studies highlight the potential of green roofs to act both as pollutant sinks and possible pollutant sources (Berndtsson et al., 2009; Carpenter and Kaluvakolanu, 2011; Gregoire and Clausen, 2011). As a green roof only receives rainwater, it may be unrealistic to expect a significant improvement in water quality. The requirement to provide a water quality benefit is evidently more relevant for ground-level SuDS receiving more polluted waters, e.g. road runoff. Of those studies that have considered green roof water quality, the most frequently investigated

pollutants are forms of phosphorus, nitrogen, and heavy metals (Hashemi et al., 2015). It has generally been found that as a result of reduced runoff volumes from the green roofs the total mass of pollutants was also reduced. The efficiency of green roofs to remove pollutants is heavily dependent on roof configuration and maintenance regimes (Berndtsson, 2010; Hashemi et al., 2015).

Whilst there are many benefits provided by the installation of a green roof there are also some disadvantages. In comparison to other SuDS devices a green roof does not infiltrate rainwater into the ground. Intensive green roof constructions can lead to high levels of structural loading that may require reinforcement of the supporting structure. Extensive systems are more appropriate for retrofit than intensive systems due to their lightweight construction (Theodosiou, 2009; Werthmann, 2007). The provision of amenity space may also be restricted for private and/or inaccessible green roof installations.

2.3.4 Green Roof Substrates

Modern commercial green roof substrates are light-weight, well drained, with adequate moisture and nutrient storage and supply capacity, and generally resistant to breakdown over time (Getter and Rowe, 2006). Typical substrate compositions include 80-90% by volume (v/v) light-weight inorganic aggregates and 10-20% v/v organic matter. The aggregate content creates a substrate matrix with pore spaces for air, water and gas exchange, whilst facilitating well drained conditions. The coarse texture of this aggregate requires supplementary organic matter to support key functions of plant growth (VanWoert et al., 2005b).

In the UK, the most common aggregate material is crushed recycled clay bricks (**Figure 2.4**), whilst crushed concrete and fly ash are occasionally used (Molineux et al., 2009). Elsewhere in the USA and New Zealand, natural volcanic material such as pumice and zeolite are common choices with similar characteristics to manufactured expanded materials (Fassman and Simcock, 2012), such as light expanded clay aggregates (**Figure 2.4**). Experimental studies have also considered additional substrate additives such as crumbed rubber, paper ash, sewage sludge and biochar. However, these have yet to become widely adopted (Beck et al., 2011; Molineux et al., 2009; Ristvey et al., 2010).
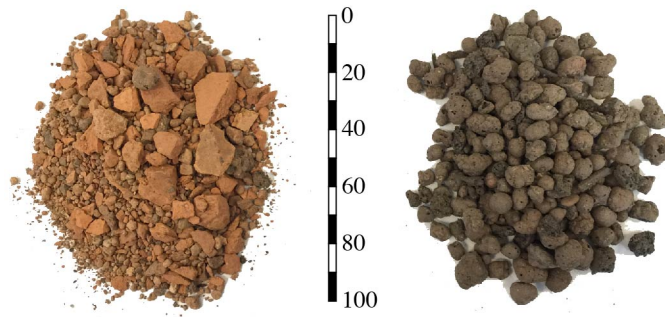
Figure 2.4 Left: Typical crushed brick-based substrate **Right:** Light Expanded Clay Aggregate (LECA) based substrate. Scale in mm.

What constitutes a suitable level of organic matter within the substrate composition is debated. The German FLL (2008) recommends a maximum of 4% (by mass, equivalent to 10-20% v/v). This upper limit was originally dictated by German fire regulations to prevent smouldering burns of green roofs (Fassman and Simcock, 2012). Other literature also proposes an organic content of between 5-20% v/v (Berghage et al., 2008; Dunnett and Kingsbury, 2004). The levels of organic matter can have significant effects on vegetation growth. High levels of organic matter favour plant growth, but can promote growth of less drought tolerant species which subsequently struggle to survive (Getter and Rowe, 2006; Molineux et al., 2009). Additionally, high levels of organic matter can increase moisture storage, potentially increasing system weight (Getter and Rowe, 2006). The decomposition of organic matter over time risks the reduction of substrate depth (Beattie and Berghage, 2004; Snodgrass and Snodgrass, 2006), which may compromise drainage (Snodgrass and McIntyre, 2010), runoff colour and quality (Berghage et al., 2008; Berndtsson et al., 2009; Moran et al., 2003). Typical sources of organic matter include peat moss and composted bark (FLL, 2008). Waste and recycled local resources are increasingly popular, such as composted bark or shredded wood (Fassman and Simcock, 2012). Suitable composted materials must be stable to prevent nutrient leaching and rapid decomposition (Snodgrass and McIntyre, 2010).

Evaluation of substrate physical properties

Given the complex interactions between substrate physical properties and hydrological performance, it is important to accurately and reliably quantify key physical properties. The German FLL (2008) '*Guidelines for the Planning, Execution, and Upkeep of Green-Roof Sites: Appendix 2'* provides a comprehensive standards for testing substrates. The document presents rigorous laboratory testing methods, apparatus, and target numerical values for various green roof configurations. The FLL

substrate characterisation methodology has been utilised in Europe (Berretta et al., 2014; Poë et al., 2015), North America (Hakimdavar et al., 2014; Hill et al., 2016; Sims et al., 2016), Australia and New Zealand (Farrell et al., 2013; Fassman and Simcock, 2008), as well as in China (Chen, 2013). The American Society of Testing Materials (ASTM) has also issued testing standards (ASTM E2397-11 and E2399-11), but does not provide target values for suitable substrates (ASTM 2011a; b).

The investigation techniques presented by the FLL guidelines can be invasive and destructive. For example: particle sizes are determined via a sieve analysis, destroying the sample's original matrix; and organic matter is determined by loss on ignition, permanently removing the organic material from the substrate. These methods also typically involve the collection and aggregation of several substrate samples into an overall sample, which is then used for physical property evaluation (Emilsson and Rolf, 2005; FLL, 2008; Thuring and Dunnett, 2014). When exploring complex interacting substrate properties (e.g. pore sizes, tortuosity and hydraulic conductivity) the re-aggregated FLL samples can result in highly variable values. These problems are compounded when exploring the delicate in-situ properties of already established green roof systems, and preclude any evaluation of substrate properties over time.

Concerns have been raised about the suitability of some FLL testing practices, particularly the FLL test for substrate permeability (approximately equal to a saturated hydraulic conductivity measure conducted with a 10 mm falling water head). Fassman and Simcock (2012) identified that the testing methodology was sensitive to the initial moisture content of the substrate, with increased initial moisture levels leading to increased permeabilities. The dissimilarity of the test to actual rain events (the methodology uses a ponded depth of water, 35-45 mm, to drive flow through the substrate, whereas substrate saturation is not expected to occur in operation) was also highlighted by Fassman and Simcock (2012). The issue of a meaningful permeability test remains unresolved. However, the standardised nature of the FLL methodology facilitates the comparison of permeability amongst varying substrate compositions and permits a basic check against recommended limits.

Alternative physical exploratory methods to the FLL do exist and mainly emanate from the Soil Science community. To maintain the particle and pore size distributions of in-situ green roof substrates, substrate cores can be taken and set in resin. This preserves the internal structure of the core, which can then be cut to examine particle

and pore sizes (Graceson et al., 2013; Poë, 2016). Whilst this technique does preserve the in-situ characteristics of the green roof substrate, it is only capable of providing discrete 2D perspectives of the core (Young et al., 2001). Similarly, it is possible to asses in-situ hydraulic conductivity via a double ring infiltrometer (Rowell, 1994). Within a laboratory environment, saturated hydraulic conductivity is measured by first saturating a substrate sample and maintaining a constant head of water above its surface. The rate of inflow to maintain the head is equal to the saturated hydraulic conductivity (Rowell, 1994).

Interest in the internal structures of soils within the Soil Science community has led to the development of non-invasive physical property evaluation techniques. Amongst these techniques, the most common is X-ray microtomography (XMT), a non-destructive 3D computed tomography (CT) imaging approach. XMT is widely used for the visualisation and quantification of an object's internal structure, exploring particle and pore sizes. Improvements in spatial resolution and image reconstruction times since the turn of the century have allowed XMT to become a commonly accepted tool for material analysis (Maire and Withers, 2014). Images are obtained by passing X-rays from a suitable source through the object to be imaged and onto a CCD detector. Typical achievable image resolutions range from <1 µm to 150 µm depending upon object size (Maire and Withers, 2014). The resulting high resolution images can be analysed to show the 3D spatial arrangement of the solid particles and pore spaces in a soil matrix.

XMT is an established technique within the soil sciences field, where the main application has been for the characterisation of physical soil properties (Menon et al., 2015). Several studies have successfully utilised XMT to observe plant roots and their interactions with soils, earthworm burrows, soil insects, and other soil microorganisms (Taina et al., 2008). However, there has been limited use of XMT to image engineered soils similar to those used as green roof substrates. One example of the application of XMT to green roof substrates is from Jelinkova et al. (2016), where the techniques was used to assess macroporosity (pores greater than 50 µm in diameter) and the internal geometries of the substrate matrix. The non-invasive nature of XMT allows for considerably greater preservation of the delicate internal structure of a green roof substrate than is possible with destructive or reconstructive testing techniques. In turn, this enables the reliable characterisation of in-situ substrate properties and further 3D analyses. Previous studies on conventional soils

have confirmed that the XMT technique provides comparable or improved porosity results over thin section analysis, vacuum analysis and mercury porosimetry (Taina et al., 2008).

The digital models of soil/substrate structure obtained from XMT allow for the numerical modelling of water flow and other common applications of computational fluid dynamics. Menon et al. (2015, 2011) have demonstrated the implementation of the Lattice Boltzmann Method (LBM) for evaluating fluid flow through soil matrices, by utilising 3D XMT images. These fluid flow simulations permit the estimation of permeability and saturated hydraulic conductivity. The LBM method is a preferable alternative to other conventional Computational Fluid Dynamics (CFD) approaches due to its ability to use large datasets with complex irregular geometries and its speed (particularly when also considering the meshing requirement of conventional CFD approaches) (Menon et al., 2011). The LBM method is uniquely suited to the saturated hydraulic conductivity modelling of complex soil/substrate matrices obtained from 3D XMT images.

Substrate Characteristics and Hydrological Performance

A substrate's soil–water characteristics are typically considered to be the key influence in a system's capacity to store rainfall (Palla et al., 2010). The field capacity, permanent wilting point (Beattie and Berghage, 2004) and water release characteristics (Manning, 1987; Miller, 2003) are all governed by a substrate's structure and texture. Adsorption of water molecules to the substrate particles and the cohesive forces between these water molecules generates a negative (matric) pressure in the soil–water (Hillel, 2004). Matric pressure (ψ_m) is the driving force for soil water fluxes under unsaturated flow conditions. The magnitude of ψ_m is dependent on pore sizes, with smaller pores generating higher matric pressures, conversely large pores have lower matric pressures (Hillel, 2004). When ψ_m is in equilibrium with gravitational forces, the substrate is at field capacity (θ_{FC}). This equilibrium exists in pores with a diameter of 50 µm or less (**Figure 2.5**). Field capacity is also often referred to as the Maximum Water Holding Capacity (MWHC) and is easily determined by allowing a substrate to drain under gravity for a sufficient period (FLL guidelines recommend 2 hours for a typical substrate). At smaller pore diameters, the elevated levels of ψ_m make it difficult for plants to extract the water from the substrate. The point at which plants can extract no further moisture from the substrate is referred to as the Permanent Wilting Point (PWP), this corresponds to a

pore diameter of 0.2 µm (**Figure 2.5**). The difference between MWHC and PWP is known as the Plant Available Water (PAW) and is considered to represent the maximum potential retention capacity of the green roof. The relationship between ψ_m and pore size means a substrate's pore size distribution will dictate its water retaining abilities.
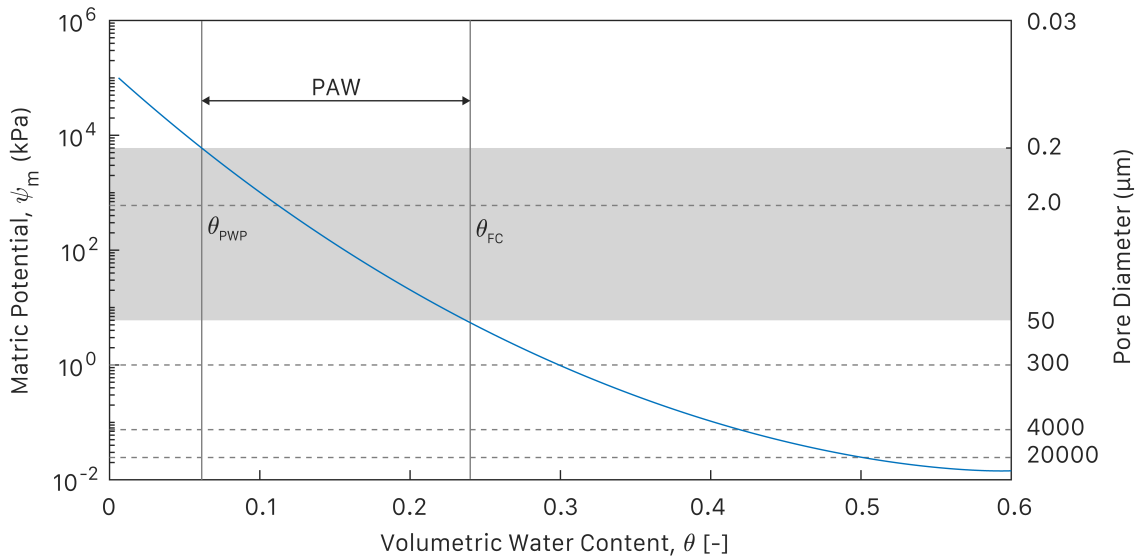
Figure 2.5 Typical Water Release Curve for a Green Roof Substrate. Shaded region indicates typical operating moisture levels.

Pore size distribution is also a controlling factor for detention performance, primarily due to its influence on substrate tortuosity and hydraulic conductivity. A typical highly porous free draining green roof substrate should only support unsaturated flow conditions during operation (FLL, 2008). The relationship between pore size and ψ_m dictates that at low moisture contents (below θ_{FC}) water will be present in only the smallest pores. During these low moisture conditions, there is a lack of connectivity between water filled pores, as such flow paths through the substrate depth can be extremely tortuous or not present at all (**Figure 2.6: A**). The hydraulic conductivity of the substrate can therefore be described as low. As moisture content increases (to above θ_{FC}) larger pores begin to fill with water. Greater connectivity of water–filled pores decreases flow path tortuosity and allows for greater flow transmission (elevated hydraulic conductivity, **Figure 2.6: B**). Continued wetting of the substrate until saturation (θ_{SAT}) causes the largest pores to become water filled and flow paths become the least tortuous. The saturated hydraulic conductivity (K_{sat}) represents the fastest transmission rate of water through the substrate (**Figure 2.6: C**). The relationship between moisture content and hydraulic conductivity is known as a K(θ) relationship. **Figure 2.7** illustrates a typical K(θ) relationship for a green roof

substrate, where it can be seen that there is a negligible hydraulic conductivity under typical operational green roof moisture levels. A significant increase in substrate moisture above field capacity is required before hydraulic conductivity becomes observably different. The K(θ) relationship of **Figure 2.7** is theoretical and the exact form of this relationship will change with differing pore size distributions and tortuosity values (Hillel, 2004).
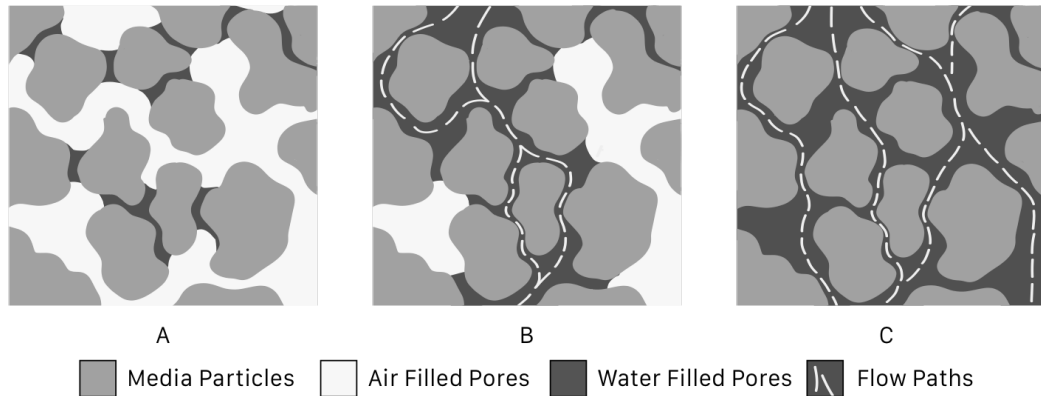
Figure 2.6 Flow of Water through a Porous Media. **A**: θ_{FC}. **B**: $\theta_{FC} < \theta < \theta_{SAT}$. **C**: θ_{SAT} (after Hillel, 2004).
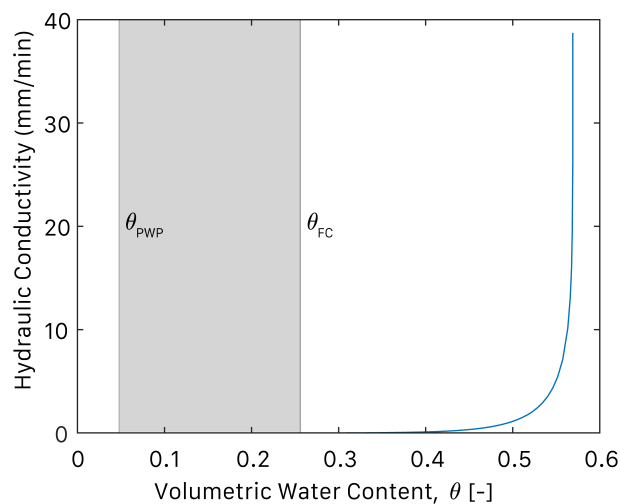
Figure 2.7 Typical K(θ) Relationship for a Green Roof Substrate. Shaded region indicates typical operating moisture levels.

The K(θ) relationship can be obtained from a substrate's soil water characteristic curve, which expresses the relationship between moisture content (θ) and soil moisture potential (ψ), e.g **Figure 2.5**. The soil water characteristic curve can be determined via the pressure plate extraction method (Carter, 1993). Water is gradually

removed from initially saturated samples by applying increasing suction pressures. Few older green roof studies (published prior to 2010) report the water release or K(θ) relationships of the substrates that they utilise (Villarreal and Bengtsson (2005) and Hilten et al. (2008) being notable exceptions). This is primarily due to difficulty, equipment availability, and time required to obtain the necessary data. In more recent years, and with a general research direction toward more physically-based models, numerous studies have actively explored the water release characteristics of green roof substrates (Berretta et al., 2014; Carson et al., 2013; Fassman and Simcock, 2012; Liu and Fassman-Beck, 2017). This characterisation of green roof substrate properties allows for the successful validation of hydrological models that represent the physical processes that control hydrological performance.

Green Roof Substrates Summary

The substrate is the major component within a green roof system, and the majority of green roof benefits can be attributed to substrate physical properties. Substrate compositions can vary widely amongst green roof systems, but there is a requirement for free drainage and suitable levels of organic material to support vegetation growth. The hydrological performance of a green roof substrate is predominantly dictated by its pore size distribution, which is a controlling factor for retention (via moisture release controls) and detention (via hydraulic conductivity controls).

2.3.5 Green Roof Vegetation & Root Systems

Potentially any plant species can be placed on a green roof provided that its specific needs are catered for. The most common vegetative treatment is generally a mix of Sedum species (*spp.*). Sedum *spp.* are a type of succulent vegetation and their widespread use on green roofs is due to their efficient use of available water which enables them to have a high drought tolerance (Dvorak and Volder, 2010). Under drought conditions some Sedum species may have the ability to switch their metabolism to Crassulacean Acid Metabolism (CAM), reducing moisture loss from foliage (Sayed, 2001). Sedum *spp.* also typically have shallow root systems enabling them to survive in thin substrate layers. However, in cold climates frequent freezing of the substrate causes damage to roots (Boivin et al., 2001).

Herbaceous perennials have also been installed in green roof environments although they are less commonly used due to their relative intolerance of drought compared to succulents. In particularly shallow substrates (<100 mm) herbaceous plants do not fare well if unirrigated after a period of two weeks. In deeper substrates (>127 mm)

some herbaceous species are capable of surviving without irrigation (Monterusso et al., 2005, Licht & Lundhdolm, 2006). Graminoids (i.e. Grasses) were found to extract water from the growing media at a faster rate than succulents (Wolf and Lundholm, 2008). Generally herbaceous plants have been found to support greater transpiration rates than succulents, which allows them to provide greater cooling and water management benefits. However, to be effectively used on a green roof a deeper substrate and some irrigation is required (Dvorak and Volder, 2010).

A wide variety of fruits, vegetables and herbs have been produced in limited quantities from green roofs worldwide as part of urban agriculture initiatives (Whittinghill et al., 2013). However, the majority of schemes use intensive substrate depths exceeding 150 mm. Extensive systems have a reduced capacity for vegetable production due to lower water availability and nutrient content. With regular irrigation and some fertiliser input, Whittinghill et al. (2013) were able to successfully cultivate tomatoes, beans, cucumbers, peppers, basil and chives in a 105 mm depth of substrate. Further research is required to ensure fertiliser application rates do not lead to detrimental water quality effects (Whittinghill et al., 2016).

Vegetation and Hydrological Performance

Plant transpiration accounts for between 20 and 40% of the total moisture lost to the atmosphere via evapotranspiration (Voyde et al., 2010). Transpiration rates differ from species to species, and are dependent on the plant's metabolic processes (Poë et al., 2015). Comparative studies into the effects different vegetation types have on hydrological performance have been conducted. Fassman and Simcock (2008) found that green roof installations with *Sedum mexicanum* supported higher ET rates than those with New Zealand Ice Plants (*Disphyma australe*), thus resulting in lower runoff volumes (i.e. stronger retention performance). Poë et al. (2011) similarly found that green roof test beds installed with a Sedum *spp.* mix reduced runoff to a significantly greater extent than equivalent systems with 'Meadow Flower' vegetation. Poë and Stovin (2012) subsequently identified that introducing vegetation to a green roof can reduce its ability to return water to the atmosphere, particularly in the initial 4 to 12 days after a rainfall event. This is due to the greater levels of evaporation from a bare dark substrate surface compared to the green planted coverage which contributes to localised air cooling. Once this initial period has passed, a 'Meadow Flower' vegetative treatment was found to regenerate the available water capacity faster than a Sedum mix treatment; this is similar to the findings of Wolf and Lundholm (2008). As

retention performance is a direct result of ET rates, those plant species that can support high levels of ET could lead to greater reductions in runoff (Lundholm et al., 2010; MacIvor and Lundholm, 2011).

A minimum vegetation cover of 20 to 25% is required to provide any additional storm water retention benefit beyond the abilities of the substrate alone (Morgan et al., 2013). Increased interception of rainfall by vegetation has the ability to reduce runoff volumes and rates from green roofs (Nagase and Dunnett, 2012). Comparisons of the interception abilities of different plant types identified that mat-forming low-growing plants had a reduced interception compared to taller plant species due to a reduced surface area (Clark, 1940, 1937). Plant species that have a very dense fibrous root system tend to reduce the porosity of the surrounding growing media, thus reducing the space available for water storage and so reducing the levels of rainfall retention (MacIvor and Lundholm, 2011).

Impacts of Vegetation Root Growth & Decay

As roots grow they push through the soil compressing the surrounding soil matrix to accommodate their own volume. In doing so the roots change the size distribution and connectivity of soil pores. A reduction in pore space of 23% is possible in the soil adjacent to the root surface (Bruand et al., 1996). Living roots secrete a complex mixture of organic compounds into the soil, including sugars, amino acids, organic acids, phospholipids, and polysaccharides. Many of these compounds are released from the root tip in order to lubricate penetration of the soil aggregates and they persist in the area surrounding the root (Bengough, 2012). These organic secretions can alter the water retention properties of the soil and is the primary cause of chemically-based changes in water holding ability. When wet, the mucilage spreads and so the concentration of solutes within it falls. However, upon drying it contracts, increasing the solute concentration and so increasing its osmotic potential (Bengough, 2012). The combination of root secretions and additional microbial exudates coating pore walls around roots is likely to influence the rate of wetting of the soil. The organic coatings may have a hydrophobic quality, which is most evident in dry soils, thus decreasing the rate of wetting. When the soil is wet the organic compounds can exhibit surfactant-like behaviour allowing water extraction from smaller pores (Hallett et al., 2003).

On a larger scale, the continuous network of branched roots that permeates a soil will lead to changes in hydrological processes due to the growth of new roots and the

decay of old ones. There is a constant turnover of root mass and this cycle may occur over a period of days for fine unbranched roots of grasses, or over several years for thick structural roots of trees (Bengough, 2012). This continual turnover creates numerous continuous flow paths through the growing media. The walls of these channels are coated in organic remains of root material and any associated microbial populations (Jassogne et al., 2007). New roots will often repopulate these channels as they present a path of low mechanical resistance compared with the surrounding soil. Whilst vacant these channels will also form flow paths, allowing faster infiltration of water. The continuous root-sized pores are responsible for much of the porosity that regulates saturated flow in a soil (Bengough, 2012). A study by Schwen et al. (2009) found that particle travel speeds were 152 times faster than the measured soil matrix conductivity values due to the presence of dead root macropores forming preferential flow paths.

Green Roof Vegetation & Root Systems Summary

Vegetation is an integral part of any green roof system and provides the necessary biodiversity and amenity benefits required by the SuDS philosophy. Any type of planting can be used on a green roof if its specific needs are met. For extensive green roof systems, the predominant vegetation choice is Sedum, due to its drought tolerance. As green roof vegetation grows its root networks move through the substrate and have the potential to alter physical and hydrological characteristics. There is considerable literature that explores the role of vegetation in controlling green roof retention performance via plant water use, but there remains little exploration of substrate/root interactions and the consequences for hydrological performance.

2.4 Green Roof Hydrological Performance

2.4.1 Green Roof Retention Performance

There are two distinct hydrological processes that occur within a green roof, retention and detention. Together they account for the stormwater management benefits that a green roof can provide. Retention is the hydrological process that reduces the volume of stormwater runoff. As rainfall falls on the green roof it is stored in the pore spaces of the substrate, over time this stored water is lost from the roof and returned to the atmosphere through evapotranspiration (ET).

Numerous pilot and full scale green roof monitoring studies have been conducted globally to assess retention performance. Retention performance is commonly reported as either a total volumetric retention, as a percentage of rainfall over a study period, or as a mean per-event retention (VanWoert et al., 2005a). For the example events of **Figure 2.8** (where total rainfall depths were 10, 20 and 30 mm respectively), the mean per-event retention is 63%. As a total of 30 mm of rainfall was retained across all three events, from a total incident rainfall of 60 mm, the volumetric retention is 50%. Small event depths with high levels of retention can skew reported metrics toward higher levels of retention performance. A selection of 32 reported monitoring studies illustrates the significance of retention as a method of volumetric control (**Table 2.1**). The range of reported retention performances, from 17 to 97%, is typical of the wider green roof literature.
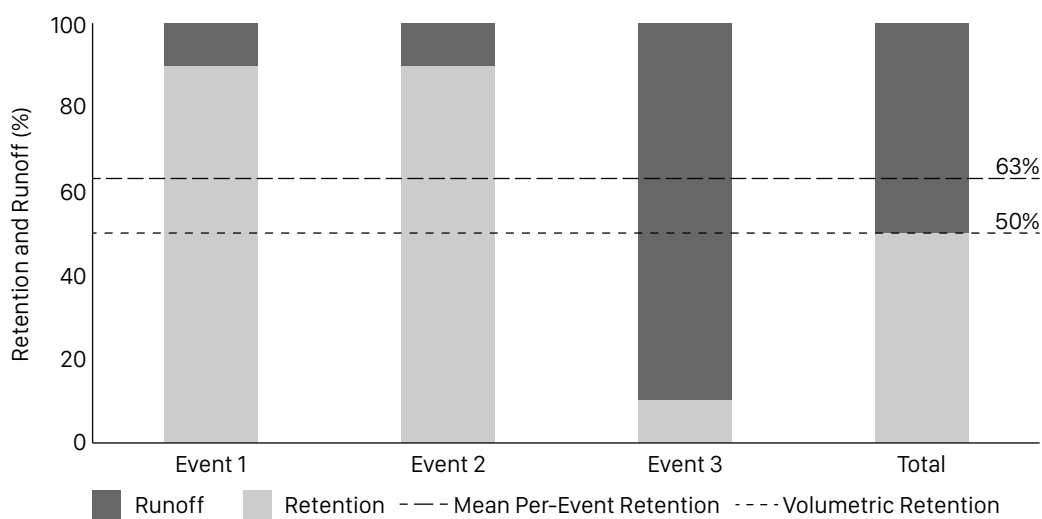
Figure 2.8 Comparison of Mean Per-Event and Volumetric Retention.

Table 2.1 Summary of reported retention performance of 32 studies.

Study	Location	Climate	Vegetation	Substrate Depth (mm)	Retention (%) Per Event	Retention (%) Volumetric	Study Duration (Months)
Hutchinson et al., 2003	Portland, OR, USA	Temperate Marine	Succulent	127	-	69	16
Moran et al., 2003	Kinston, NC, USA	Humid Subtropical	Sedum	100	-	63	17
	Goldsboro, NC, USA	Humid Subtropical	Sedum	50-100	-	62	3
Liu, 2004	Ottawa, Canada	Humid Continental	Wild Flower	150	54	-	22
DeNardo et al., 2005	Raleigh, NC, USA	Humid Subtropical	Sedum	76	45	-	2
Liu & Minor, 2005	Toronto, Canada	Humid Continental	Unspecified	75-100	57	-	24
Carter & Rasmussen, 2006	Athens, GA, USA	Humid Subtropical	Sedum	76	79	-	13
Connelly et al., 2006	Vancouver, Canada	Oceanic	Sedum	150	-	26	12
TRCA, 2006	Toronto, Canada	Humid Continental	Sedum	140	65	-	2
Getter et al., 2007	East Lansing, MI, USA	Humid Continental	Sedum	60	80	-	17
Teemusk & Mander, 2007	Tartu, Estonia	Humid Continental	Sedum	100	29	-	11
Berkompas et al., 2008	Seattle, WA, USA	Temperate Marine	Sedum	150	-	17	11
Spolek, 2008	Portland, OR, USA	Temperate Marine	Sedum	150	25	-	36
Bliss et al., 2009	Pittsburgh, PA, USA	Humid Continental	Sedum	140	22	-	6
Kurtz, 2009	Portland, OR, USA	Temperate Marine	Sedum	125	-	56	36
Berghage et al., 2010	Chicago, IL, USA	Humid Continental	Sedum	76	74	-	24
Fioretti et al., 2010	Genoa, Italy	Hot Mediterranean	Unspecified	200	68	-	15
Gregoire & Clausen, 2011	Storrs, CT, USA	Humid Continental	Sedum	102	-	43	3

Table 2.1 Cont. Summary of reported retention performance of 32 studies.

Study	Location	Climate	Vegetation	Substrate Depth (mm)	Retention (%) Per Event	Volumetric	Study Duration (Months)
Palla et al., 2011	Genoa, Italy	Hot Mediterranean	Unspecified	200	52	-	12
Burszta-Adaniak, 2012	Wroclaw, Poland	Maritime Temperate	Perrenial	Unspecified	83	-	13
Stovin et al., 2012	Sheffield, UK	Maritime Temperate	Sedum	80	29	43	29
Carson et al., 2013	New York, NY, USA	Humid Subtropical	Sedum	32	-	36	12
Eksi, 2013	Istanbul, Turkey	Humid Subtropical	Sedum	90	54	-	12
Fassman–Beck et al., 2013	Auckland, New Zealand	Oceanic	Native Mix	100	-	39	28
Hakimdavar et al., 2014	New York, NY, USA	Humid Subtropical	Sedum	32	48	-	12
Wong & Jim, 2014	Hong Kong, China	Humid Subtropical	Perrenial	40–80	44	14.1	10
Razzaghmanesh and Beecham, 2014	Adelaide, Australia	Mediterranean	Native Mix	100	66	-	24
			Native Mix	300	82	-	24
Harper et al., 2015	Rolla, MO, USA	Humid Continental	Sedum	102	-	60	9
Nawaz et al., 2015	Leeds, UK	Maritime Temperate	Sedum	30	66	-	20
Arias et al., 2016	Mions, France	Maritime Temperate	Sedum	60	38	-	2
Carpenter et al., 2016	Syracuse, NY, USA	Humid Continental	Sedum	102	97	-	11
Franzaring et al., 2016	Hohenheim, Germany	Maritime Temperate	Sedum–Grass	120	-	40	24
Sims et al., 2016	London, Canada	Humid Continental	Sedum	150	77	48	26
	Calgary, Canada	Humid Continental	Sedum	150	90	67	26
	Halifax, Canada	Humid Continental	Sedum	150	60	34	26

It is now widely acknowledged that retention performance is influenced by roof configuration (slope, aspect, drainage layer, substrate type and depth, and vegetation), rainfall characteristics (duration, depth, intensity), and antecedent conditions (primarily as a function of variable ET rates) (Berndtsson, 2010). A large portion of early green roof literature lacked critical evaluation of the physical processes driving retention performance. Studies conducted since 2010 have generally been more focused on exploring the effects of roof configuration or study climate. However, there is continued reporting of one-off roof configurations under specific climatic conditions. The usefulness of these 'local' case-studies is perhaps limited for the scientific community, although it remains important to stormwater managers and other decision makers in driving the adoption of green roofs.

Monitoring studies in the literature range from 2 months in duration (Denardo et al., 2005) to greater than 18 months (Fassman-Beck et al., 2013; Stovin et al., 2012). Study duration is important in contextualising reported retention performance, due to the influential effects of rainfall characteristics and climatic conditions. Longer duration studies may represent more typical climatic conditions for a location, whereas a short-term study is susceptible to abnormal weather conditions. In an extreme case, Teemusk and Mander (2007) only considered 3 rainfall events where retention performance for each event was 2, 87 and 85% respectively. This yields a mean per-event retention of 58%, which is quite clearly skewed by the one very low retention value. Stovin (2010) reported a total volumetric retention of 34% using 4 months of data collected in Sheffield, UK, yet with continued collection Stovin et al. (2012) reported a retention of 50% when analysing 29 months of data from the same test bed. Studies by Voyde et al. (2010) and Fassman-Beck et al. (2013) in Auckland, New Zealand, with 12 and 28 month durations exhibited 66% and 56% retention respectively.

Green Roof Retention Performance and Roof Configuration
A clear trend between roof configuration and retention performance is difficult to discern from the information presented in **Table 2.1**, primarily as many other variables differ from study to study. By co-locating various green roof configurations, such that they experience the same climate and rainfall, the effects of configuration can be explored in isolation. The presence of vegetation is perhaps the most visible difference in roof configuration. VanWoert et al. (2005b) identified that vegetated configurations could provide marginally greater retention performance than identical

unvegetated systems, but suggested more significant improvements could arise from altering substrate physical properties. Similar explorations by Wolf and Lundholm (2008) identified that the moisture loss from vegetated systems was only greater at low substrate moisture levels, a finding also reported by Poë et al. (2015).

Razzaghmanesh and Beecham (2014) ran a comparative study between different substrate types and depths, with a consistent vegetation type, where a 24% improvement in retention was seen for tripled substrate depths (300 mm vs. 100 mm). A doubling of media depth, from 40 to 80 mm, led to 16% increase in retention performance for Wong and Jim (2014). A laboratory analysis of substrate properties and retention performance undertaken by Graceson et al. (2013) identified that retention was more significantly affected by the substrate's physical properties (particularly its pore size distribution and maximum water holding capacity) than by its depth. The two substrates investigated by Razzaghmanesh and Beecham (2014) had a 4% difference in MWHC; the substrate with an elevated MWHC experienced a 23% point increase in mean per-event retention performance. Similar associations between MWHC and retention have been reported in the wider literature (Poë et al., 2011; Fassman and Simcock, 2012). A more critical exploration of substrate properties and hydrological performance is undertaken in section 2.3.4.

The inclusion of substrate additives and additional roof layers have been explored to maximise retention. Rock wool layers have been trialled by Teemusk and Mander (2007) and Wong and Jim (2014), amongst others. Teemusk and Mander (2007) incorporated an 80 mm rock wool layer beneath the substrate, whilst Wong and Jim (2014) incorporated a 40 mm layer. However, the inclusion of this layer did not result in elevated levels of retention in either study. Specialist drainage layers incorporating clay pellets and/or sub irrigation wicks have proven to be more successful in increasing retention performance. These systems restrict runoff volumes through an outflow control, retaining water in the drainage layer for subsequent return to the substrate through capillarity and ultimately being lost by ET. The incorporation of these systems led to almost a doubling of retention performance, compared to a traditional drainage layer (Arias et al., 2016). Farrell et al. (2013) incorporated common soil additives (hydrogels and silicate-based granules) into green roof substrates to increase the levels of moisture available to plants. These additives were found to increase substrate MWHC, but with varying levels of effectiveness dependant on substrate properties (particularly pore size distribution). Farrell et al. (2013) suggest

this elevated MWHC could increase retention performance, although no experimentation was conducted to confirm this. Biochar is an alternate substrate additive that has seen much success in agricultural soils and containerised horticulture (Cao et al., 2014). Biochar is the carbon-rich product of high temperature combustion of biomass (Jha et al., 2010). (Beck et al., 2011) found that a substrate with 8% biochar (by mass) increased retention performance by 4%.

Getter et al. (2007) investigated the effects of roof slope by using a series of green roof test plots, it was found that increasing roof slope led to reduced retention performance, similar to the conclusions of Villareal & Bengtsson (2005). However, Getter et al. (2007) and Mentens et al. (2006) cite several pieces of German literature that suggest no correlation between retention performance and roof slope.

Green Roof Retention Performance and Climate

The greatest impact climatological factors (excluding rainfall patterns) have on green roof retention performance is through the control of evapotranspiration (ET). ET is the only process by which the available storage capacity of a green roof can be recovered between rainfall events. Solar radiation, air temperature, relative humidity, and wind speed have all been identified to affect ET rates (Fassman and Simcock, 2008; Koehler and Schmidt, 2008; Rezaei and Jarrett, 2006). The variation in these factors partially explains the geographical differences in green roof retention performance. Retention performance has been typically observed to be elevated under warmer drier conditions (e.g. 74% in Australia, Razzaghmanesh and Beecham, 2014) compared to more temperate climates (e.g. 32-57% in Scandinavia, Locatelli et al., 2014). Seasonal changes in climatological factors produce seasonal changes in ET rates (Koehler and Schmidt, 2008; Marasco et al., 2014; Rezaei and Jarrett, 2006), with the greatest rates of ET being observed under warm summer conditions. However, seasonal variations in rainfall patterns are also important factors for retention performance (Hakimdavar et al., 2014). Typically, retention levels are greatest in the summer months (Elliott et al., 2016; Uhl and Schiedt, 2008) although Carson et al. (2013) and Stovin et al. (2012) observed their greatest retention performance in either spring or autumn. The northern-hemisphere winter months of December, January, and February resulted in the lowest retention performance for all the above studies.

The design of a monitoring study to explore the effects of climate is arguably more challenging than attempting to explore the effects of roof configuration. The establishment of the exact same roofing system in differing climates is almost

impossible to achieve given substrate heterogeneity and differing vegetation growth. Sims et al. (2016) identified this gap in empirical data. Using 3 near identical roof configurations spread across Canada, Sims et al. (2016) identified greater retention in drier climates with reduced rainfall and longer inter-event periods, where water loss through ET was high. In wetter climates, total retention volumes are higher, but represent a lower proportion of total rainfall. The same set of conclusions were reached by Stovin et al. (2013) in a modelling study of long term green roof retention performance across the UK.

Green Roof Retention Performance and Rainfall Characteristics

It its widely reported in the literature that greater retention performance can be achieved for smaller rainfall events, given the greater probability that the rainfall volume is less than the available storage of the system. For example, a 10-month study conducted in Hong Kong by Wong and Jim (2014) quantified retention performance for 63 rainfall events, grouped by event size. It was found that the levels of retention performance decreased with increasing event size (Rainfall depth, P). For P<2 mm retention was 83.9%, 2<P<10 mm was 46.7%, and P>10 mm was 18.9%. Similar trends were also found by Carpenter and Kaluvakolanu (2011), Carter and Rasmussen (2006), Fassman-Beck et al. (2013), and Getter et al. (2007). However, due to inconsistent grouping of event size, the reported retention performance varied greatly. Contrary to the majority of green roof literature, a study by (Speak et al., 2013) conducted in Manchester, UK, for an intensive roof system (170 mm substrate depth) found retention performance to be higher for medium rainfall events (2<P<10 mm) than for light rainfall events (P<2 mm). This result remains unique.

Further to the quantification of retention under different rainfall event sizes, both Stovin et al. (2012) and Sims et al. (2016) have highlighted a need to understand retention for significant rainfall events with large return periods. Stovin et al. (2012) identified 'significant' rainfall events as having a return period of greater than 1 year. In their 29-month study, 21 events were considered to be significant and retention for these events was reported as 30%. Sims et al. (2016) identified up to 6 significant rainfall events (>2-year return period) in a 14 month period over their 3 locations; retention was found to be 16%, 21% and 15% in London, Calgary and Halifax respectively. This performance is slightly elevated over the 11.8% calculated from Stovin et al. (2012) for events with a return period of greater than 2 years, but differences can be largely attributed to differences in other climatological factors

(Sims et al., 2016). Other literature has quantified retention for very large rainfall events (P>45 mm) where reported retention ranges from 0 to 60% (Carpenter and Kaluvakolanu, 2011; Carter and Rasmussen, 2006; Speak et al., 2013; Stovin et al., 2012a).

Green Roof Retention Performance Summary

The retention performance of green roof systems is widely reported, and is often the focus of hydrological performance studies. Whilst monitoring studies provide insight into the performance of different roof configurations, they are often too short in duration to capture long-term climate trends. Extended monitoring studies of greater than 24 months provide more insight into the long-term performance of green roof systems and facilitate the exploration of seasonal effects as well as other temporal patterns. More fundamental exploration of the drivers of retention indicate that the green roof substrate's ability to store, and then release water via ET, is often the most important factor for determining retention performance.

2.4.2 Green Roof Detention Performance

Detention describes the hydrological processes within the green roof that lead to a delay between rainfall and associated runoff. Compared to a conventional roof, incident rainfall on a green roof must make its way through the vegetation, substrate and drainage layer before entering a receiving system, all of which take time. This time delay can be defined using a multitude of metrics as seen in **Figure 2.9** and outlined in **Table 2.2**. Whilst detention performance can be reported via various metrics, the literature provides evidence that detention is affected by roof configuration and rainfall characteristics as was retention performance.

Detention metrics derived from monitoring studies contain the effects of retention processes. In such cases the reported detention metrics are affected by antecedent rainfall and ET processes (Uhl and Schiedt, 2008). Wong and Jim (2014) highlighted a lack of understanding of the peak delay and peak attenuation behaviours in green roof systems, stating that peak delay is a function of retention and not detention. The hydrographs presented in **Figure 2.9** indicate approximately 20% retention, if this retention percentage were greater, the runoff profile would likely begin later. Therefore, the peak runoff rate may also occur later and so the detention metric 'peak delay' is increased for increased retention performance.

Green Roof Detention Performance and Roof Configuration

The majority of detention literature that considers roof configuration is based on altering roof area (Hakimdavar et al., 2014), drainage pathway lengths (Vesuviano and Stovin, 2013) and drainage layer materials (Arias et al., 2016). A monitoring study of three full scale green roofs in New York, USA by Hakimdavar et al. (2014) identified improvements to peak attenuation for increasing roof scale. This increase in performance was attributed to the increased drainage pathway lengths. Laboratory studies conducted by Vesuviano and Stovin (2013) demonstrated a similar relationship. Hakimdavar et al. (2014) also identified a reduction in the range of peak attenuation values (suggesting a more consistent level of performance) from larger green roof systems. The positioning of monitoring equipment to calculate peak attenuation is also critical, Fassman-Beck et al (2013) observed that the downstream collection system may have contributed to differences in the 5-minute peak attenuation observations for four different green roof configurations in Auckland, New Zealand.
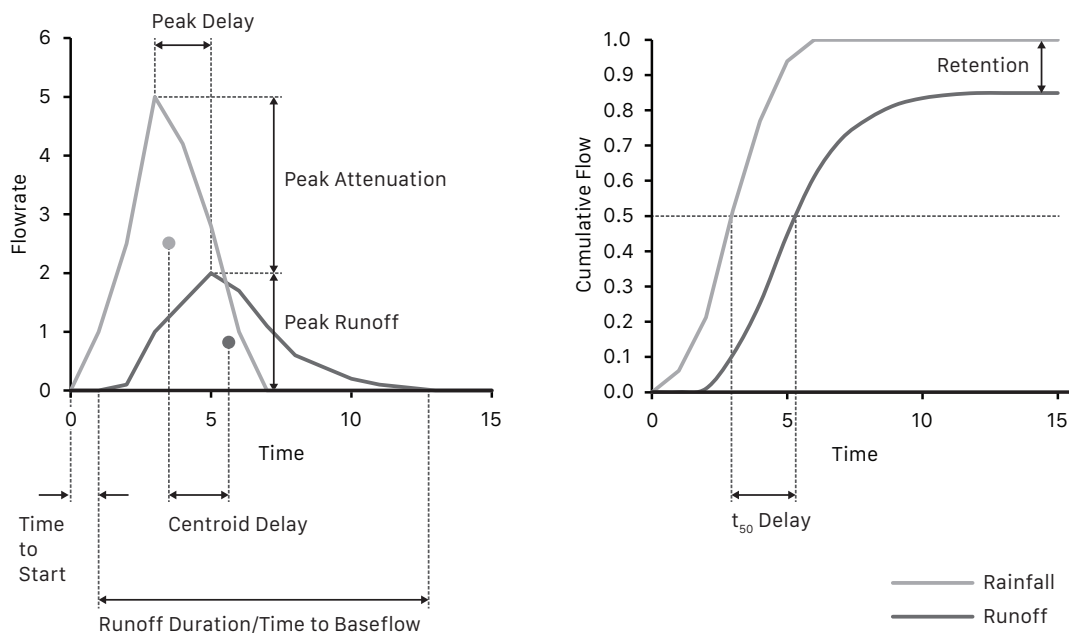
Figure 2.9 Common Detention Metrics (adapted from Stovin et al., 2015b).

Table 2.2 Summary of Common Detention Metrics

Metric	Units	Comments
Peak Delay	min	The time difference between the maximum rate of inflow and outflow
Peak Attenuation	%	The difference in the maximum rate of inflow and outflow
Peak Runoff	mm/min	The maximum rate of runoff
Centroid Delay	min	The time difference between the centroid of the inflow profile and the outflow profile
Time to Start of Runoff	min	The time taken for runoff to emerge since the onset of rainfall
Runoff Duration	min	The total time that runoff is occurring
t_{50} delay	min	The time difference between reaching 50% cumulative inflow and cumulative outflow

Increasing substrate depths have been found to lead to greater detention performance, increasing peak attenuation and temporal delay metrics (Alfredo et al., 2010; Buccola and Spolek, 2011). For a doubling of substrate depth (from 40 to 80 mm), Wong and Jim (2014) observed a 43% increase in peak attenuation and a 10 minute increase in peak delay as part of a 10 month monitoring study. Greater increases in depth, like the tripling of Razzaghmanesh and Beecham (2014) from 100 to 300 mm, result in greater increases in peak attenuation (+50%) and peak delay (+865 minutes). Such results are not unexpected given the greater flow travel distances associated with deeper substrates. Yio et al. (2013) also identified significant increases to overall detention performance due to increased substrate depth. In addition to substrate depth, Yio et al. (2013) observed increases in overall detention performance for decreasing substrate permeability. The physical mechanisms by which substrates affect detention performance are considered in more detail in Section 2.3.4.

Whilst increasing substrate depth can enhance detention performance, the added substrate mass will also increase structural loading. An alternative approach for enhancing detention is to engineer green roof drainage layers to temporarily store water by controlling discharge rates. Beck et al. (2014) and Arias et al. (2016) present two different systems that utilise an outlet control to increase detention performance. Beck et al. (2014) controlled outlet flows through a series of interchangeable orifices, varying from 1.6 to 6.4 mm, whereas Arias et al. (2016) restricted outflow to 0.1 l/s, although the exact mechanism was not disclosed. Beck et

al. (2014) reported increases in detention times of >400% for the smallest orifice size (1.6 mm), but noted no difference in performance for orifices greater than 3.2 mm. Arias et al. (2016) saw a 91% increase in peak attenuation over a traditional green roof system. Whilst these outlet controls can clearly provide enhanced detention, the maintenance of orifice controls has not been fully explored. Beck et al. (2014) noted at their smallest orifice levels, the flow restriction was too great, causing saturation of the drainage and substrate layers, leading to surface runoff. Further work is required to strike a balance between enhancing detention, preventing surface runoff, and ensuring blockage-free operation (particularly important at low orifice sizes).

Green Roof Detention Performance and Rainfall Characteristics

There is very little reporting of the effect of rainfall characteristics on detention performance, despite the strong associations between retention and rainfall characteristics. Hakimdavar et al. (2014) do present detention — peak attenuation and time to start of runoff — by rainfall depth, intensity, and duration. Peak attenuation was found to decrease with increasing rainfall depth and duration, whilst there was no observable difference for varying intensity. The time to start of runoff showed no relationship to rainfall depth, but increasing intensity led to reductions in time to start of runoff, and increasing rainfall duration corresponded with increased times to start of runoff. However, the above observations are from monitored data and so these detention metrics also include the effects of retention. This is perhaps best seen from the time to start of runoff relationships with rainfall intensity, the heavier the rainfall the quicker the available storage is used and so the earlier runoff emerges. The controlled laboratory study of Yio et al. (2013) also identified decreasing levels of detention performance with increasing intensity, although only two rainfall intensities were trialled. In the case of Yio et al. (2013) this change was not attributed to retention effects as the substrates were at field capacity at the beginning of rainfall simulations. The complex interactions between moisture content and substrate hydraulic conductivity is the likely source of this variation in performance with intensity.

Isolating Green Roof Detention Using Hydrological Models

The co-dependent nature of detention and retention performance makes it difficult to evaluate detention performance in isolation from monitoring study data. To overcome this co-dependency, laboratory studies have explored detention effects in isolation by applying synthetic rainfall events to green roof systems at field capacity,

i.e. there is no available retention storage (Villarreal, 2007; Yio et al., 2013). In addition to laboratory testing, calibrated hydrological models that suitably characterise retention processes can be used to identify detention performance. For example, Kasmin et al. (2010) argue that by accounting for retention processes, reservoir routing model parameters can be used as a descriptor of detention performance (this approach is explored in more detail in section 2.4.3).

Green Roof Detention Performance Summary

Whilst less reported than retention performance, detention performance plays an important role in overall green roof hydrological performance. In fact, under conditions where retention storage is rarely recovered (e.g. persistent wet weather) detention performance provides the sole hydrological benefit of a green roof. The under-reporting of detention performance is not helped by the multitude of available metrics or the confounding effects of retention processes. By isolating detention processes through hydrological model parameterisation, a greater understanding of the affecting factors of detention performance can be obtained.

2.4.3 Green Roof Hydrological Modelling

There are predominantly three categories of green roof hydrological models: statistical regression approaches, conceptual approaches, and mechanistic approaches. Statistical regression models can predict hydrological performance for specific roof configurations in specific climates (Carson et al., 2013; Fassman-Beck et al., 2013). However, the use of physically-based models provides a more generic modelling option (Stovin et al., 2012). It has been identified that proper representation of evapotranspiration processes is critical for the continuous simulation of green roof retention performance (Jarrett and Berghage, 2008; Stovin et al., 2013). This representation is commonly achieved in conceptual models through a substrate moisture flux approach, which has been shown to reliably predict retention performance (Locatelli et al., 2014; Stovin et al., 2012).

Combining retention and detention processes allows the prediction of temporal runoff profiles. Techniques used to model detention include: finite element solutions of the unsaturated flow equations (Hilten et al., 2008; Palla et al., 2012); a unit hydrograph-based approach (Villarreal and Bengtsson, 2005); and a simple reservoir routing technique (Jarrett and Berghage, 2008; Kasmin et al., 2010). Each method has been shown to demonstrate acceptable levels of accuracy for stormwater modelling requirements (Villarreal and Bengtsson, 2005; Hilten et al., 2008; Jarrett and

Berghage, 2008; Kasmin et al., 2010; Palla et al., 2012). Whilst the unit hydrograph and the reservoir routing approaches rely on previously-monitored data for calibration, the physically-based finite element models potentially provide a generic approach capable of estimating detention processes in unmonitored systems. However, these models are reliant on the parameterisation of many substrate properties, several of which are difficult to identify using traditional laboratory techniques (e.g. water release curve, pore size distribution, see Section 2.3.4).

Statistical Regression Approaches

Numerous statistical regression models have been developed to predict hydrological performance for specific roof configurations in specific climates (Stovin et al., 2012; Carson et al., 2013; Fassman Beck et al., 2013). Both Carson et al. (2013) and Fassman-Beck et al. (2013) used second order polynomial equations regressed from monitored data. Both studies found roof runoff could be predicted to an acceptable level. Stovin et al. (2012) undertook a regression analysis for 29 months of monitored data to assess relationships between total rainfall, ADWP and retention. However, the resulting equations did not prove to be effective, even when applied to the data from which they were derived. Stovin et al. (2012) suggested this was due to the regression equations being unable to capture the complex inter-event processes that give rise to retention. As identified by (Li and Babcock, 2014), these regression models are specific to their locations and roof configurations. This makes them unsuitable for understanding physical processes or designing new green roofs.

Conceptual Modelling Approaches

Several conceptual modelling approaches have been presented in the literature. Palla et al. (2012) presented a conceptual model based around a series of three cascading reservoirs. The first reservoir represented green roof vegetation, the second the substrate, and the third the drainage layer. For a series of 10 rainfall events this model predicted runoff hydrographs with a Nash Sutcliffe efficiency exceeding 0.7, indicating good levels of prediction. The model used 6 parameters and required a set of initial conditions, including initial moisture content. Locatelli et al. (2014) also deployed a series of three reservoirs for their conceptual model in a similar approach to Palla et al. (2012). Locatelli et al. (2014) noted that some model parameters could be obtained from the physical roof configuration as opposed to being determined from calibration to hydrological data.

A well-documented conceptual method is the reservoir routing approach of Kasmin et al. (2010), Stovin et al. (2013), Yio et al. (2013), Vesuviano and Stovin (2013) and Vesuviano et al. (2014). A substrate moisture flux model accounts for retention and a reservoir routing technique simulates detention processes. Moisture content in the substrate is determined through time by the addition of precipitation and losses via ET using the following relationships:

$$R_t = \begin{cases} 0, & S_{t-1} + P_t - ET_t \leq S_{max} \\ P_t - (S_{max} - S_{t-1}) - ET_t, & S_{t-1} + P_t - ET_t > S_{max} \end{cases} \quad (2.1)$$

where R is runoff, S is the storage level, P is precipitation, ET is evapotranspiration and S_{max} is the maximum substrate retention capacity, all in mm; t is the discretised time-step. Substrate moisture content is then updated:

$$S_t = \begin{cases} S_{t-1} + P_t - ET_t, & S_{t-1} + P_t - ET_t \leq S_{max} \\ S_{max}, & S_{t-1} + P_t - ET_t > S_{max} \end{cases} \quad (2.2)$$

When the substrate's available storage is exceeded, this additional moisture is placed into transient storage and runoff is determined using the following relationships:

$$h_t = h_{t-1} + Qin_t \Delta t - Qout_t \Delta t \quad (2.3)$$

in which Qin and Qout are the flow rates into and out of the substrate layer respectively, in mm/min. h is the depth of water temporarily stored within the substrate, in mm. Δt is the discretisation time step. Qout is given by:

$$Qout_t = kh_{t-1}^n \quad (2.4)$$

where k and n are the scale and exponent reservoir routing parameters. For h in mm and Q in mm/min, k has the units $mm^{(1-n)}$/min, whilst n is dimensionless. Kasmin et al. (2010) identified suitable values of k (0.03) and n (2.0) for their typical extensive green roof test bed, resulting in a coefficient of determination (R^2) of 0.97 between monitored and modelled runoff. These parameters include the detention effects from all roof layers (vegetation, substrate and drainage layer) as well as specific drainage distances to the runoff monitoring location.

Yio et al. (2013) used the same reservoir routing model formulation to explore substrate detention in isolation. A fixed value of n was found to not negatively impact runoff prediction over a model where both k and n had been optimised. Vesuviano et al. (2014) proposed the inclusion of two storage reservoirs, to represent the substrate

and drainage layer as separate components. The accuracy of runoff prediction was not adversely affected by this change and an R^2 value of 0.97 was attained.

Both Yio et al. (2013) and Vesuviano et al. (2014) explored the relationship between physical roof configurations and the model parameters. Increasing substrate depth and drainage lengths leads to reductions in the value of k, whilst increasing roof slope decreases the value of n. The exact relationships of these links between physical roof configuration and model parameters have not been fully explored. As such, conceptual model parameters remain configuration specific, although they are more generic than regression models due to their independence from climatic conditions.

Mechanistic Approaches

In contrast to the regression and conceptual modelling approaches, mechanistic models focus on the underlying structures and processes responsible for green roof hydrological performance. Starry et al. (2016) note that mechanistic models are usually much more flexible to a variety of data sources. The majority of reported mechanistic models are adaptations of the HYDRUS 1D-3D model (Hilten et al., 2008; Palla et al., 2012) or Storm Water Management Model (SWMM) (Alfredo et al., 2010; Burszta-Adamiak and Mrowiec, 2013; Cipolla et al., 2016; Krebs et al., 2016; She and Pang, 2010).

HYDRUS is s commercial soil physics model that can be utilised for simulations of water, heat, and solute movement in porous media (Šimůnek et al., 2008). The model numerically solves the Richards' equation for saturated-unsaturated water flow. For water flow applications, the input data are surface moisture fluxes (precipitation and evapotranspiration) and soil properties (hydraulic conductivity, water retention curve parameters). Outputs include the spatial and temporal distribution of water content, surface runoff, and infiltration runoff. Hilten et al. (2008) utilised HYDRUS 1D to simulate runoff from a modular green roof system, where it was found that model accuracy decreased with increasing rainfall depth. Palla et al. (2012) directly compared the performance of HYDRUS-1D to a conceptual model. HYDRUS required twice the number of parameters compared with the conceptual model (12 vs. 6) but yielded more accurate results.

Green Roof Evapotranspiration Modelling

Numerous authors have highlighted the need for accurate estimates of evapotranspiration (ET) to reliably predict green roof hydrological performance using

a variety of modelling techniques (Jarrett and Berghage, 2008; Krebs et al., 2016; Stovin et al., 2013). ET is difficult to predict due to the range of factors that affect it, including: solar radiation, surface albedo, humidity, wind speed, substrate moisture, and vegetation properties (Allen et al., 1998; MacIvor and Lundholm, 2011; Mawdsley and Ali, 1985; Salvucci and Gentine, 2013) Due to experimental difficulties in the measurement of ET, several models have been developed to predict ET from available environmental data (Zhao et al., 2013). Some of the most commonly utilised models are the Hargreaves (Hargreaves and Allen, 2003), Priestley and Taylor (1972), Penman (1948), and Penman-Monteith (Monteith, 1965) models which estimate potential evapotranspiration (PET). PET represents the energy-limited ET; actual ET rates may be lower due to other restrictions such as substrate moisture. The Hargreaves and Priestly-Taylor models are based on energy and temperature data, whereas the Penman and Penman-Monteith models also incorporate wind speed and humidity (Marasco et al., 2014).

PET estimates can be tailored to specific roof configurations through the application of crop coefficients and soil moisture extraction functions (Berretta et al., 2014; Starry et al., 2016; Stovin et al., 2013; Zhao et al., 2013). There is little agreement on which PET model is most suitable to green roof scenarios, with data availability being the biggest dictator of model choice (Starry et al., 2016). Many authors have identified suitable crop coefficients for specific roof configurations, but entirely generic values are not available. Morasco et al. (2014) highlight a need for robust validation of any PET model against measured green roof ET data. With this robust validation, and provided roof configuration is similar, previously determined crop coefficients are thought to be applicable to predicting green roof ET under differing climatic variables (Morasco et al., 2014).

2.5 Green Roof Ageing

Berndtsson (2010) noted that the vegetated substrates of green roofs undergo various chemical and physical changes over time: particles may be lost, dissolvable substances are removed with runoff, organic content may fluctuate, and root development impacts on substrate porosity. Yet, in their extensive review of green roof literature, Li & Babcock (2014) identified very few studies discussing the impact that green roof ageing may have upon substrate properties or hydrological performance over time. Whilst this partly reflects the scarcity of long-term hydrological records, the effect that natural climatic variation has on observed hydrological performance is likely to mask any subtle changes in the underlying hydrological characteristics of the system. Those studies that have considered green roof age and associated substrate property changes have identified very different trends, with no clear consensus on what to expect with increasing system age.

Mentens et al. (2006) found no correlation between green roof age and yearly runoff quantity for a series of differently-configured German green roofs when analysing less than 5 years of data. Similarly, Hill et al. (2016) found no statistical correlation between roof age and substrate depth or particle size. However, Hill et al. (2016) attribute these results to the large range of substrate types and particle sizes seen in the 30 sampled green roofs. Although consolidation post installation is typically expected to occur (FLL, 2008), substrate depths were thought not to have decreased due to paedogenesis mechanisms adding decomposing biological material to the substrate profile, a similar hypothesis to Köhler and Poll (2010).

Getter et al. (2007) found that substrate organic content and pore volume both doubled over a 5-year period. Getter et al. (2007) hypothesised improvements to retention performance due to an increase in microporosity (< 50 μm), but noted these improvements may come at the expense of detention performance due to an increased presence of macropore (>50 μm) channels. Despite these clear changes in substrate properties over 5 years, a limited 17-month monitoring period prevented the observation of any variation in hydrological performance. Köhler and Poll (2010) also identified significant increases to total substrate porosity, >20% in 10 years. By using non-invasive XMT characterisation, Jelinkova et al. (2016) identified reductions in macroporosity near the substrate surface and observed reductions in overall macropore connectivity in a 2-year study. Jelinkova et al. (2016) also observed changes in hydrological performance, with retention falling by around 46-65%.

However, a lack of critical evaluation of hydrological performance over time means these changes are likely to be attributed to the differences in rainfall patterns from year to year as opposed to the small changes in substrate properties.

In contrast to Getter et al. (2007), Emilsson and Rolf (2005) observed a net loss of organic matter from 3 to 1% (m/m) over a single year in a study of green roof establishment. Bouzouidja et al. (2016) identified similar falls in organic content over a 4 year-period and reported a reduction in the mass of particles smaller than 2 mm in diameter. Beattie and Berghage (2004) state that the levels of organic content will stabilise at around 2 to 5% (m/m) once the roof has become well established, these levels are consistent with the findings of Getter et al. (2007). The impact that organic matter fluctuations can have on green roof hydrological performance is demonstrated by Yio et al. (2013), where a threefold increase in organic content (Coir) was associated with a peak attenuation increase from 15 to >50%. In this instance, changes in organic matter content are thought to be a surrogate indicator of pore size distribution changes.

Gaches et al. (2013) identified that freeze/thaw weathering was responsible for severe reductions in particle sizes of 5 mature green roofs, between 3 and 7 years old, in the Mid-Atlantic USA. Particle size reductions were so large that none of the 5 aged substrate mixes met the FLL (2008) guidelines, despite being deemed suitable during construction. Gaches et al. (2013) hypothesised that the reductions in particle sizes would increase water holding capacity and reduce air space making plant growth more difficult.

Speak et al. (2013) investigated the runoff retention performance of an aged intensive green roof. The green roof was found to have good retention performance, but the study lacked any initial performance data and so determination of any performance changes with age were not made. Literature examples such as this highlight the need for specific studies focused on ageing, using continuous rainfall/runoff monitoring and detailed tracking of changes in substrate properties over time.

2.5.1 Ageing of Other Green Infrastructure and Conventional Soils

Beyond the limited range of green roof ageing literature, other SuDS devices provide evidence of ageing effects. Biofilters are prone to sedimentation and clogging as they age, although the media's hydraulic conductivity may be maintained through the presence of plant roots (Virahsawmy et al., 2013). Further literature from the

agro/forestry fields provides evidence of the effects that plant-life can have on soil porosity and infiltration rates. Root growth can reduce pore volumes due to local compression and pore filling (Dexter, 1987), thereby reducing hydraulic conductivity. The decay of dead roots leaves channels which may increase pore spaces and act as flow paths, increasing hydraulic conductivity (Schwen et al., 2009). Plant activity can also influence soil aggregation (Lado et al., 2004) and desiccation cracking (Materechera et al., 1992). However, the majority of agro/forestry literature is based on observations of plant species and growing media not typically found on a green roof, which potentially limits its relevance in a green roof context.

2.6 Chapter Summary

Given the pressures of predicted climate change there is a need for alternative strategies for urban stormwater management. Green roofs, and the wider array of SuDS devices, can help alleviate some of the current and future stresses on urban drainage networks through the reduction and delay of runoff volumes. Stormwater reductions are achieved via retention processes, whilst the remaining runoff experiences a slower entry into receiving systems due to the detention processes.

Green roof monitoring studies are often too short in duration (<12 months) and are susceptible to atypical climatic conditions. Longer duration studies (>24 months) can provide much greater insight into long-term green roof hydrological performance under more typical climatic conditions. These longer duration studies also provide a greater wealth of data to allow exploration of seasonal effects on performance, amongst other temporal trends. However, even for the longest term studies identified in this review, there is little reporting of variations in hydrological performance from year to year. This is partly due to the overriding influences of climate on hydrological performance, which often masks the subtle changes that are expected in performance over time. Therefore, the outputs of monitoring studies are not the best identifiers of the evolution of hydrological performance. But, with the application of hydrological modelling techniques and sufficient laboratory validation, monitoring studies can provide the necessary data to determine whether green roof performance does change with time.

The development and validation of green roof hydrological modelling techniques requires accurate and reliable characterisations of substrate properties. Existing techniques of characterisation are often destructive, preventing the observation of

fine-scale changes in substrate properties over time. Such limitations have led to a reliance on virgin substrate or re-aggregated substrate characterisation as a basis for model development, thus precluding the incorporation of substrate, and substrate/root, evolution. Non-invasive imaging techniques developed by/for the soil-science community provide an alternate means for assessing substrate property development over time. The application of non-invasive techniques can allow for the observation of true in-situ green roof substrate properties to better validate models of mature green roof systems.

Given the conflicting state of the current knowledge surrounding green roof hydrological performance with time, there is a novel opportunity to explore the resulting changes in hydrological performance of green roof substrate development. A coupled non-invasive imaging and long-term monitoring study will provide the new knowledge required to better inform the future development and modelling of green roof systems.

3. *Materials & Methods*

3.1 Chapter Overview

This chapter presents the experimental materials and methods employed to answer the research question posed in Chapter 1. The research comprised three parallel studies: monitoring; cored microcosms; and longitudinal microcosms. The methodologies can be broadly classified into two distinct approaches, the first investigates the hydrological performance of green roof test beds over a period of 6-years, whilst the second uses X-ray imaging techniques to look inside green roof substrate microcosms and explore their physical properties. A large portion of the methodology presented in section 3.2 and 3.3 has been published in the following journal papers:

Stovin, V., Poë, S., **De-Ville, S.** and Berretta, C., 2015a. 'The influence of substrate and vegetation configuration on green roof hydrological performance'. *Ecological Engineering*, 85, 159–172.

Stovin, V., Vesuviano, G. and **De-Ville, S.**, 2015b. 'Defining green roof detention performance', *Urban Water Journal*, pp. 1–15.

De-Ville, S., Menon, M., Jai, X., Reed, G. and Stovin, V., 2017. 'The impact of green roof ageing on substrate characteristics and hydrological performance'. *Journal of Hydrology*, 547, 332–344.

3.2 Parallel Investigation Approach

The research comprised three parallel studies conducted to provide insight into the evolution of substrate physical properties and hydrological performance at multiple temporal scales (**Figure 3.1**). The three studies can be broadly defined as having two distinct methodologies, the first is a 6-year long-term monitoring study of pre-existing green roof test beds, whilst the second applies a non-invasive X-ray imaging technique to explore the internal structures of green roof substrates. The coupling of these investigative methods provides the new knowledge required to better inform the long-term management, future development, and modelling of green roof systems.
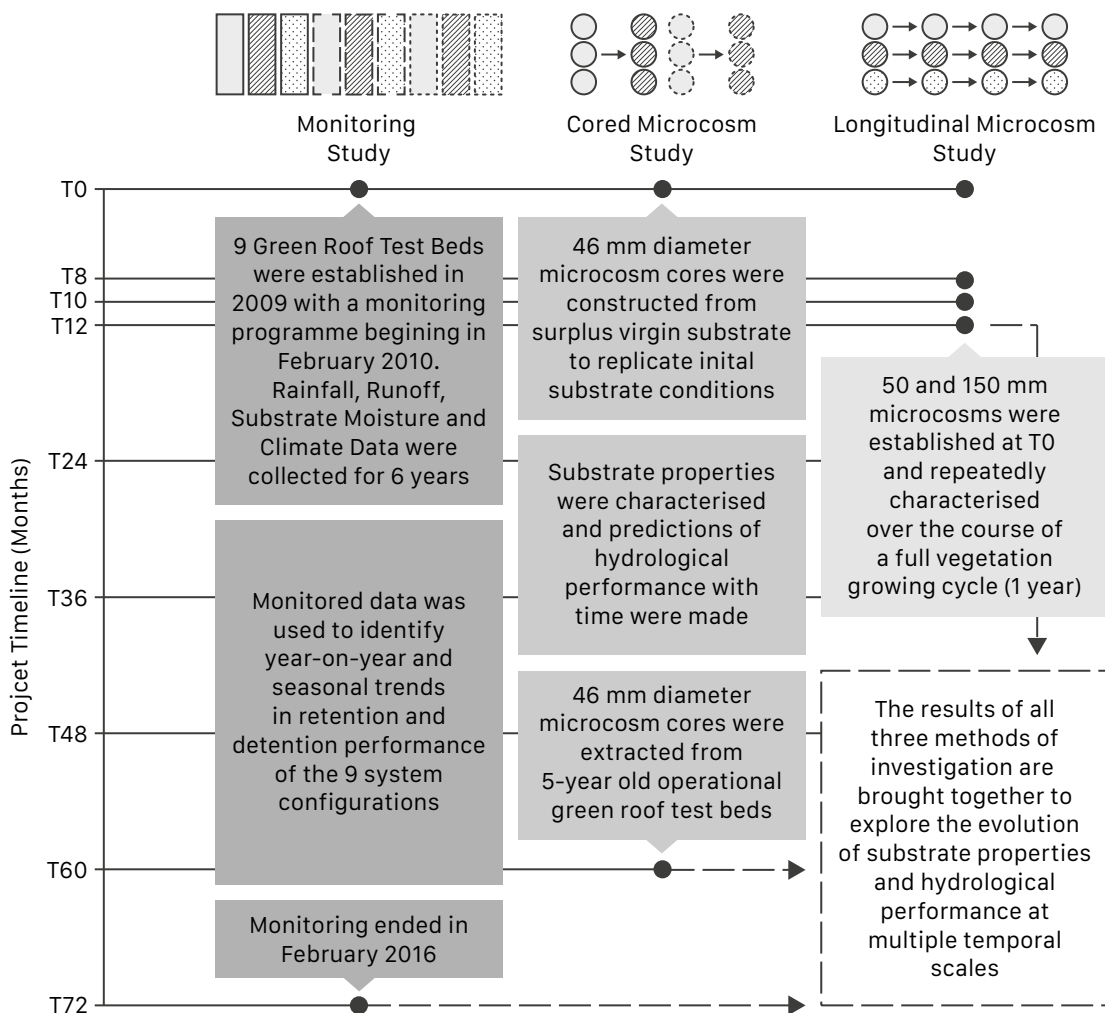
Figure 3.1 Overview of the three parallel investigations presented in this thesis.

3.3 Experimental Field–Scale Monitoring Study

3.3.1 Hadfield Test Beds

The Hadfield Test Beds (**Figure 3.2**) are a series of 9 differently configured green roof test beds located at the University of Sheffield's Green Roof Centre on a third-floor terrace of the Sir Robert Hadfield Building (Grid Reference 53.3816, -1.4773). Test bed design was finalised in 2009, so the following is a description of the inherited experimental design. Each test bed (TB) configuration has a different substrate composition and vegetation treatment pairing (**Figure 3.3**). The test beds are 1 m wide by 3 m long and are installed at a 1.5° slope. The test bed physically comprises, from base to surface, a hard plastic tray, a drainage layer (ZinCo Floradrain FD 25-E), a filter sheet (ZinCo Systemfilter SF), one of three substrates to a depth of 80 mm, and one of three vegetation treatments.
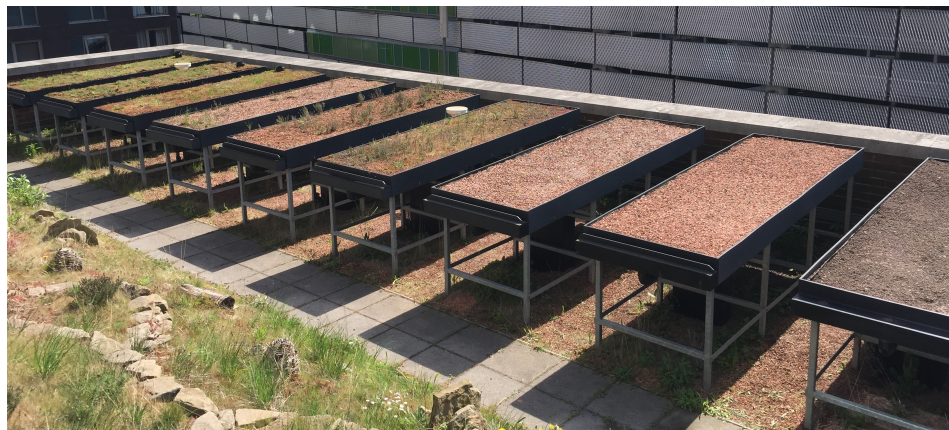
Figure 3.2 The Hadfield Test Beds in April 2015.

| TB1 | TB2 | TB3 | TB4 | TB5 | TB6 | TB7 | TB8 | TB9 |

Substrate: HLS   Vegetation: □ Sedum   ● Rain Gauge
SCS   Vegetation
LECA   Unvegetated
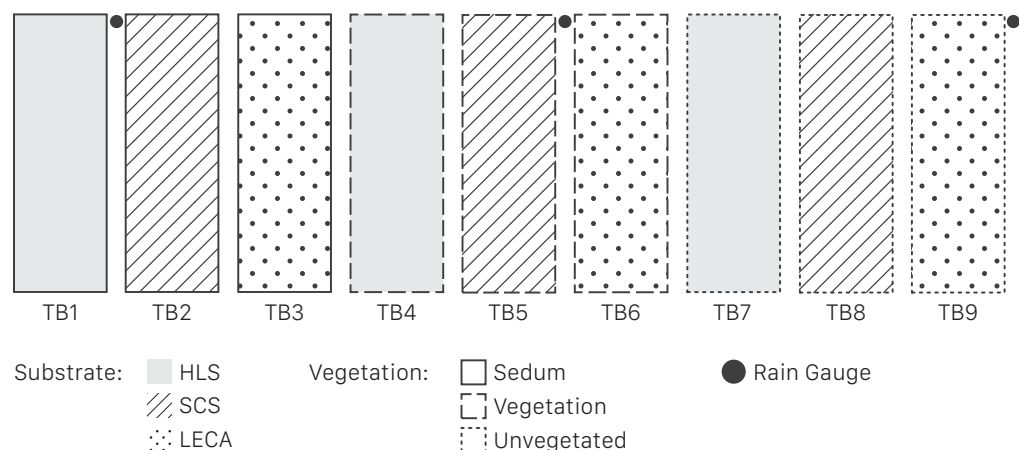
Figure 3.3 Test bed configuration layout. The nine test beds are grouped by the three vegetation treatments (indicated by exterior line style) with a repeating substrate order (indicated by shading style).

The first two substrates are commercially available substrates manufactured by Alumasc ZinCo — Heather with Lavender (HLS) and Sedum Carpet Substrate (SCS). HLS is installed in test beds 1, 4 and 7 with SCS being installed in test beds 2, 5 and 8. The third substrate is a bespoke mix based on Lightweight Expanded Clay Aggregate (LECA) and is installed in test beds 3, 6 and 9. HLS is a semi-intensive commercial substrate consisting of crushed brick and pumice (ZincolitPlus), enriched with organic matter including compost with fibre and clay materials (Zincohum). SCS is a typical extensive green roof substrate consisting of crushed bricks (ZincoLit), enriched with Zincohum. The LECA-based substrate contains LECA as the sole mineral component, with loam and compost. The three substrates are shown in **Figure 3.4**.
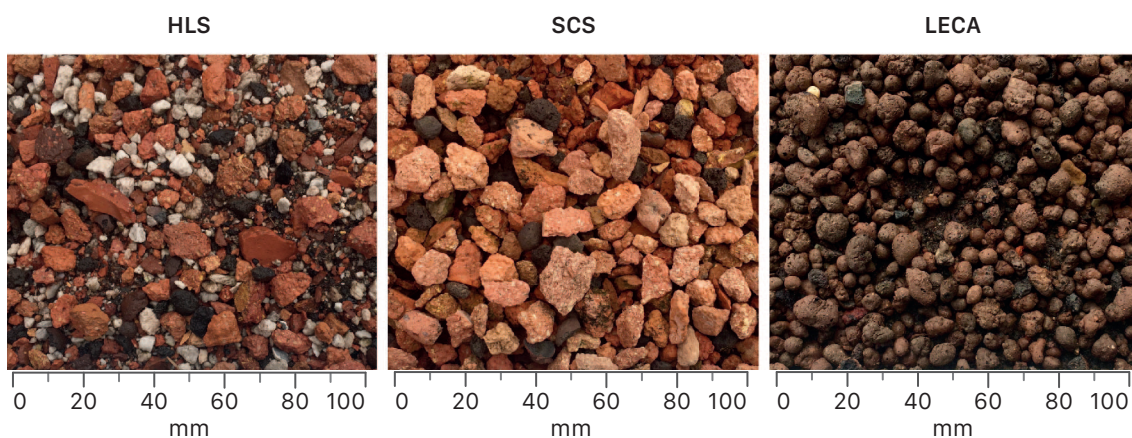
Figure 3.4 Photographs of the three substrate types, taken from the unvegetated test beds, July 2015.

The three vegetation treatments comprise two planted test groups (**Figure 3.5**) and a single un-vegetated group. Test beds 1 through 3 were vegetated with Alumasc Blackdown Sedum Mat, test beds 4 through 6 were vegetated with a Meadow Flower mix, and test beds 7 through 9 remained unvegetated. The sedum vegetation was chosen as it is a commonly adopted species for extensive green roof applications due to its tolerance of drought, extreme temperatures and high wind speeds (VanWoert et al., 2005). The Meadow Flower treatment comprises a mix of flowers, grasses and succulents. These species exhibit a lower drought tolerance (Lu et al., 2014) but greatly increase the biodiversity potential compared to Sedum (Benvenuti, 2014). The unvegetated test bed configurations were created to provide a basis against which the contribution of vegetation could be evaluated.

Sedum   **Meadow Flower**

Figure 3.5 Photographs of the two vegetation treatments, taken from TB3 and 9 respectively, June 2014.

Hadfield Test Bed Substrate Properties

All of the substrates used in the Hadfield Test Beds were subjected to laboratory tests in accordance with the *Guidelines for the Planning, Construction and Maintenance of Green Roofing* as set out by the German Landscape Development and Landscaping Research Society (FLL, 2008) prior to installation. These tests included Particle Size Distribution (PSD), apparent density (at dry conditions (105° for >24h) and at maximum water capacity), total pore volume, maximum water holding capacity (MWHC), permeability and organic content (**Table 3.1**). To address the uncertainty associated with sub-sampling heterogeneous media, a sample splitter was used and up to 6 replicates were tested, depending on the analysis.

Table 3.1 Substrate characteristics according to FLL (2008) test methods (Stovin et al., 2015).

		HLS		SCS		LECA	
		μ	σ	μ	σ	μ	σ
Particle Size <0.063 mm	% w/w	2.1	1.4	1.4	0.3	0.4	0.0
Median Particle Size, d_{50}	mm	4.7	0.7	5.2	0.3	5.0	0.1
Dry density	g/cm^3	0.95	0.04	1.06	0.05	0.41	0.00
Wet density	g/cm^3	1.36	0.02	1.45	0.07	0.76	0.02
Total Pore Volume	% v/v	63.8	1.6	59.8	2.0	84.8	0.0
MWHC (field capacity)	% v/v	41.2	2.3	39.1	2.1	35.0	1.6
Air content at MWHC	% v/v	22.6	0.8	20.7	4.1	49.8	1.5
Permeability	mm/min	1 - 15		10-35		>30	
Organic Content	% w/w	3.8	0.1	2.3	0.5	6.0	0.3

There is considerable uncertainty surrounding the permeability characterisations presented above. This is due to the FLL method for determining permeability (mod. K_f), where a relatively small sample (150 mm diameter by 100 mm deep) and head drop (10 mm) are assessed, leading to considerable variation in repeat and replicate determinations. LECA samples proved particularly difficult to characterise due to the

porous nature of the particles which makes them buoyant, and the rapidity of the head drop, with permeabilities in excess of 150 mm/min being estimated for some samples. However, from repeated testing, where confidence in the results is high, the permeability of LECA is presented as >30 mm/min (**Table 3.1**). The FLL method is primarily intended as a check against performance thresholds rather than an accurate physical characterisation. Fassman and Simcock (2012) have also commented that additional work is required to define a meaningful standard permeability test for green roofs. Hence, the permeabilities above are presented as ranges of typically observed values. The three substrates generally comply with the FLL permeability requirements for vegetated extensive systems (0.6-70 mm/min), although some LECA samples may exceed this guideline. HLS is evidently the least permeable substrate and the permeability of LECA is one order of magnitude higher.

Berretta et al. (2014) presented soil moisture release curves obtained using a Pressure Plate Extractor, which suggested lower values for the field capacity than had been determined in the FLL tests for both HLS and SCS at 25.0% and 22.4% (v/v) respectively. However, the test did not produce reliable values for the LECA-based substrate. It is important to note that much of the pore space in the LECA-based substrate (as with volcanically-derived aggregates such as pumice) is occupied by ineffective pores (i.e. internal to the expanded clay particles) that do not actively contribute to water retention at field capacity. It is therefore expected that the LECA-based substrate will provide less retention and less detention when compared with brick-based substrates.

Hadfield Test Bed Monitoring

The experimental setup includes a Campbell Scientific weather station that records hourly wind speed, temperature, solar radiation, relative humidity and barometric pressure. Rainfall depth was measured at one minute intervals using three 0.2 mm resolution ARG-100 tipping bucket rain gauges manufactured by Environmental Measures Ltd. The rain gauges were located at the same height as the test beds, between TB1 and TB2, TB5 and TB6, and TB9 and TB10 (**Figure 3.3**. Note that TB10 was not part of the comparative experiment reported here). Runoff was measured volumetrically in collection tanks equipped with Druck Inc. PDCR 1830 pressure transducers. The collection tank located under each test bed was designed for increased measurement sensitivity at the beginning of each rainfall event and to avoid direct discharge on the sensor. The pressure transducers were calibrated

against collected volumes on site. An electronic solenoid valve empties the tank when maximum capacity is reached and every day at 14:00. Runoff is recorded at one minute intervals. Data are recorded through a Campbell Scientific CR3000 data logger.

Water content reflectometers were located at three different soil depths to measure the soil moisture profile and behaviour in four of the nine test beds (TB1, 2, 3 and 7). The sensors used were Campbell Scientific CS616 Water Content Reflectometers (Campbell Scientific Inc., 2006). The probes were installed horizontally at the centre of each test bed and the rods were located at 20 mm (bottom), 40 mm (mid) and 60 mm (top) above the drainage layer and filter sheet (Figure 3.6). Considering the proximity of the probes in each test bed, the rods of the mid and top probes were installed at 90° and 180° respectively from the lower one, in order to avoid distortion of the measurement reading taken by the enabled probe. The orientation of each probe was pre-determined to ensure that the wires did not interfere with the accuracy of the measurements from nearby probes. Furthermore, to avoid inter-probe interference, the probes are differentially-enabled, with each of the four sub-scans measuring three probes in different test beds. Moisture content measurements were recorded at 5 min intervals.

Vegetation Substrate Moisture Probe Filter Sheet Drainage Layer
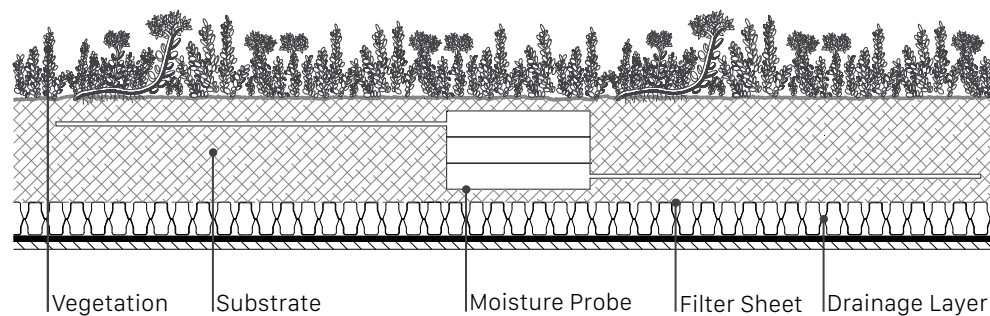
Figure 3.6 Green roof test bed section showing the vertical locations of the water content reflectometer moisture probes. Adapted from Beretta *et al*. (2014).

Hadfield Test Bed Maintenance

Throughout the 6-years of data collection the green roof test beds were regularly maintained. Weeding of the testbeds was undertaken to ensure that vegetation represented the original treatment as closely as possible. The test beds were infrequently irrigated during extended dry periods, these occasions are noted and any associated runoff has been removed from the data record. Pressure transducer calibrations were repeatedly assessed to account for settlement of the collection

barrels. Automatic outlet valve leakages were remedied as soon as they were identified.

3.3.2 Hadfield Test Bed Data Record

The Hadfield test beds have been in place since late June 2009. After a commissioning period, rainfall and runoff data collection began in February 2010. Climate data was collected from June 2010 and moisture data from January 2011. This study uses data collected from all sources between February 2010 – February 2016.

Throughout the monitoring period the runoff collection system experienced a series of failures. The failures were caused by clogging of the automatic barrel emptying valves with fine particulate material washed out from the test beds. Even with regular maintenance the collected rainfall/runoff dataset is not complete, this prevents the reporting of annual volumetric retention metrics and requires the adoption of 'per-event' analysis. The 6-year data record is made up of 503 individual rainfall events where total precipitation exceeded 2 mm and the inter-event period exceeded 6 hours. An inter-event period of 6 hours was chosen to allow comparability with previous studies (Stovin et al., 2012), whilst a 2 mm minimum rainfall depth is considered to be the amount of rainfall typically retained by a non-green roof (Voyde et al., 2010).

Hadfield Test Bed Runoff Barrel Calibration

The pressure transducers in the runoff collection system of the Hadfield test beds record pressure in Volts; this pressure is interpreted as runoff volume, with voltage increasing for increasing runoff volumes. Calibration of this raw data converts the voltages into mm/m^2 depths. The shape of the collection barrel – with high and standard-sensitivity regions – implies that calibrations are described by two linear equations. The first applies to the high sensitivity region of the barrel (the first to fill) and the second the remainder of the barrel depth (**Figure 3.7**).
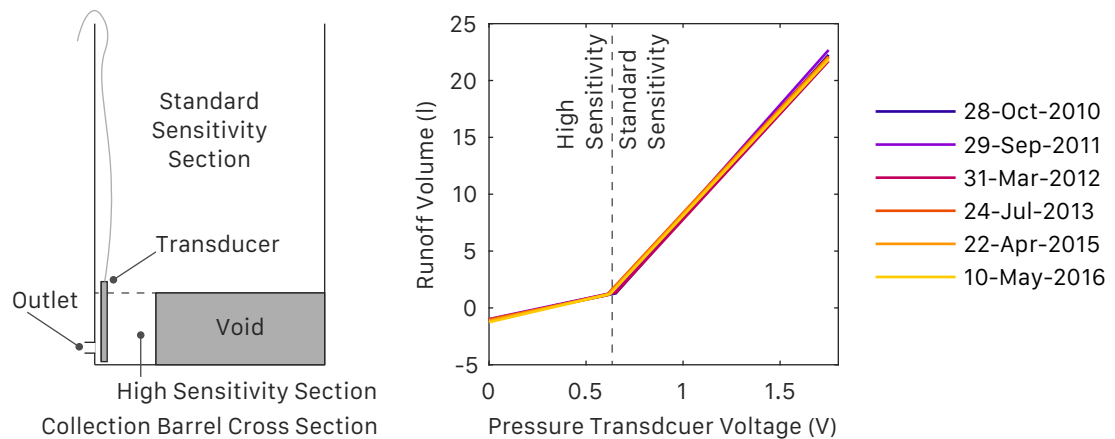
Figure 3.7 *Left:* Collection barrel cross section, indicating regions of high and standard sensitivity. *Right:* Calibration curves for TB1 over the entire study period.

Calibration was repeated annually during the study period, except in 2014. It was found that the calibrations fluctuated over the course of the study period. These changes were slight and are attributed to the movement of the collection barrels and pressure transducers. The effect that each of these fluctuations would have had on the final collected volume of runoff, if used exclusively, can be seen in **Figure 3.8**. The red horizontal line in **Figure 3.8** represents the final collected volume of runoff determined using a time-varying calibration incorporating each calibration event. Variation between individual calibration volumes and the time-varying calibration range from between <0.1% and 2.2%. These small differences provide confidence in the runoff volume of individual events, particularly when a runoff threshold of 2 mm is applied.
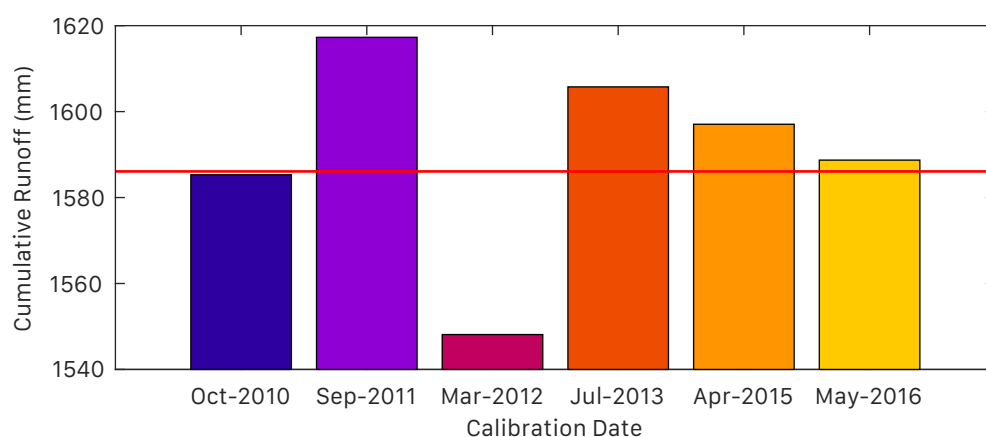
Figure 3.8 Variation in total cumulative runoff by calibration date for TB1. Red horizontal line indicates final collected volume using time-varying calibration.

Hadfield Test Bed Rainfall Event Runoff Validation & Datasets

The experimental problems with the automatic emptying valves of the runoff collection barrels required inspection of raw runoff data to ensure there was no barrel leakage during each identified event. Such leakage was readily identifiable given the cumulative nature of the raw data, whereby when operating correctly the collection barrel fills up gradually, empties rapidly, then refills (**Figure 3.9**, Top plot). Over the course of the monitoring period there were two modes of valve failure: either the valve did not fully re-close after an automatic opening, leading to subsequent leakage (**Figure 3.9**, Centre plot); or the continuing failure of a valve where leakage was present throughout an event (**Figure 3.9**, Bottom plot).

Runoff data validation was achieved by assessing the raw trace from the pressure transducer in volts (V), the calculated runoff in mm and the event rainfall in mm. From these data it could be seen if there was any reduction in tank volume that was not attributed to a valve opening event, or any significant inflows to the system unlikely to be attributed to rainfall. If all traces were normal in appearance, the runoff profile was deemed to be fit for further analysis. This process was repeated for each test bed and every identified storm event.

Removal of events with clear leakage patterns resulted in $40 - 80\%$ of all identified events (AIE) per test bed being carried forward for further analysis. **Table 3.2** details the number of valid events in each study year for each test bed; this data forms the VIE dataset (valid identified events). TB9 is consistently the worst performer and limits the number of events where all 9 beds (ATB dataset) were fully operational to 60 (12% of AIE). For retention analysis it should be recognised that any comparisons between test beds will be strongly influenced by the event rainfall characteristics, so the absence of one or more events from an individual test bed record could severely skew the results. Therefore, all per-event retention comparisons are made using only the ATB dataset. Detention analysis is not expected to be influenced by rainfall characteristics and so the VIE dataset is suitable for analysis.
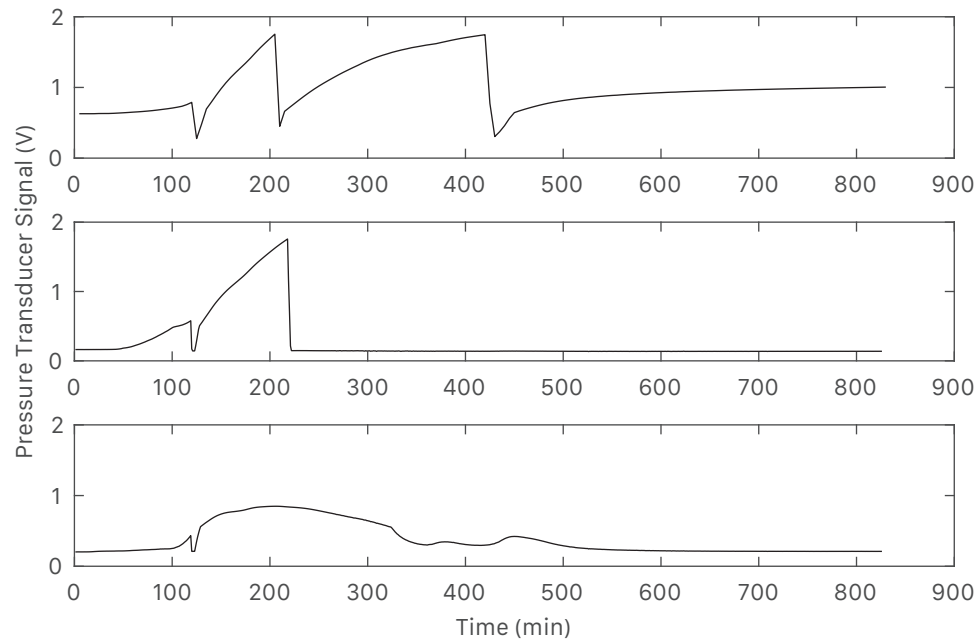
Figure 3.9 Examples of Runoff Voltage Traces from a rainfall event in October 2010. ***Top:*** A valid runoff trace with only ever increasing voltage except for sharp drops at valve openings. ***Centre***: An invalid profile exhibiting valve failure after the second opening, as indicated by the flat line. ***Bottom:*** An invalid profile exhibiting valve leakage, as indicated by voltage drops not caused by valve openings.

3.3.3   Hadfield Test Bed Hydrological Performance Data Analysis

The long-term Hadfield Test Bed data record provides a wealth of information on the effects of green roof configuration. The length of the data record also permits the identification of any trends in performance over time. **Figure 3.10** provides an overview of how retention and detention performance were characterised. The methodologies for these analyses are presented below.

Table 3.2 Number of valid events for each test bed and study year. Includes total number of events and the percentage of all 503 identified events (AIE).

Study Year	Test Bed									ATB
	1	**2**	**3**	**4**	**5**	**6**	**7**	**8**	**9**	
1	65	48	56	56	57	53	65	59	46	17
2	68	56	42	46	55	64	69	45	37	13
3	53	53	35	59	51	75	53	73	41	8
4	69	75	46	36	78	78	66	80	31	8
5	85	85	41	38	79	79	76	79	19	9
6	77	64	27	41	77	66	59	67	29	5
Total	417	381	265	276	397	415	388	413	203	60
% of AIE	83%	76%	53%	55%	79%	83%	77%	82%	40%	12%
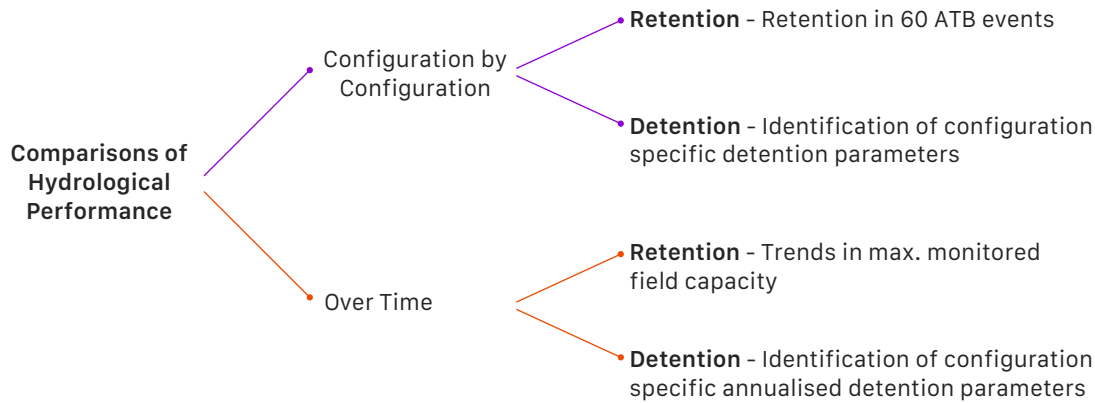
Figure 3.10 Overview of the Hadfield Test Bed Data Analysis.

Retention by Roof Configuration

Differences in retention performance amongst the various configurations of green roof tests beds were evaluated using the ATB dataset, where runoff data was available for all 9 test beds. It was necessary to ensure that all 9 test beds experienced the same rainfall events and ADWPs due to the controlling effects of both factors on retention performance. Per-event retention performance was determined via:

$$Retention = \frac{Rainfall - Runoff}{Rainfall} \times 100 \tag{3.1}$$

where retention is a %, rainfall and runoff are the total event depths in mm.

Retention via Field Capacity Monitoring

The identification of any year-on-year trends in retention performance from conventional metrics using rainfall and runoff data is highly subjective due to the dominant effects of climatic factors. Additionally, failures of the experimental equipment precluded the generation of complete annual metrics. Therefore, a physical property monitoring approach was adopted to assess the potential maximum retention depth of the green roof over time. The MWHC (field capacity) of the substrate was monitored continuously using the moisture content probes installed into TB1, 2, 3 and 7. When runoff occurs from a green roof, the substrate *should* have reached field capacity. Therefore, after the point of runoff initiation the substrate should be at/around its MWHC. Due to the highly permeable nature of green roof substrates, any significant saturation above MWHC is unexpected. The substrate's field capacity was therefore defined as the moisture content of the substrate 2 hours after the cessation of rainfall.

The ageing study utilised all three data types collected from the Hadfield beds: climate; rainfall/runoff; and moisture content. Each rainfall event where rainfall (P) and runoff (R) was greater than 2 mm was identified from the 6-year data record (between 98 and 198 events depending on the test bed). The moisture level recorded 2 hours after the cessation of rainfall was determined for all three moisture depths in each of the four test beds. The raw moisture content sensor data was first corrected for temperature effects using the relationship:

$$P_{corr} = P_{uncorr} + (20 - T) * (0.526 - 0.052 * P_{uncorr} + 0.00136 * P_{uncorr}^{2}) \qquad (3.2)$$

where P_{corr} is the corrected moisture probe period, P_{uncorr} is the raw probe data and T is the ambient temperature in °C (Western and Seyfried, 2005). This period was then converted into the observed field capacity ($\Theta_{0,FC}$) according to the following rules:

$$\begin{cases} P_{corr} < 20.299 & \Theta_{O,FC} = 0.0658 \cdot P_{corr} - 1.0802 \\ P_{corr} \geq 20.299 & \Theta_{O,FC} = 0.0200 \cdot P_{corr} - 0.1505 \end{cases} \qquad (3.3)$$

The resultant observed field capacity values were then statistically analysed using non-parametric methods for correlation (Spearman's Rank-order) and significant differences in distribution (Kruskall-Wallis Test) to identify trends over time.

3.3.4 Detention Performance Analysis and Modelling

To allow for comparisons to existing studies, common detention metrics have been calculated for each identified rainfall event and test bed, these are: peak delay; peak attenuation; t_{50} delay; centroid delay; time to start of runoff; and time to baseflow (see **Figure 2.9**). These metrics can be defined as:

- Peak delay — the time between the peak 5-minute rainfall intensity and the peak 5-minute runoff intensity;
- Peak Attenuation — defined as the percentage reduction in the peak 5-minute runoff compared with the peak 5-minute rainfall depth;
- The t_{50} delay — the time delay between 50% of the rainfall occurring to the same volume of runoff occurring, requiring runoff to be greater than 50% of rainfall;
- Centroid delay is the time delay between the centroid of the rainfall profile and that of the runoff;
- Time to start of runoff — the time between the first recorded rainfall and the first recorded runoff

- Time to baseflow — the time between the first occurrence of runoff and the last, can also be described as a runoff duration.

It should be noted that these methods do not distinguish between detention effects resulting from initial losses (retention) and actual physical delays inherent in the system, and thus fail to provide a good indication of actual detention processes. Only when a system is at field capacity at the onset of a storm event will detention metrics reflect the effects of detention processes alone. Stovin et al. (2015) proposed an alternative approach which assumes that the roof's detention characteristics are properties of the physical system and therefore independent of rainfall event characteristics. Assuming that a suitable hydrological model for the detention process can be identified, the observed rainfall-runoff data may be used to identify the model parameter(s) that uniquely define each individual system's detention characteristics.

Several different approaches to modelling green roof detention processes have been presented in the literature, including finite element (Hilten et al., 2008; Palla et al., 2012) and unit hydrograph-based (Villarreal and Bengtsson, 2005) methods. However, many authors have shown that a simple reservoir routing model is suitable for characterising green roof detention processes (Kasmin et al., 2010; Yio et al., 2013).

Modelling detention processes using reservoir routing techniques

Kasmin et al. (2010) suggested that the detention performance of a green roof test bed could be modelled using reservoir routing concepts, whereby:

$$h_t = h_{t-1} + Qin_t - Qout_t \tag{3.4}$$

in which *Qin* and *Qout* represent the flow rates into and out of the substrate layer respectively (mm/min), *h* represents the depth of water temporarily stored within the substrate (mm), and *t* represents the discretisation time step. *Qout* is given by:

$$Qout_t = D_S . h_{t-1}^{D_E} \tag{3.5}$$

in which D_S and D_E are the reservoir routing parameters (scale and exponent respectively). For *h* in mm and *Q* in mm/min, D_S has the units mm$^{(1-n)}$/min, whilst D_E is dimensionless. Note: in previous literature, the scale and exponent of the reservoir routing equation (3.5) have been referred to as *k* and *n* respectively, they have been altered in this study to avoid confusion with other physical properties and model parameters.

When considering only the influence of the substrate layer, Yio et al. (2013) demonstrated that a model based on a fixed value of D_E was capable of predicting observed runoff profiles with almost no loss of accuracy when compared with a model for which both parameters had been optimised. For the present study D_E was fixed at the literature suggested value of 2.0, and the best-fit value of the reservoir routing parameter D_S was identified for each rainfall event. Initial losses (or retention, defined simply as Rainfall (*P*) minus Runoff (*R*) in mm) were removed from the start of the monitored rainfall data to generate the net-rainfall profile prior to reservoir routing. The *lsqcurvefit* optimisation function in MATLAB (Mathworks, 2007), and an iterative approach, were utilised to identify the best-fit value of D_S for each individual event based on maximising the model fit — R_t^2 (Young et al., 1980) — between the routed and monitored runoff profiles. The routing employed a 5-minute time-step.

As the value of D_S is considered to be a system property, and therefore should not be affected by rainfall characteristics, the full VIE dataset was used for this analysis. However, as it is not meaningful to assess detention for rainfall events that do not generate runoff, a minimum runoff threshold of 2 mm was applied. This resulted in between 98 and 198 events being used to identify the best-fit D_S value for each test bed. For each test bed the individual event-based calibrated D_S values were combined by year of study to determine the test bed's median D_S value for each study year. The derived values of D_S were compared both on a configuration-by-configuration basis and year-on-year. Independent-samples Kruskal-Wallis tests with Dunn's pairwise comparisons were carried out to determine whether the identified annual D_S values were statistically independent.

Model Sensitivity to D_S

When using D_S as a descriptor of detention performance it is necessary to be mindful of what the differences in the value of D_S physically represent. **Figure 3.11** demonstrates that the optimisation of D_S is well-posed, with each event optimisation having only one peak R_t^2 value. However, these plots also highlight a general insensitivity to D_S at higher values, as seen from the long, shallow descending limbs. Sensitivity can be seen to much higher at lower values of D_S, with R_t^2 values rising quickly toward a peak value.
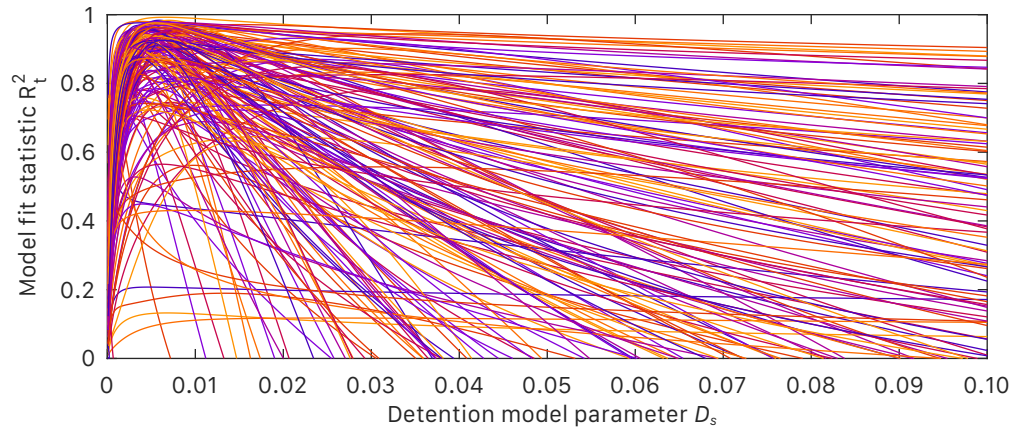
Figure 3.11 Plot of R_t^2 against D_s for all valid TB1 events.

Reductions in model fit (R_t^2) of 5% (e.g. 0.950 becomes 0.903, still indicating a strong model fit) result in a range of D_S values between 52 and 190% of the peak D_S value. A reduction or increase to the value of D_S by 5% typically results in changes to R_t^2 of less than 1%, further reinforcing the insensitivity of the model to the value of D_S. There is currently no solution to the model's insensitivity to D_S, but where relevant the limitations of predictions based around D_S values are clearly stated.

3.4 X-Ray Microtomography Microcosm-Scale Facilities & Methods

3.4.1 Substrate types for investigation

Previous studies by Berretta et al. (2014), Poë et al (2015) and the current monitoring study all considered the same three types of green roof substrate; introduced in section 3.3.1. Stovin et al. (2015a) identified that there were minimal differences in the hydrological performance of the two brick-based substrates. Therefore, the XMT study evaluated a single crushed brick-based substrate and an expanded clay-based substrate. The crushed brick-based substrate (BBS) is typical of many extensive green roof substrate mixes. The mineral component consists of crushed terracotta brick (55%) and pumice (30%). The organic components are coir (10%) and bark (5%). The second substrate is based on a light expanded clay aggregate (LECA), which is the sole mineral component (80%). The organic component is compost (10%) and loam (10%). This LECA substrate is quite different in physical appearance (**Figure 3.12**) and characteristics compared to BBS.
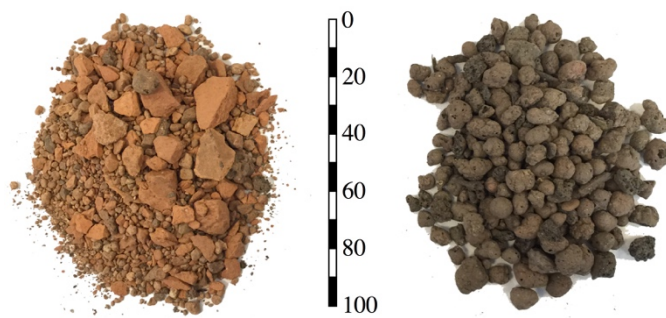
Figure 3.12 Left: Crushed brick based substrate (BBS). Right: Light expanded clay aggregate based substrate (LECA)

3.4.2 X-Ray Microtomography Facilities

All XMT imaging was conducted at The University of Nottingham's Hounsfield Facility for 3D X-ray imaging using a *General Electric - Phoenix v|tome|x M* microfocus CT system. An X-ray source is used to generate an X-Ray cone which passes through the object to be imaged, before reaching a digital detector. After a specified integration time the sample is slightly rotated and a subsequent image is captured. The sample continues to rotate for 180°, which provides sufficient images for the reconstruction of a sample within a holder of symmetrical cross-section. The machine is capable of imaging samples as large as 400 x 290 x 290 mm, with spatial image resolutions of between 5 and 150 µm (depending on sample size). **Figure 3.13** illustrates how sample size is related to image resolution, smaller samples can be placed closer to the X-ray

source, allowing the X-ray cone to fan out more on the detector side of the sample. This results in greater geometric magnification than is possible with a larger sample.
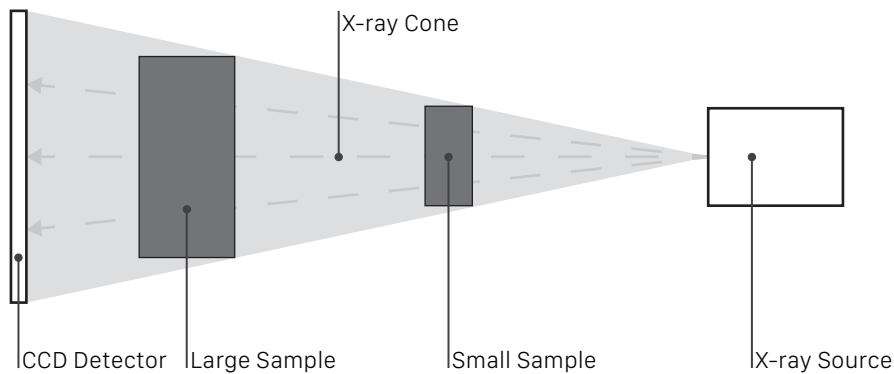
Figure 3.13 Diagram of X-Ray image capture and how sample size affects image resolution

3.4.3   Phase 1 — Cored Microcosm Study

The aim of the cored microcosm study was to observe and quantify the changes in substrate physical properties between virgin and aged substrate samples from two green roof test beds of differing configuration and predict hydrological response using appropriate hydrological modelling tools.
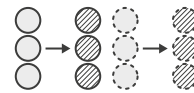
Extraction and preparation of substrate cores

Three aged and three virgin cores were obtained for each substrate type. The virgin cores (BBS_V and $LECA_V$) were formed from surplus substrate material used to construct two active green roof test beds. The aged cores (BBS_A and $LECA_A$) were taken from these two green roof test beds, which included an additional *Sedum spp.* vegetation layer not present in the virgin cores. The aged BBS_A cores were taken from the Mappin Test Bed (Stovin et al. (2012) provides a full description of this facility) and the aged $LECA_A$ cores were taken from TB3 of the Hadfield Test Beds (see section 3.3).

The core holders were 68 mm in height with an internal diameter of 46 mm, these sizes were dictated by the loading gauge of the originally intended XMT machine. The core holders were constructed from *Poly(methyl methacrylate)* (PMMA, commercially known as Perspex) as a non-metallic material is required for the XMT imaging process in order to prevent poor image quality.

Physical testing of substrates

To maintain the substrate cores' 'in-situ' status for as long as possible some physical characterisations were not made. However, each of the substrate cores was characterised in line with the FLL (2008) guidance for determining apparent density and maximum water holding capacity. The solid base of the core holders prevented hydraulic conductivity measurements from being undertaken. Upon completion of the XMT imaging, samples were destructively tested to determine particle size distributions using a sieve analysis in accordance with BS ISO 11277:2009. Cores were not then reconstructed for further testing. Where experimental technique prohibited the determination of certain substrate properties, previously reported values in the literature were used for comparison (see **Table 3.3**).

Table 3.3. Substrate Physical Properties explored in this phase of study and methods of characterisation.

Property	Substrate Physical Property Source		
	Literature	**Physical Testing**	**XMT Image Analysis**
Particle Size Distribution	✓	✓	✓
Pore Size Distribution	–	–	✓
Dry Density	✓	✓	-
Density at Field Capacity	✓	✓	-
Max. water holding capacity	✓	✓	-
Hydraulic Conductivity	✓	-	✓
Tortuosity	-	-	✓

XMT Imaging

All 12 cores were imaged only once, with a spatial resolution of 30 µm/pixel. All scans were performed at 180 keV and 110 µA, taking 2400 projections with an exposure time of 250 ms. Total imaging time was 30 minutes per core, producing ~15 GB of image data per scan.

3.4.4 Phase 2 – Longitudinal Microcosm Study

The aim of the longitudinal microcosm study was to observe and quantify the changes in substrate physical properties and hydrological performance repeatedly over time for specific microcosms across a full year of vegetation growth.
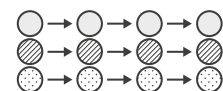
Preparation of Microcosms

Two microcosm sizes were utilised for the longitudinal study (**Figure 3.14**), larger microcosms conforming to the standardised FLL test container guidelines (150 mm in diameter, 100 mm depth of substrate), and smaller microcosms suitable for XMT

investigation (50 mm in diameter, 100 mm depth of substrate). The greater depth of the longitudinal microcosms as opposed to the cored microcosm study (100 vs. 80 mm) was to meet FLL guidelines. The larger microcosms were utilised to confirm that the smaller 50 mm diameter microcosms sufficiently represented the properties of larger microcosms.

50 mm   150 mm
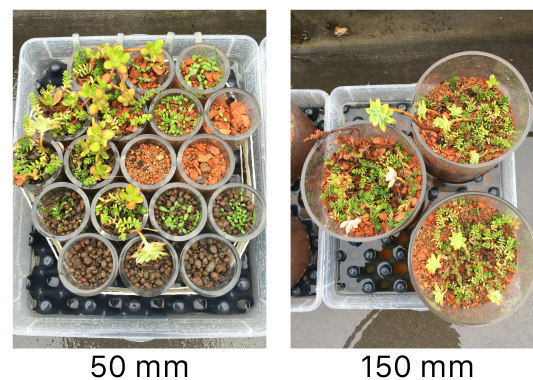
Figure 3.14 Two microcosm sizes. 150 mm examples are BBS and Sedum Vegetation. Image taken 07/10/15.

For each microcosm size there were 2 substrate treatments, 3 vegetation treatments and 3 replicates of each configuration, totalling 18 microcosms of each size. The two substrate treatments were those presented in section 3.4.1, a crushed brick-based substrate and a light expanded clay aggregate based substrate. The three vegetative treatments are an unvegetated control, a planted sedum vegetation and a seeded meadow-flower vegetation, like those described in section 3.3.1.

Physical testing of substrates

Each 150 mm diameter microcosm was tested in accordance with the FLL (2008) guidelines for determining apparent density, maximum water holding capacity, hydraulic conductivity and particle size distribution. The smaller 50 mm diameter microcosms were also tested using the same methodologies, although testing deviated from the guidance as the samples were only 1/3 the recommended FLL diameter. Full characterisation was undertaken on virgin samples and again after 1 year of growth (**Figure 3.15**).

Additionally, the 50 mm microcosms were subject to basic detention testing. A constant intensity (5 mm/min) 5-minute duration 'rainfall' was applied to each microcosm using a peristaltic pump and pressure-compensating irrigation dripper. Microcosm runoff depths were monitored using a pressure transducer in a collection

vessel, in a similar approach to the monitored Hadfield Test Beds. These detention tests allowed the determination of a D_s value, by the fitting of a reservoir routing model, for each 50 mm microcosm in virgin (T0) and aged (T12) states.

XMT Imaging Schedule

The 50 mm diameter microcosms were initially imaged in a virgin state, with no vegetation present in August 2015. Microcosms were planted/seeded and allowed to develop for 8 months under normal climatic conditions before being imaged again. The second images were taken in April 2016 (T8). The third set of images were acquired 2 months later in June 2016 (T10) and the final image set was acquired in August 2016 (T12, **Figure 3.15**). Repeated imaging of the growing microcosms was spaced 2 months apart to allow for significant growth to occur. The total scanning period covers one calendar year to capture the full first year growth cycle of the vegetation. Unvegetated control microcosms were scanned at the same intervals. All 18 microcosms were imaged with a spatial resolution of 40 μm/pixel. All scans were performed at 180 keV and 110 μA, taking 2400 projections with an exposure time of 250 ms. Total imaging time was 30 minutes per microcosm, producing ~15 GB of image data per scan.
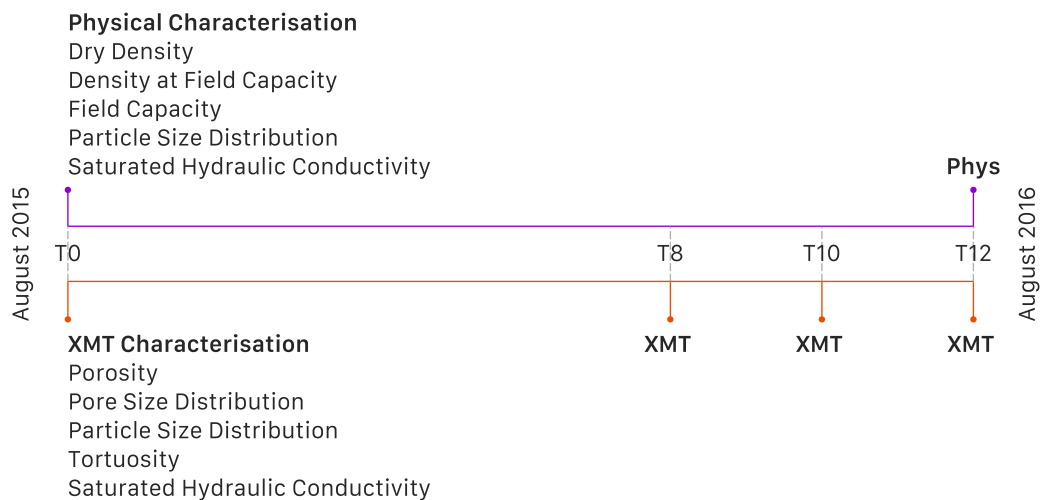
Figure 3.15 Timeline of substrate property characterisations. TX indicates time passed in months, i.e. T8 is after 8 months of ageing.

3.4.5 Image Analysis

Analysis was undertaken to obtain physical properties from the X-ray images. Image pre-processing was handled using the ImageJ software (Schneider at el., 2012). Image stacks were cropped to remove areas not of concern (outside of core area) and then, to meet computational limits, split into 2 sub-stacks (top and bottom). Image

processing was undertaken using Avizo 9 (FEI, 2015), ImageJ and DigiUtility (SVL, 2015). Each of the image sub-stacks underwent the same image processing protocol (**Figure 3.16**), which is detailed below. After the image processing steps, sub-stacks were recombined to allow analysis across full core and microcosm heights.

Image filtering & segmentation

The pre-processed XMT images contain image noise (random variation of brightness) which may be incorrectly interpreted as small particles. To mitigate against this misidentification a median filter was applied to the image sub-stacks. The median filter reassigns each voxel (3D pixel) with the median value of the surrounding 26 voxels. This filtering technique creates a clear distinction between the solids and voids of the image. Images were then segmented by picking threshold 8-bit greyscale values from the image histogram. To minimise the effects of subjective thresholding, constant thresholding based on known materials (the core or microcosm holder) was used. Images were segmented into 4 label bins: exterior regions not for analysis; particles; effective pore volumes (inter-particle voids); and ineffective pore volumes (intra-particle voids). Binary image sets were then generated for particle regions, whereby the individual pixel values represented either a particle (1) or nothing (0). Similar binary image sets for pore space were created where individual pixel values represented pores (1) and solids (0). These binary image sets are the inputs for the physical property characterisation steps.

Porosity Determination

The porosity of the substrate was determined from the segmented binary images. The effective porosity (inter-particle voids) was determined from contiguous regions of voxels with a value of 0. The ineffective porosity (intra-particle voids) was determined in a similar way, except these pores are bounded on all sides by voxels with a value of 1, indicating that the pore is encased by solid material. Labelling of these regions in Avizo allowed the application of a *Volume Fraction* module, which calculated the volume of each labelled region. These volumes were then substituted into the following formulae:

$$\phi_T = \frac{V_E + V_I}{V_T} \qquad\qquad\qquad (3.6)$$

$$\phi_E = \frac{V_E}{V_T} \qquad\qquad\qquad (3.7)$$

Raw XMT image: 8-bit greyscale

Filtering

Median filtered image: 8-bit greyscale

Reduced image noise
with retained particle
structures

Segmentation

Segmented image

■ Particles

▨ Effective Pore Space

□ Ineffective Pore Space

Separated particle image - Particles Shaded

Separation

Same shading does not
necessarily imply
connected particles
where clearly
seperated

Separated pore image - Pores Shaded

Figure 3.16 Image processing protocol including typical 2D perspectives of outputs for BBS.

$$\phi_I = \frac{V_I}{V_T} \qquad\qquad (3.8)$$

where ϕ_T is total porosity, V_E is the inter-particle void volume in voxels, V_I is the intra-particle void volume in voxels, V_T is the total sample volume in voxels, ϕ_E is effective porosity and ϕ_I is ineffective porosity. Porosity was calculated for full 3D volumes in addition to a series of 2D horizontal slices, which were used to assess how porosity varied with depth.

Particle size distribution

To determine particle size distribution, contiguous regions of solid needed to be discretised into individual particles. To achieve this, any identified intra-particle volume was first filled to create entirely solid particles. This step avoids the fracturing of highly porous particles. The *Separate Objects* module was applied in Avizo (FEI, 2015). Separation lines were drawn where two (or more) convex particles met. The intra-particle volume was subtracted from the separated image to create separated porous particles. The *Label Analysis* module was applied to characterise the individual particles in terms of a selection of custom metrics, including: equivalent diameter; length; breadth; width; volume; surface area and sphericity.

Length, breadth and width are the particle's calculated Feret diameters (FEI, 2015). Length is taken as the longest dimension of the object; breadth is then taken as the next largest dimension, perpendicular to the length. The width is taken as the third perpendicular dimension. The breadth measure is used to analyse particle sizes, as it is the limiting dimension if physically sieved. Particle size distributions are plotted as the percentage of particles (N/N) finer than given particle sizes. This is different to physically-derived particle size distributions which are presented as a percentage by mass.

Pore size distributions

To determine the pore size distribution, the pore space needed to be discretised into a pore network. A similar method to that of Youssef et al. (2007) was applied. The first step was the skeletonisation of the pore space. The skeleton is the thinnest representation of the pore space, yet it retains the topology of the original pattern. Secondly a pore space thickness map was computed to determine the distance between any pore space voxel and the edge of the pore space. The combination of the pore space skeleton and the thickness map allowed for the division of the pore space skeleton at points of minimum thickness (pore throats) to create individual pore

spaces. The same *Label Analysis* module as that used for particle size distributions was then applied to determine pore volume and equivalent diameter. Pore size distributions were plotted as the percentage of pores (N/N) finer than given pore sizes.

Tortuosity

Tortuosity is the square of potential pathway lengths through a media relative to the media depth. Higher values of tortuosity indicate longer paths and would imply longer travel times through the media (assuming constant velocities). For example, a value of 4 would imply the path length from top surface to bottom surface is twice the media thickness. Tortuosity values were computed in DigiUtility (SVL, 2015) from binary pore images. A random selection of 1000 starting locations each with 100 repeats was averaged to provide a mean value of tortuosity for each substrate core.

Root Tracking

For the second phase of XMT exploration the root networks of the ageing cores were analysed where sufficient contrast between the roots and surrounding substrate existed. To distinguish the roots from the surrounding mineral particles the root tracking software RooTrak (Mairhofer et al., 2012) was used. RooTrack utilises a top-down approach to the segmentation of the filtered XMT images. The XMT images are viewed as a sequence of horizontal slices. As the sequence is traversed root cross sections appear to move around the image, those movements reflect the shape of the scanned root. Strategies used for the visual tracking of moving objects in 3D are then applied to segment the root architecture from the surrounding soil. The resultant 3D root model can be used to determine the physical dimensions of the root network.

3.4.6   Lattice Boltzmann Method for determining hydraulic conductivity

The Lattice Boltzmann Method (LBM) is a computational method for simulating flow based on Lattice Gas Cellular Automata (LGCA). It harnesses the Boltzmann equation to explicitly solve fluid dynamics problems (Succi, 2001). LBM simulations were undertaken using DigiFlow (SVL, 2015). The method offers a numerical solution that quantifies a superficial velocity in terms of lattice units (lu — i.e. one pixel) and time steps (t_s) with velocity given in units of $lu \cdot t_s^{-1}$ and kinematic vicosity in $lu^2 \cdot t_s^{-1}$ (Menon et al., 2011). These quantities can then be converted back into physical properties, assuming that Reynolds number is the same in both lattice and physical units, using the following formulae:

$$Re_{phys} = \frac{K_{XMT} \cdot L_{phys}}{v_{phys}} \quad \equiv \quad Re_{lat} = \frac{U_{lat} \cdot L_{lat}}{v_{lat}} \tag{3.9}$$

where Re_{phys} is the physical Reynolds number, Re_{lat} is the LBM Reynolds number, K_{XMT} is the hydraulic conductivity in m/s, U_{lat} is the superficial velocity of the LBM simulation, L_{phys} is a characteristic physical dimension in m, L_{lat} is the corresponding simulation dimension of the characteristic length, v_{phys} is the kinematic viscosity of water, and v_{lat} is the simulated kinematic viscosity of the LBM simulation fluid. Within the DigiFlow LBM implementation:

$$v_{lat} = \frac{2\tau - 1}{6} \tag{3.10}$$

$$\beta = \frac{L_{lat}}{L_{phys}} \tag{3.11}$$

where τ is a simulation relaxation factor and β is the ratio of physical to simulated length scales in pixels/m. Hence, to determine hydraulic conductivity:

$$K_{XMT} = \frac{6v_{phys}U_{lat}\beta}{2\tau - 1} \tag{3.12}$$

where in this study v_{phys} = 1.004x10^{-6} m^2/s, β = 3,333 pixels/m for a 30 µm image and β = 2,500 pixels/m for a 40 µm image , and τ = 1.The inputs for the LBM simulations are binary images of each substrate sample, including the effective pore spaces and solids. The simulations each result in a value of K_{XMT}. The simulations were considered to be complete when the flow velocity had converged, typically within 10000 iterations.

3.4.7   Statistical Analysis of Resultant Property Values

All individual measures of substrate physical properties, both physically-derived and XMT-derived, were grouped by physical configuration and age. Non-parametric statistical tests performed in Matlab, Kruskal-Wallis, were used to identify the presence of any significant differences in property values between physical configurations, ages and between methods of determination.

3.4.8   Modelling of Hydrological Performance

Potential Retention Performance

Retention processes within the substrate were modelled using a conceptual hydrological flux model as presented in Stovin et al. (2013). Runoff was predicted from moisture fluxes within the substrate due to precipitation and evapotranspiration. Runoff volumes were calculated from the following relationships:

$$R_t = \begin{cases} 0, & S_{t-1} + P_t - ET_t \leq S_{max} \\ P_t - (S_{max} - S_{t-1}) - ET_t, & S_{t-1} + P_t - ET_t > S_{max} \end{cases} \tag{3.13}$$

where R is runoff, S is the storage level, P is precipitation, ET is evapotranspiration and S_{max} is the maximum substrate retention capacity (equal to PAW), all in mm; t is the discretised time-step. Substrate moisture content is then updated:

$$S_t = \begin{cases} S_{t-1} + P_t - ET_t, & S_{t-1} + P_t - ET_t \leq S_{max} \\ S_{max}, & S_{t-1} + P_t - ET_t > S_{max} \end{cases} \tag{3.14}$$

ET is calculated as a function of Potential Evapotranspiration (PET) by use of a Soil Moisture Extraction Function (SMEF):

$$ET_t = PET_t \times \frac{S_{t-1}}{S_{max}} \tag{3.15}$$

The retention performance was then calculated by subtracting the total runoff from the total precipitation and dividing by total precipitation.

Potential retention performance in the cored microcosm study was determined for four design storm scenarios. Two values of S_{max} were assessed; corresponding to an 80 mm depth of virgin and aged substrate. Additionally, two values of PET were assessed; corresponding to typical spring and summer conditions for Sheffield, UK, where PET was 1.8 and 4.5 mm/day respectively (Poë et al., 2015). All runoff volumes were in response to a 1-hour duration 1-in-30-year design rainfall event for Sheffield, UK, and a variable 1 to 28 day antecedent dry weather period (ADWP). On day zero, S was set equal to S_{max} to simulate field capacity conditions.

For the longitudinal microcosm study potential retention performance was determined for two scenarios for each substrate. Two values of S_{max} were assessed; corresponding to an 100 mm depth of virgin and aged substrate and determined from:

$$S_{max} = PAW = d.(\theta_{FC} - \theta_{PWP}) \tag{3.16}$$

where PAW is plant available water in mm, d is the substrate depth in mm, θ_{FC} is field capacity (equal to MWHC) as a % v/v, and θ_{PWP} is the permanent wilting point as % v/v. A single spring value of PET was assessed (1.8 mm/day, Poë et al., 2015). All runoff volumes were in response to a 1-hour duration 1-in-30-year design rainfall event for Sheffield, UK, and a variable 1 to 28 day antecedent dry weather period (ADWP). On day zero, S was set equal to S_{max} to simulate field capacity conditions.

Detention Performance

Detention performance was determined in isolation from the effects of retention using a Finite Element (FE) model developed by Bayton (2013). The FE model uses a numerical solution of Darcy's Law and the Moisture-Mass Conservation Law to predict runoff volumes for an unsaturated media in response to an input rainfall. The model was validated against laboratory data collected by Bayton (2013) and Yio et al. (2013), and replicates similarly configured HYDRUS-1D outputs (Šimůnek et al., 2008). An 80 mm substrate depth was modelled for the cored microcosm study, whilst a 100 mm depth was modelled in the longitudinal microcosm study. A constant vertical spatial discretisation of 1 mm and a 0.5 s time-step were employed. The initial model moisture content was set equal to the physically-derived field capacity. The upper substrate surface was subject to a flux, corresponding to a relevant rainfall profile. For the cored microcosm study two rainfall inputs were used, a 1-hour duration 1-in-30-year design rainfall and a monitored rainfall event. For the longitudinal microcosm study, again two rainfall inputs were used, the same design rainfall and 5 mm/min constant intensity 5 min duration event to replicate laboratory detention tests. The lower surface was set as a free draining boundary.

The FE model requires the parameters of a van Genuchten water release curve model (van Genuchten, 1980) and a value of K_{sat}. The van Genuchten model parameters (**Figure 3.17**) were determined via the RETC software (van Genuchten et al., 1991) using pressure plate extraction data for comparable brick-based substrates presented by Berretta et al. (2014). The runoff responses for XMT-derived and physically-derived values of K_{sat} were assessed. The lack of pressure plate data for LECA limits detention performance predictions to the BBS substrate only.
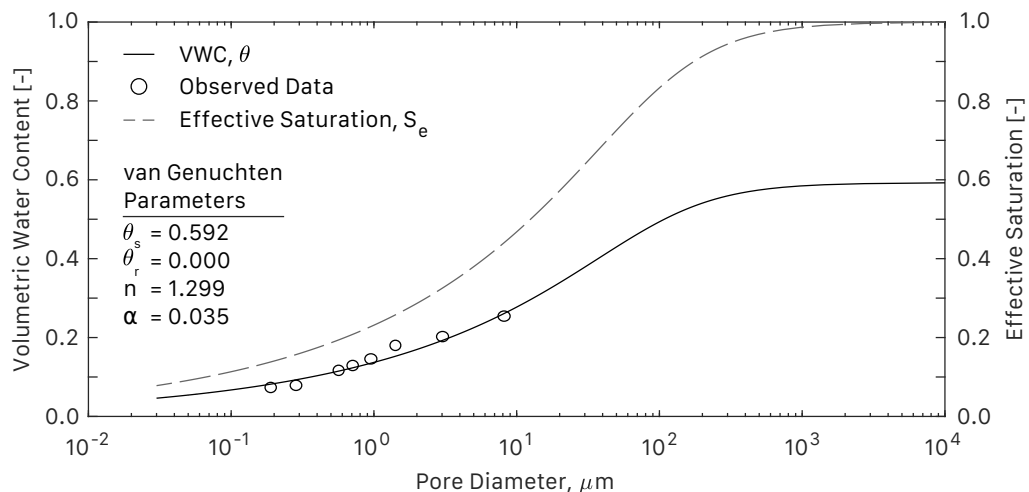
Figure 3.17 Observed pressure plate data of Berretta et al. (2014) with fitted van Genuchten model.

3.5 Chapter Summary

The methodologies presented here can be broadly classified into two distinct approaches. The first investigates the hydrological performance of green roof test beds over a period of 6-years. This approach builds upon the work of several authors, additionally providing new insight into the evolution of hydrological performance over time. A novel approach is introduced for evaluating temporal changes in maximum retention capacity, based on substrate moisture content measurements, whilst hydrological modelling techniques are used to assess detention performance.

The second approach uses X-ray imaging techniques to look inside green roof substrates to explore their physical properties, something that has not been undertaken before. This portion of the experimental programme is split into a further two distinct phases, the first being the investigation of a virgin substrate compared to a 5-year old sample, whilst the second (longitudinal study) employs a much higher temporal resolution to assess changes in substrate properties over a single year. Together these approaches provide multiple perspectives of the changes in hydrological performance over time and the physical processes underpinning these changes. The following chapters present the results of each of these experimental components.

Monitoring Study Results & Discussion

4.1 Chapter Overview

This chapter outlines the results from the long-term monitoring study of the Hadfield Green Roof Test Beds. Consideration is given to the effects of roof configuration on hydrological performance, and the presence of temporal trends, both sub-annually and multi-annually. The implications of differences in hydrological performance and the potential drivers for these changes of configuration, system age and season are discussed. Finally, predictions of performance for design storms are made, highlighting the importance of the identified differences in hydrological performance.

Analysis of hydrological performance by season and age has not been previously presented. However, some identification of hydrological performance from data used here is incorporated into the following publication:

Stovin, V., Poë, S., **De-Ville, S.** and Berretta, C., 2015a. 'The influence of substrate and vegetation configuration on green roof hydrological performance'. *Ecological Engineering*, 85, 159–172.

4.2 Identified Storm Events

The monthly rainfall depths (**Figure 4.1**) highlight the typically high levels of variability associated with a temperate climate. It is also apparent that, compared to the long-term mean (UK MET Office, 2016), summers during the study period were wetter and autumns were drier. **Figure 4.1** also aids in understanding the difficulty of observing similar rainfall characteristics over time, with the exception of January almost all other months receive vastly different levels of rainfall from year to year.
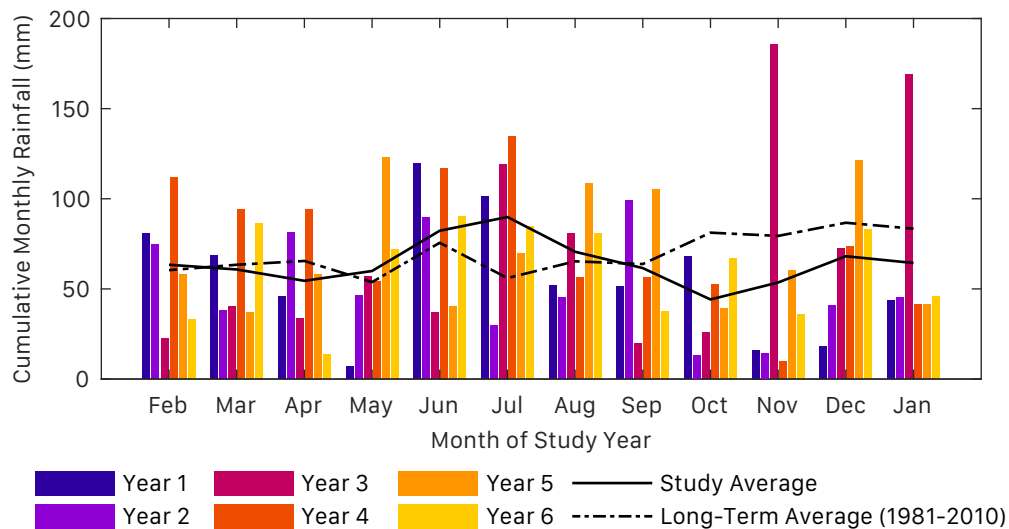
Figure 4.1 Monthly rainfall data for the 6-year study period compared to long term climate averages for Sheffield, UK.

Application of a precipitation threshold of ≥2 mm and a minimum inter-storm period of 6 hours resulted in the identification of 503 rainfall events over the 6-year study period. Cumulative rainfall for these events totals 4224 mm, out of a total recorded 4670 mm, representing 90.5% of all rainfall. The characteristics of these storm events are shown in **Figure 4.2**, where it can be seen that the vast majority of storms can be classified as having a return period of less than 1 year. Only 4 events are classified as having a return period in excess of 2 years.

Figure 4.3 presents 6 rainfall and runoff responses for all 9 test bed configurations and illustrates a range of observed rainfall patterns and runoff responses. Several consistent behaviours can be observed in the runoff responses. In each case there is a clear delay between the onset of rainfall and the onset of runoff. This period represents retention processes whereby rainfall is subjected to initial losses, either intercepted by vegetation or retained within the substrate. The length of this period

and the subsequent depth of rainfall that is retained depends on the moisture losses from the system as a result of ET in the antecedent period. For the events from years 3 and 4 a high degree of variation in the depth of initial losses between the nine test beds can be observed, for example, ranging from between 6 and 20 mm for the event depicted in year 3. Key summary statistics for these events can be seen in **Table 4.1**.
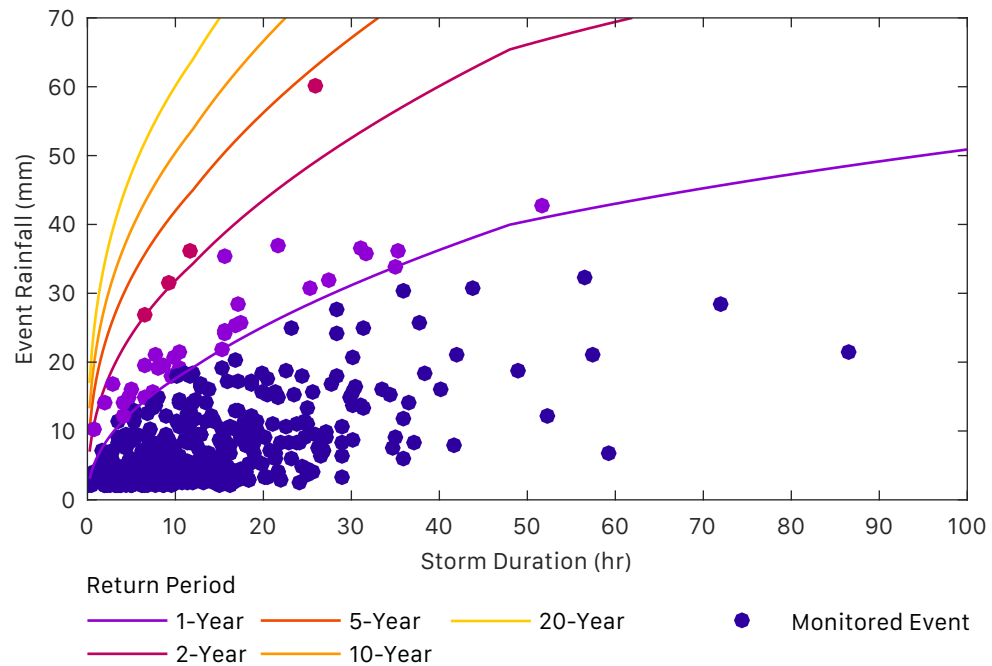
Figure 4.2 Intensity-duration-frequency plot for monitored rainfall events in Sheffield, UK.

Table 4.1 Summary of key event parameters for identified events in Figure 4.3.

Year	Event	Start date	Rainfall depth (mm)	Rainfall duration (h)	ADWP duration (h)
1	23	06-Jun-2010 01:20:00	11.2	10.7	177.6
2	107	25-Aug-2011 01:36:00	14.8	4.6	96.0
3	156	03-Apr-2012 22:32:00	21.8	15.3	399.5
4	257	02-Dec-2013 23:20:00	6.6	19.0	136.0
5	344	31-Mar-2014 19:33:00	9.5	8.8	87.4
6	441	08-May-2015 13:02:00	19.7	8.7	42.8
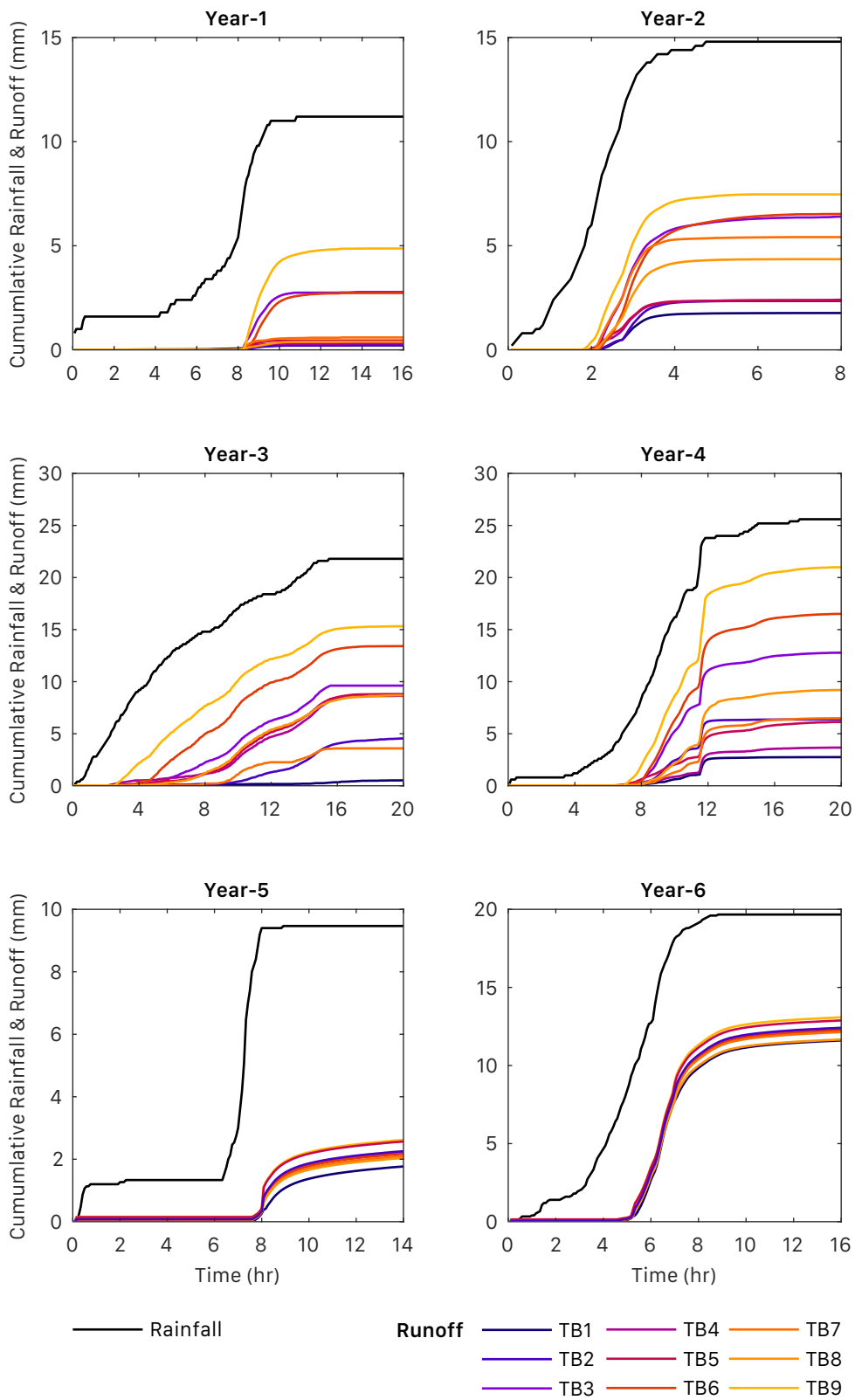
Figure 4.3 Cumulative runoff responses for the nine test-beds for six rainfall events that generated runoff, one from each study year.

4.3 Retention Performance Analysis

4.3.1   Retention Performance by Roof Configuration

The distributions of per-event retention values for the 60 events of the ATB dataset (where all 9 beds were fully operational) are presented in **Figure 4.4**. For those events where rainfall (P) was greater than 2 mm the distributions are strongly influenced by the high retention performance associated with frequently occurring small rainfall events. However, those test beds installed with LECA (TB3, 6, and 9) exhibit lower median values of per-event retention than their brick-based counterparts, irrespective of vegetation treatment. From within the LECA sub-group the lowest median per-event retention performance is seen for TB9, the unvegetated LECA test bed. Whilst these observations can be made, statistically there is no significant difference between the per-event retention performance of the nine configurations for P≥2 mm.
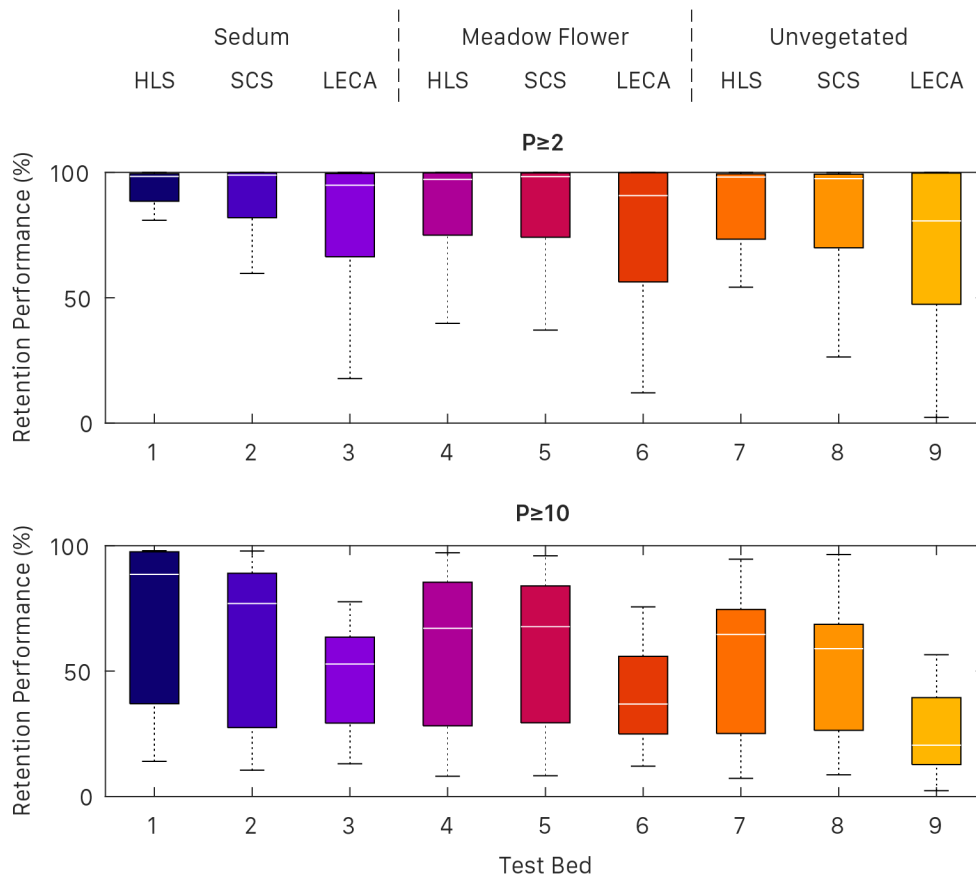
Figure 4.4 Boxplot of retention performance for the 9 test bed configurations. ***Top:*** events where rainfall (P) exceeded 2 mm. ***Bottom:*** events where rainfall exceeded 10 mm.

When considering only the events where rainfall exceeded 10 mm (**Figure 4.4 Bottom**) the influence of substrate and vegetation becomes more evident. Again, the LECA test beds are seen to be the worst performers compared to their brick-based counterparts. Of the two brick based substrates, HLS consistently provides an elevated median level of per-event retention compared to SCS across all vegetation treatments. Sedum vegetated beds (TB1 - 3) exhibit the highest levels of per-event retention performance irrespective of substrate type, with Meadow Flower beds (TB4 - 6) performing slightly worse. The un-vegetated test beds (TB7 - 9) demonstrate the lowest levels of per-event retention. However, due to the small sample size and heavily overlapping distributions — a result of highly variable retention performance — there is no statistical significance to the difference in per-event retention performance by roof configuration.

The observed differences in retention performance are most greatly influenced by substrate type. The increased levels of retention performance for the brick-based substrates (HLS and SCS) over LECA-based configurations can be attributed to the physical properties of the substrate. Both HLS and SCS have a higher MWHC than LECA, which allows for a greater maximum potential retention capacity. Providing there is a sufficiently lengthy antecedent dry weather period, the HLS and SCS roof configurations can retain greater levels of rainfall than LECA configurations. Examples of this behaviour can be seen in **Figure 4.3**, particularly for years 2, 3 and 4.

Observed differences in retention can also be attributed to the presence, or absence, of vegetation. The actual substrate moisture retention capacity at the start of a rainfall event is dependent upon the volume of losses generated during the antecedent dry period. For vegetated systems, the plants add to the long-term losses by transpiring additional water compared to the evaporative processes alone of the unvegetated test beds. Observations have been made of unvegetated substrates having higher initial rates of ET (Poë at al., 2015), but vegetated systems exhibit larger overall losses. Further losses can also be attributed to the presence of vegetation, as plant leaves provide greater surface areas for the interception of rainfall. Hence, vegetated test beds exhibit higher available storage volumes at the onset of rainfall events, leading to improved retention performance over their unvegetated counterparts.

> *The main conclusions from the analysis of retention performance by configuration are that brick-based substrates exhibit higher levels of retention*

> *performance compared with LECA-based substrates. Similarly, vegetated systems exhibit greater retention performance than their unvegetated counterparts. Storm event rainfall depths are also a controlling factor of retention performance, with retention performance decreasing with increasing event rainfall depths.*

4.3.2 Retention Performance with Roof Age

The overriding influence of climatic factors means that conventional retention metrics provide a poor descriptor of any changes over time. Identical events with the same ADWP and rainfall characteristics would need to occur repeatedly to allow for any direct comparisons to be made. However, the moisture-holding properties of the substrates are thought to be less likely influenced by climatic factors and may provide a more reliable estimate of any changes to potential retention performance (i.e. maximum retention capacity) over time. As outlined in section 3.3.3, the monitored field capacity of the substrates has been used as an indicator of trends in the maximum potential retention capacity of the green roof configurations.

When comparing the monitored field capacity data against FLL-derived field capacity measurements (**Table 4.2**), the two vegetated brick based substrates (TB1 and TB2) have mean field capacity values that fall within one standard deviation of the FLL-derived value. However, both the middle and top layers of the substrate in TB1 and TB2 exhibit median levels of field capacity below those of the FLL-derived result. Berretta *et al*. (2013) presented a second set of field capacity values for the HLS and SCS substrates — TB1 and TB7, and TB2 respectively — which were determined using a Pressure Plate Extractor, which are considerably lower than monitored values at 25.0% and 22.4% (v/v) respectively. Yet, in monitoring observations using the same equipment as in this study, Berretta et al. (2014) observed comparable substrate moisture levels to those presented here. The disparity in FLL-derived values of field capacity and those from the pressure plate extractor were attributed to the sieving of pressure plate samples and the use of smaller sample sizes, which potentially induced boundary effects.

All monitored values of field capacity for TB3 and TB7 are below those identified by FLL methods. Berretta et al. (2014) was unable to determine a value of field capacity for the LECA substrate of TB3 using the pressure plate extractor method. Characterisation of the in-situ LECA substrate of TB3 is presented in chapter 5, where these disparities are discussed.

Table 4.2 Comparison of FLL-derived field capacity values and median monitored field capacity of the four test bed configurations across all monitored depths, and depth averaged.

Test Bed	FLL-derived field capacity (% v/v)	Observed median field capacity (% v/v)			
		Bottom	**Middle**	**Top**	**Full Depth**
1	41.2 ± 2.3	44.6	39.3	37.4	40.4
2	39.1 ± 2.1	40.4	36.2	34.7	37.1
3	35.0 ± 1.6	32.5	26.3	26.1	28.3
7	41.2 ± 2.3	36.6	37.5	35.3	36.5

Figure 4.5 displays the monitored field capacity of TB1, 2, 3, and 7 across the entire study period. Data was not available for the first year of the study, and so a 5-year period is used for the evaluation of any trends over time. Consistently, the bottom of the substrate exhibits a higher moisture content than either the middle or top. After a rainfall event such behaviour is expected due to the high permeability of green roof substrates, as rainfall quickly makes its way to the underlying drainage layer. The vertical gradient is also likely a result of preferential drying at the surface of the substrate. It has additionally been suggested that the effects of substrate compaction and ageing, causing the leaching of fines into deeper substrate layers, may contribute to the establishment of a vertical moisture profile (Berretta et al., 2014; Morbidelli et al., 2014, 2011); these claims will be addressed more closely in chapters 5 and 6.

The presence of a vertical moisture profile is exaggerated in the vegetated test beds (TB1-3) when compared to the unvegetated TB7. This would suggest that plant and root activity also contribute to the development of the vertical profile. Comparisons between TB1 and TB7, which share the same substrate but have different vegetation treatments, reveal that moisture levels are consistently elevated in TB1 over TB7. Berretta et al. (2014) suggested this phenomenon was due to the moisture retention effects of plants and roots, a result of greater entrained organic content. However, inspection of **Figure 4.5** also reveals the presence of a sub-annual cycle by which monitored field capacities were highest in the winter months — vertical dotted lines indicate February of each study year — and lowest in the summer. If differences are to be solely attributed to the vegetative processes, seasonal trends are unlikely to also be present in the unvegetated TB7. The effects of seasonal differences on substrate properties that may result in altered field capacity values will be discussed further in chapter 6.
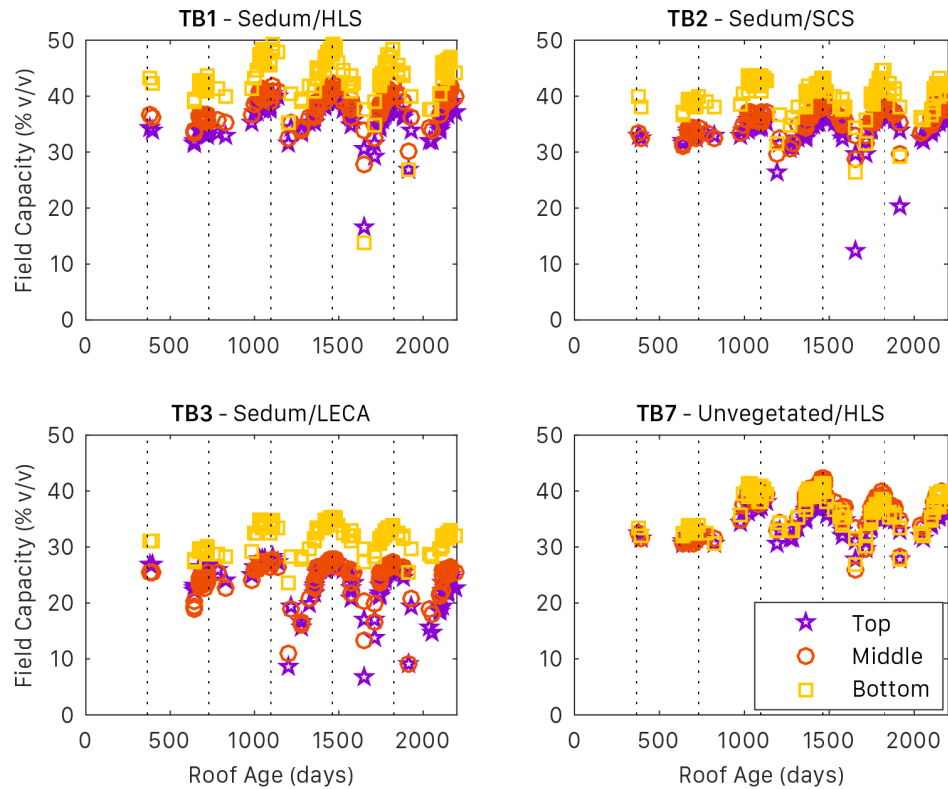
Figure 4.5 Scatter plot of monitored post-event field capacity over time. Dotted lines indicate study years.

The results of a non-parametric correlation determination, Spearman's rho (**Table 4.3**), identified significant statistical correlations between roof age and monitored field capacity for every test bed but not at all monitored depths. For test bed 1, statistically significant correlations existed in the top (very-weak positive) and middle (weak positive) layers of the substrate. **Figure 4.6** illustrates this relationship, where the bottom layer of substrate in TB1 exhibits only minor fluctuations in monitored field capacity over time compared to the middle and top layers. The strongest correlation is seen for the top and middle layers of TB2 which both exhibit a moderate positive correlation between monitored field capacity and roof age. TB1 and TB2, both sedum vegetated test beds on brick-based substrates, demonstrate similar relationships over time. However, the Sedum vegetated LECA test bed (TB3) exhibits a different relationship with no significant correlation seen in the top substrate layer but the presence of a weak positive correlation in the bottom layer. This suggests a different mechanism by which the field capacity is being altered for the different substrate types. The unvegetated TB7 displays a third relationship where the only significant correlation is in the middle layer of the substrate (very-weak positive), further suggesting that vegetation has a role in altering field capacity over time.

Table 4.3 Spearman's rho correlation coefficient values for statistically significant correlations (P≤0.05) between monitored field capacity and roof age.

Test Bed	N	Field Capacity Observation Depth		
		Top	Middle	Bottom
1	144	+0.194	+0.362	-
2	161	+0.452	+0.526	-
3	111	-	+0.275	+0.297
7	159	-	+0.184	-
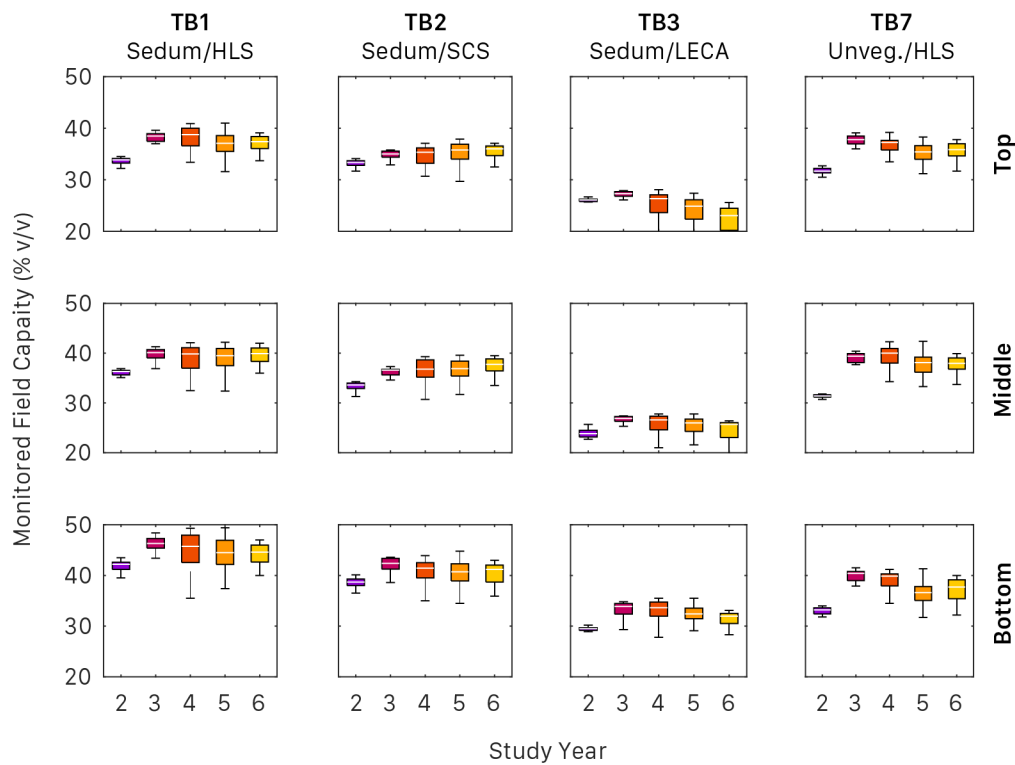
Figure 4.6 Boxplot of monitored field capacity for the four test bed configurations across each study year. Outliers not shown. Each row indicates a vertical location within the cross-section.

Table 4.4 Year 2 to Year 6 changes in median monitored field capacity for the four substrate configurations across all monitored depths.

Test Bed	Change in monitored field capacity (%)		
	Bottom	Middle	Top
1	2.4	3.3	3.5
2	2.0	3.9	2.5
3	3.0	3.0	-1.5
7	2.5	5.4	3.2

Categorising the monitored field capacity values by study year (as per **Figure 4.6**) clearly displays the results of the correlation measure above. Further statistical testing – Kruskal-Wallis test of independence – revealed significant differences (P≤0.05) in the distribution of monitored field capacity over time for the full depth of TB1 and TB2. Supplementary Dunns pairwise comparisons revealed only a significant difference between year 2 monitored field capacity values and all other years for the two uppermost substrate layers. From year 3 onward there is no significant statistical difference in the value of monitored field capacity. The bottom layer of TB1 and TB2 indicated a statistically significant difference between year 2 and years 3, 4, and 5 but falling levels of monitored field capacity in year 6 resulted in no significant difference. For the LECA test bed (TB3) there is no statistical significance in the difference of monitored field capacity between year 2 and year 6. The unvegetated test bed (TB7) exhibits a significant difference in monitored field capacity between year 2 and all subsequent years, yet years 3, 4, 5, and 6 are not significantly different from one another.

In most cases, the presented data suggest that something occurred late in year 2/early in year 3 resulting in increases to field capacity, particularly in the lower substrate layers. Such a clear divide between year-2 and year-3 could indicate the end of the primary consolidation process of the substrate. Consolidation reduces pore sizes, leading to more pores being capable of holding water against gravity, thus improving field capacity. The HLS and SCS substrates are supplied with compaction factors from the manufacturer of 1.25 and 1.12 respectively (Alumasc, 2012). This means that for every square metre and 100 mm of substrate depth (i.e. a volume of 0.1 m^3) 0.125 or 0.112 m^3 of substrate should be ordered to negate the effects of consolidation. FLL characterisation of substrate field capacity is undertaken on compacted substrate samples to replicate established roof conditions. A compaction factor of approximately 1.2 is used, whereby 120 mm of substrate is compacted to a 100 mm depth for testing. The similarity of monitored field capacity values and FLL-derived values from year 3 onward could indicate a similar level of compaction of the in-situ substrates as the FLL test samples. This further suggests that prior to year 3 the in-situ substrates were less consolidated.

Whilst substrate consolidation may have led to the increased values of MWHC, the retention storage capacity of the roof may not have also increased. As MWHC is measured as a percentage, with reducing substrate depths (consolidation) retention

capacity decreases if MWHC is constant. The substrate depths of the Hadfield Test Beds were not monitored over the course of the monitoring programme and so it cannot be definitively said that the identified increases to MWHC have led to corresponding increases in retention capacitates. Assuming consolidation in line with the manufacturer's recommendations for HLS, PWP values equal to those identified by Poë (2016), an initial substrate depth of 100mm, a final substrate depth of 80 mm, and utilising the median values of monitored field capacity for TB1, retention capacity in an unaged TB1 would have been approximately 28 mm compared to 26 mm in an aged TB1. This example highlights the importance of understanding the relationships between substrate physical properties and hydrological performance.

In the upper substrate layers the differences between median monitored field capacity in years 2 and 3 are reduced for vegetated substrate configurations compared to lower layers and unvegetated configurations. This suggests that the vegetation is playing a role in preventing substrate consolidation, an observation that has also been made in bio-filter media (Virahsawmy et al., 2013).

> *The main conclusion from the analysis of retention with roof age is that there is generally evidence of an increase in MWHC between year 2 and year 3, but there is little significant change after this point. If these increases in MWHC are a result of consolidation then substrate depths are required to assess changes in the potential retention capacity of the system.*

4.3.3   Retention Performance by Season

Given that the sub-annual fluctuations in monitored field capacity appear to be greater than multi-annual trends, the data has been aggregated over time and categorised by season to assess the magnitudes of seasonal fluctuations. **Figure 4.7** illustrates the seasonal changes that were observed for monitored levels of field capacity. It can be seen that for every test bed configuration and at every monitored substrate depth, summer field capacity values are lower than those of all other seasons, with winter values being the highest.
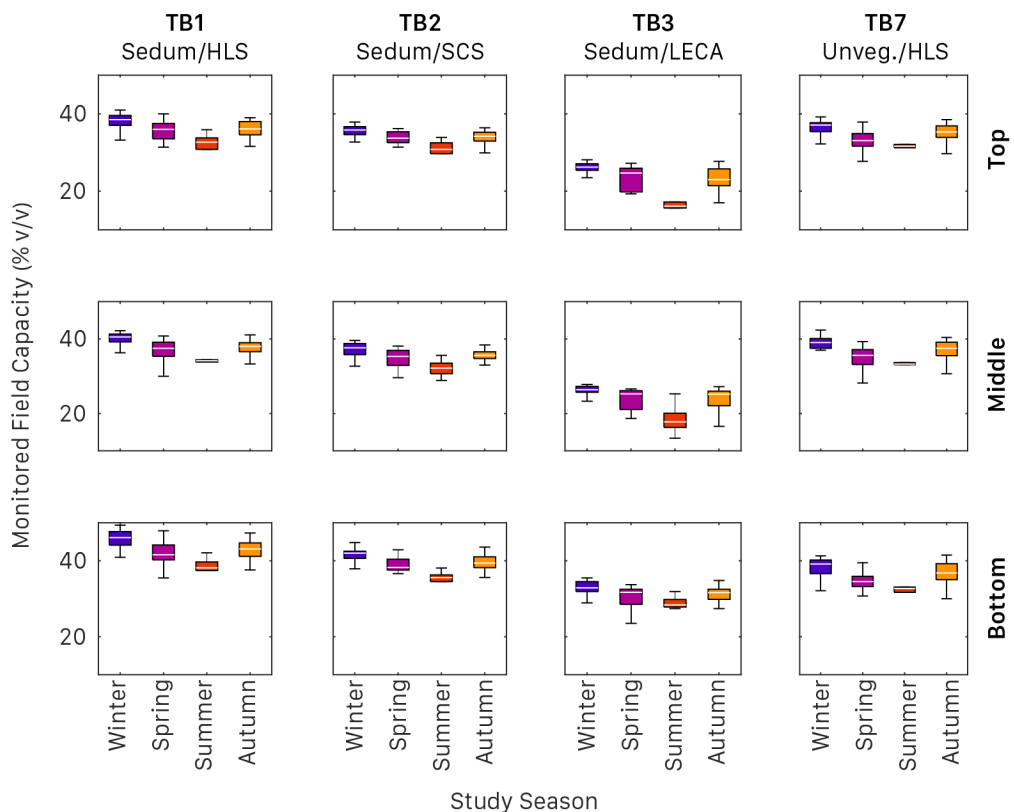
Figure 4.7 Boxplot of monitored field capacity for the four test bed configurations by season. Outliers not shown. Rows of graphs indicate vertical location within cross-section.

An independent Kruskal–Wallis test with Dunn's pairwise comparisons found that for every substrate configuration and at every monitored depth there was a significant statistical difference in the monitored field capacity between winter and summer (P<0.05). The magnitudes of these differences can be seen in **Table 4.5**. In every case autumn and spring results were not statistically different from one another; given the relatively similar climate at these times of year, this was not unexpected.

Table 4.5 Change in median monitored field capacity in Winter compared to Summer for the four test bed configurations and all monitored substrate depths.

Test Bed	Change in monitored field capacity (%)		
	Bottom	**Middle**	**Top**
1	7.8	6.4	5.8
2	5.9	4.3	3.3
3	6.0	9.4	10.2
7	7.0	5.9	5.4

The presence of seasonal trends within the monitored field capacity data closely follows expectations of seasonal vegetation behaviour. However, the presence of seasonal changes also in TB7, which is unvegetated, indicate that this may not be the sole cause. It is possible that a seasonal variation in the substrate's wetting and drying response is being observed. As a substrate dries, just like an ordinary soil, the organic secretions of roots and soil microorganisms become more concentrated. In doing so, these secretions become hydrophobic, actively repelling water. During winter months, frequent rainfall events and low levels of ET prohibit the substrate from drying excessively, preventing the formation of hydrophobic films on substrate particles. Low levels of hydrophobicity allow water to adhere to substrate surfaces, increasing the moisture content. Contrastingly, in summer, there are fewer rainfall events and higher temperatures, allowing for greater depletion of substrate moisture through ET. These conditions allow for the generation of a hydrophobic environment such that at the onset of the next rainfall event water is repelled from substrate particles. This causes rainfall to leave the green roof more quickly and prevents the ingress of water to smaller pores, resulting in lower substrate moisture levels than may otherwise be theorised.

> *The main conclusion from the analysis of retention by season is that there is considerably greater seasonal variation in monitored field capacity than that identified from year-to-year. This significant variation may be of more importance to stormwater engineers than the moderate annual increases.*

4.4 Detention Performance Analysis

4.4.1 Detention Performance by Roof Configuration

Six common detention metrics are presented in **Figure 4.8** for the 9 test bed configurations using the AIE dataset and a minimum runoff threshold of 2 mm. The majority of metrics show marginal differences between roof configuration, with the exception of peak attenuation. For peak attenuation a similar trend to that of retention performance can be seen, with the three LECA substrate test beds (TB3, 6, and 9) having a reduced median peak attenuation compared to the brick-based substrate test beds. An independent samples Kruskal-Wallis test identified two groupings where statistically significant differences existed. Those test beds with either a LECA substrate or that are unvegetated exhibit significantly different peak attenuation performance compared to brick based and/or vegetated test beds. The best performing test bed was TB1 with a median peak attenuation of 81.5%, whilst the worst performer was TB9 with 59.6% when using a 5-minute time step.

As previously stated, common detention metrics like those presented in **Figure 4.8**, including peak attenuation, have their limitations as each metric is not necessarily independent from retention effects. In the case of peak attenuation, the resultant metric can be influenced by the specific rainfall events and the size of time-step used for determination. To address these deficiencies a reservoir routing model, based on that proposed by Kasmin et al. (2010), has been used to provide a more objective and independent mechanism for characterising detention. The optimised values of the reservoir routing scalar D_s parameter fitted using the AIE dataset and a minimum runoff threshold of 2 mm are presented in **Figure 4.9**.

The use of the detention model parameter D_s makes differences between test bed configurations more clear than the common detention metrics presented in **Figure 4.8**. **Figure 4.9** further highlights the presence of previously identified trends in configuration, whereby LECA test beds exhibit the worst performance for each vegetation treatment (a higher value of D_s indicates more rapid runoff, i.e. poorer detention performance). Similar to the results of the retention analysis, unvegetated test beds (TB7-9) exhibit the poorest levels of performance, with very little difference between the performance of sedum or meadow flower vegetation treatments.
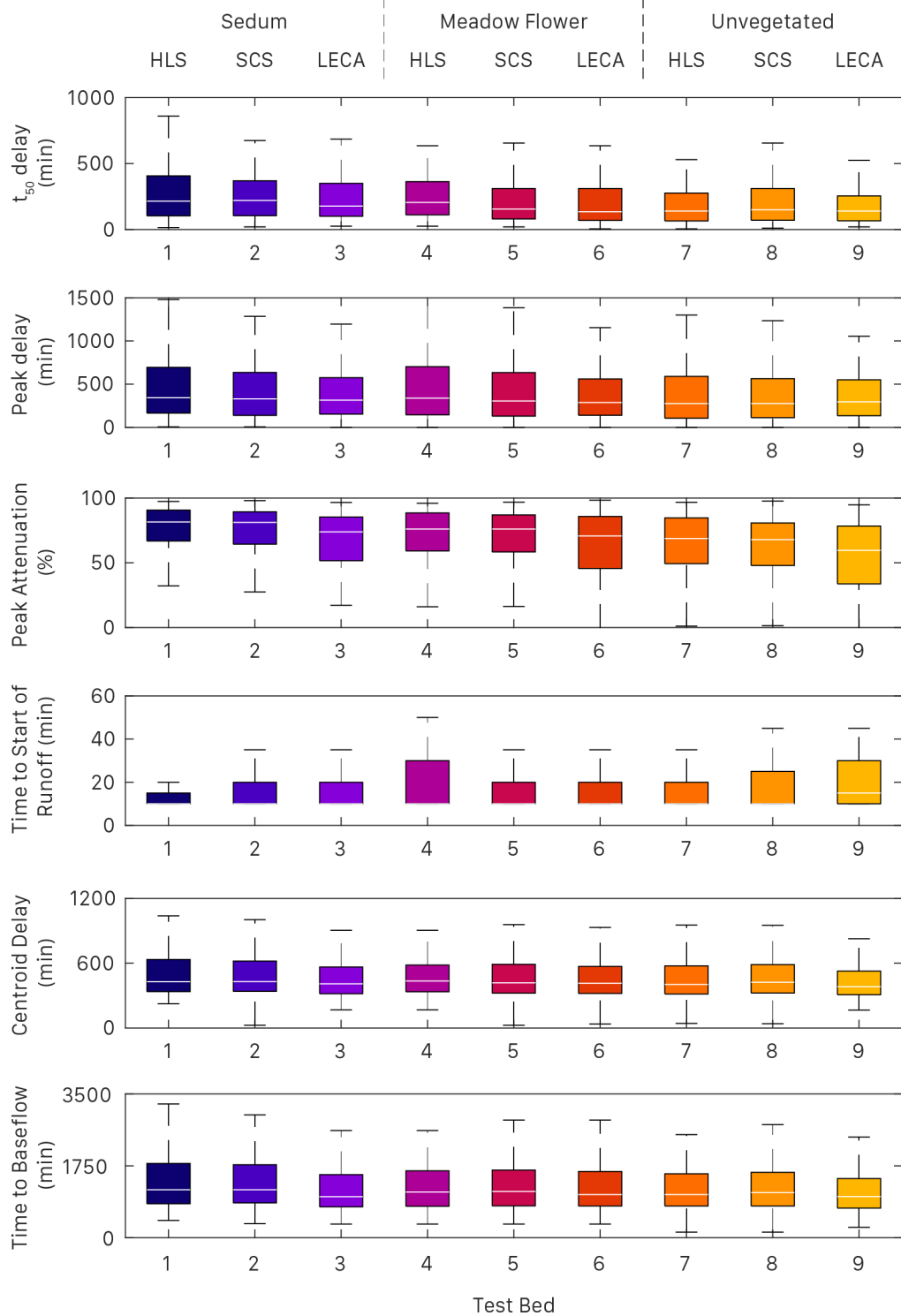
Figure 4.8 Detention metrics for the 9 test bed configurations. Outliers not shown.
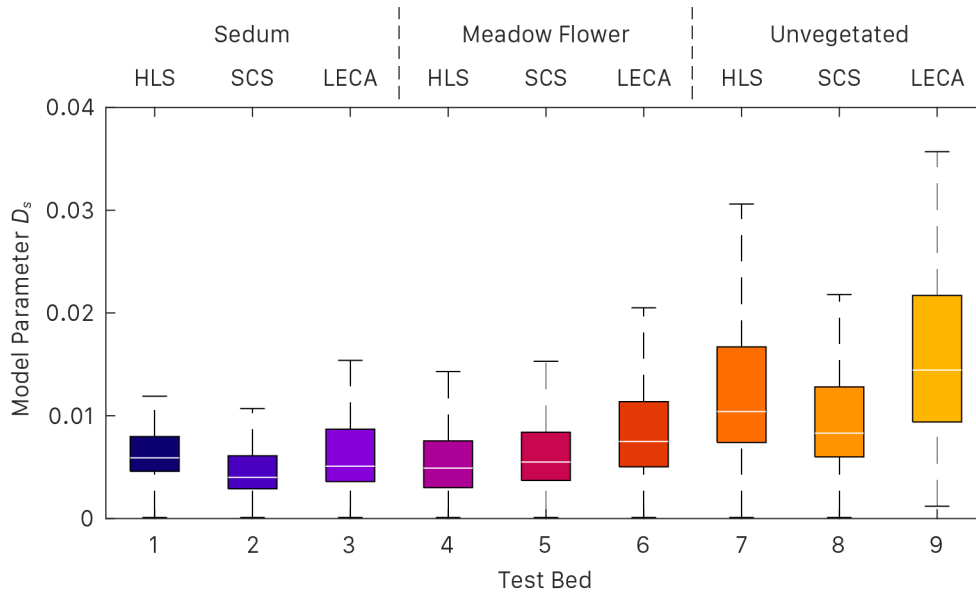
Figure 4.9 Detention model parameter *k* for the 9 test bed configurations. Outliers not shown.

The observed variation by configuration is a facet of many physical substrate properties. Substrate composition has been observed to influence detention performance (Vesuviano and Stovin, 2013), with hydraulic conductivity being an important factor (Yio et al., 2013). The differences in substrate hydraulic conductivity are apparent in the results presented above, with the LECA substrate (highest saturated hydraulic conductivity) having the lowest peak attenuation and highest D_S value. The brick-based substrates (HLS and SCS), with lower saturated hydraulic conductivities, conversely exhibit improved detention performance.

The physical composition of the substrate particles themselves is also important. LECA has 58% of particles between 4 and 8 mm in diameter, compared with 35% for HLS and 40% for SCS. The higher proportion of large, uniformly-sized and rounded particles of LECA results in a substrate with a higher porosity than the angular and varied particles of the brick based substrates. FLL testing methods do not consider substrate tortuosity, but the graded distribution of particle sizes and shapes within the brick-based substrates is likely to increase the number of tortuous paths through the substrate, reducing permeability and increasing detention times (Miller, 2003).

Vegetation type also has a significant effect on detention. The vegetated test bed configurations exhibit lower values of D_S and greater peak attenuation compared with the unvegetated test beds. As no direct observations of soil/root/moisture interactions were made, it is only possible to speculate on exactly how the vegetation

affects the system's detention characteristics. Several mechanisms have been highlighted in related literature, but these remain to be proven for green roof systems. The above-ground vegetation may introduce small delays to the runoff, and it is reasonable to assume that the dense year-round coverage of Sedum will be associated with greater delays that the less-dense seasonal Meadow Flower. The presence of roots is expected to change the size distribution and connectivity of pores compared with the bare/virgin substrate. Soil matrix porosity has been observed to fall by >20% in a conventional soil as a result of plant activity (Bruand et al., 1996). Any reduction in porosity is expected to be reflected in a reduction in permeability and consequently in increased detention. The differences in the detention performance between the two vegetated configurations may also reflect their contrasting rooting types. The mixed Meadow Flower vegetation contains species that have a deeper rooting system compared with the shallower fibrous rooting system of the Sedum vegetation (Snodgrass and Snodgrass, 2006). Root die-back may lead to the development of preferential flow paths and this effect would be expected to be more evident in the seasonal Meadow Flower. In a horticultural setting, particle travel speeds have been found to be 152 times faster than the measured soil matrix conductivity values due to the presence of dead root macropores (Schwen et al., 2011). Further detailed characterisation and discussion of substrate properties is presented in chapters 5 and 6.

> *The main conclusion from the analysis of detention performance by configuration is that conventional detention metrics are not independent of retention effects and are poor descriptors of differences in detention performance arising from system configuration. The application of a hydrological model to simulate detention processes, and its parameters, provide an independent and more descriptive overview of varying detention performance by system configuration.*

4.4.2   Detention Performance with Roof Age

Categorising the generated detention metrics by study year allows for the determination of any trends over time. The majority of common detention metrics displayed limited sensitivity between contrasting configurations, and their ability to describe the subtler effects of ageing is questionable. Of the 6 metrics displayed in **Figure 4.8**, only peak attenuation highlighted any differences in performance associated with test bed configuration. Thus, trends in peak attenuation over time are presented in **Figure 4.10**, where considerable variation can be seen. This variation is more likely to be a result of climatic variation and changes to retention performance than it is a reflection of ageing processes influencing detention performance.
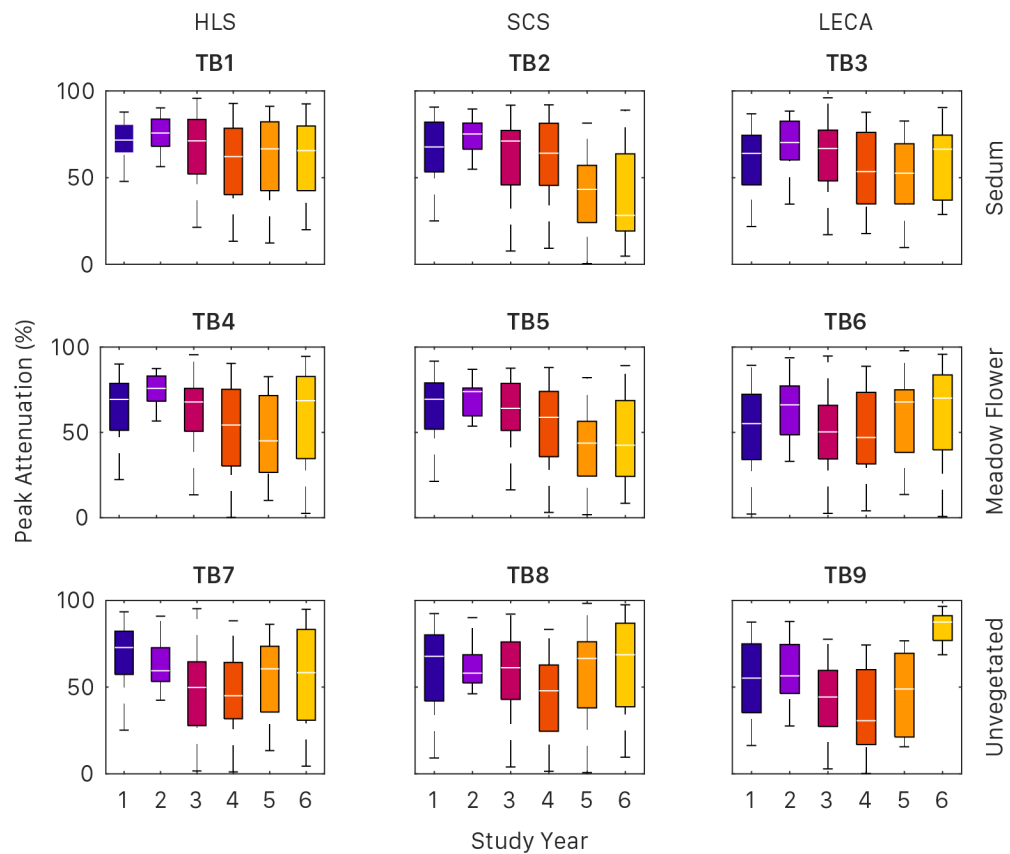
Figure 4.10 Boxplot of peak attenuation over time for the 9 test bed configurations. Outliers not shown.

Using the more objective detention model parameter D_S as an indicator of detention performance over time yields more consistent results than those seen in **Figure 4.10**. A scatter plot of D_S values over time is presented in **Figure 4.11**, where it becomes clear that there is considerable variation in the data. Sub-annual trends are less apparent than those seen for the retention analysis. Best-fit linear trend lines are plotted and clearly show the greatest increase in D_S over time for the unvegetated test beds (TB7-9). This increase in D_S indicates worsening detention performance with age.
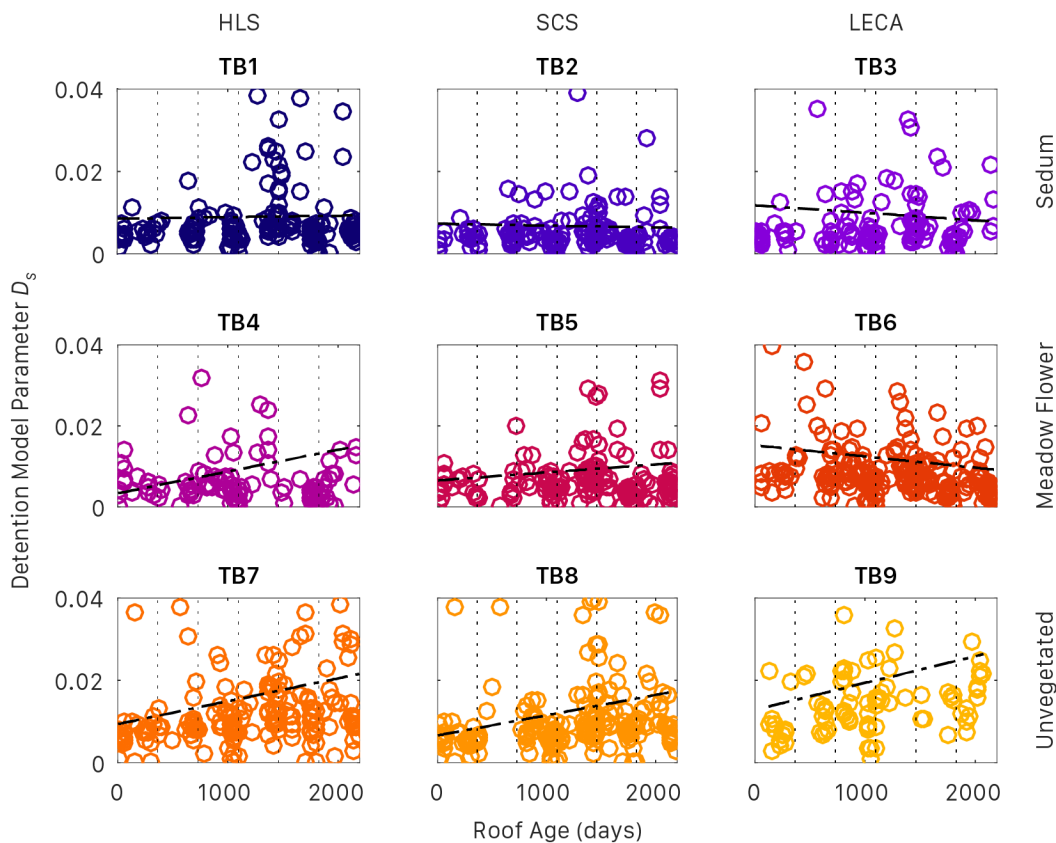
Figure 4.11 Scatter plot of detention model parameter D_S with roof age. Only those points $D_S \leq 0.04$ shown. Dot-dash line represents best-fit linear trend calculated from all data points. Dotted lines indicate study years.

The grouping of D_S values by study year makes the trends over time more visible (**Figure 4.12**) where the increases in D_S for unvegetated test beds can be seen to exceed the vegetated test beds. Vegetated test beds exhibit little or no change in detention performance over the six-year study period when compared to unvegetated systems. The vegetated test beds (TB1-6) exhibit no statistically significant variation in yearly-median D_S and any observed variation does not appear to be systematically related to age. The unvegetated test beds (TB7-9) experience a large variation in the

yearly-median value of D_S, with TB9 showing a steady year-on-year increase. These unvegetated beds have a statistically significant difference in D_S between year 1 and year 6 of the study. Any trends in median D_S for substrate type are harder to identify due to the dominant effects of vegetation. Yet, in the unvegetated test beds, the LECA substrate has a far greater and more consistent increase in median D_S year-on-year compared to its brick-based counterparts.
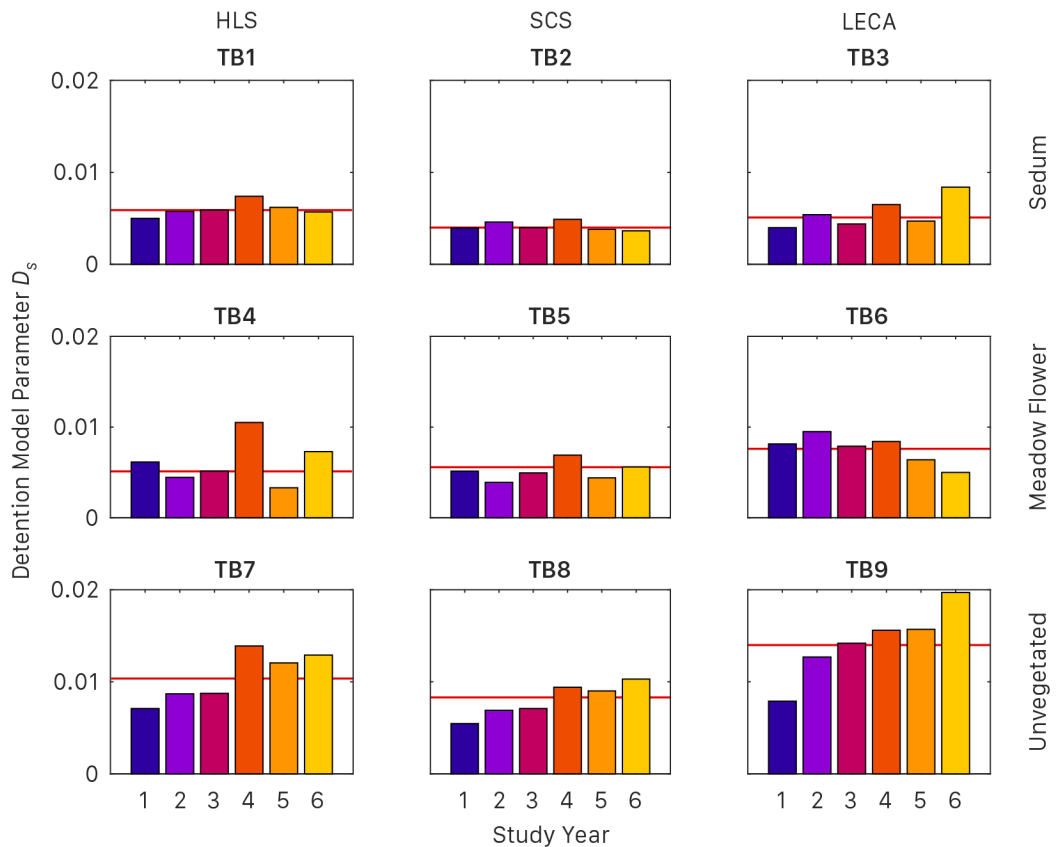
Figure 4.12 Median values of D_S for each test bed configuration across the study period. Red horizontal line indicates overall study median value of D_S.

Table 4.6 Configuration-specific D_S parameter values and goodness of fit statistics.

Test Bed	1	2	3	4	5	6	7	8	9
Median R_t^2	0.91	0.92	0.91	0.92	0.90	0.89	0.89	0.88	0.92
Median D_S (x10^{-3})	5.9	4.0	5.1	5.0	5.5	7.5	10.4	8.3	14.2
Median R_t^2 at median D_S	0.89	0.84	0.86	0.86	0.81	0.82	0.84	0.85	0.81
Change in D_S (Y1 to Y6, %)	11.8	-7.6	95.4	18.7	8.7	64.9	81.7	89.0	160.9

Whilst statistically significant differences in yearly-median D_S have been identified, the model fit of these D_S values is also of importance. The optimal value of D_S, as determined for each test bed and storm event (test bed event-specific D_S), has an associated R_t^2 value of fit. **Figure 4.13** shows that these R_t^2 values have median values typically well in excess of 0.75, indicating a good model fit (1.0 being perfect). Application of the test bed yearly-median and study-median values of D_S to predict runoff results in a reduced R_t^2 compared to the test bed event-specific D_S values. The yearly-median values provide a stronger fit than the study-median value. Therefore, the yearly-median value of D_S provides a better estimation of runoff compared with the study-median value. This observation implies that the six values of yearly-median D_S differ from the study-median, which would not be expected if detention performance were constant throughout the study period.
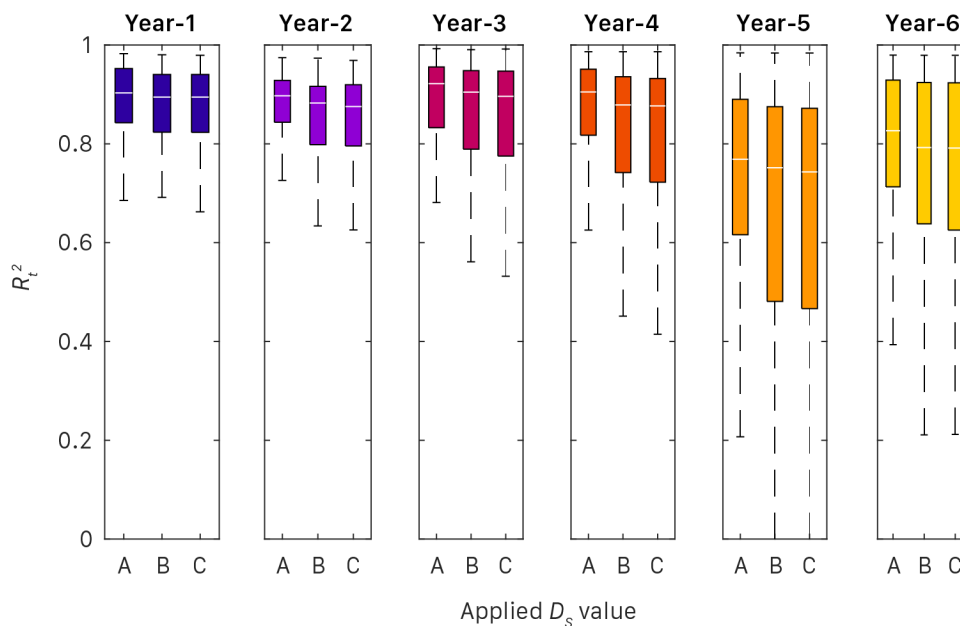
Figure 4.13 R_t^2 distributions of each year of study for different applied D_S values: A = Test Bed Event Specific D_S; B = Test Bed Yearly-Median D_S; C = Test Bed Study-Median D_S.

The steady increase in the value of D_S seen for unvegetated test beds would suggest the cause is a continuously occurring process. The more consistent values of D_S over time for vegetated beds suggest that vegetation helps mitigate against the negative effects of this unidentified process on detention performance. A reduction in detention performance is perhaps unexpected, if substrate consolidation is occurring — as hypothesised from monitored field capacity observations — then detention

performance may be expected to increase. Consolidation reduces substrate pore sizes, potentially reducing the cross-sectional area for water flow, resulting in a reduced hydraulic conductivity and a theorised improved detention performance.

The steady increases in D_s in the unvegetated beds could indicate the steady decay of the initial organic matter content over time. This loss of organic content has been observed in the literature, with Emilsson and Rolf (2005) observing a net loss of organic matter from 3 to 1% over a single year. The impact that organic matter fluctuations can have on green roof hydrological performance are demonstrated by Yio et al. (2013), where a threefold reduction in organic content (Coir) saw peak attenuation fall from >50 to 15%. For TB9, the trend seen in the first 5 years of the study would support this hypothesis of organic content decay, with detention performance deterioration slowing until a steady level is reached around year 4 to 5. However, further deterioration is seen in year 6, which is somewhat unexpected. Further detailed characterisation and discussion of substrate properties is presented in chapters 5 and 6.

> *The main conclusion from the analysis of detention performance with roof age is that for a conventional green roof system, with a crushed brick-based substrate and Sedum vegetation, detention performance is relatively consistent over time. Green roof systems without vegetation or using a LECA-based substrate exhibit an overall reduction in detention performance with age.*

4.4.3 Detention Performance by Season

The retention analysis highlighted that seasonal trends could be more important in defining green roof hydrological performance than year-on-year trends. **Figure 4.14** presents the median D_S values for the nine test bed configurations by season. Similar to the results of the retention analysis, seasonal variation is greater than that seen annually over the entire study period.
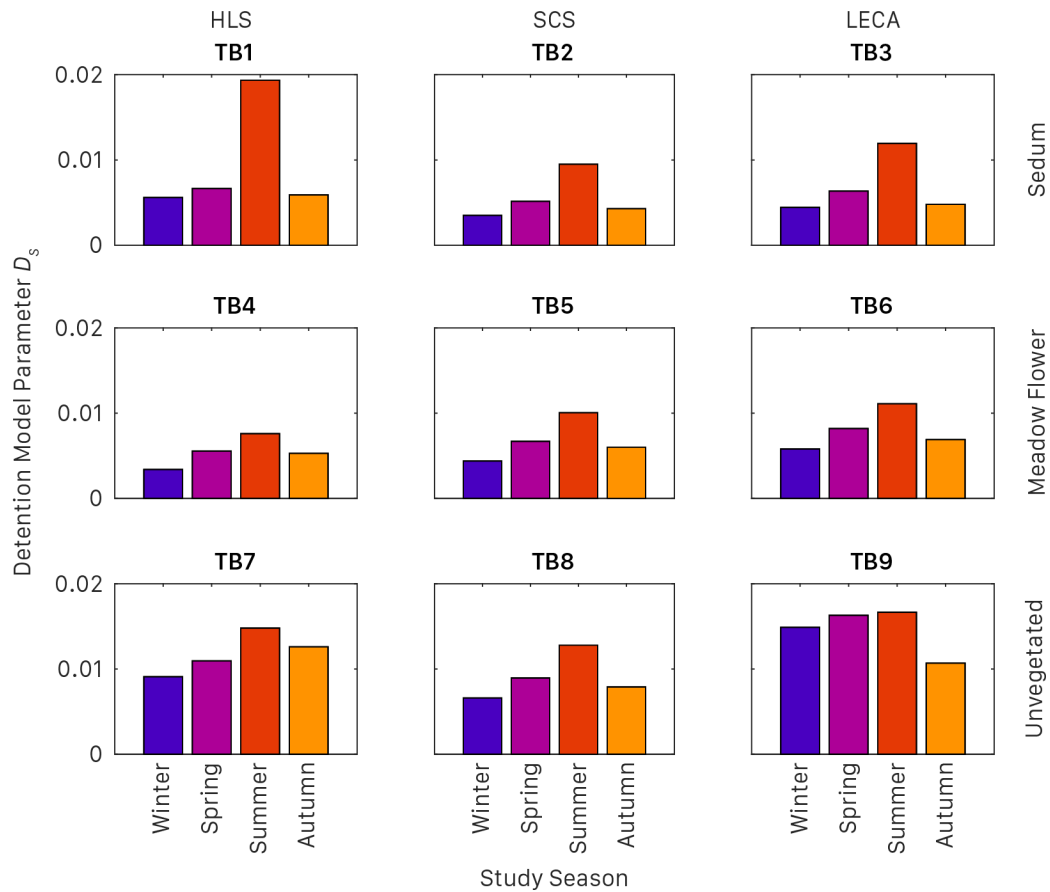
Figure 4.14 Median detention model parameter D_S by season.

Table 4.7 Configuration-specific D_S parameter value changes from Winter to Summer.

Test Bed	1	2	3	4	5	6	7	8	9
Change in D_S (%, Winter to Summer)	245	171	168	123	128	98	62	94	12

Sedum vegetated test beds exhibit the biggest seasonal changes, with D_S increasing by 245% for TB1 in summer compared to winter. Meadow flower test beds exhibit the next highest levels of variation, with the unvegetated test beds having some of the

smallest variation (**Table 4.7**). This relationship is almost directly inverse to that identified for year-on-year trends, with TB9 experiencing the greatest change in D_s over the study period annually, but the smallest change seasonally.

These seasonal trends are thought to be a result of many processes, with the most likely cause being vegetation growth phases, evidenced by the reduced variation seen for unvegetated test beds. Greater levels of variation were anticipated for the meadow flower test beds (TB4-6) due to the deciduous nature of many of the species, which greatly reduced vegetation coverage in winter months. Another key driver of these seasonal changes is thought to be the substrate wetting and drying behaviour, as identified in the retention analysis. Greater substrate moisture during winter months prevents the generation of hydrophobic substrate conditions. Water is then able to move through the small pore networks of the substrate, leading to increased travel times and greater detention performance. Whilst in summer, the more frequent occurrence of extended dry periods generates hydrophobic films on substrate particles. These films prevent water ingress into smaller pores and direct it into preferential flow paths, reducing travel times and thereby reducing detention performance.

The reduced levels of seasonal variation in the unvegetated test beds likely arise from the reduced levels of organic matter and absence of roots. Without these, the generation of hydrophobic conditions is greatly reduced. Combining observations for TB9's year-on-year decline in detention performance — hypothesised to be associated with reducing organic levels — with these seasonal trends, adds additional support to the hypothesis of substrate wetting and drying response being the main driver of seasonal performance variation.

> *The main conclusion from the analysis of detention performance by season are that in conventional green roof systems, with a crushed brick-based substrate and Sedum vegetation, detention performance varies greatly by season. Unvegetated systems see considerably less variation by season, but variation is still observed. This significant variation in detention performance by season is likely of more importance to stormwater engineers than the consistency from year-to-year.*

4.5 Implications of Hydrological Performance Changes

Increases of up to 160% have been seen in the detention model parameter D_S over the 6-year study period, and field capacity has also been seen to increase by up to 5.4%. The effect that this combination of changes has on green roof runoff response will be explored here using an FEH 1–in–30–year 1–hour design storm for Sheffield, UK, with a total rainfall of 29.6 mm (NERC, 1999).

4.5.1   Annual change simulations

Brick-based substrate simulations

Figure 4.15 demonstrates the differences for two test beds installed with the HLS brick based substrate, and incorporates changes in the detention model parameter D_S and the changes in monitored field capacity. Initial losses for the modelling simulation were set at 10 mm in year 1. With a mean 3.1% increase in field capacity seen for TB1 the initial losses for year 6 were adjusted to 10.31 mm. The increased year 6 field capacity translates into an increase in per-event retention of 1.0% for this simulated rainfall event. For TB7, year 6 initial losses increased to 10.37 mm, representing a 1.2% rise in per-event retention performance.
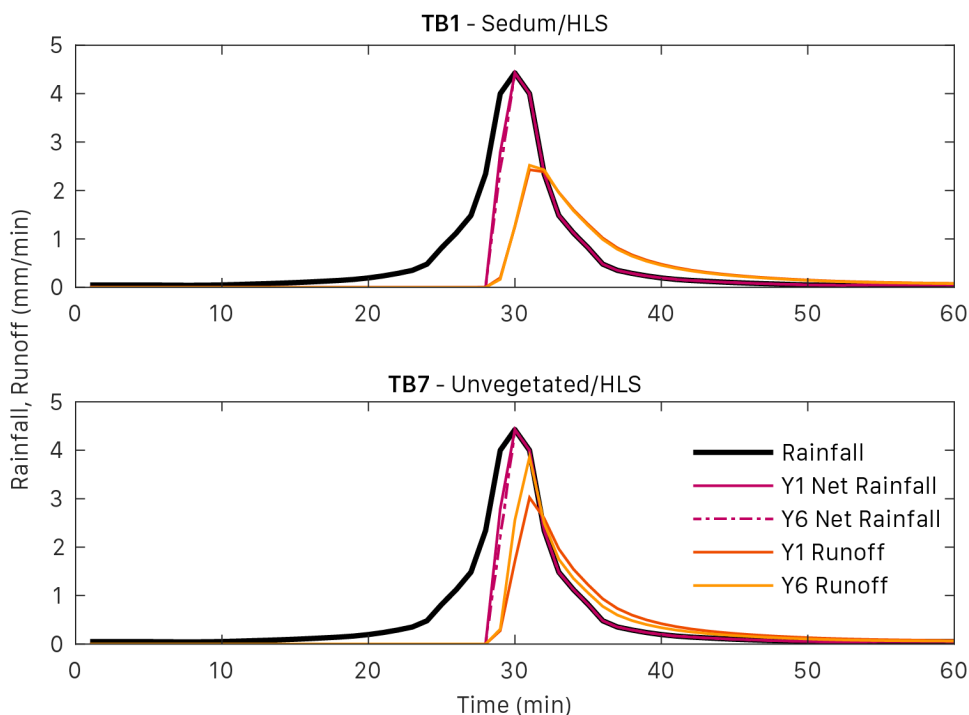
Figure 4.15 Comparison of changes in runoff response for HLS test beds to a 1 in 30 year 60 minute design storm for Sheffield, UK. Runoff profiles are generated using yearly-median values of D_S, and incorporate changing initial losses based on observed changes in field capacity. *Top:* TB1 from Year 1 to Year 6. *Bottom:* TB7 from Year 1 to Year 6.

The detention model parameter, D_S, for TB1 increased by 11.8% from year 1 to year 6, indicating a decline in performance. Inspection of **Figure 4.15** highlights just how small a difference this increase makes to the shape and position of the runoff response profile. Quantifying the change in detention performance using a common detention metric such as peak attenuation — where a 2% reduction is observed — reinforces the greater sensitivity of D_S as a detention metric, first identified in section 4.4.1. Much larger differences are seen in the runoff profile of TB7 from year 1 to year 6, with an 81.6% increase in D_S leading to a 19% reduction in peak attenuation.

LECA substrate simulations

Figure 4.16 presents the results of a similar modelling exercise for LECA test beds. As moisture data were unavailable for TB9, the change in field capacity element of the simulation has been excluded for these test beds and the results only reflect changes in detention performance. Initial losses for the modelling simulation were set at 10 mm. TB9 saw the greatest increase in the detention model parameter D_S of all test beds, increasing by 160% from year 1 to year 6, with TB3 exhibiting the second largest increase (95.4%). These large changes in D_S result in markedly different runoff response profiles for year 6 compared to year 1. For TB9, there is a very minimal detention effect present in year 6, with the runoff profile almost replicating the rainfall from the 31st minute. Whilst TB9 saw the greatest change in D_S, TB3 saw a larger change in peak attenuation, falling by 24.8% compared to a 22.1% reduction for TB9.

These diminishing declines in peak attenuation as D_S increases are not unexpected. As D_S increases the runoff profile will begin to conform to the inflow profile and so detention effects, like peak attenuation, will be minimal. **Figure 4.17** illustrates the relationship between peak attenuation and D_S, which is observed in the peak attenuation reductions of TB3 and 9.

4.5.2 Seasonal change simulations

Seasonal changes in the value of D_S were two orders of magnitude higher than year-on-year changes, being particularly evident in vegetated test beds. **Figure 4.18** highlights the significance of this difference in simulated runoff response for TB1. The seasonal changes lead to a radically different runoff response compared to the multi-annual changes, with summer runoff nearly matching the rainfall from the 31st minute of the storm event, compared to a much more delayed runoff response in winter. As discussed previously, TB1 saw a 2% reduction in peak attenuation from year 1 to year 6, but experiences a 35% reduction from winter to summer. This provides

further evidence that sub-annual (seasonal) trends are more important in understanding *vegetated* green roof hydrological performance than multi-annual trends.
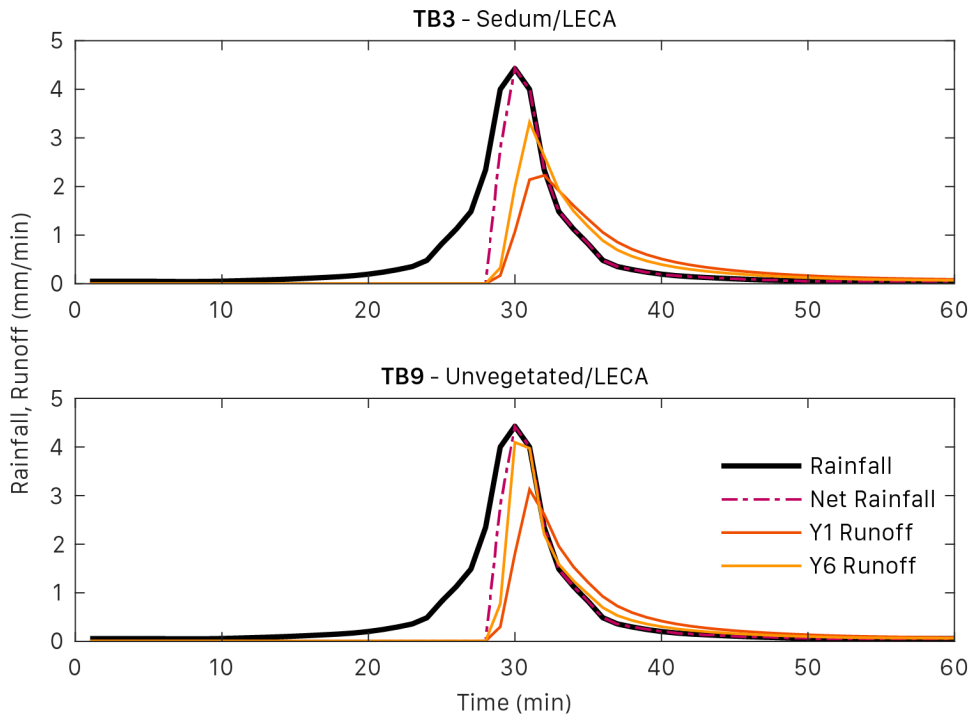
Figure 4.16 Comparison of changes in runoff response for LECA test beds to a 1 in 30 year 60 minute design storm for Sheffield, UK. Runoff profiles are generated using yearly-median values of D_S, and incorporate changing initial losses based on observed changes in field capacity. *Top:* TB3 from Year 1 to Year 6. *Bottom:* TB9 from Year 1 to Year 6.
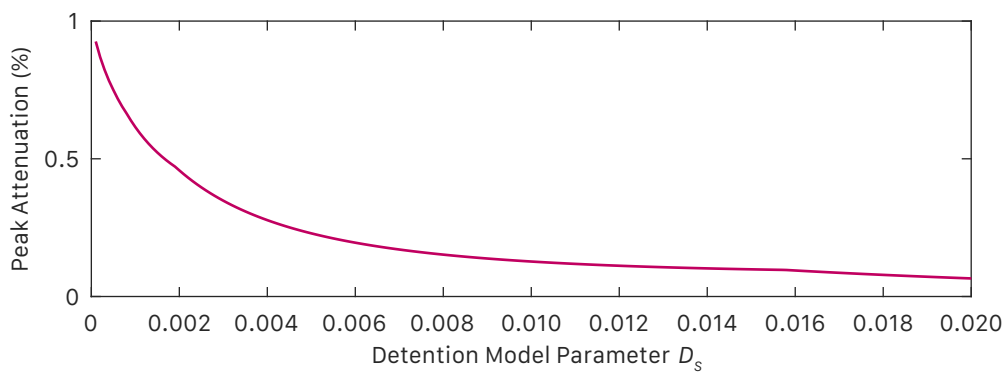
Figure 4.17 Relationship between peak attenuation and detention model parameter D_S for a 1-in-30-year 1-hour design storm for Sheffield, UK, using a 1 minute time-step.
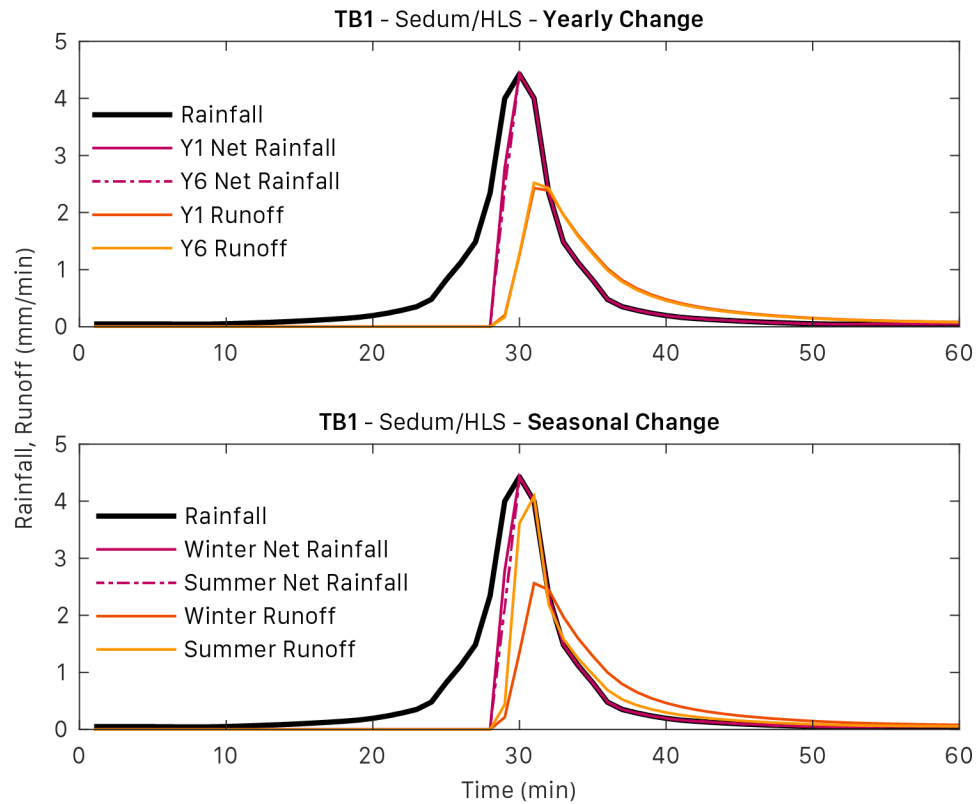
Figure 4.18 Comparison of changes in runoff response to a 1 in 30 year 60 minute design storm for Sheffield, UK. *Top:* TB1 runoff profiles are generated using yearly-median values of D_S, and incorporate changing initial losses based on observed changes in field capacity. *Bottom:* TB9 Runoff profiles are generated using seasonal-median values of D_S, and incorporate changing initial losses based on observed changes in field capacity.

4.6 Chapter Summary

From the identified 503 storm events it was established that roof configuration has an impact on retention and detention performance. The predominant driver of this variation is differences in the physical properties of the substrate, with substrates with a higher MWHC capable of greater levels of retention. In this study, there is very little performance difference between the two brick-based substrates as they have relatively similar physical properties. The contrasting LECA substrate systematically displays the poorest levels of performance due to its lower MWHC and elevated levels of hydraulic conductivity. The type of vegetation treatment exhibited little differentiation between the two types of planting, but contrasted greatly to unvegetated systems where performance was always poorest. This is thought to be due to a combination of effects from the vegetation, whereby plants intercept rainfall and transpire it back into the atmosphere increasing retention performance, and through root action which is thought to stabilise substrate organic content levels enabling increased detention performance.

Monitored trends in substrate field capacity over time suggest an overall increase in retention performance over the study period. The small improvements in retention performance are likely to be the result of substrate consolidation generating more small substrate pores capable of holding water against gravity. Increased consolidation in the unvegetated test bed indicates that root action helps to stabilise retention performance over time. However, the magnitude of these improvements is exceeded by seasonal performance variations and balanced by reduced substrate depths.

For detention performance, seasonal variation again proved to be more evident compared with annual trends. The steady decline in detention performance for unvegetated test beds, compared to the relatively stable yearly performance of vegetated test beds, indicates that organic matter decay is the likely cause of long-term detention performance deterioration.

For both retention and detention seasonal trends the likely driver is the varying wetting and drying response of the substrate. During winter conditions, with frequent rainfall and low ET, substrate moisture levels remain high and substrate hydrophobicity low. This allows water to adsorb onto substrate particles and enter small pores, promoting stronger potential retention and detention performance. Conversely in summer, with more frequent extended dry periods and high ET,

substrate moisture levels are much lower. These low substrate moisture levels lead to the generation of hydrophobic soil conditions, promoting the formation of preferential flow paths. These preferential flow paths prevent the ingress of water into smaller pores and direct it quickly away from the green roof, reducing both the retention and detention performance of the system.

The observed changes in retention and detention performance can be seen to lead to altered runoff responses for both year-on-year and seasonal scenarios. Retention improvements remain small, with sub 1 mm increases to potential storage. Detention performance is greatly altered in some instances, with peak attenuation falling by up to 35% (TB1, seasonal).

All of the above findings help to explain why a Sedum vegetated green roof with a brick-based substrate has become a global industry standard. This configuration is capable of supporting strong levels of retention and detention performance, without significant variation in performance from year-to-year. However, what has been highlighted is the need for further understanding of the substrate wetting and drying response over time. Multiple data sources and methods of analysis suggest that this could be the driver for significant seasonal variation in both retention and detention performance.

The results and discussion presented here will be brought together with the findings of chapters 5, 6 and 7 to provide an overall synthesis and discussion, which will be presented in chapter 8.

5. *Cored Microcosm Study Results & Discussion*

5.1 Chapter Overview

This chapter presents the results from the first phase of X-ray Microtomography experiments, which examined a set of virgin and aged cored microcosms. Extensive image analysis output is presented which characterises substrate porosity, pore size distributions, particle size distributions and tortuosity. The results of numerical modelling of fluid flow using the Lattice Boltzman Method to estimate hydraulic conductivity are also outlined. Physical determinations of substrate characteristics are presented; these results are compared to XMT observations to determine the effectiveness of image analysis methods. The differences in virgin and aged samples, alongside the implications of these changes for hydrological performance, are then discussed. This chapter forms the core of the following publication:
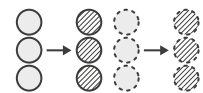
De-Ville, S., Menon, M., Jai, X., Reed, G. and Stovin, V., 2017. 'The impact of green roof ageing on substrate characteristics and hydrological performance'. *Journal of Hydrology*. 547, 322–344.

5.2 Physically derived properties

All 12 microcosm cores (2 substrate types, at virgin and aged conditions, each with 3 replicates) were characterised in line with the FLL (2008) guidance for determining apparent density and MWHC. A determination of hydraulic conductivity could not be made due to the solid bases of the core holders. **Table 5.1** lists all physically determined characteristics for the two substrate types and ages.

Table 5.1 Physically determined properties of the BBS and LECA substrates (Mean values ± Standard Deviation).

Property	Unit	BBS		LECA	
		Virgin	Aged	Virgin	Aged
Particle Size < 0.063 mm	% m/m	0.38 ± 0.34	1.41 ± 0.13	0.66 ± 0.21	1.57 ± 0.28
Median Particle Diameter, d_{50}	mm	4.05 ± 0.40	2.67 ± 0.16	5.07 ± 0.40	5.01 ± 0.49
Dry Density	g/cm^3	0.94 ± 0.00	0.75 ± 0.01	0.66 ± 0.03	0.65 ± 0.02
Density at Field Capacity	g/cm^3	1.21 ± 0.05	1.08 ± 0.04	0.87 ± 0.10	0.93 ± 0.03
Max. water holding capacity, MWHC	% v/v	27.44 ± 5.08	33.34 ± 2.76	21.19 ± 6.89	28.48 ± 1.05

Both substrate types show an increase in the fraction of finer particles for aged samples (**Figure 5.1**). For BBS, this change is across all particle sizes, whereas LECA retains the same percentage of particles over 5 mm in size. This observation is clearly demonstrated in the median particle diameter (d_{50}) values of both substrates and the percentage of particles finer than 0.063 mm. The dry density of the BBS substrate differs greatly between virgin and aged samples, with reductions in density for aged samples. This difference is more likely a facet of substrate heterogeneity and the coring process, than the direct result of ageing processes. LECA samples exhibit a negligible change in dry density with age. The MWHC of both substrate types has increased with age. For BBS there is a 5.9% increase, whereas LECA experiences a greater increase of 7.3%. This change in MWHC represents a restructuring of the substrate's pore space. Compared with previous LECA substrate samples from the literature, the LECA substrate samples of this study are generally more dense, this results in a lower porosity and lower MWHC. There are no previous literature values for the BBS substrate. However, BBS is comparable to the two brick-based substrates described in Chapter 3 (see **Table 3.1**). Unlike LECA samples, the BBS samples of this study are less dense than their literature counterparts and also exhibit lower MWHC values.
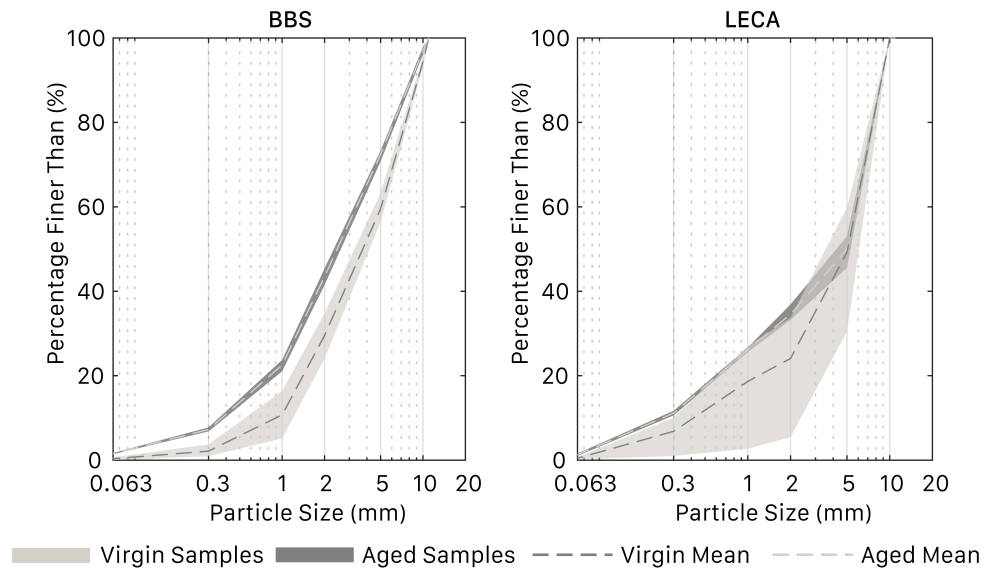
Figure 5.1 Physically derived particle size distributions for the 12 substrate cores. Percentage by mass.

The differences in substrate property values between this study and previous literature may also be a result of substrate sample size. Traditional FLL testing uses substrate volumes of approximately 1.770 l. The cored microcosms of this study have a volume of 0.113 l, 6% of the standard FLL volume. Such small volumes of substrate increase the likelihood of encountering the effects of substrate heterogeneity and of boundary effects. To mitigate against these problems, future studies should consider greater numbers of replicates or a parallel series of full-scale FLL samples to ensure good microcosm representation. Data on the variation of substrate properties as a function of sample size is presented in Chapter 6 as part of the longitudinal microcosm study.

> *The main conclusion from the physically-derived substrate properties is that particle sizes have reduced in both substrate types over time. These particle size changes have led to a reorganisation of the substrate matrix over time such that aged samples exhibit elevated levels of MWHC over their virgin counterparts.*

5.3 XMT derived properties

All 12 cores were imaged with a spatial resolution of 30 μm/pixel. All imaging scans were performed at 180 keV and 110 μA, taking 2400 projections with an exposure time of 250 ms. Total imaging time was 30 minutes per core, producing ~15 GB of image data per scan. Using the image processing protocol set out in Chapter 3 (Section 3.4.5) the raw XMT images have been used to determine substrate porosity; particle size distribution, pore size distribution, tortuosity and an estimate of hydraulic conductivity.

5.3.1 Visual Observations

The images of the substrate presented in Chapter 3 (**Figure 3.12**) provided some insight into the typical geometries of the substrate particles. The un-processed XMT images allow for a more complete observation of the substrates' internal structures and the overall packing matrices. **Figures 5.2** (BBS) and **5.3** (LECA) show a horizontal and vertical section of each microcosm core.

From these figures, the largest BBS particles can be clearly identified to be more irregular and angular than the largest LECA particles, which are more rounded. The angular geometry of BBS creates a more dense particle matrix. The internal structure of the LECA particles is also revealed, with significant internal pore space. These two observations are supported by the substrates' physically determined densities (**Table 5.1**), where the density of BBS is 50% greater than LECA. The finer particles of the substrate matrices can be seen to be unevenly distributed with core depth (particularly $LECA_V2$ and $LECA_V3$) and core position (particularly the horizontal sections of BBS_V2 and BBS_V3, where the lower-right quadrant has significantly more fine particles than any other). This uneven distribution will alter local hydraulic conductivities within the substrate and may also influence the rooting behaviour of overlying vegetation.

The inherent heterogeneity of the substrates is also apparent in the un-processed XMT images, with clear differences in particle sizes and spacing between replicate cores of the same substrate. This heterogeneity, in addition to use of independent virgin and aged cores (as opposed to repeated imaging of the same sample), makes changes that can definitely be attributed to age difficult to identify with confidence in these 2D representations alone.
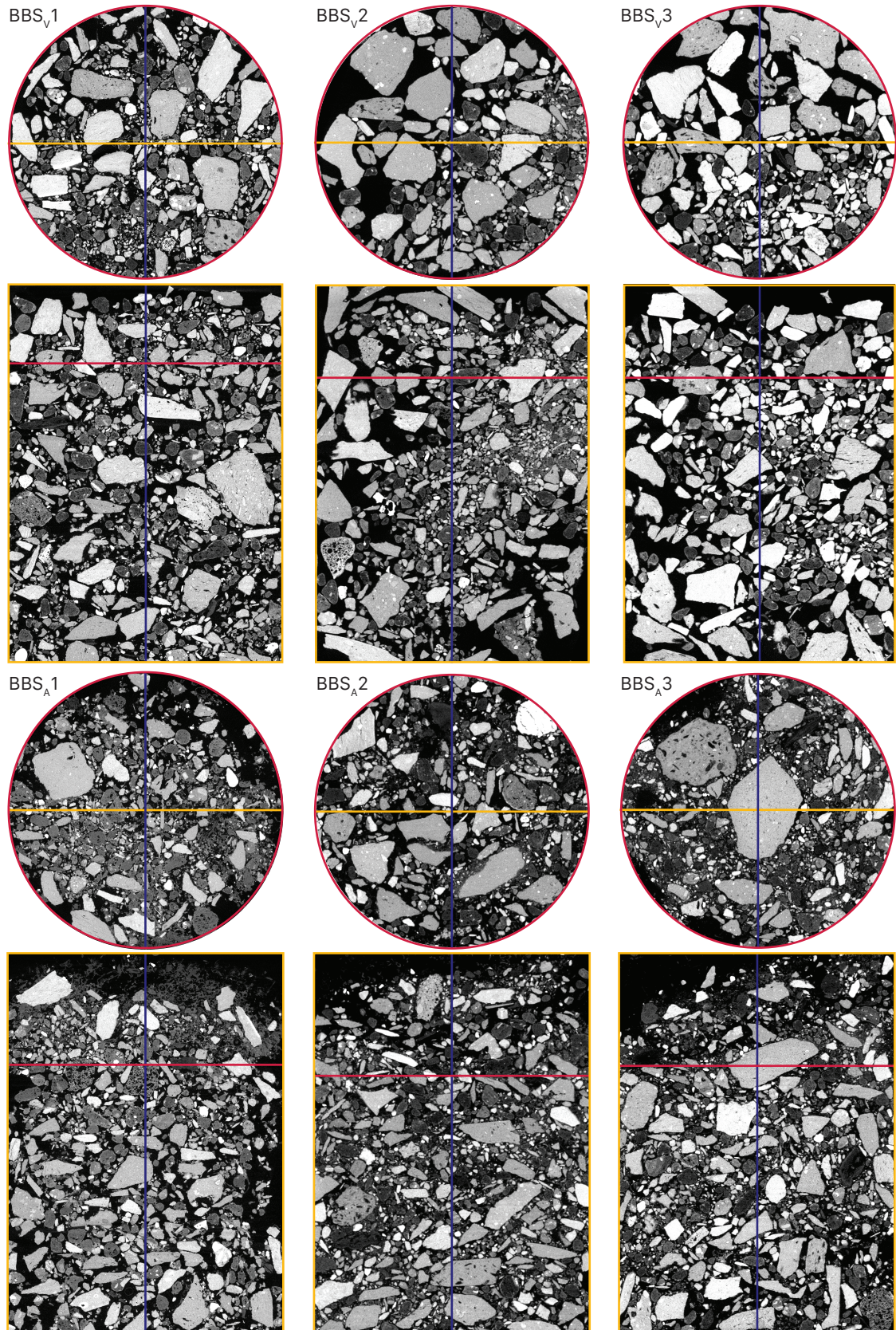
Figure 5.2 Examples of raw XMT output for BBS. 2D slices through the horizontal axis (Red lines) and a central vertical axis (Yellow lines), all samples are 46 mm across.
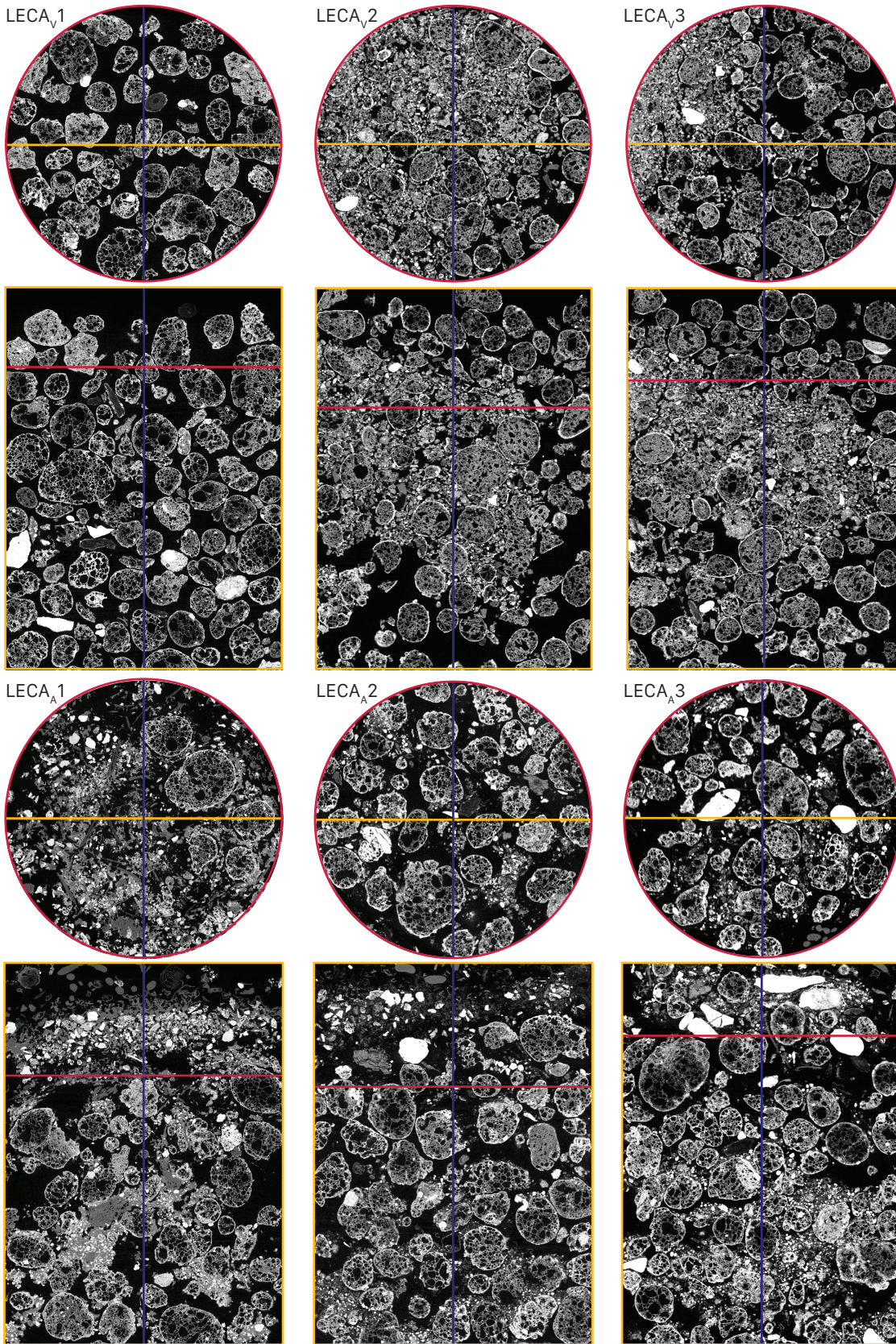
Figure 5.3 Examples of raw XMT output for LECA. 2D slices through the horizontal axis (Red lines) and a central vertical axis (Yellow lines), all samples are 46 mm across.

5.3.2 Porosity

Microcosm porosity is determined by the segmentation of the median filtered XMT images into particle and pore regions. Typical output of this segmentation is shown in **Figure 5.4** for the same horizontal 2D slices shown in **Figures 5.2 and 5.3**.

The quality of segmentation is very important to achieving a reliable image processing result, as it influences all subsequent processing steps. Image segmentation is highly subjective, small variations in thresholding limits can significantly alter the volumes of pore or particle regions. It is therefore the key step in the image processing protocol. Comparing the 2D core representations in **Figures 5.4 and 5.2/5.3**, it is clear that the particles with the greatest contrast between themselves and the surrounding pore space are reliably segmented. However, those particles and clusters of particles where this contrast is much lower are less reliably resolved. This problem arises due the large difference in density of the particles that make up the substrate matrices. If all particles were of the same density, greater contrast could be achieved between pore space and particles, allowing for a higher quality segmentation. To mitigate the effects of subjective thresholding, constant greyscale values were assigned to known materials (the core holder and background) and thresholds decided based on these values.

Compared with the BBS samples, total porosity is elevated in LECA samples (**Table 5.2** and **Figure 5.5**), due to a significantly higher amount of ineffective pore space, internal to the LECA particles. This is not unexpected given the nature of the expanded clay mineral component of LECA. Inspection of **Figure 5.3** in conjunction with **Figure 5.5** shows that for the first virgin LECA sample (LECA$_V$1) there is a visibly greater pore space area (more black pixels) than either LECA$_V$2 or LECA$_V$3. This clearly demonstrates the heterogeneity that exists even within replicate samples of the same substrate and age. Mean values of porosity (**Table 5.2**) show a decline in both effective and ineffective porosity in aged LECA when compared with the virgin samples.

Table 5.2 Mean and standard deviation porosity, ϕ, values for the two substrate types

Substrate	Total, ϕ_T (%)		Ineffective, ϕ_I (%)		Effective, ϕ_E (%)	
	Virgin	Aged	Virgin	Aged	Virgin	Aged
BBS	35.80 ± 0.38	33.29 ± 6.37	0.17 ± 0.01	0.17 ± 0.07	35.63 ± 0.38	33.07 ± 6.44
LECA	46.45 ± 8.55	41.81 ± 7.30	6.56 ± 3.14	6.36 ± 0.98	39.89 ± 5.51	35.45 ± 8.16
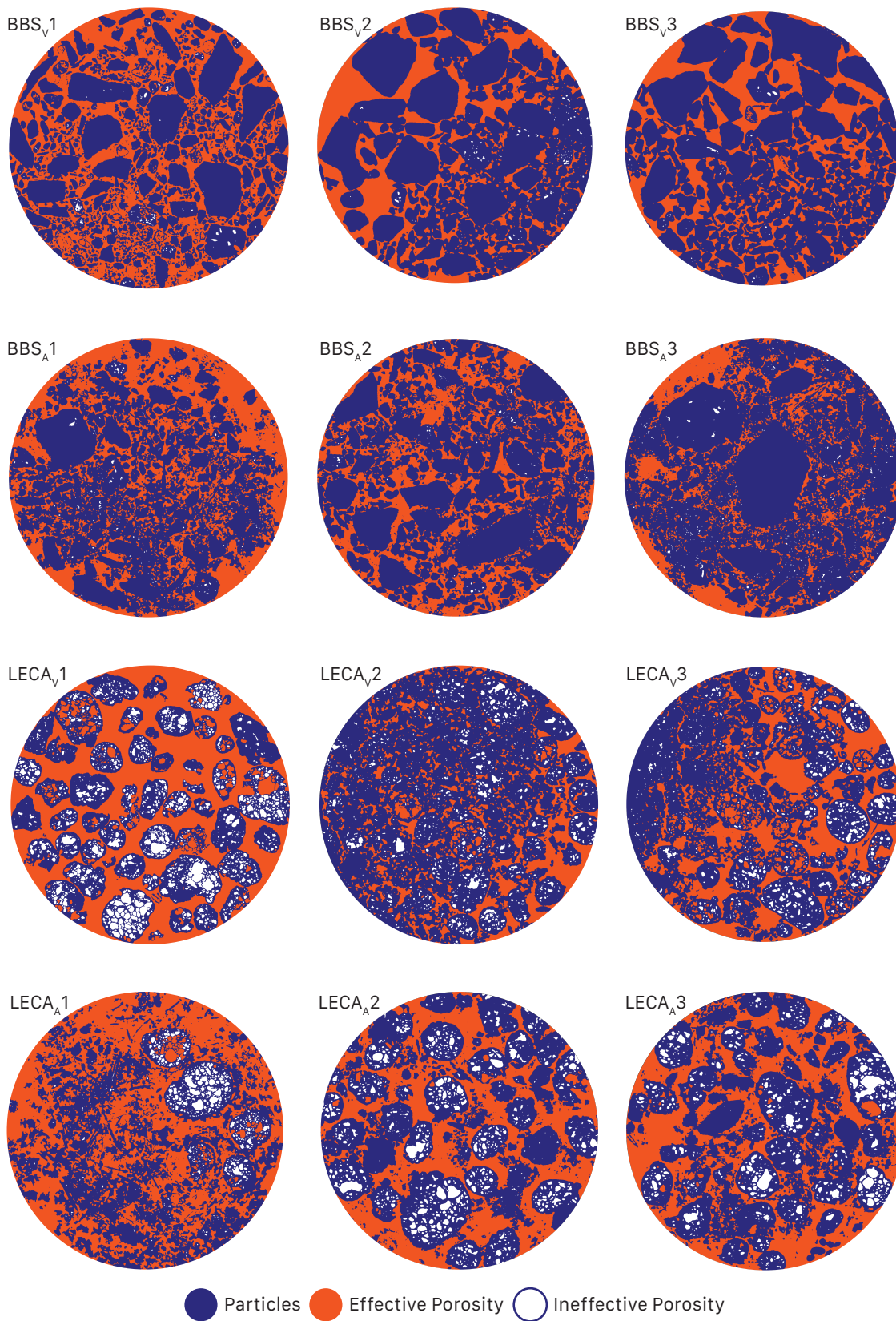
Figure 5.4 Segmented porosity images of the 12 cores.
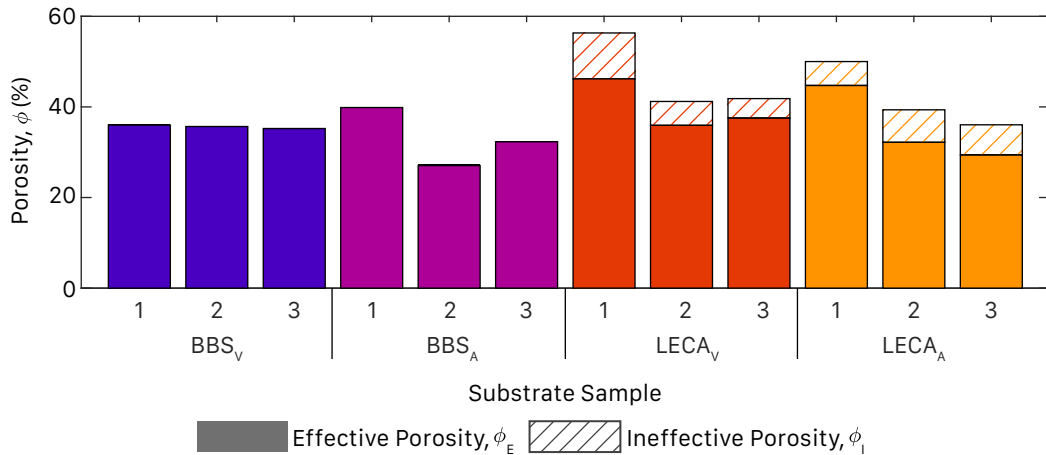
Figure 5.5 Porosity values for the 12 substrate cores

5.3.3 Particle Size Distribution

The particle regions of the binary images shown in **Figure 5.4** were separated into individual particles using the *Separate Objects* module of *Avizo*. The separated particles within the 3D volumes were then analysed and a particle size distribution determined. Due to a lack of information on individual particle density, XMT particle size distributions are presented as a 'number of particles finer than.' This differs from a physically determined PSD which is typically presented as a 'mass of particles finer than.'

Figure 5.6 illustrates the results of particle separation for the same 2D horizontal slices as **Figures 5.2 and 5.3**. The quality of separation is generally good, particularly for the virgin BBS samples. Where small particles are heavily clustered (e.g. the lower right quadrant of BBS_A3) separation is poorer, with clusters of touching particles being misidentified as a single object. Greater separation performance for these types of particle clusters could be achieved with raw images of higher contrast and subsequent re-segmentation. However, this would be difficult to achieve for the reasons discussed in Section 5.3.2. Analysis was performed using the data as presented, but with awareness that the number of small particles was systematically underestimated. The highly porous nature of the LECA particles also presents a challenge for the separation algorithms. In almost all LECA images there are cases where a single LECA particle (as identified in **Figure 5.3**) is seen to be separated into multiple sub-particles. Attempts to mitigate this were taken by filling ineffective pores before particle separation. However, the presence of effective pore space internal to the particles still generated these fractured LECA particles. Therefore, larger particle sizes are systematically underestimated for LECA.

BBS$_V$1 BBS$_V$2 BBS$_V$3

BBS$_A$1 BBS$_A$2 BBS$_A$3

LECA$_V$1 LECA$_V$2 LECA$_V$3

LECA$_A$1 LECA$_A$2 LECA$_A$3
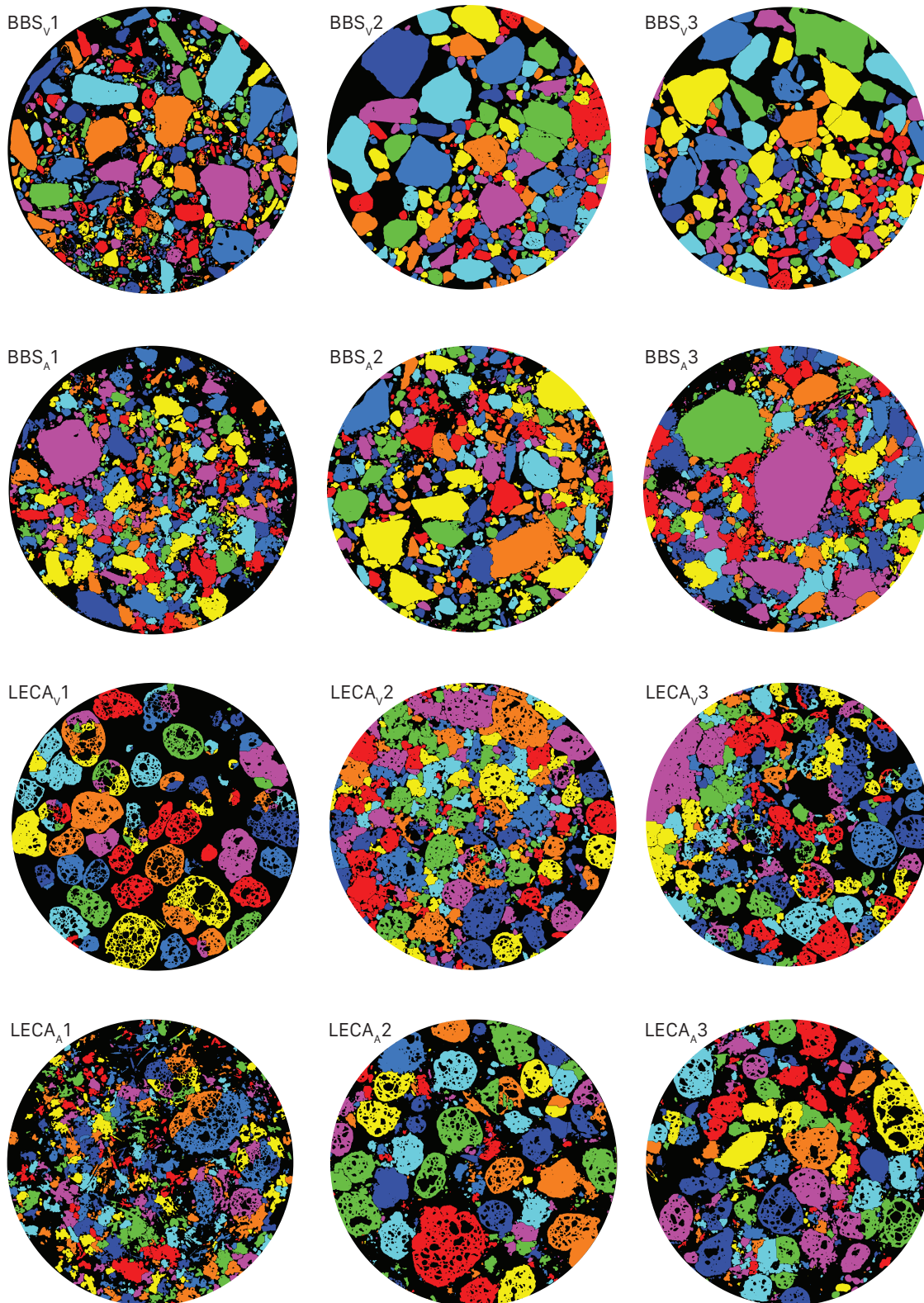
Figure 5.6 Separated particle images of the 12 cores. Note that particles are randomly coloured to aid identification, colours do not relate to any physical property, the same colour does not necessarily indicate that particles are connected where they are clearly separated.

Given the difficulties highlighted above it is possible that the determined PSDs underestimate the number of the largest and smallest particles within each core. However, as **Figure 5.7** illustrates, the majority of particle size differences between the virgin and aged cores occurred in the central regions of the pore size distributions (i.e. from 0.1 to 2 mm).

The particle size distributions for both substrate types indicate a shift towards a matrix with more finer particles with age (**Figure 5.7**). The median particle diameter (d_{50}) decreased from 2.16 mm to 0.59 mm for BBS samples, this represents a 73% reduction. LECA samples see a larger decrease in median particle diameter, falling from 2.62 mm to 0.27 mm, a reduction of 90%. These values are not directly comparable with d_{50} values from the physically-derived PSDs, with the reduction in the XMT-derived d_{50} for the LECA samples over time not being observed in the physically-derived PSD results. However, the XMT-derived BBS particle size distribution exhibits similar trends to the observed physical reduction in d_{50} between virgin and aged samples. The complexity of LECA's internal structure and the difficulties encountered in particle separation of LECA cores are the likely cause of this disparity between the XMT-derived and physically-derived results.
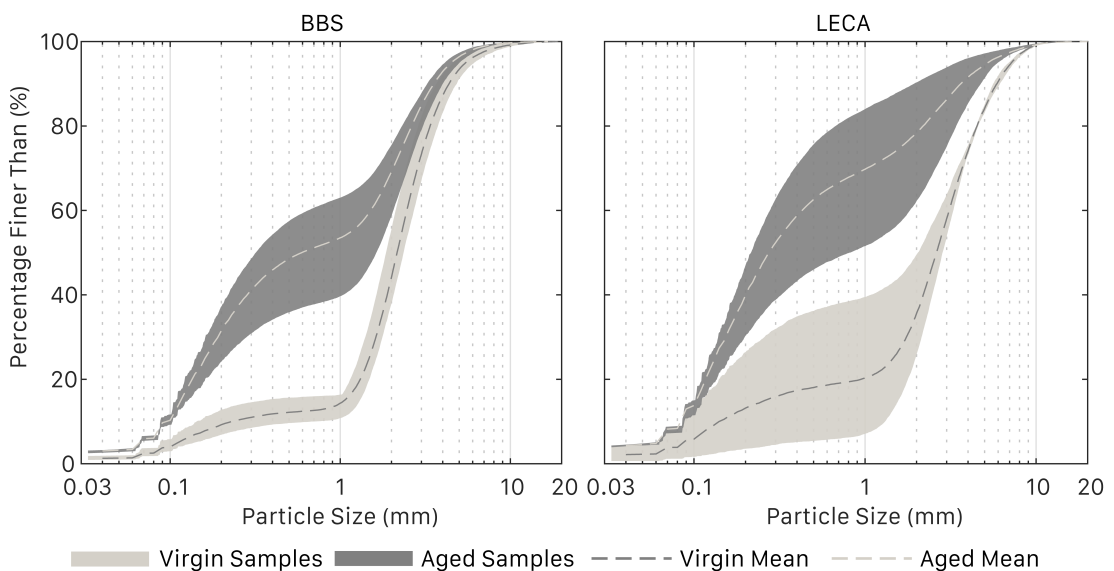
Figure 5.7 Particle size distributions for the two substrate samples. Percentage by number of particles.

The heterogeneity between the samples of the same substrate type and age can also be clearly seen by the indicated range of values. The virgin BBS samples are much more alike than any other set of replicate age samples. This is consistent with the narrow range of porosity values identified for the virgin BBS substrate. Whilst particle

size distribution is a controlled characteristic by the FLL guidance, this is mainly as a surrogate indicator of pore size distribution, which is the dominant characteristic for the control of hydraulic functions. With this in mind, the potential inaccuracy of the XMT-derived PSD is unimportant, provided a reliable measure of pore size distributions can be determined.

5.3.4 Pore Size Distribution

The pore regions of the binary images of **Figure 5.4** were processed in *ImageJ*, using the *BoneJ* plugin (Doube et al., 2010), to determine the pore size distributions. The resulting pore size maps of **Figure 5.8** show the typical output of this analysis for the same 2D slices as **Figures 5.2 and 5.3**. Note the missing internal pores of some LECA particles, this is due to a sizing of only the effective pore space within the core. A continuous colourmap is applied to the image to identify the pore diameter at every point within the pore space region. Using this colourmap it is possible to infer the regions of the substrate that will retain water for a greater length of time, with the smaller pores retaining water longer than larger free-draining pores.

The 2D pore size maps (**Figure 5.8**) show a general trend of larger pore spaces within the LECA substrates, with BBS substrates having only localised occurrences of large pore spaces. This can be seen to be true of the entire core volumes when inspecting the pore size distributions shown in **Figure 5.9**. Greater volumes of smaller pore spaces can result in higher levels of MWHC, provided that these pores have a diameter of 50 µm or less. Physical determination of MWHC showed elevated levels in BBS compared to LECA, this is a direct result of the greater volume of small pores, as identified using XMT. The resolution of the XMT images, 30 µm, prevents the full identification of regions where water is held against gravity (0.2 to 50 µm) and so an XMT-derived estimate of MWHC is not possible.

The greater disconnection of the larger pore spaces in BBS is also responsible for its reduced hydraulic conductivity compared to LECA (**Table 3.9**). This disconnection inhibits the free flow of fluids through the pore matrix and results in lower values of hydraulic conductivity. More heterogeneity can be seen in the pore size distribution for BBS than LECA, this is contrary to many of the other determinations of BBS properties. This observation is due to the increased complexity of the BBS matrix — with its angular particle shapes — compared to the more uniform LECA matrix.
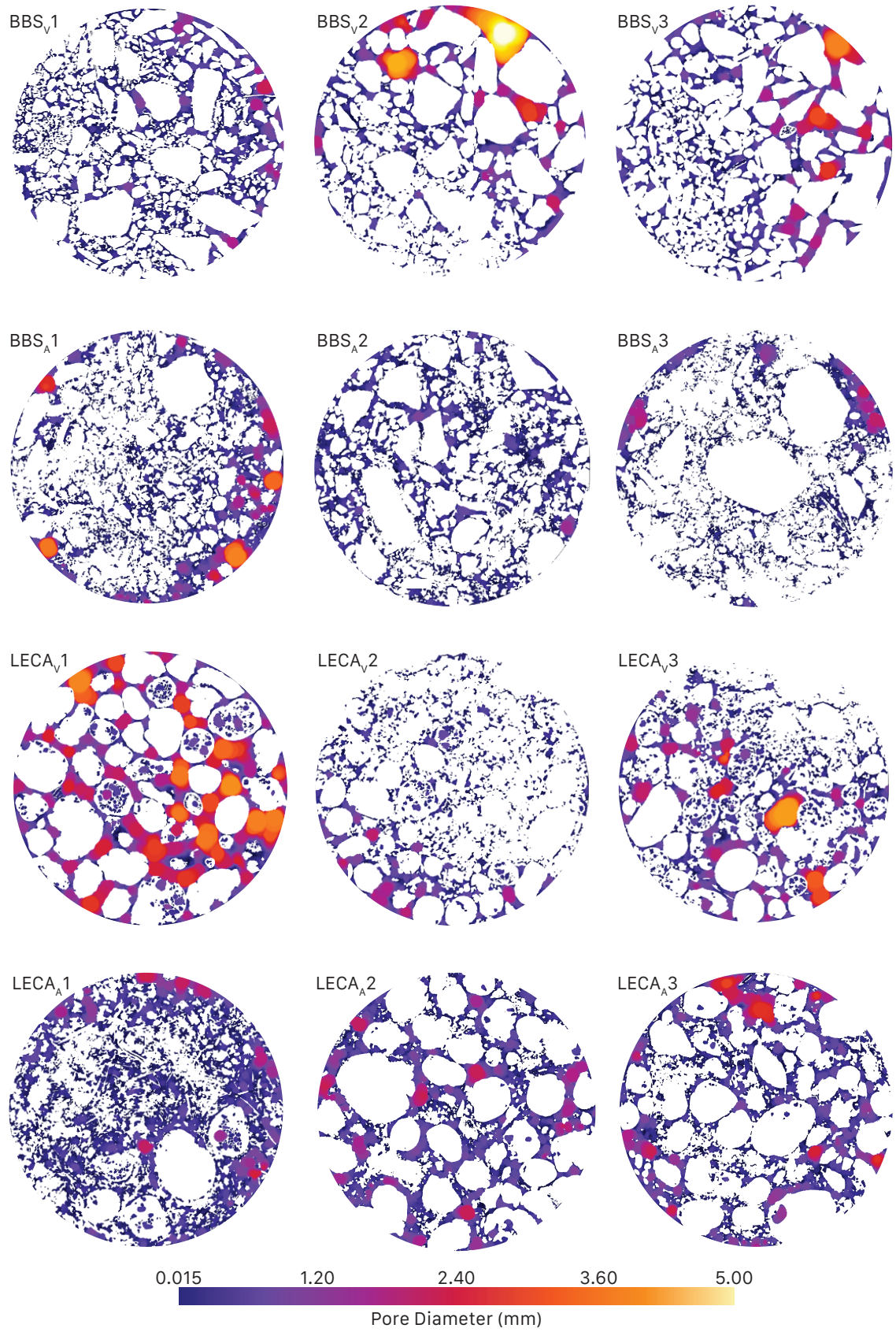
Figure 5.8 Pore size maps of the 12 cores.

Like the particle size distributions, the pore size distributions also exhibit a shift to finer pores with age (**Figure 5.9**). This shift in pore sizes is more subtle than that seen for particle sizes. The median pore diameter of BBS samples fell by 55% from 1.07 mm to 0.47 mm. LECA samples exhibit a smaller reduction in median pore diameter, falling from 1.55 mm to 1.05 mm, a reduction of 33%.
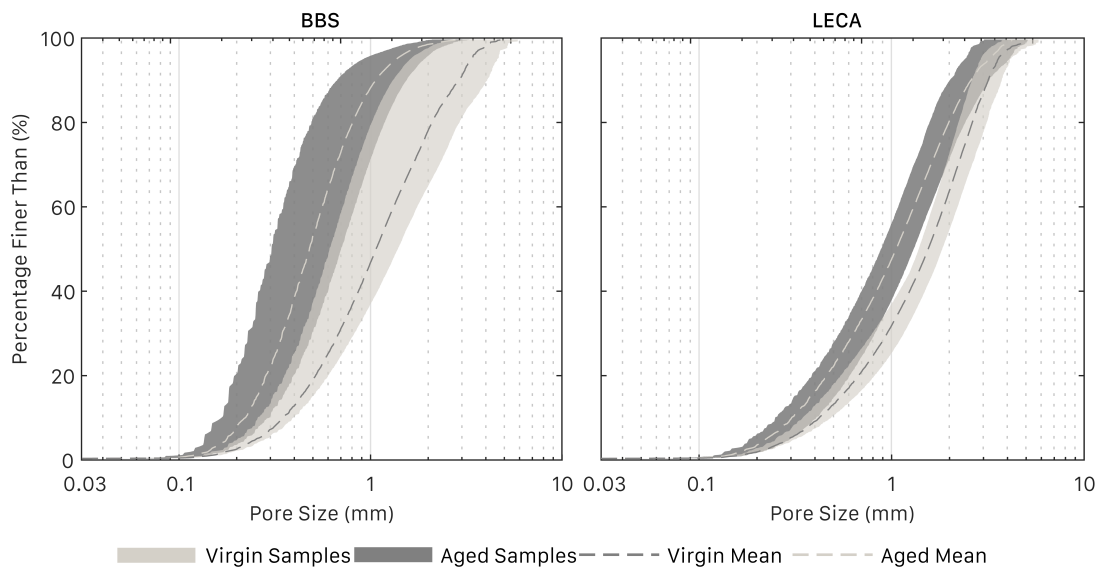
Figure 5.9 Pore size distributions for the two substrate samples. Percentage by volume of pores.

Physically-derived pore size distributions are difficult to obtain, due to the required use of hazardous materials (i.e. mercury, in traditional porosimetry techniques) or prohibitively small samples (as used in water release methods). Previous characterisation of the water release behaviour for BBS, and the subsequent transformation of this data to obtain a pore size distribution, proved to be ineffective due to sieving of substrate samples prior to testing. This sieving altered the particle size distribution of the substrate and subsequently the substrate matrix. Pore size comparisons between this previously tested matrix and the matrices of this study are therefore not possible.

Pore size distribution and the establishment of a vertical moisture profile

The presence of a vertical moisture profile was identified in Chapter 4 (Section 4.3.2). The exact mechanism behind its existence was hypothesised as being a result of the leaching of fines into deeper substrate layers, leading to a reduction in pore sizes (Berretta et al., 2014; Mordibelli *et al.*, 2011, 2013). The flexibility of the XMT image analysis technique allows for the characterisation of pore sizes with sample depth, enabling investigation of this hypothesis.

The moisture probes located within the Hadfield Green Roof Test Beds, from which the presence of a vertical moisture profile was observed, are spaced at 20 mm intervals over the central 20 to 60 mm of the full 80 mm substrate depth. Whilst the cored microcosms of this study extend to only 68 mm of the full substrate depth, they do encompass the positions of the 3 moisture probes.

Characterising changes in a complete pore size distribution over depth is particularly challenging due to the significant amount of data that is generated. To efficiently assess any changes in pore size distribution with depth, two pore size metrics were examined: median pore diameter; and the percentage of pores with a diameter <100 μm. This pore diameter is twice that of the corresponding field capacity suction, but the identification of smaller pores is compromised with a working image resolution of 30 μm.

Figure 5.10 illustrates the median pore diameter, d_{50}, for the all 12 cores over their full 68 mm depths. To support greater levels of MWHC a greater volume of small pores is required, and a greater volume of small pores will reduce the value of d_{50}. At substrate depths of between 0 (the surface) to 10 mm, d_{50} rapidly reduces as the number of pores directly open to the atmosphere reduces. With increasing depth below 20 mm, the value of d_{50} does not generally continue to decline but remains relatively stable. At a depth of 60 mm (the location of the deepest moisture probe) d_{50} is typically the same, or greater than, at a depth of either 20 or 40 mm. This does not support the hypothesis of reduced pore sizes lower in the profile being responsible for the presence of a vertical moisture profile.

Figure 5.11 presents the percentage of pores with a diameter of <100 μm for the all 12 cores over their full 68 mm depths. A greater number of pores with a diameter of <100 μm may be an indicator of increased moisture retention potential. Greater variation can be seen across the depth of the substrate compared to values of d_{50}. **Figure 5.11** also helps to explain the increased MWHC of the BBS substrate samples compared to LECA, as all BBS samples typically have greater quantities of pores <100 μm across their full depths. $LECA_A2$ and $LECA_A3$ begin to show steep rises in the percentage of pores <100 μm at depths below 60 mm, this could indicate an increased potential for moisture retention at depth for aged LECA substrates. However, there is no significant evidence of a greater number of small pores at depths corresponding to the location of the deepest moisture probe (60 mm).
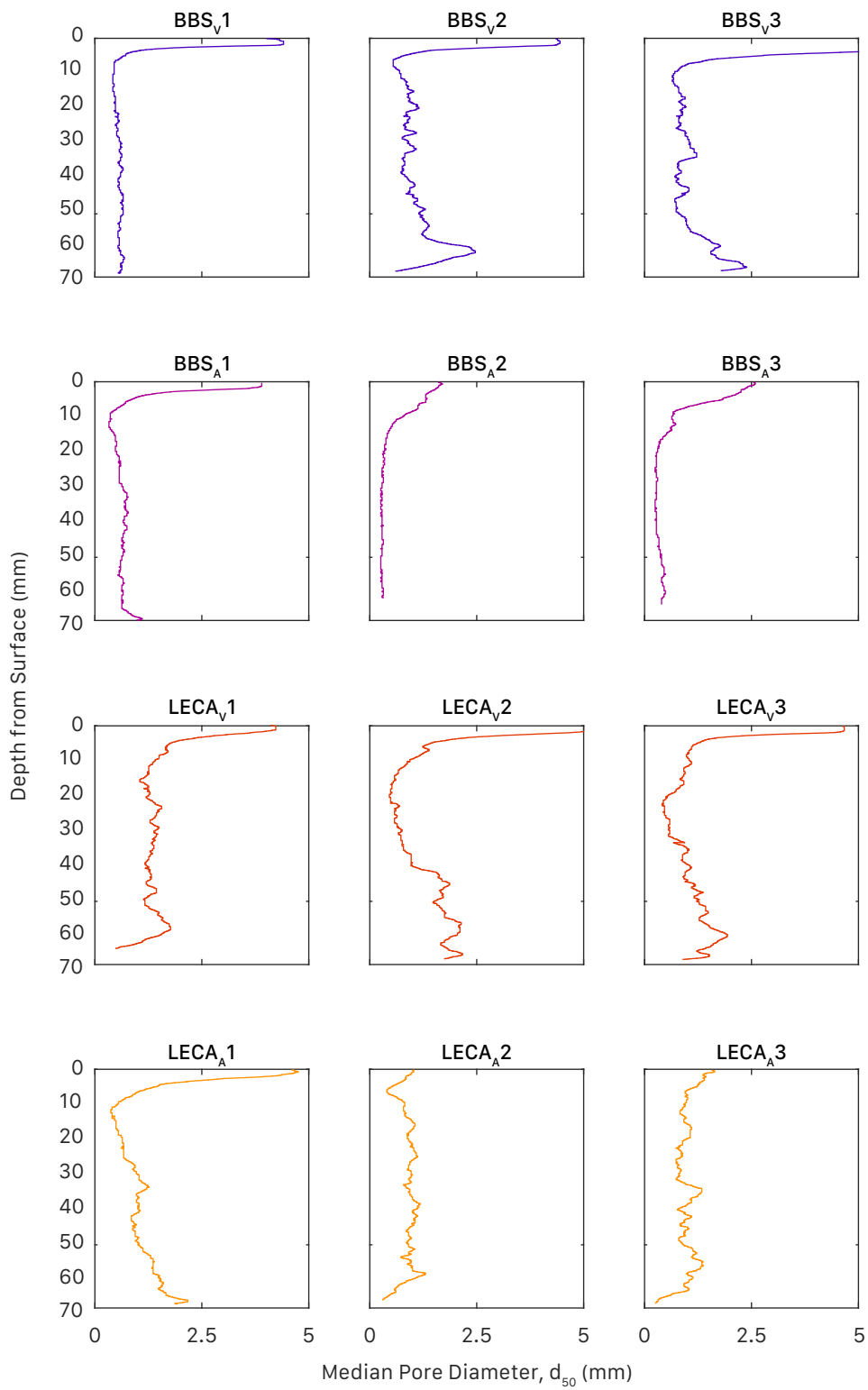
Figure 5.10 Median pore diameter, d50, across core depth
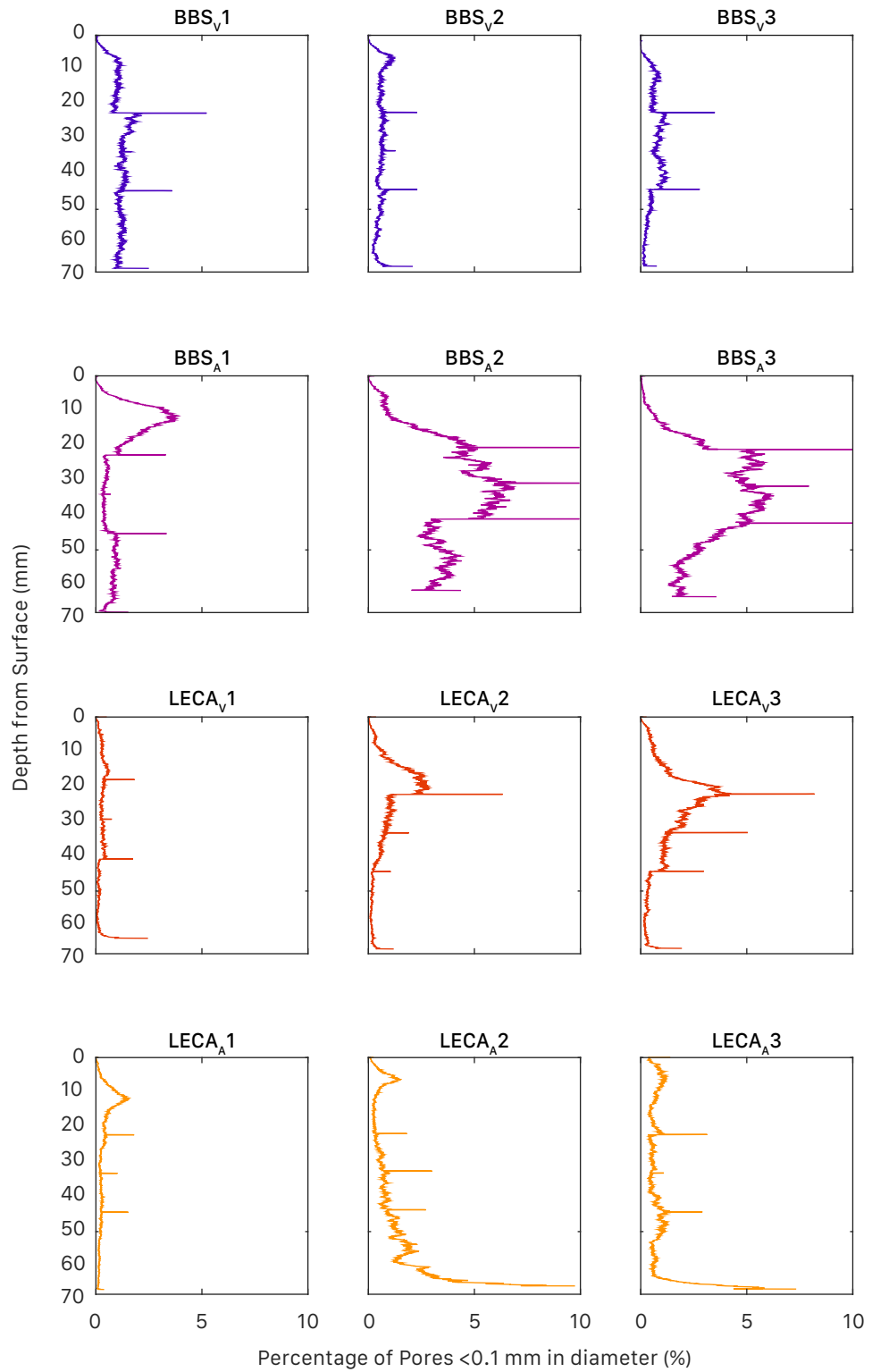
Figure 5.11 Percentage of pores smaller than 0.1 mm in diameter across core depth

It is worth noting that the evidence presented here represents only a very small fraction of the substrate volume of the operational test bed, and so the results may not be representative of the entire system. Additionally, the LECA cores used for XMT evaluation were not taken from locations near to the moisture probes to prevent any disturbance. The BBS cores were taken from a test bed without moisture monitoring equipment, yet its similar composition to the HLS and SCS of the Hadfield Green Roof Test Beds would indicate that it too would support a vertical moisture profile. The resolution limitations of the XMT technique also prevent the exploration of the range of pore sizes predominantly responsible for moisture retention.

5.3.5 Tortuosity

Tortuosity was determined from the pore space regions of the binary images shown in **Figure 5.4**. Analysis was conducted using *DigiUtility*.

LECA substrates, of both ages, have a lower tortuosity compared to their BBS counterparts (**Figure 5.12**). This observation is in line with prior identification of hydraulic conductivity (**Table 3.9**), the less complex matrix of the LECA substrate and the greater disconnection of large pore spaces in BBS. The tortuosity of BBS samples fell by 13% with age, whereas for LECA samples the reduction in tortuosity was greater, at 23%. Significant variation in the tortuosity values exists, which is expected for samples of a heterogeneous media. However, due to the large number of values (N = 1000 per substrate core) Kruskal–Wallis tests indicated a significant statistical difference ($P<0.05$) between the virgin and aged samples of both substrates.
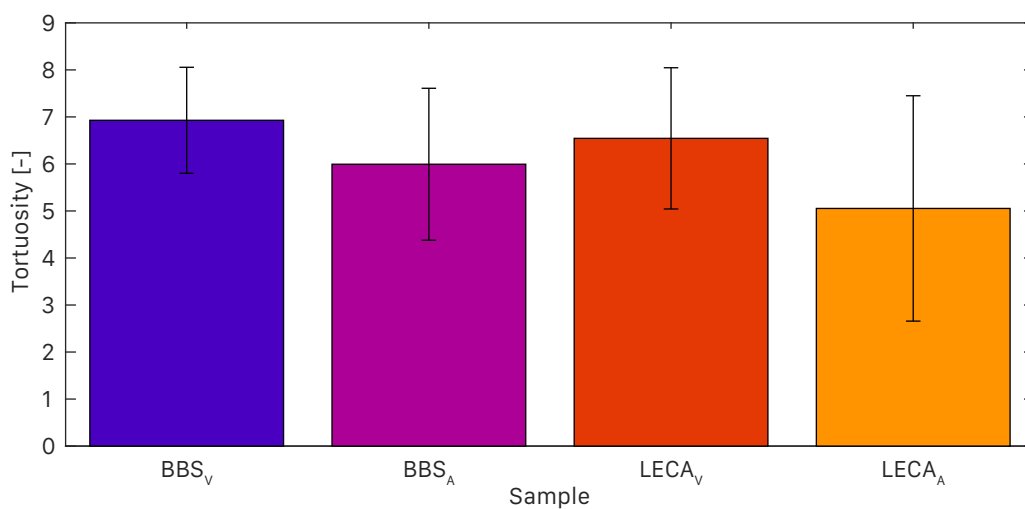
Figure 5.12 Mean tortuosity values for the 12 substrate cores. Error bars indicate +/- 1 standard deviation.

5.3.6 Hydraulic Conductivity

Hydraulic conductivity estimates were determined from the pore space regions of **Figure 5.4**. Using the *DigiFlow* implementation of the Lattice Boltzmann Method, the flow of water through the pore space of each core was numerically modelled.

Flow field visualisations from the LBM simulations show the formation of flow paths through the substrate mixes. These visualisations are typical of the flow conditions seen throughout the substrate samples. However, the 2D images only represent a fraction of the samples, and features of interest have been highlighted to show the type of output generated by LBM simulations. The BBS examples (**Figure 5.13**) show a single large flow path for the virgin sample compared to many smaller flow paths for the aged sample. The LECA examples (**Figure 5.13**) both exhibit a flow path on the left edge of the image, the size and peak flow of the flow path in $LECA_A$ is narrower and slower compared to that of $LECA_V$.
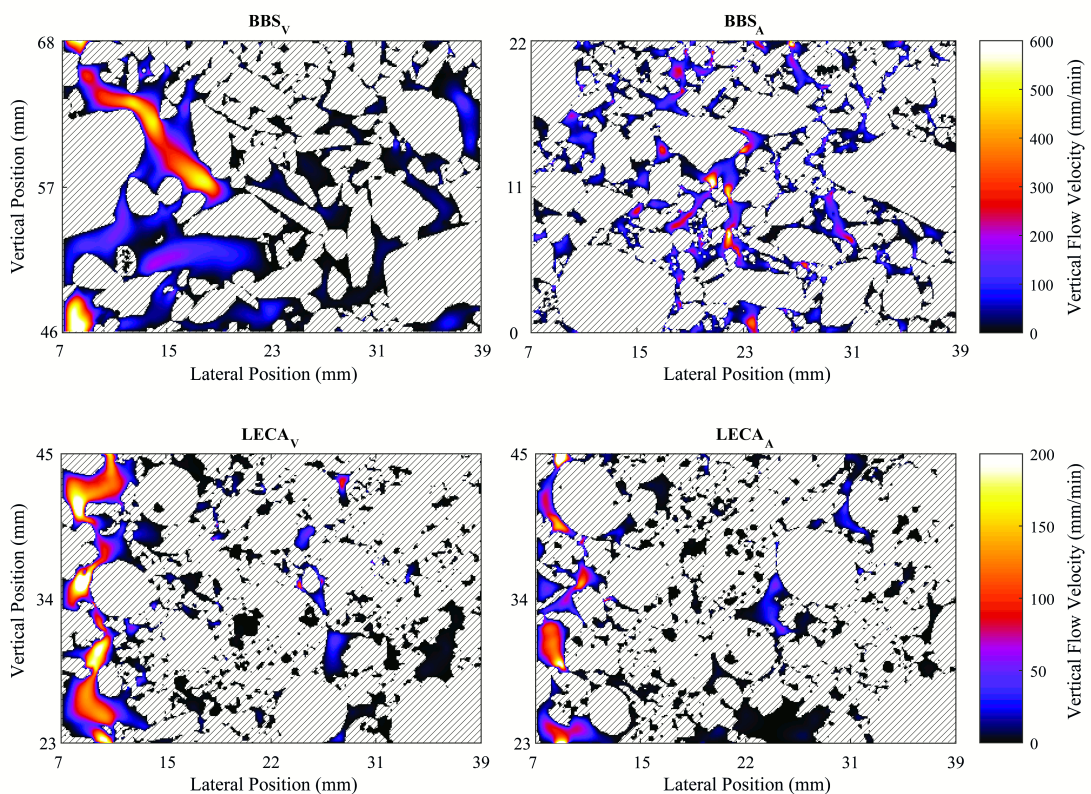
Figure 5.13 LBM flow field visualisations for BBS (top) and LECA (bottom).

Overall, aged samples have a lower hydraulic conductivity than their virgin counterparts (**Figure 5.14**). This is to be expected given the reduction in porosity for aged samples, as seen from the XMT image analysis. With fewer pore spaces there are

fewer flow paths, thereby restricting flow through the substrates. The relationship between BBS and LECA results is the same as that seen in the literature whereby LECA has a higher hydraulic conductivity than BBS (Berretta et al., 2014; Poë et al., 2015). The virgin LECA samples experience very high levels of standard deviation compared with all other samples. This is caused by sample $LECA_V1$ — which has been found to be consistently different across many properties — having a much higher hydraulic conductivity than the other two virgin LECA samples.
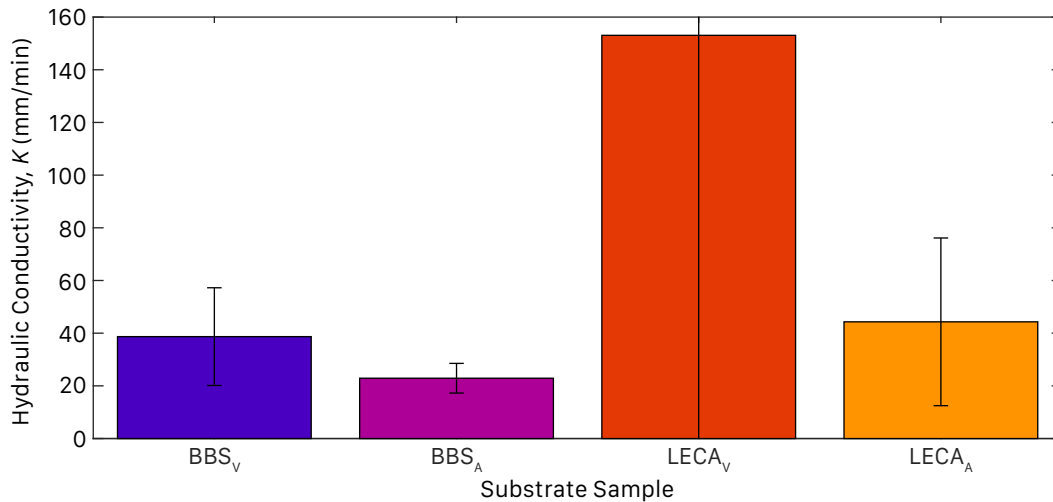
Figure 5.14 Mean hydraulic conductivity values for each substrate category. Error bars indicate ± 1 standard deviation. Error bars on LECA V extend above and below axis bounds (± 225 mm/min).

Hydraulic conductivity compares favourably between the physically-derived (K_{phys}) and numerically-derived values (K_{XMT}), with LECA substrates showing elevated levels of hydraulic conductivity over BBS. K_{XMT} values are slightly elevated (when not including virgin LECA samples) over K_{phys}, this is a result of the resolution limit on the XMT data. Only those flow paths with a diameter of >30 µm are modelled, with narrower flow paths — which may support slower velocities — being excluded. As K_{XMT} is determined from the superficial velocity of the fluid flow (mean velocity across only fluid sites) the omission of zones with slower flow skews the result toward a higher value of hydraulic conductivity.

> *The main conclusions from the XMT-derived substrate characterisations are that the non-invasive XMT methodology can identify differences between substrate types and ages, with aged substrates exhibiting reduced particle and pore sizes compared to their virgin counterparts. The numerical modelling of fluid flows within the substrate also results in physically comparable values of saturated hydraulic conductivity.*

5.4 Hydrological Performance

Section 3.4.8 explained how hydrological models were used to explore the influence of physical property changes on hydrological performance.

5.4.1 Retention performance

The BBS and LECA substrates exhibited increased mean MWHC values in aged samples, +6 and +7% respectively (**Table 5.1**). A 7% increase in MWHC will lead to a 1.4 mm increase in S_{max} for an initial value of 20 mm, assuming PWP is constant with age. **Figure 5.15** shows the impact of this increase in S_{max}. Retention increases with increased ADWP due to the cumulative effects of ET. At a 28 day ADWP the difference in retention performance between virgin and aged substrates reaches its greatest extent of 4.7 percentage points for summer and 4.3 percentage points for spring. At low ADWPs (<4 days) the difference in retention performance between the virgin and aged substrates is just 2.5 percentage points in summer and 2.3 percentage points in spring. **Figure 5.15** also demonstrates the influence of climate on retention performance, where summer conditions – with greater PET – result in significantly enhanced retention performance compared to spring. For a 7-day spring ADWP the difference in aged retention performance resulting from climatic factors is 23.3 percentage points. This is 10 times greater than the difference resulting from ageing processes (2.3 percentage points).
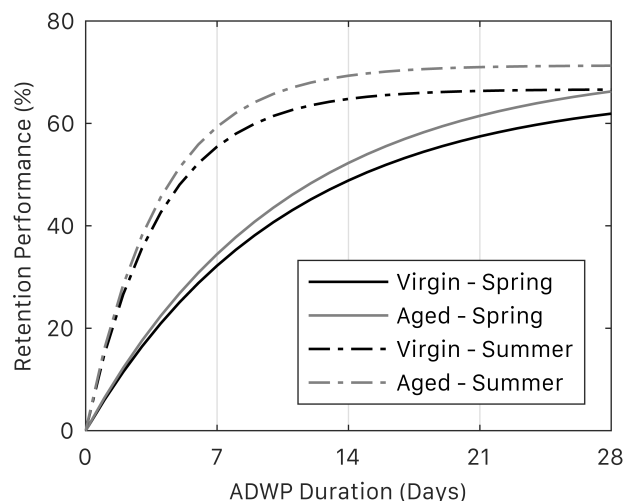
Figure 5.15 Comparison of the potential retention performance of a virgin and aged green roof in response to a 1-in-30-year 1-hour design storm for Sheffield, UK, at varying durations of ADWP.

5.4.2 Detention performance

The determined van Genuchten parameters (Section 3.4.8) of the BBS substrate allow an exploration of the relationship between hydraulic conductivity (K) and moisture

content (θ). The K(θ) relationships for the two values of K_{sat} (Section 3.4.6) are presented in **Figure 5.16**. At the onset of a rainfall event, moisture levels within the green roof substrate will be between the permanent wilting point (θ_{PWP}) and field capacity (θ_{FC}). Within this operational range, the differences between virgin and aged hydraulic conductivity are negligible. As the moisture content approaches saturation, the differences in hydraulic conductivity increase. However, even at typically observed maximum moisture contents (θ_{maxO}) (Berretta et al. 2014), the difference in hydraulic conductivity is still small compared to the difference in K_{sat} (0.14 vs. 16 mm/min).
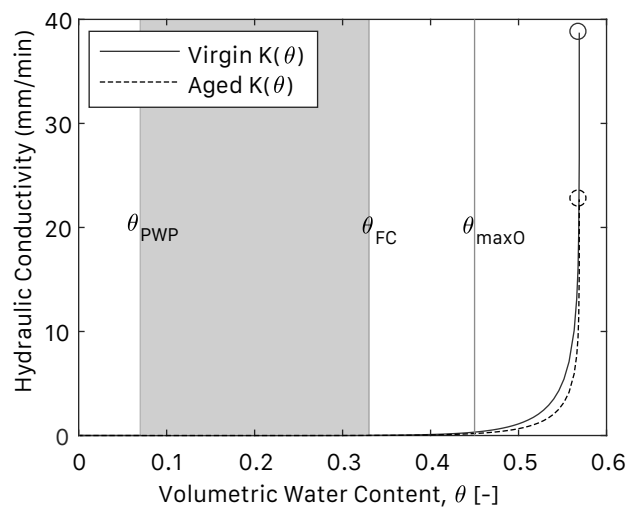
Figure 5.16 K(θ) relationship for BBS mean virgin and aged K_{sat}. Circular points indicate K_{sat}. Shaded region indicates typical operational moisture content at initiation of rainfall.

In response to the design rainfall event, the virgin and aged saturated hydraulic conductivity values both result in significant reductions in the peak runoff rate (**Figure 5.17**). The virgin BBS (K_{sat} = 38.9 mm/min) and aged BBS (K_{sat} = 22.9 mm/min) result in 70 and 80% peak attenuation respectively. However, the rainfall intensities of the design rainfall event are high in comparison to routine rainfall events. When exploring the runoff detention response of the two differently-aged systems to monitored rainfall patterns, the observable differences between them become much smaller (**Figure 5.17**). For the virgin green roof system, peak attenuation of 28% is achieved, whilst the aged roof exhibits 31% peak attenuation. Again, the lower values of K_{sat} in the aged roof result in greater detention performance. However, in response to this monitored rainfall event the improvement between the virgin and aged systems is just 11% compared to a 14% increase for the design storm.
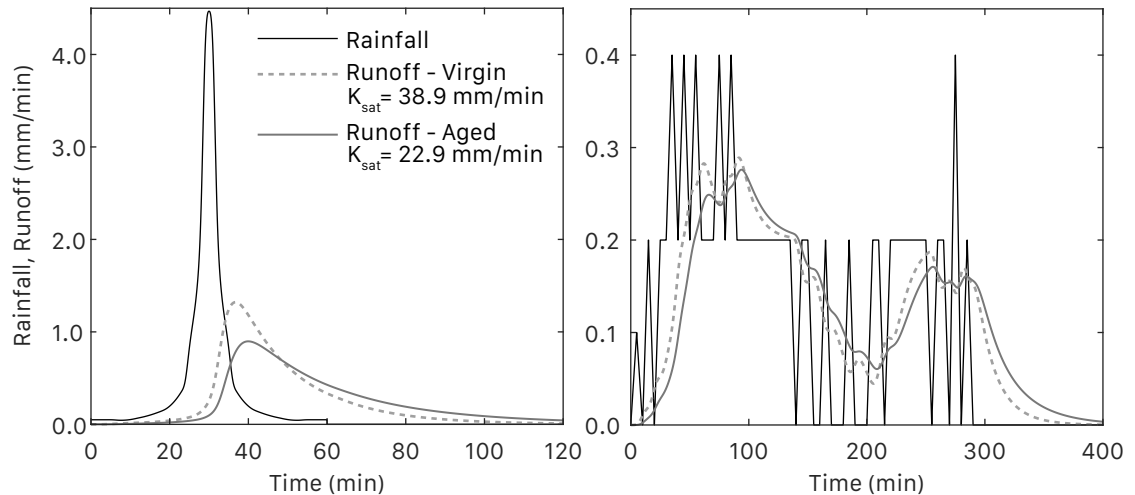
Figure 5.17 Detention only runoff response for two values of K_{sat} corresponding to virgin or aged BBS. **Left:** Response to a 1 hour 1-in-30-year design storm for Sheffield, UK, P = 30.28 mm. **Right:** Response to a monitored rainfall event in Sheffield, UK, P = 9.5 mm.

5.5 Discussion

5.5.1   Key Differences in virgin and aged substrate properties

For both methods of investigation (physical and XMT), particle sizes decreased with age. XMT-derived particle size distributions show greater reductions in median particle size for LECA than BBS. This is thought to demonstrate the fragility of the highly porous expanded clay aggregate within the LECA substrate, which is more prone to the destructive effects of weathering and root growth than the dense crushed brick of BBS. The observation of more fine particles in aged substrates is contrary to that reported by Bouzouidja et al. (2016), where the mass of particles with a diameter smaller than 2 mm in a pozzolana based substrate fell by up to 6% over a four-year period. This disparity, and the differences between BBS and LECA, highlight the variability in the impacts of ageing on differing substrate compositions.

Pore size reductions were observed in the physically-derived MWHC values. As moisture is only held against gravity inside pores with a diameter smaller than 50 μm (Rowell, 1994), if MWHC has increased then the total volume of pores with a diameter of <50 μm has also increased. As both virgin and aged samples are of the same total volume, then pores below 50 μm are more abundant in aged cores than their virgin counterparts, indicating a shift to smaller pore sizes. This is particularly evident in the LECA substrate, where sample density changes negligibly with age, but MWHC increases by 7%. Increases in MWHC were also seen by Getter et al. (2007) for a 60 mm depth of substrate. These increases in MWHC were also attributed to increases in

micropore (<50 μm) volumes. The XMT-derived pore size distributions also confirmed this shift toward smaller pore sizes with increasing age. However, resolution limitations prevent accurate observation of changes in <50 μm diameter pore volumes. The increase in the number of smaller pores is believed to be a result of root presence and the increased number of smaller particles within the aged substrate matrices.

Pore size reductions are also indicative of substrate consolidation (Menon et al., 2015). Networks of smaller pores reduce the cross sectional area for fluid flow, inhibiting free movement and reducing the resultant hydraulic conductivity. The effect of this reduction in cross sectional area for fluid flow may be somewhat mitigated in this instance by the reductions in tortuosity for aged samples. Such reductions to tortuosity indicate a reduction in flow path lengths through the substrate, which would increase hydraulic conductivity if it occurred in isolation (Schanz, 2007). However, results from the LBM simulations indicate that even with reductions in tortuosity, hydraulic conductivity is lower for aged samples. In this instance, it appears that pore size reductions have greater influence on hydraulic conductivity than tortuosity, as identified in non-engineered media by Vervoort and Cattle (2003).

Whilst differences are present between the virgin and aged cores, care needs to be exercised in solely attributing these changes to age. The same manufacturer's substrate specification was used for both the aged and virgin cores. However, the samples were taken from different batches. Additionally, the aged samples were clearly not the original samples that had aged, but a different set of samples. Differences in substrate properties may therefore be attributable to substrate heterogeneity, given the relatively high standard deviations observed in most properties. Future studies of this type will need to take account of this, and it is recommended that the same sample be repeatedly examined throughout time as it ages. Such an experimental method is only practical using non-destructive analysis techniques such as XMT, as demonstrated here. This methodology is employed as part of the longitudinal microcosm study presented in Chapter 6.

5.5.2   Disparities between physically-derived and XMT-derived properties

Two of the key physical properties that determine hydrological performance — porosity and saturated hydraulic conductivity — have been evaluated using both physical tests and XMT image analysis. This allows for a comparison of the resultant

property values and an evaluation of the usefulness of XMT. Whilst particle size distributions were also determined physically and via XMT-based methods, the two cannot be compared directly. The physically-derived particle size distribution is presented as a percentage by mass, whereas the XMT-derived particle size distribution is presented as a percentage by number.

The XMT-derived porosity values for both substrates are lower than the physically-derived values (**Figure 5.18**). The greatest disparity is for aged LECA samples, where XMT-derived porosity (ϕ_{XMT}) is 25% lower than the observed porosity (ϕ_{Phys}). This discrepancy is caused by the XMT images having a resolution of 30 μm. Any features smaller than this cannot be resolved and so are not represented in characterised property values. Values of MWHC determined from physical tests give some indication of the porosity for pores smaller than 50 μm, as this approximate pore size corresponds to field capacity conditions. Addition of the MWHC values to XMT derived porosities typically gives total porosity values in excess of those determined physically (**Figure 5.18**). This is to be expected as there is some overlap between the 30 μm XMT limit and the 50 μm criteria for field capacity. Given the above, ϕ_{XMT} appears to be a reasonable characterisation of sample porosity for pore sizes greater than 30 μm.
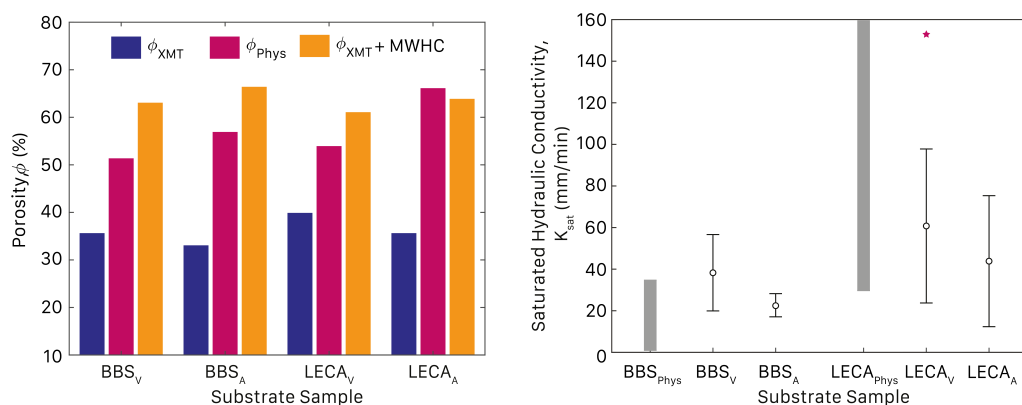
Figure 5.18 Comparison of Physically-derived and XMT-derived property values. **Left:** Porosity, mean values for each sample group. Including XMT-derived porosity + physically observed MWHC. **Right:** Range of Saturated Hydraulic Conductivities. Physically-derived Stovin et al. (2015) values (BBS$_{phys}$, LECA$_{phys}$) plotted as a shaded range; saturated hydraulic conductivity results of this study (BBS$_V$, BBS$_A$, LECA$_V$, LECA$_A$) plotted as mean and standard deviation; pentagram indicates mean of LECA$_V$ including result for LECA$_V$1.

K_{sat} compares favourably between the physically-derived values of Stovin et al. (2015a) (BBS$_{Phys}$ and LECA$_{Phys}$) and XMT-derived values (BBS$_V$, BBS$_A$, LECA$_V$, LECA$_A$), with LECA substrates consistently showing elevated levels of saturated hydraulic conductivity over BBS (**Figure 5.18**). XMT-derived values are slightly elevated (when

not including the LECA$_V$1 sample) over physically-derived values, this is expected as a result of the resolution limit on the XMT data. Only those flow paths with a diameter of >30 µm are modelled, with narrower flow paths — which may support slower velocities — being excluded. As the XMT-derived values are determined from the superficial velocity of the fluid flow (mean velocity) the omission of zones with slower flow skews the result toward a higher value of K$_{sat}$.

The disparities between physical and XMT-based determinations of porosity and saturated hydraulic conductivity can be largely attributed to the resolution of the XMT scan, and highlight the importance of acquiring images with sufficient resolution to resolve the features of interest. With current equipment, high image resolutions (<5 µm) require very small sample sizes (<5 mm in diameter). Soil science studies advocate the use of the smallest sample possible to maximise image resolution, with a core diameter of 50 mm being optimal (Rab et al., 2014). In this study, the heterogeneity of the substrate prevented the use of smaller diameter samples. Previous XMT studies of heterogeneous media (glass beads and sands) identified that the effects of heterogeneity are minimised for samples where the core diameter is 2–20 times the largest particle diameter (Costanza-Robinson et al., 2011). For the 46 mm diameter cores of this study a core diameter to maximum particle diameter ratio of 2.87 (median value) was achieved, i.e. within the target 2-20 range. It may be argued that a successful compromise has been achieved in maximising XMT image resolution whilst mitigating against excessive heterogeneity influences.

Whilst some disparities between physically and XMT-derived properties were noted, consistent general trends in the relative differences between the quantified properties of the two substrates over time were observed. The XMT technique allowed for the non-destructive characterisation of key substrate properties. It is this non-destructive nature that is the greatest benefit of using XMT for assessing the evolution of green roof substrate properties over time. The repeated imaging of the same substrate sample will allow for the determination of key property evolutions associated with ageing whilst removing the uncertainty of substrate heterogeneity.

5.5.3   Implications of substrate property changes on hydrological performance

Retention performance

The improvements seen in retention performance due to increasing substrate age are small (<5%, at their greatest extent). Long-term simulation of retention performance yields improvements that are a third the size of those seen for the design storm after

a prolonged (28-day) ADWP. This is not unexpected, as natural ADWPs are typically much lower than 28 days.

To determine an aged and virgin value of S_{max} for the retention modelling it was assumed that PWP and substrate depth were constant over time. Such an assumption may not be correct. The XMT-derived pore size distributions for both substrates suggest a reduction in pore diameters. Any increase in the total volume of pores below 0.2 μm will lead to increases in the value of PWP. Bouzouidja et al. (2016) observed moderate increases in PWP from 7 to 12% over a 4-year period in a pozzolana-based green roof substrate. This increase in PWP was directly attributed to the number of pores <0.2 μm in diameter and contributed to PAW reducing from an initial 11%, to just 2% within 4 years. The virgin BBS samples of this study have a PAW of >20% using the PWP value of comparable brick-based substrates from Berretta et al. (2014). Given that aged substrates have a MWHC of 33% (compared to 27% for virgin substrates), PWP would have to double to result in any overall reduction in PAW. To see similar declines in PAW as Bouzouidja et al. (2016), the PWP of BBS would need to of have quadrupled in 5 years. It is therefore possible that actual retention performance improvements may be smaller than those modelled here. However, from current observations, it is unlikely that the retention performance of a crushed-brick-based substrate will decline within a 5-year period due to changes in substrate properties.

Detention performance

Reductions in saturated hydraulic conductivity for the aged substrate samples are associated with an improvement in detention performance. Such an observation was expected due to the increase in the physical travel times of flow through the substrate. These observations are in line with the laboratory study findings of Yio et al. (2013) and those of the Stovin et al. (2015a) monitoring study. As there are no statistically significant differences between the virgin and aged values of K_{sat} for the BBS substrate, the resulting runoff profiles also have no statistically significant differences.

The input data for the modelling approach employed within this study is a simplification of the very complex relationships between hydraulic conductivity, tortuosity and pore size distributions. A single set of van Genuchten parameters was used to describe both the virgin and aged BBS substrate. Given the absence of water release data for the samples of this study, the results of comparable brick-based substrates were used from Berretta et al. (2014). Whilst there is little deviation

between the water release curves of the two substrates presented in Beretta et al. (2014) and other unpublished works, the subtleties of differences in tortuosity and pore size distributions will have an impact on hydraulic conductivity, particularly for low moisture contents.

Practical Implications

The small improvements to both retention and detention expected over time are unlikely to be detected in practical field monitoring programmes. Any variation resulting from substrate property changes is small compared to climatic and seasonal variations. This, alongside the lack of statistical differences between the virgin and aged substrates, supports the findings of Mentens et al. (2006), where no statistical significance was found between green roof hydrological performance and system age. The fact that there are no indications that hydrological performance will have declined in a 5-year period of normal operation may be of most importance to urban planners and stormwater engineers.

5.6 Chapter Summary

Virgin and aged substrate samples — of a brick-based and LECA-based substrate — display differences in physical properties, with aged samples exhibiting properties that would support enhanced hydrological performance over their virgin counterparts. This enhanced hydrological performance can be attributed to the changing substrate matrix. Aged samples consistently show smaller particles and pores which can support a greater MWHC and reduced hydraulic conductivity. However, the small magnitude of these enhancements to hydrological performance mean they are unlikely to be detected in full-scale monitoring studies given the dominant effects of climatic and seasonal variations.

X-Ray microtomography has proved to be a powerful tool for the visualisation of the internal structure of green roof substrates. In turn, this has allowed for the non-destructive determination of several physical properties that are key to understanding hydrological performance. Whilst some disparities were noted, general trends in the relative differences between the quantified properties of the two substrates over time were consistently observed with both measurement techniques. Some disparities were observed and these are believed to be attributable to the XMT image resolution. It is therefore important that guidance presented in previous literature is followed regarding sample size, with sample core diameters exceeding twice the largest particle diameter. Such steps help to mitigate heterogeneity effects, reduce required sample replication, maximise image resolution and therefore maximise XMT data quality. The second problem of not using the same cores over time is addressed via the longitudinal microcosm study described in Chapter 6, where non-intrusive XMT methods are used to monitor changes in substrate properties over time.

The results and discussion presented here will be brought together with the findings of chapters 4, 6 and 7 to provide an overall synthesis and discussion, which will be presented in chapter 8.

6. *Longitudinal Microcosm Study Results & Discussion: Substrate Properties*

6.1 Chapter Overview

This chapter presents the substrate property evolution results from the second phase of X-ray microtomography experiments, which repeatedly characterised green roof microcosm substrate properties over a full year of vegetation growth. Physically-derived characterisations performed at the start and end of the study are outlined before being supplemented by X-ray imaging data analysis conducted at intervals throughout the year of the study. The influence of microcosm size on heterogeneity and ageing processes is evaluated, alongside an exploration of X-ray imaging resolutions. Substrate root architectures and root growth are also identified. A brief discussion of the trends in substrate evolution and comparisons of physically and XMT-derived substrate properties concludes the chapter. The impacts of substrate evolution on hydrological performance are discussed in chapter 7.
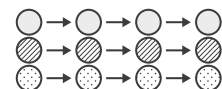
6.2 Physically-derived Substrate Properties

Two different sizes of microcosm were trialled to determine whether sample size was an affecting factor of any apparent property changes over time. **Figure 6.1** illustrates the similarities between the 50 and 150 mm diameter microcosms in their virgin state (at time T0). Statistical tests (Kruskal Wallis) identified no significant statistical difference in dry density, density at field capacity, and hydraulic conductivity for BBS samples (**Table 6.1**). For LECA samples dry density, density at field capacity, and MWHC were all found to have no statistically significant differences between 50 and 150 mm cores (**Table 6.1**).

Statistically significant differences in T0 substrate properties were observed for MWHC, percentage of particles <0.063 mm, and median particle diameter for BBS substrate samples (**Table 6.1**). The difference in MWHC is attributed to the difference in median particle diameter. The reduced median particle size in the 150 mm microcosms will result in a more densely packed substrate matrix with smaller pore spaces. The density of 150 mm microcosms is slightly greater than the 50 mm equivalents, which supports this theory, although the difference is not statistically significant. The larger median particle sizes of 50 mm microcosms likely results in larger pore spaces, and so MWHC is reduced.

For LECA substrate samples, only percentage of particles <0.063 mm and median particle diameter were found to be statistically different (**Table 6.1**). The increased number of particles finer than 0.063 mm in the 50 mm microcosms, as opposed to the 150 mm samples, coincides with an unexpected elevation in median particle diameter. A greater percentage of fine particles may be expected to reduce median particle diameters. This, alongside the full particle size distributions shown in **Figure 6.2**, highlights that the 50 mm microcosms are not as well graded as their 150 mm counterparts.

Characterisation of saturated hydraulic conductivity could not be completed for the majority of LECA samples for two reasons. Firstly, the highly porous LECA particles are buoyant and so when the substrate samples were saturated the substrate matrix disassociated. Therefore, any measured hydraulic conductivity was not representative of a compact substrate matrix. Secondly, the hydraulic conductivity of some samples exceeded the rate of inflow into the system. For these samples the saturated hydraulic can be said to be >460 mm/min (highest observed value).
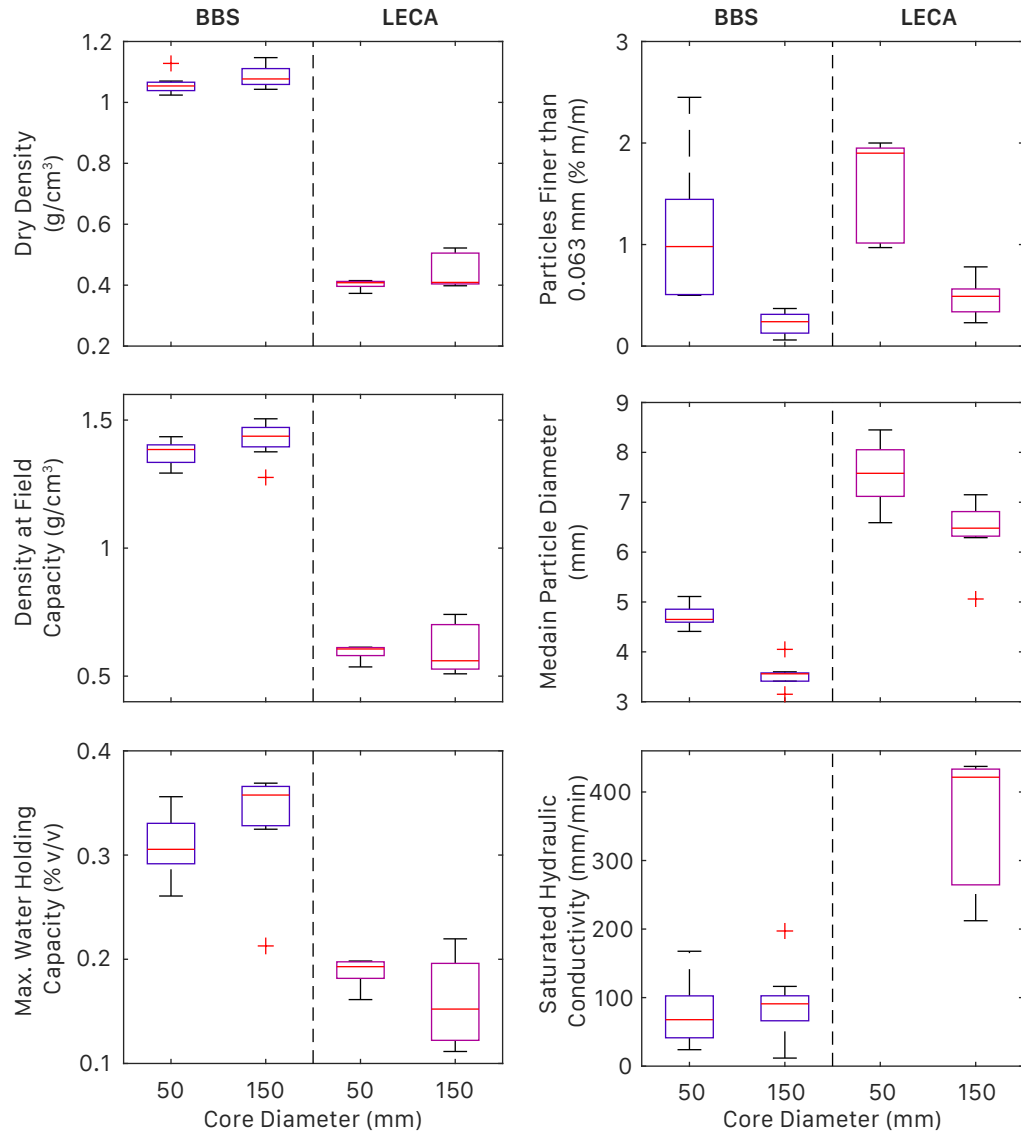
Figure 6.1 Boxplots to compare the range of physically-derived property values for both substrate types and microcosm diameters at the beginning of the study (T0).

Table 6.1 Kruskal Wallis P values comparing 50 and 150 mm substrate core physical properties at T0. * indicates significant statistical difference at P<0.05. Insufficient data for determination of LECA hydraulic conductivity

	BBS	LECA
Dry Density	0.0636	0.1992
Density at Field Capacity	0.0576	0.5074
MWHC	0.0271*	0.1219
Percentage of Particles <0.063 mm	0.0003*	0.0003*
Median Particle Diameter	0.0003*	0.0031*
Hydraulic Conductivity	0.2697	-
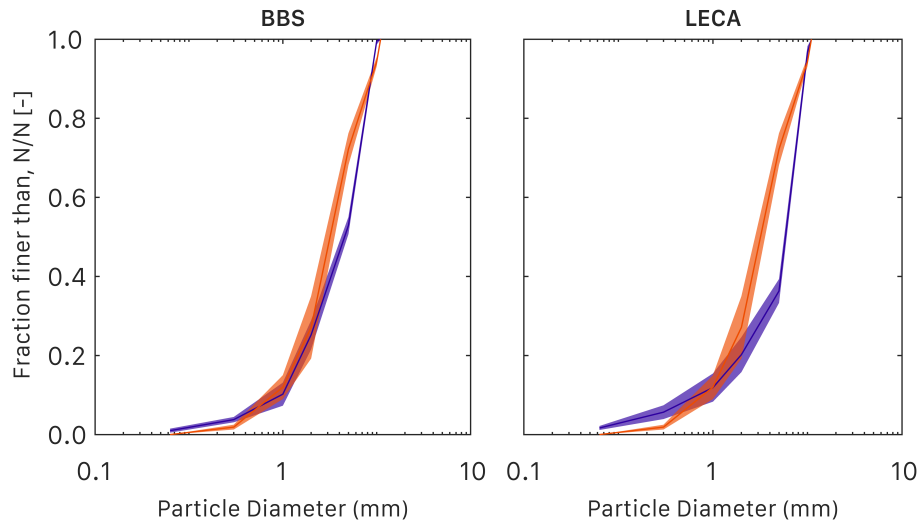
Figure 6.2 Physically-derived mean particle size distributions for 50 mm samples (Purple) and 150 mm (Orange) for BBS and LECA. Shaded regions indicate ± 1 x standard deviation.

The samples developed over the course of a year, from August 2015 (T0) to August 2016 (T12), in an outdoor environment alongside the Hadfield Test Beds (Section 3.4.4). Given the heterogeneities present between the 50 and 150 mm microcosms, all subsequent reporting of property evolution will be presented as a percentage difference from T0 values (%Δ from T0) as opposed to each specific property's units. Physical re-characterisation was undertaken after 12 months (T12) for all previously identified properties.

Figure 6.3 and **Figure 6.4** illustrate the percentage differences seen at T12 compared with T0 for BBS and LECA microcosms respectively. Inspection of **Figure 6.3** reveals that the majority of 50 and 150 mm vegetated BBS microcosms experience a similar %Δ from T0. The only statistically significant difference between 50 and 150 mm vegetated microcosms is for dry density in sedum samples (**Table 6.2**). The only mechanism by which density could be reduced in the 150 mm microcosms is through particle loss. Yet, the percentage of fine particles has doubled in 150 mm microcosms, although this still represents <1% of total mass. Density at field capacity and median particle diameter exhibit a range of %Δ from T0 indicating both reductions and increases over time. Given the lack of any statistically significant differences, the evolution of these properties is inconclusive. MWHC, particles finer than 0.063 mm and saturated hydraulic conductivity all underwent positive increases over time in vegetated samples. Increased MWHC is beneficial to retention performance (provided there are no adverse changes in PWP). Increased saturated hydraulic conductivities would suggest a reduced detention performance as flow travel times through the

substrate would be reduced. The unvegetated BBS microcosms (control) saw much greater variation between 50 and 150 mm diameters compared to their vegetated counterparts (**Figure 6.3**). Statistically significant reductions in dry density also resulted in reductions in density at field capacity for 150 mm microcosms (**Table 6.2**). Saturated hydraulic conductivity values were also statistically significantly different, with 50 mm microcosms indicating an increase with time, whilst 150 mm microcosms exhibited a decline. The significant reductions in density for the 150 mm microcosms suggest a wash-through of smaller particles from upper layers, some of which being lost from the microcosm and the remainder clogging pores deep within the substrate and thereby reducing hydraulic conductivities.
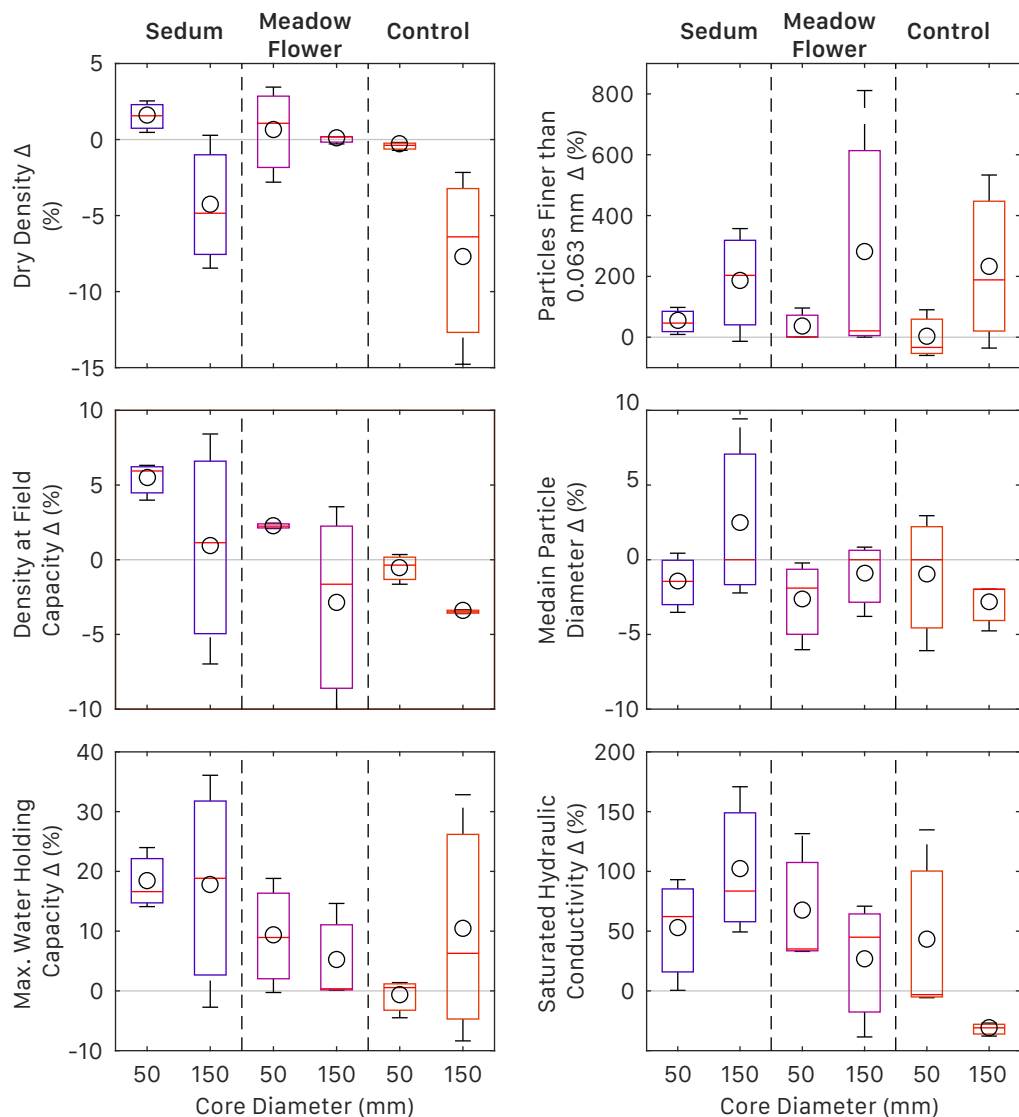
Figure 6.3 Changes in property values of the BBS substrate cores (50 and 150 mm) from T0 to T12. Circles indicate mean values.

Table 6.2 Kruskal Wallis P values comparing the difference between T0 and T12 substrate properties for the 50 and 150 mm substrate cores. * indicates significant statistical difference at P<0.05. Insufficient data for determination of LECA hydraulic conductivity.

	BBS			LECA		
	S	MF	NV	S	MF	NV
Dry Density	0.0495*	0.5127	0.0495*	0.5127	0.0495*	0.0495*
Density at Field Capacity	0.5127	0.6579	0.2752	0.0495*	0.0495*	0.0495*
MWHC	0.5127	0.5127	0.0495*	0.8273	0.0495*	0.1266
Percentage of Particles <0.063 mm	0.5127	0.2752	0.5127	0.5127	0.0495*	0.5127
Median Particle Diameter	0.8273	0.8273	0.5127	0.1266	0.0495*	0.0495*
Hydraulic Conductivity	0.5127	0.8273	0.0495*	-	-	-
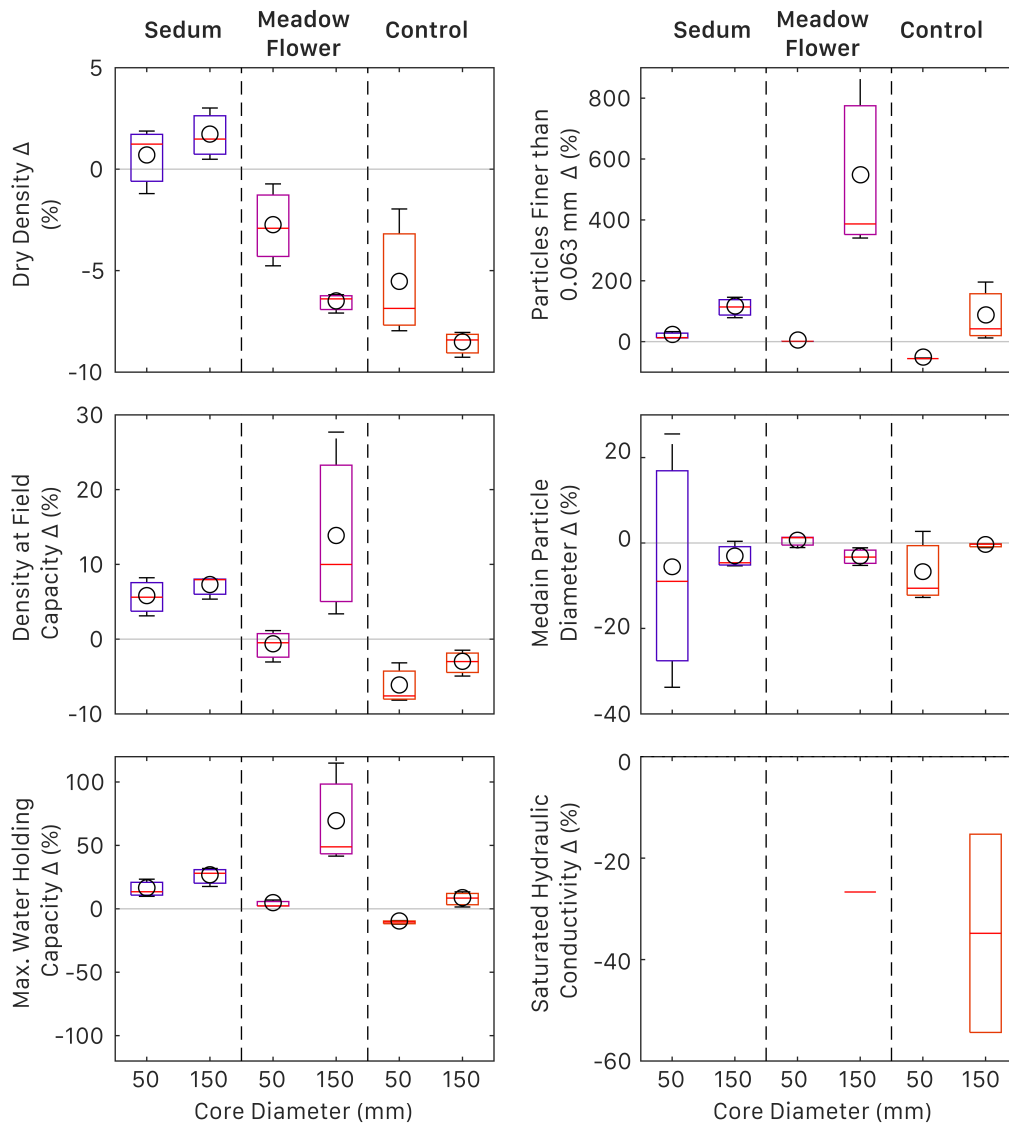
Figure 6.4 Changes in property values of the LECA substrate cores (50 and 150 mm) from T0 to T12. Circles indicate mean values.

Only minor differences were observed betweem the two sizes of Sedum treatment LECA microcosms (**Figure 6.4**). A statistically significant difference between 50 and 150 mm diameters is observed for density at field capacity (**Table 6.2**). However, this does not translate into a significant difference in MWHC, which may have been expected. All properties increased in value for both diameter Sedum vegetated LECA microcosms except for median particle diameter, where there was a reduction over time. Meadow-Flower LECA microcosms exhibit statistically different results for all properties between the 50 and 150 mm microcosms. This is predominantly a result of poor vegetation growth within the 50 mm LECA microcosm. The small diameter, low MWHC of LECA, and high water use of Meadow-Flower species caused the microcosms to dry out faster than their BBS counterparts. As such, vegetation growth was reduced. The unvegetated control microcosms exhibited statistically significant differences in both measures of density and median particle diameter (**Table 6.2**). Yet, for all 3 of these properties there was a negative change over time. Reduced particle diameters and reduced densities suggest a wash-through of fine material, like that seen for unvegetated BBS control microcosms. Again, the percentage of particles finer than 0.063 mm has increased but remains <1% of total mass (**Figure 6.5**).
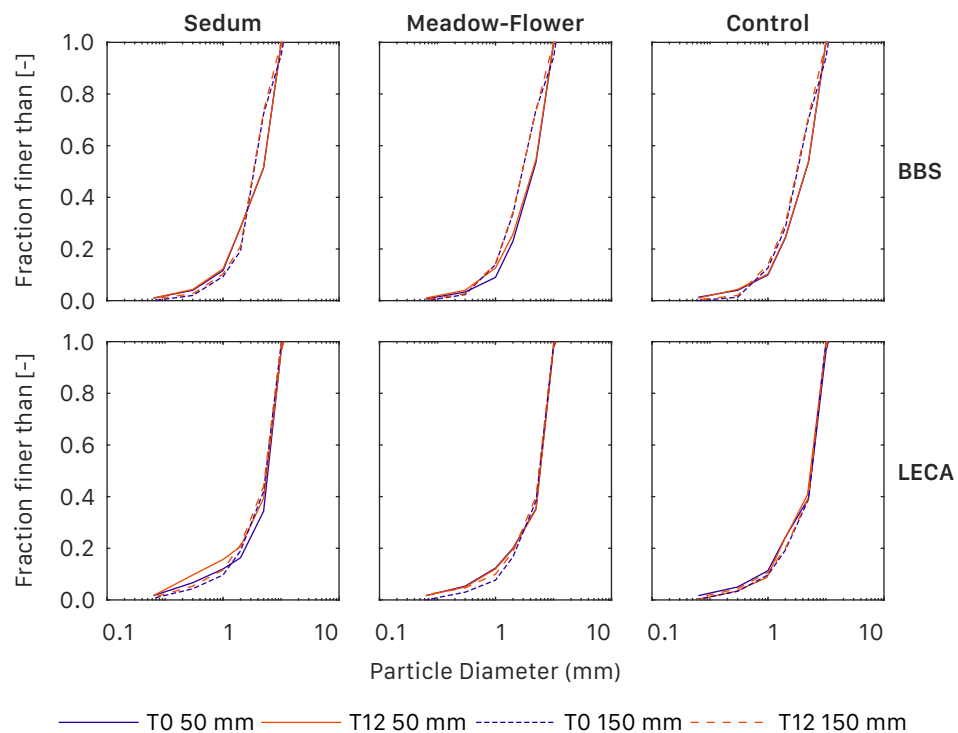
Figure 6.5 Physically-derived particle size distributions for each treatment group at T0 and T12.

The physically-derived particle size distributions of **Figure 6.5** indicate that there is very little change in particle size distributions from T0 to T12, but the variation in 50 and 150 mm microcosms highlighted in **Figure 6.2** remains.

Statistical tests conducted using property units, as opposed to %Δ, largely reveal no significant statistical differences between T0 and T12 property characterisations, for either microcosm diameter. However, there are some instances where property changes are statistically significantly different, even without accounting for substrate heterogeneity. **Figure 6.6** presents the mean and standard deviations of all physically-derived substrate properties at T0 and T12, and includes both microcosm sizes. Inspection of **Figure 6.6** and Kruskal–Wallis tests identified that the 50 mm LECA control microcosm exhibits significant statistical differences in dry density, density at field capacity, particles < 0.063 mm, and MWHC. For each of these differences there is no identified significant statistical difference in the 150 mm LECA control microcosm. No other microcosm exhibits as many significant statistical differences from T0 to T12. LECA cores account for 66% of all identified statistical differences. Also identified as having significant statistical differences with age were: dry density of 150 mm BBS control microcosm; percentage of particles <0.063 mm in the 150 mm LECA Meadow Flower microcosm; median particle diameter of the 150 mm BBS control microcosm; and the MWHC of the 50 mm BBS and LECA Sedum microcosms. All other substrate/vegetation/microcosm diameter combinations exhibited no significant statistical difference from T0 to T12.

> *The main conclusions from the physically-derived substrate characterisations are: an increased microcosm diameter does not significantly affect ageing processes or the magnitude of heterogeneity; the statistical differences of observed changes in substrate properties, of both types, are largely not statistically significant due to the high levels of substrate heterogeneity; increases to MWHC with age, for both substrates, suggest potential improvements in hydrological performance for aged samples.*
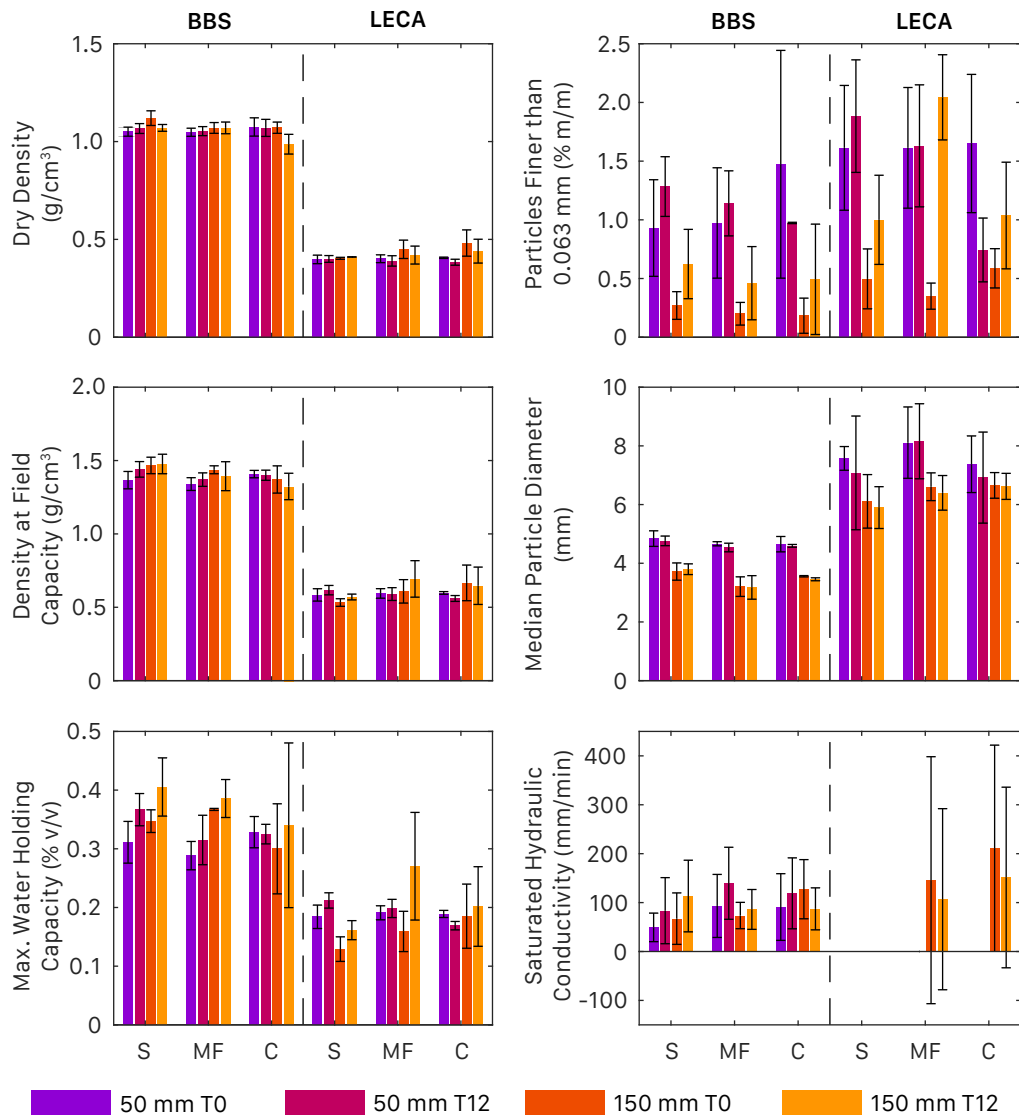
Figure 6.6 Comparison of physically-derived 50 mm and 150 mm properties at the beginning (T0) and end (T12) of the 12-month study period. **S** – Sedum. **MF** – Meadow Flower. **C** – Control.

6.3 XMT-derived Substrate Properties

The 50 mm microcosms were imaged using XMT four times over the course of the year. T0 and T12 image sets were obtained to tally with physically-derived characterisation. Additional image sets were acquired after 8 months of growth (T8) and again at 10 months (T10). These additional intermediate image sets allow for identification of substrate property evolution at a higher temporal resolution.

Figure 6.7 and **Figure 6.8** present unprocessed 2D projections of one microcosm from each of the 6 treatment groups across all 4 image acquisition dates. The BBS images (**Figure 6.7**) demonstrate the angular nature of the crushed brick aggregate and the close packing of particles, compared to the more loosely packed round LECA particles of **Figure 6.8**. Changes in the matrix over time are difficult to spot, particularly for BBS substrates. However, there are identifiable differences in the vegetated LECA cores from T0 to T8. In the upper left quadrant of the T8 LECA-Sedum image there is additional material present compared to T0. This material has fallen through from the upper layers and settled in the available pore space. Similar movement is observed across the entire LECA-Meadow Flower image set.

Separated particle images (**Figure 6.9** and **Figure 6.10**) and pore thickness maps (**Figure 6.11** and **Figure 6.12**) were extracted from the unprocessed images via the image processing protocol established in Section 3.4.5. Particle separation performed well for the BBS substrate, with clearly defined particles that reflect the unprocessed image sets (**Figure 6.9**). Separation of the LECA from the wider substrate matrix was less successful. The highly porous nature of the LECA particles resulted in significant subdivision of particles, as such the separated particle images (**Figure 6.10**) do not accurately represent the unprocessed images of **Figure 6.8**. However, as this is a systematic limitation, all LECA cores will be equally affected and so temporal changes in LECA particle sizes may still be identified. The exact values of LECA particle sizes are unlikely to represent physically-derived measures. The pore thickness maps experience little difference with time for the BBS cores (**Figure 6.11**) but LECA image sets further highlight the movement of material into pore spaces (**Figure 6.12**). As for the unprocessed images, in the upper-left quadrant of the T8 LECA-Sedum image pore sizes are much smaller than in the T0 image. Similarly, changes in pore size can be identified across the entire image set of the LECA-Meadow Flower images.
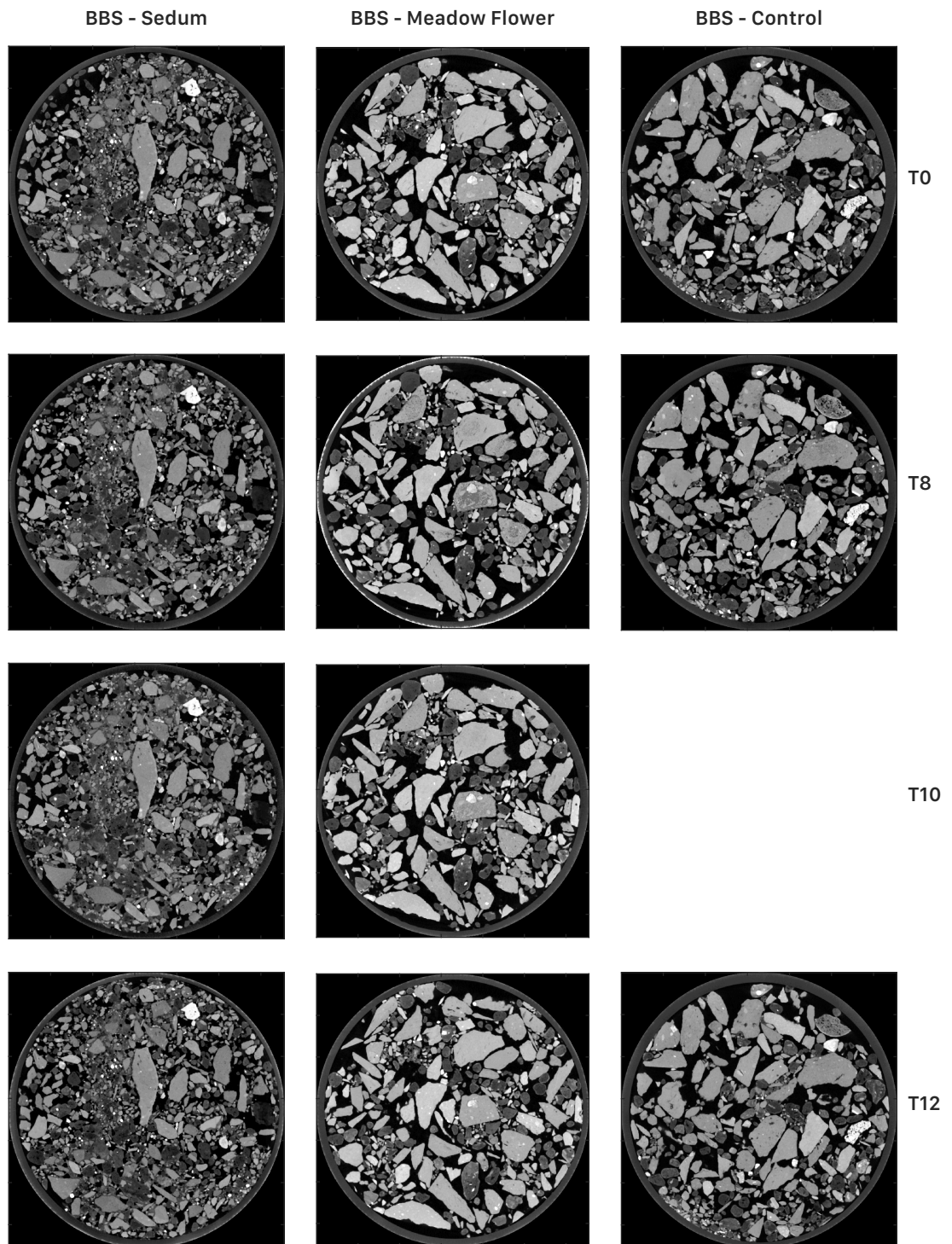
Figure 6.7 Example slices of unprocessed XMT images for BBS substrate cores, all images are 52.4 mm across. Note: no image was acquired for BBS-Control at time T10.
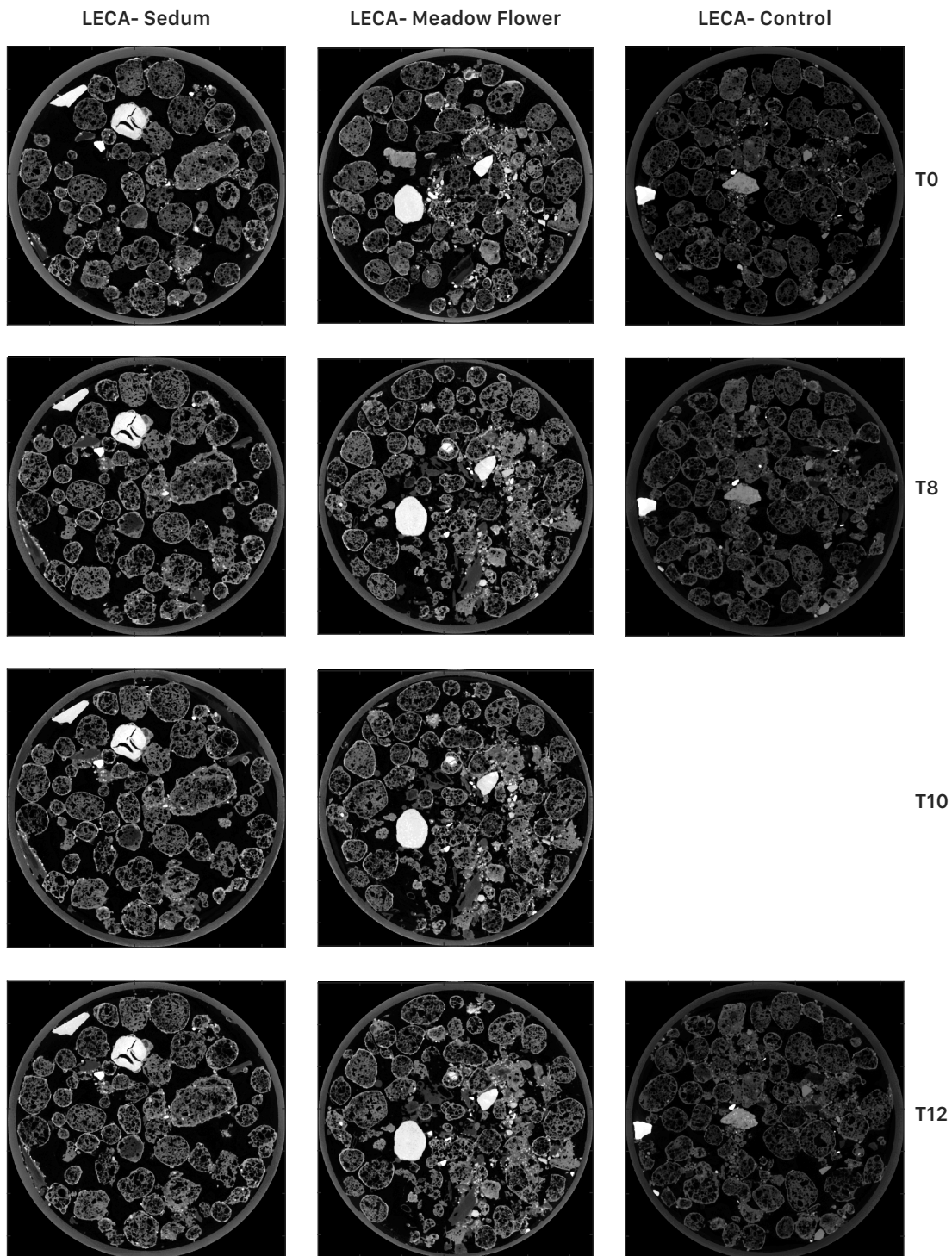
Figure 6.8 Example slices of unprocessed XMT images for LECA substrate cores. Note: no image was acquired for LECA-Control at time T10.
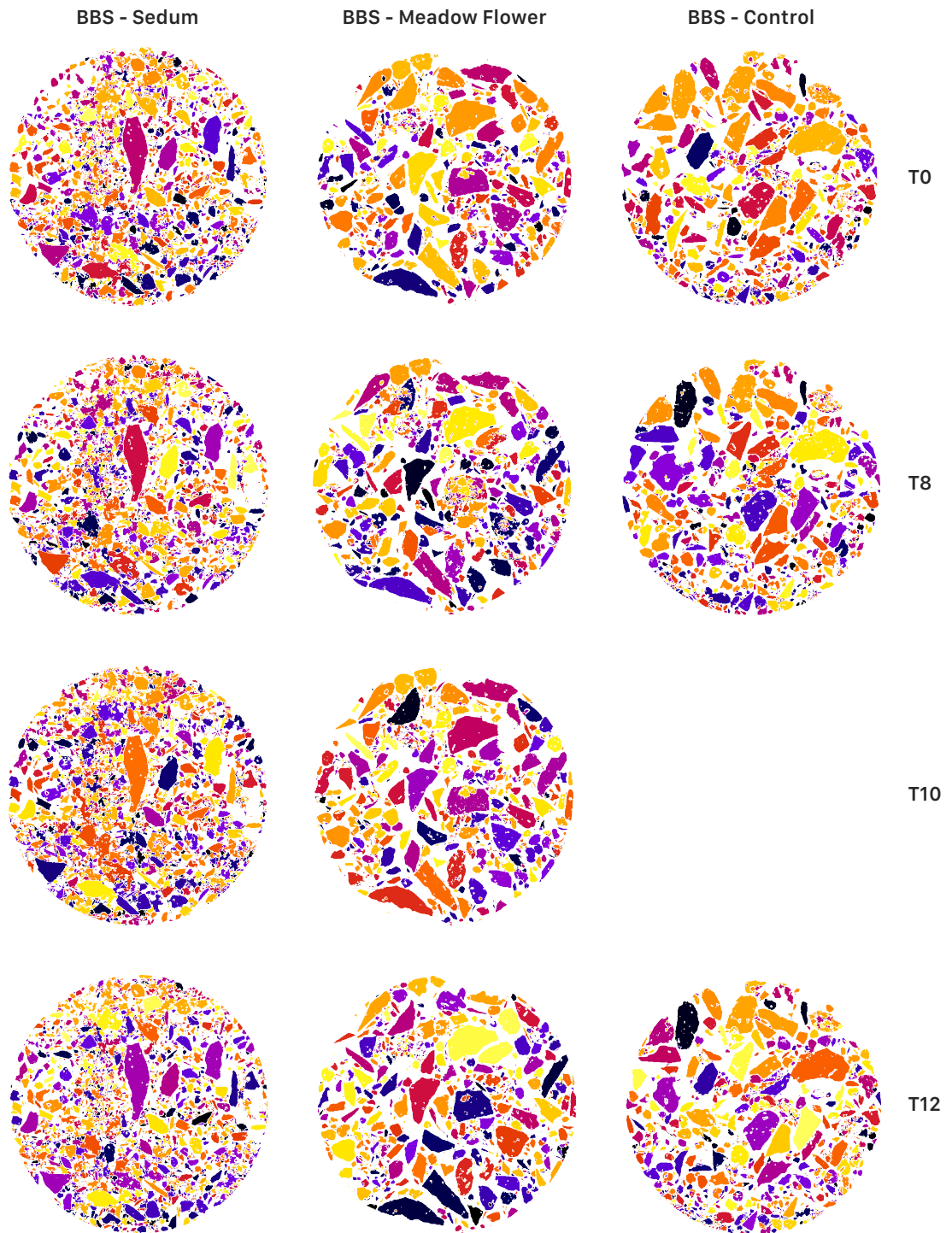
Figure 6.9 Separated particle images for the same example BBS cores as Figure 6.7. Particle colours randomised. Note: no image was acquired for BBS-Control at time T10.

LECA- Sedum **LECA- Meadow Flower** **LECA- Control**

T0

T8

T10

T12
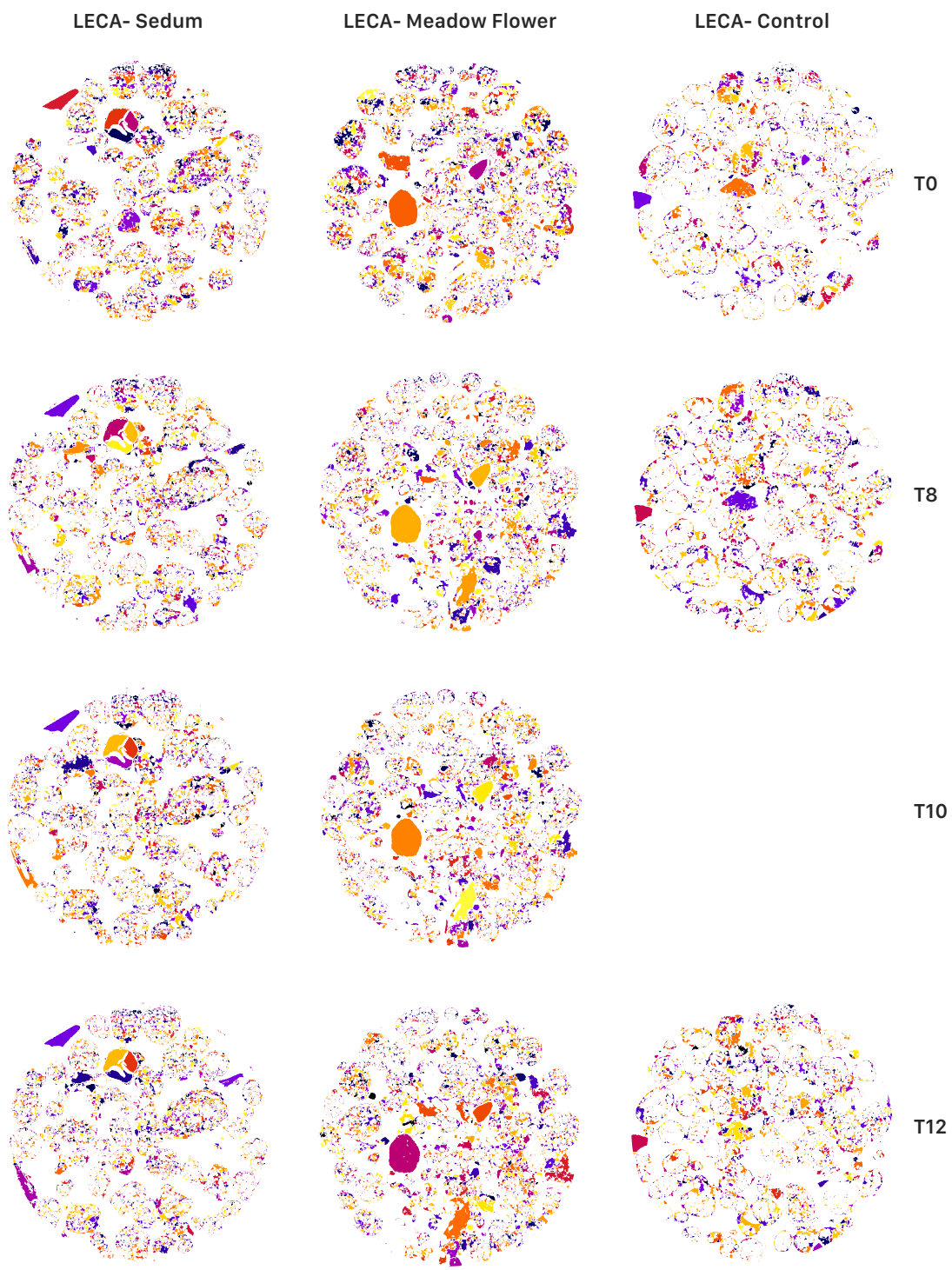
Figure 6.10 Separated particle images for the same example LECA cores as Figure 6.8. Particle colours randomised. Note: no image was acquired for BBS–Control at time T10.
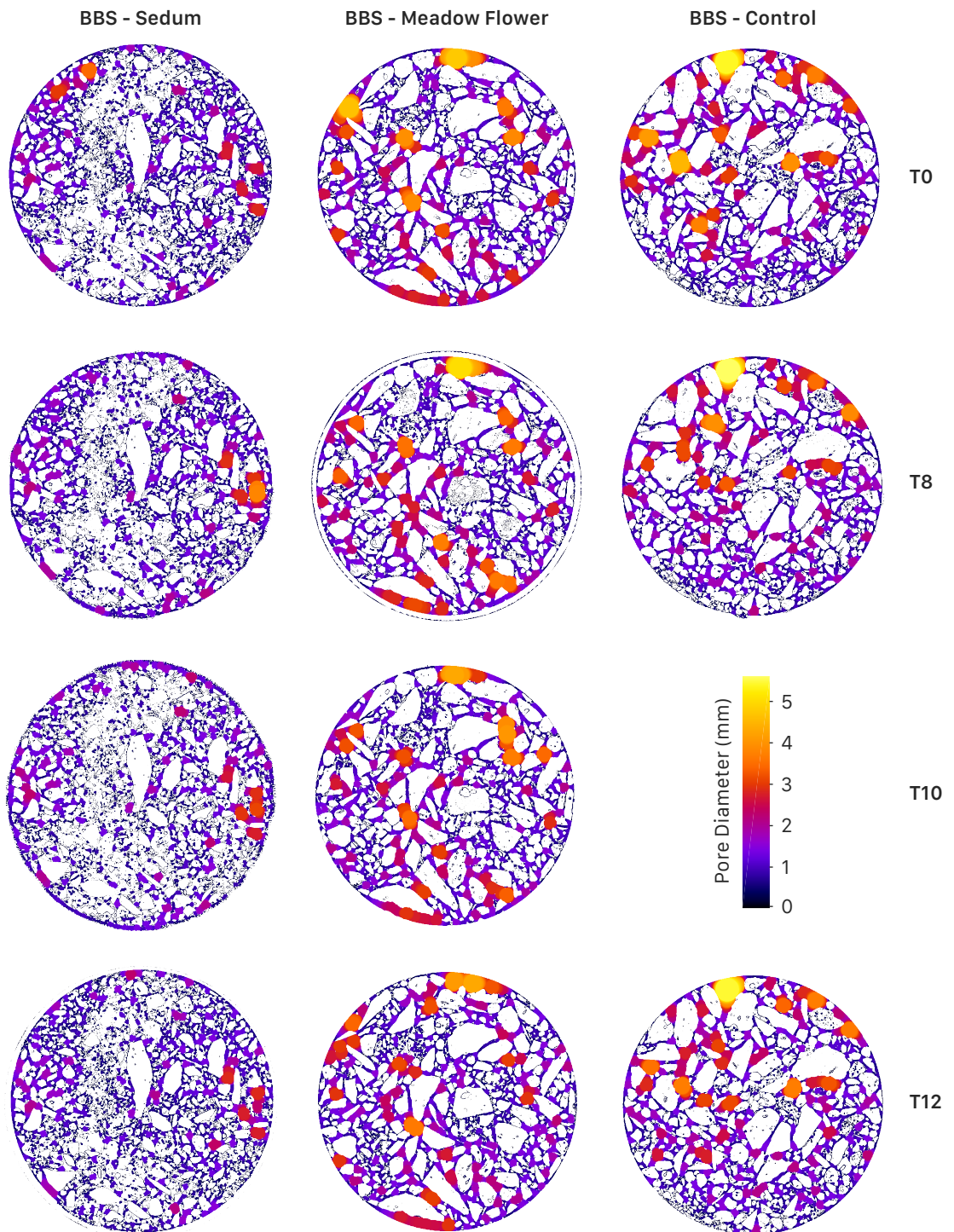
Figure 6.11 Pore thickness images for the same example BBS cores as Figure 6.7. Note: no image was acquired for BBS-Control at time T10.
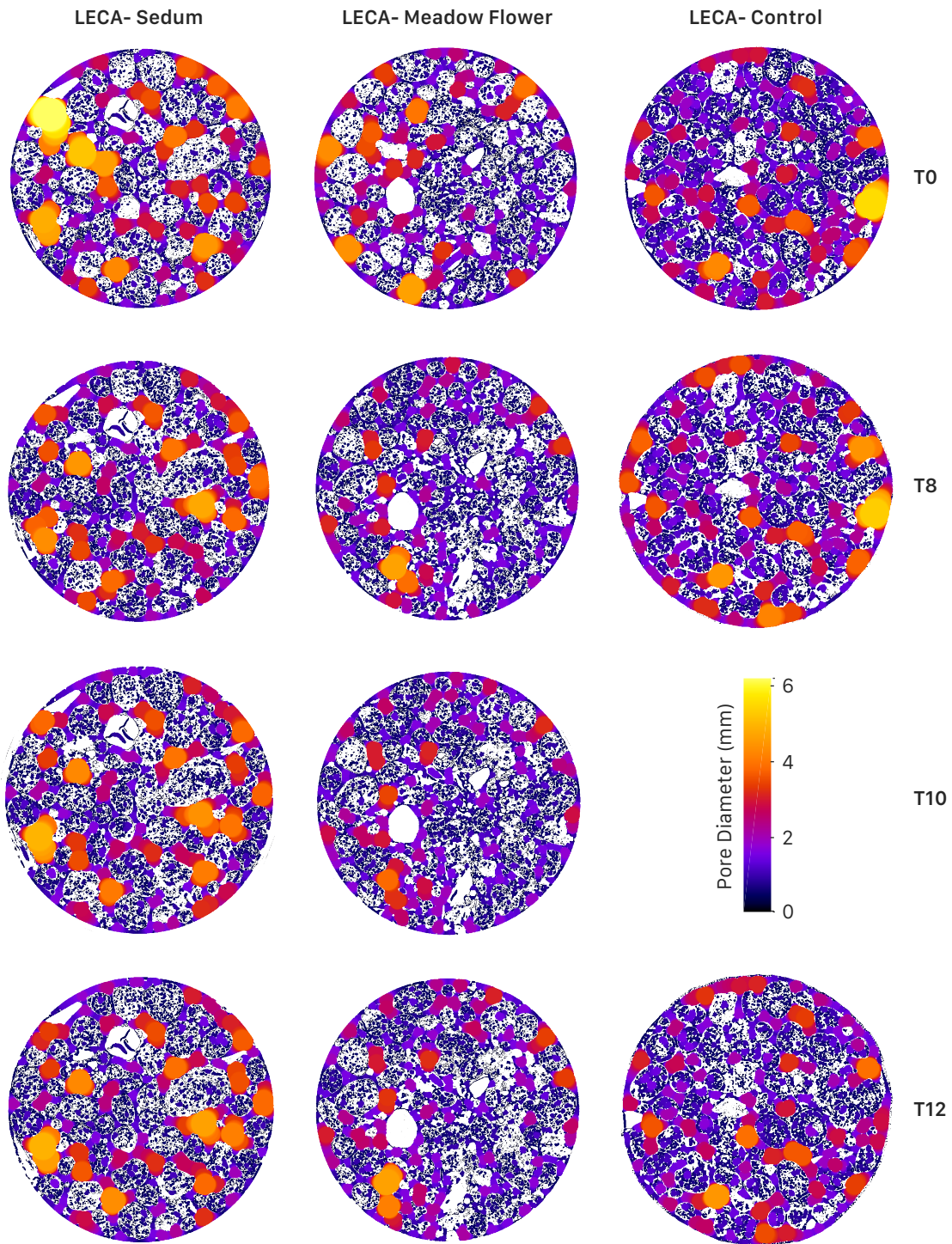
Figure 6.12 Pore thickness images for the same example LECA cores as Figure 6.8. Note: no image was acquired for LECA-Control at time T10.

The image sets were processed to determine median particle and pore diameters, total porosity, tortuosity and saturated hydraulic conductivity. The differences between the two substrate types were assessed at T0 (**Figure 6.13**). LECA microcosms have larger particles and pores compared to BBS microcosms. LECA microcosms have a much higher porosity than their BBS counterparts, due to the highly porous nature of the LECA particles themselves. This can also be observed in **Figure 6.11** and **Figure 6.12**, where LECA microcosms have a greater proportion of shaded areas compared to BBS. The larger pore networks result in reduced tortuosity in LECA microcosms, and ultimately lead to a significantly higher saturated hydraulic conductivity.
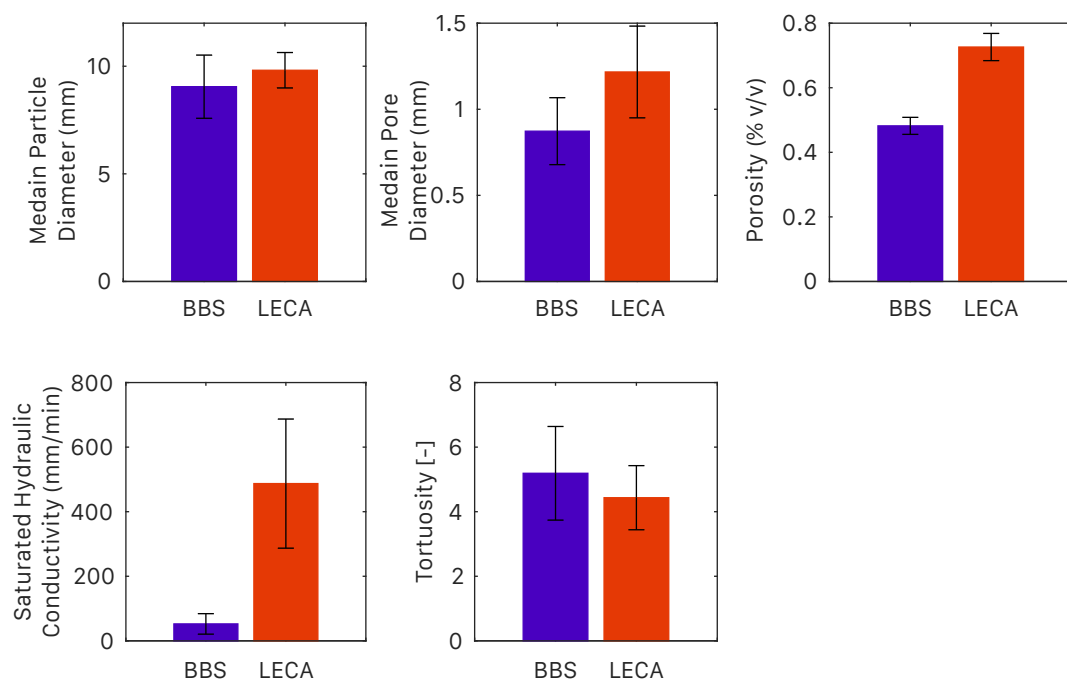
Figure 6.13 XMT-derived substrate property values at T0. Mean and Standard Deviation.

As for the physically-derived substrate characterisations, comparisons of XMT-derived properties will be presented as a percentage difference from T0 values (%Δ from T0) to mitigate against microcosm heterogeneity. **Figure 6.14** illustrates the changes seen in the 6 treatment groups across the 12-moth study period for median particle and pore diameters, and porosity.

For the BBS microcosms, there is no statistically significant difference in median particle diameter Δ (Δd_{50}) for any of the three vegetation treatments with respect to time (**Figure 6.14**). Whilst all vegetation treatments exhibit an increase in the median Δd_{50} at T8 and into T10, by T12 the median Δd_{50} has become negative indicating a slight

reduction in median particle diameter. There is a large amount of variation in the median Δd_{50} over time, particularly for the BBS Meadow Flower microcosm where median Δd_{50} falls from +55% to -3% from T8 to T12.
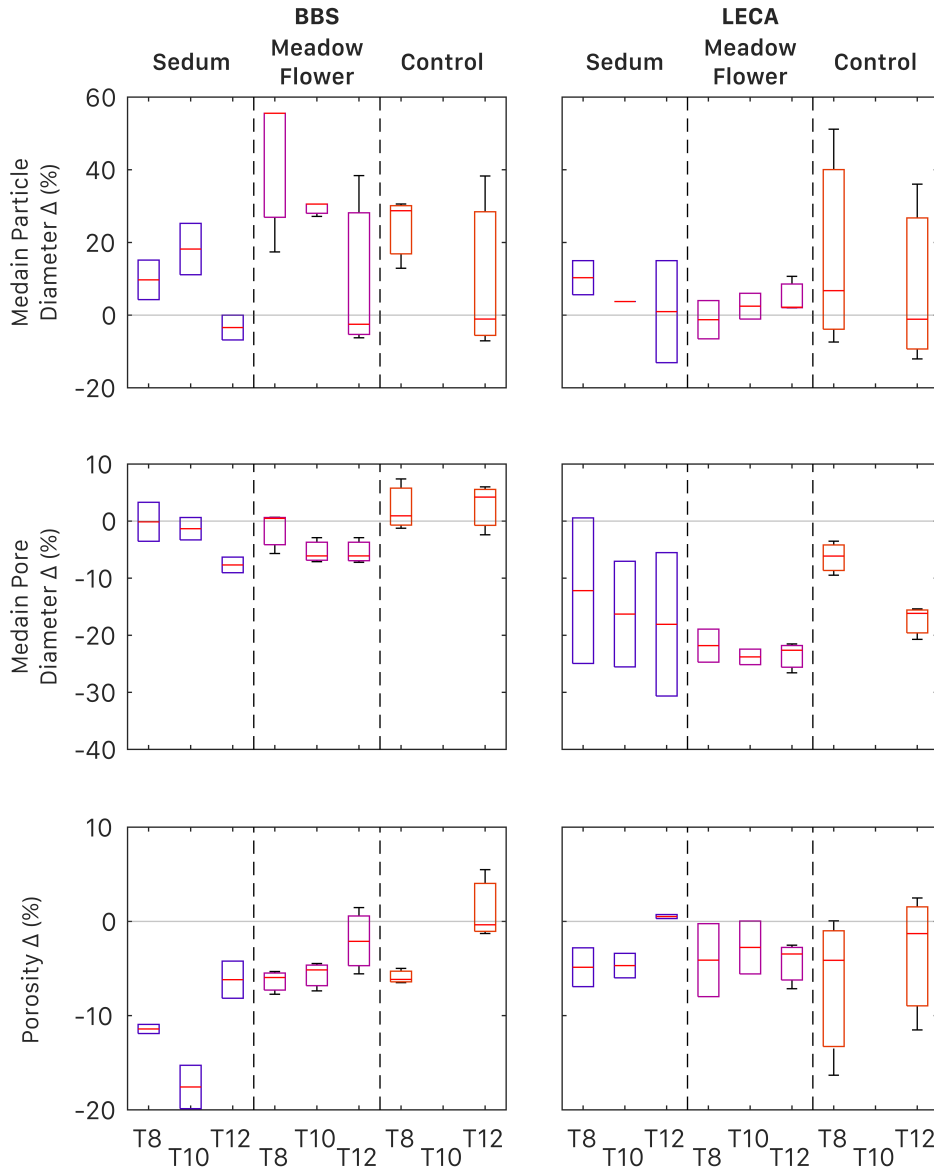
Figure 6.14 XMT-derived median particle diameter, median pore diameter, and porosity. %Δ from T0.

Similarly for LECA, there is no statistically significant difference in median particle diameter for any of the three vegetation treatments. However, unlike the BBS microcosms, vegetated LECA microcosms exhibit a positive median Δd_{50}, indicating a slight increase in median particle diameters with time. Both types of vegetated LECA microcosms see gradual changes in median Δd_{50} from T8 to T12, with median particle diameters reducing over time for Sedum vegetation but increasing under a Meadow Flower treatment.

The large variation in *median particle diameter Δ* observed in the BBS cores can be attributed to weaknesses in the performance of the particle separation algorithm. Whilst for a single image set (e.g. T0) the algorithm is repeatable (i.e. every result will be the same) when applied across multiple image sets (e.g. T0, T8, T10 and T12) the drawn separation lines can be in different places, dividing particles differently, resulting in different particle size distributions. All input parameters for the particle separation algorithm were kept constant to minimise the differences in separation across the different temporal image sets. Particle separation problems appear to be more of an issue for LECA microcosms (see **Figure 6.9** and **Figure 6.10**) as LECA particles are fractured into several pieces, but greater variability is seen for BBS microcosms. The full particle size distributions of all microcosms over time (**Figure 6.15**) also illustrate a larger level of variability in BBS microcosms compared to their LECA counterparts. It appears that the fracturing of LECA particles into several pieces is more consistent than the division of BBS particles. The deficiencies within the particle separation algorithm therefore preclude any useful identification of XMT-derived particle sizes from the repeated temporal imaging.

The BBS microcosms exhibit no statistically significant differences in median pore diameter Δ (Δp_{50}) with time (**Figure 6.14**). The Sedum vegetated BBS microcosms exhibit a distinct negative median pore diameter Δ in T12, yet due to the small number of samples, this result remains statistically insignificant compared to the positive median pore diameter Δ of T8 and T10. All vegetated BBS microcosms exhibit a negative median Δp_{50} in T12 indicating an overall reduction in median pore diameter with time. The unvegetated control BBS microcosms exhibit the opposite behaviour with median Δp_{50} being elevated in both T8 and T12, indicating an increase in the median pore diameter with time. Inspection of the full pore size distributions over time (**Figure 6.16**) highlights the general lack of variability in pore sizes with age for BBS microcosms. Sedum vegetated BBS microcosms experience some large-scale changes in some of the smallest pores (order of 100 μm), but these do not affect median pore diameter values.

All LECA microcosms exhibit negative median Δp_{50} values, indicating a reduction in median pore diameter with time. The magnitude of these reductions is almost 3 x that seen for BBS microcosms. Trends in the median Δp_{50} for vegetated microcosms suggest a stabilising of pore diameters as time progresses, with the biggest changes occurring from T0 to T8. However, the only statistically significant difference in Δp_{50}

with time is for the unvegetated control LECA microcosm. This suggests that the bulk of median pore diameter reductions occurs within the time from T0 to T8. The full LECA microcosm pore size distributions of **Figure 6.16** further support this theory, with T0 distributions (purple lines) being distinct from all other temporal characterisations.

The porosity Δ of vegetated BBS microcosms is not statistically significant with respect to time. Yet, for the unvegetated control BBS microcosm porosity Δ is significantly different from T8 to T12. Whilst there is a lack of statistical significance between T8, T10 and T12 data, median porosity Δ is always negative in all vegetation treatments of BBS microcosms. This suggests that there is a reduction in porosity with time, but that the reduction occurred between T0 and T8. For the BBS unvegetated control microcosm there is an initial reduction in porosity from T0 to T8, but this lost porosity is recovered by T12. The exact mechanisms by which this result was achieved are unknown, with little supporting data from other characterised properties. All LECA microcosms also exhibit a general trend toward reduced porosity over time, with similar magnitudes of reduction as seen in BBS. None of the LECA treatment groups exhibit a statically significant difference in porosity Δ with time. As for BBS microcosm, this suggests that the porosity reductions occurred prior to the acquisition of the T8 images.

The tortuosity Δ for all microcosms is presented in **Figure 6.17** as mean and standard deviations values. For BBS there is a clear division in trends between vegetated and unvegetated microcosms. Vegetated BBS microcosms exhibit reduced tortuosity values with time, whilst the unvegetated control exhibits increased tortuosity with time. There is no statistically significant difference in tortuosity Δ, suggesting that any changes occurred prior to T8 imaging. The reduced tortuosity with time of the vegetated BBS microcosms suggests shorter travel paths through the substrate with time, due to downward root growth forming preferential flow paths. Increased tortuosity of unvegetated samples provides more evidence of the wash-through of finer particles to lower substrate layers, causing flow paths to be longer.
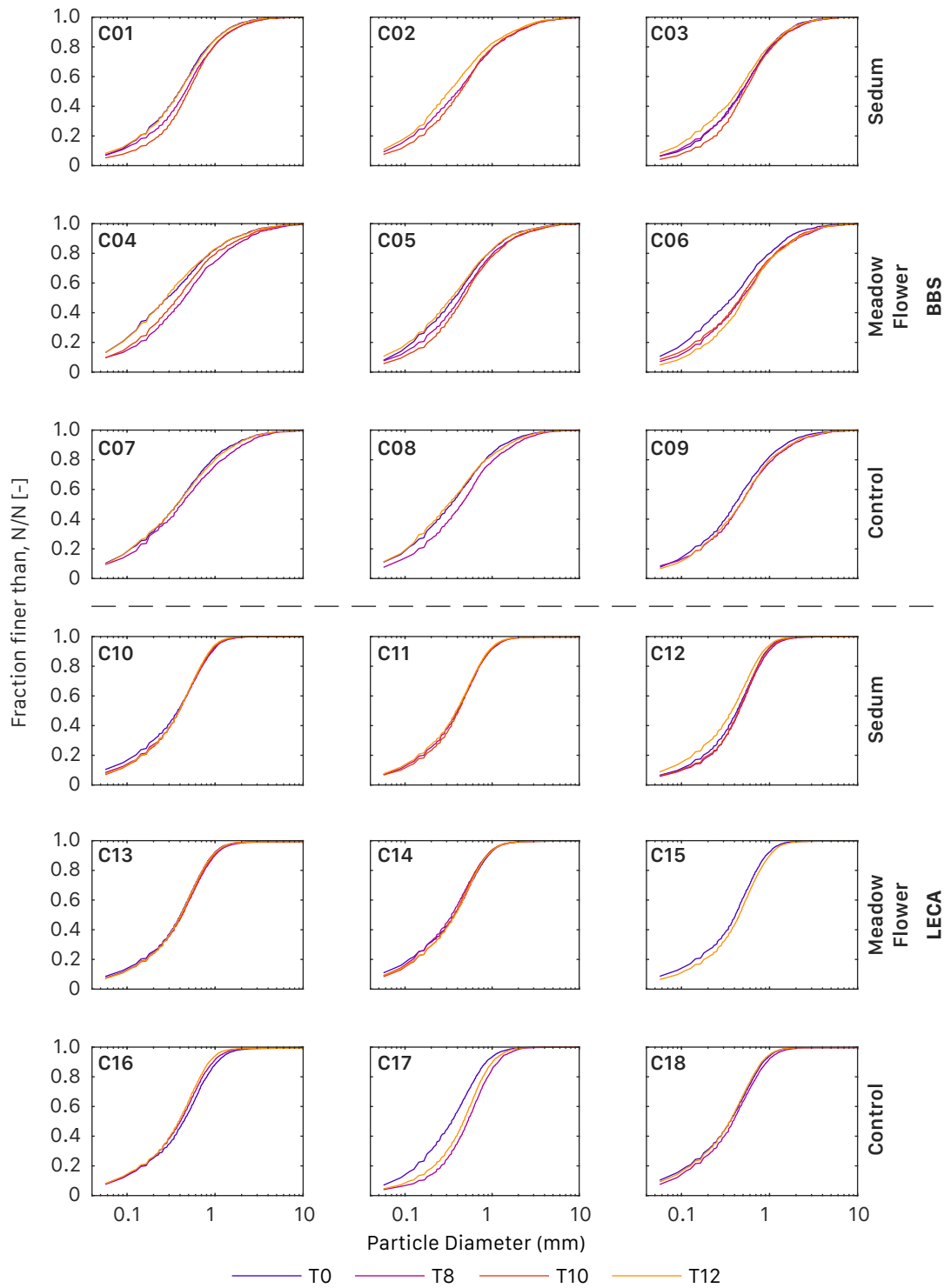
Figure 6.15 XMT–derived particle size distributions over time for the 18 50 mm substrate cores.
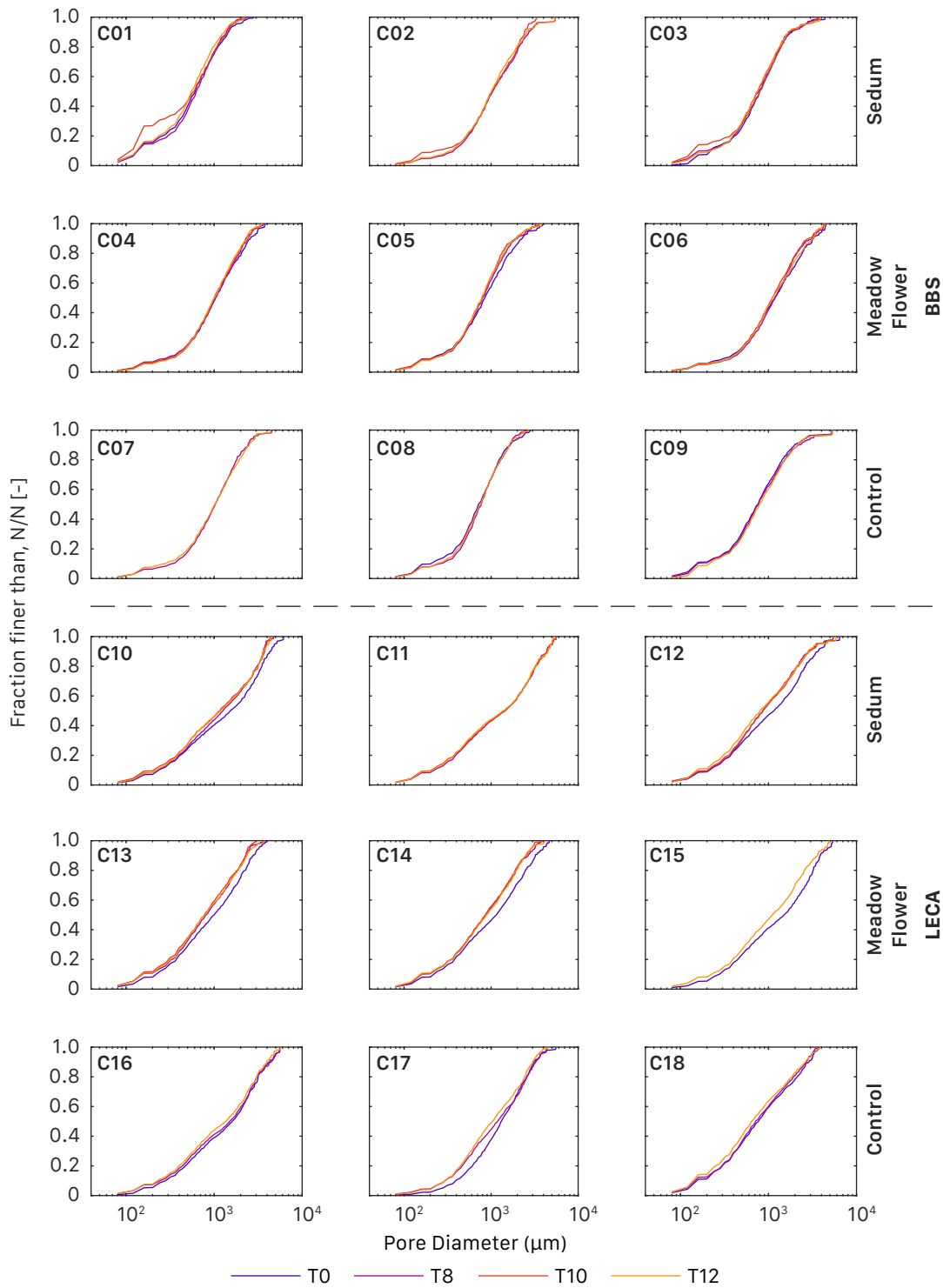
Figure 6.16 XMT-derived pore size distributions over time for the 18 50 mm substrate cores.
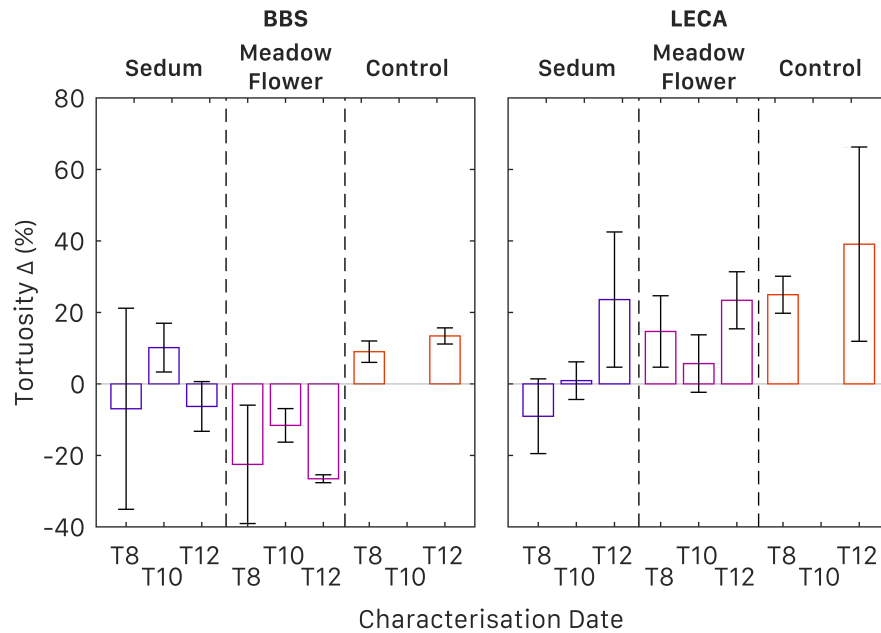
Figure 6.17 XMT-derived mean tortuosity, %Δ from T0. Error bars indicate ± 1x standard deviation.

LECA microcosms experienced increases in tortuosity for all treatment groups (**Figure 6.17**), although, as for BBS, there is no statistical significance to the differences with time. Sedum LECA microcosms experienced an initial reduction in tortuosity at T8, but exhibited continual increases from T10 onwards. The increases in tortuosity suggest a lengthening of flow paths through the LECA substrate. Both vegetated configurations result in an overall (T12) mean tortuosity Δ of approximately 23%, whilst the unvegetated configuration sees increases in tortuosity of approximately 40%. The changes in tortuosity of the control microcosms suggest a filling of deep substrate pores with fine material, extending flow paths. This theory is supported by the observed reductions in median pore diameter.

XMT-derived saturated hydraulic conductivity values were determined from LBM models of flow through the substrate matrix. The greater the porosity and pore sizes within the substrate, the longer the LBM simulations take to converge. For BBS substrates with their low porosities and relatively small pore diameters, compared to LECA, LBM models converged within 10000 iterations taking approximately 8 hours. The large pore systems of LECA only began to converge after 15000 iterations, and with each iteration taking more time than BBS, a single model runtime could be > 20 hours. Given the lack of physically-derived LECA hydraulic conductivity data for valid comparisons to XMT-derived values, only one microcosm from each LECA treatment group underwent LBM modelling to ascertain saturated hydraulic conductivity values.

Figure 6.18 presents the changes in XMT-derived saturated hydraulic conductivity values for all BBS microcosms and a single LECA microcosm of each treatment group across the 12-month study period. Vegetated BBS samples exhibit negative values of saturated hydraulic conductivity Δ, indicating reductions in saturated hydraulic conductivity over time. Both the Sedum and Meadow Flower treatments have increasingly negative mean values of saturated hydraulic conductivity Δ, suggesting a gradual decline in saturated hydraulic conductivity over time. However, there is significant variability in the saturated hydraulic conductivity Δ of each treatment group at each characterisation date and so there is no statistically significant difference in saturated hydraulic conductivity Δ from T8 to T12. The trends in mean saturated hydraulic conductivity Δ for the vegetated BBS microcosms most closely follow those of the median pore diameter data (**Figure 6.14**). Saturated hydraulic conductivity is a function of porosity, pore diameters, and tortuosity. The observation of similar trends between saturated hydraulic conductivity and median pore diameters indicates that pore diameters are more influential on saturated hydraulic conductivities than porosity or tortuosity. The unvegetated BBS control microcosms exhibits mean increases to saturated hydraulic conductivity over time, although these differences are not statistically significant from T8 to T12.
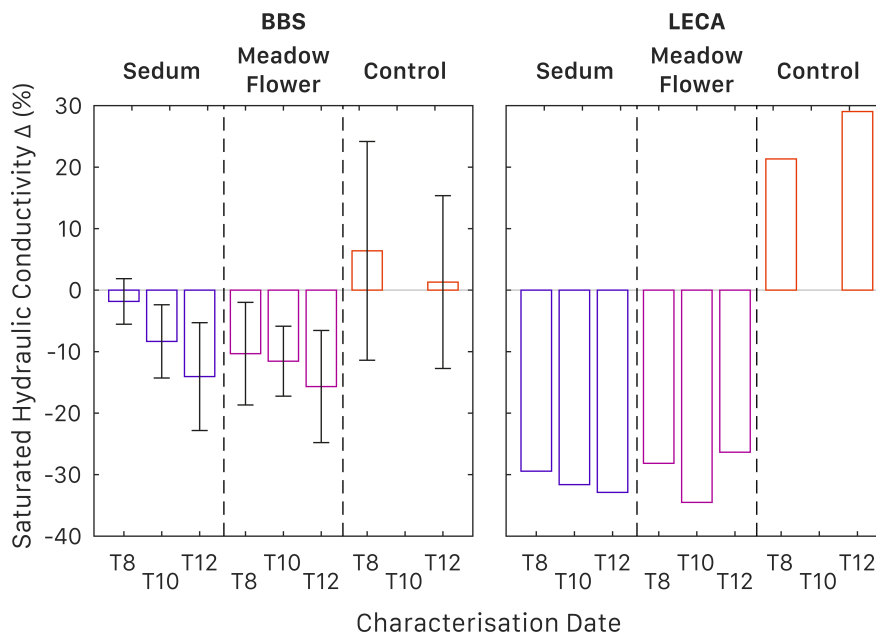
Figure 6.18 XMT-derived saturated hydraulic conductivity, %Δ from T0. **BBS**: Mean ± 1x standard deviation. **LECA**: single value per treatment group and characterisation date.

The contrasting saturated hydraulic conductivity Δ results between vegetated and unvegetated BBS microcosms is also present for their LECA counterparts. Vegetated LECA microcosms exhibit reductions in saturated hydraulic conductivity over time, but at a larger scale than those seen for BBS. For the Sedum LECA microcosm there is a gradual decrease in the value of saturated hydraulic conductivity over time, whilst the Meadow Flower treatment experiences a greatest decline at T10. As seen in BBS, the trends in saturated hydraulic conductivity Δ of vegetated LECA microcosms closely resemble the trends in median pore diameter (**Figure 6.14**), further evidence that pore diameters are more influential on saturated hydraulic conductivities than porosity or tortuosity. As only one microcosm from each LECA treatment group was subject to LBM modelling there is no available standard deviation data. However, from the T0 samples (where there were 3 repeats for LECA), LECA has a significantly greater variation in saturated hydraulic conductivity than BBS (**Figure 6.13**). Given this, it is assumed that there would be no statistically significant difference in the saturated hydraulic conductivity Δ of LECA microcosms from T8 to T12.

Statistical tests have identified that for most XMT-derived properties there are no statistically significant differences in the changes in property values at T8, T10 or T12. However, some substrate property changes are substantial (>10%) and there is a need to identify whether changes from T0 to T12 are statistically significant. **Figure 6.19** presents the mean and standard deviations of the XMT-derived substrate properties at T0 and T12, whilst **Table 6.3** summarises the results of a Kruskal Wallis test. Inspection of **Figure 6.19** reveals the high levels of heterogeneity between the T0 samples of each of the 6 treatment groups, particularly for tortuosity. It is this heterogeneity that necessitated the observation of %Δ from T0 values as opposed to comparisons in specific property units. **Table 6.3** reveals that for all properties and all treatment groups there is no statistically significant difference between T0 and T12 values. This statistical outcome is likely a result of the small number of replicates within each treatment group (N=3) and the small size of the microcosms (50 mm diameter). Irrespective of the statistics, all microcosms in all treatment groups exhibited at least minor, in some cases major, changes to substrate properties over time. Subsequent analysis of the impacts these property changes have on hydrological performance will be undertaken using the mean property values from each treatment group and characterisation data in Chapter 7.

> *The main conclusions from the XMT-derived substrate characterisations are: current particle separation algorithms are unsuitable for the repeated imaging methodology of this study, dividing particles differently for each temporal image set; changes to substrate properties have been identified to have largely occurred prior to the second imaging of the microcosms at 8-months into the study, with marginal differences identified from T8 to T12; observed differences in T0 and T12 properties for all microcosms are not statistically significant due to the high levels of heterogeneity.*
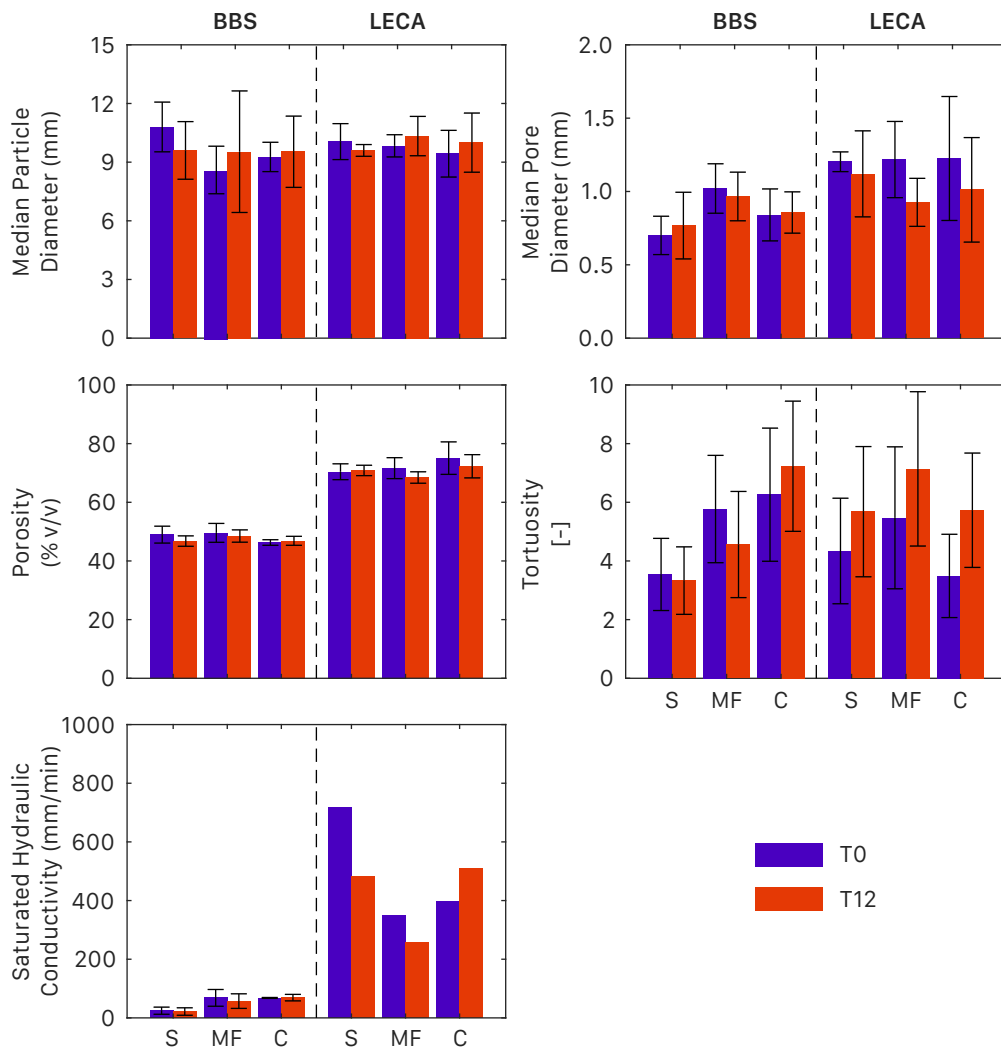
Figure 6.19 Comparison of XMT-derived properties at the beginning (T0) and end (T12) of the 12-month study period. **S** – Sedum. **MF** – Meadow Flower. **C** – Control.

Table 6.3 Kruskal-Wallis P values comparing T0 and T12 XMT–derived substrate properties. * indicates significant statistical difference at P<0.05. Insufficient data for determination of LECA hydraulic conductivity.

	BBS			LECA		
	S	MF	NV	S	MF	NV
Median Particle Diameter	0.3743	0.8273	0.8273	0.5637	0.5127	0.5127
Median Pore Diameter	1.0000	0.5127	0.6579	1.0000	0.1266	0.5127
Porosity	0.2482	0.8273	0.8273	0.5637	0.1266	0.5127
Tortuosity	0.3173	0.3173	0.3173	0.3173	0.3173	0.3173
Saturated Hydraulic Conductivity	0.4386	0.5127	1.0000	–	–	–

6.4 XMT-derived Root Network Chatacterisation

6.4.1 Differences in rooting architecture

The XMT images permit the extraction of the vegetation root networks where there is sufficient contrast between the root material and substrate particles. Sedum and Meadow Flower vegetation are believed to have different rooting architectures. **Figure 6.20** illustrates the identified root networks of a Sedum and Meadow Flower BBS microcosm at T8. The rooting systems of sedum and meadow-flower vegetation are clearly very different, as expected. Sedum roots are much more dense and extend only to a shallow depth (<30 mm). Meadow-flower roots extend much deeper into the substrate but the network appears less dense that for Sedum. In some instances Meadow Flower roots were observed emerging from the bottom of the microcosm.
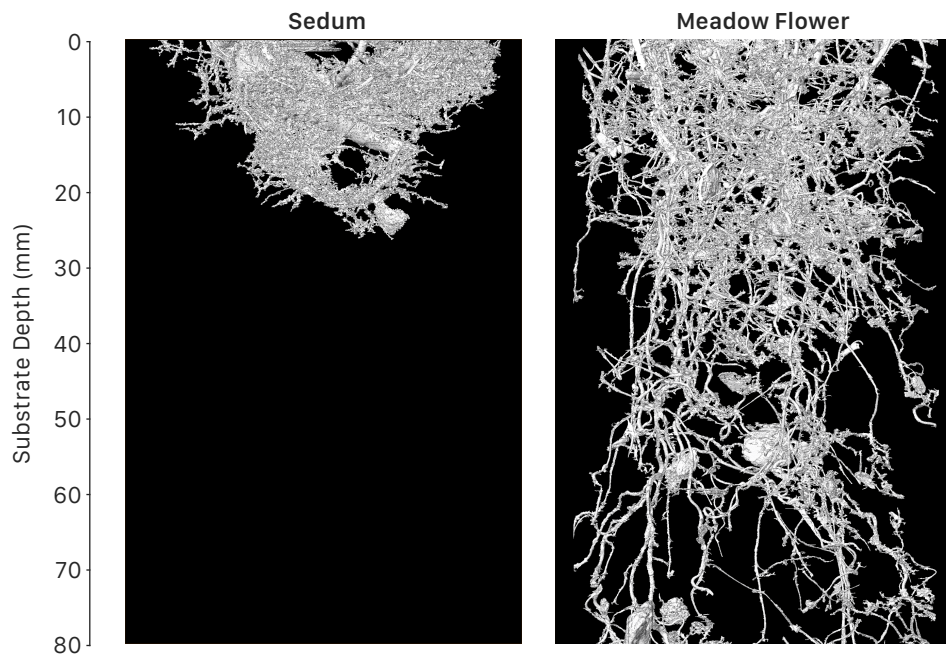
Figure 6.20 3D volume of surface-connected root networks for sedum and meadow flower vegetation types, identified from XMT data.

The root segmentation of **Figure 6.20** is not perfect, there is some evidence of particles being included in the Meadow Flower root network. These errors arise from insufficient contrast between the root material and surrounding aggregate pieces. Stronger contrast between the root and aggregate material could be attained from an uncompressed 16-bit image. However, this would double the image memory size thus requiring more computational resources.

6.4.2   Root development from T8 to T12

The root network of a single Sedum BBS microcosm was extracted for the full study period (**Figure 6.21**). As there was no network present at T0, all of the root network present in the T8 image has developed since the sedum was planted. As time advances the root network can be seen to enlarge, with significant new growth from T8 to T10, and again from T10 to T12. The root network expands greatly within the first 10 mm of substrate depth, as seen in the upper left-hand corner of each image in **Figure 6.21**. Root depth extends from 26 mm to 33 mm in the 4 months from T0 to T12. Root density increases as the large central root present in the T8 images becomes increasingly less visible until it cannot be seen in T12.

> *The main conclusions from the XMT-derived root network characterisations are: Sedum and Meadow Flower vegetation have very different rooting architectures, with Sedum exhibiting a shallow fibrous root system and Meadow Flower a deep yet sparse root network; additional contrast between root material and substrate particles is required for further root network and root-substrate interaction studies.*
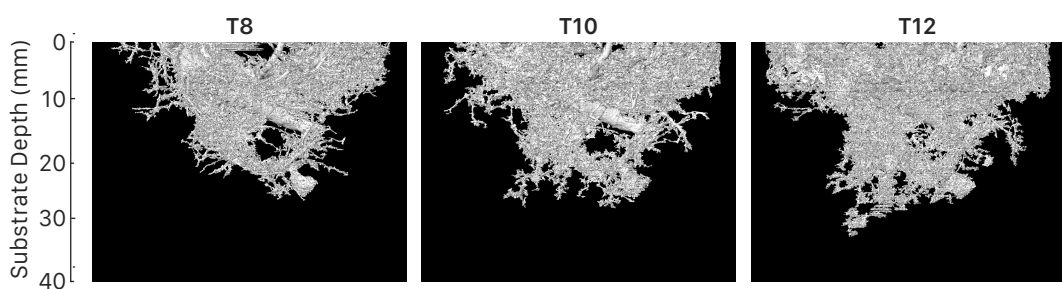
Figure 6.21 3D Volume of surface connected sedum root networks over time, identified from XMT data.

6.5 Image Resolution Exploration

The relatively high image resolutions used in this part of the study, 40 μm, result in very large image files for complete substrate cores. An exploration of higher resolution images captured at 17 μm was undertaken to assess the impact of image resolution on quantified characteristics. These large files take a large amount of time to process and require a considerable amount of computational resources, notably RAM. To speed up analysis, image resolution can be downscaled, with a 3D volume a 2 x reduction in resolution (from 17 to 34 μm) results in an 8 x reduction in image size (2^3). However, reductions in file size by downscaling increase the size of the smallest observable feature within the image, leading to poorer characterisation.

Downscaling a 17 μm image by a factor of 2 to create a 34 μm image resulted in the loss of 0.41% of identified porosity (**Figure 6.22**). Downscaling the image by a factor of 6 to 102 μm resulted in a greater loss of porosity (4.40%). However, **Figure 6.23** demonstrates that there is little visually observable difference in a 17 and 102 μm image. To keep porosity losses to below 1% a downscaling factor of 3, resulting in a 51 μm image, can be applied.
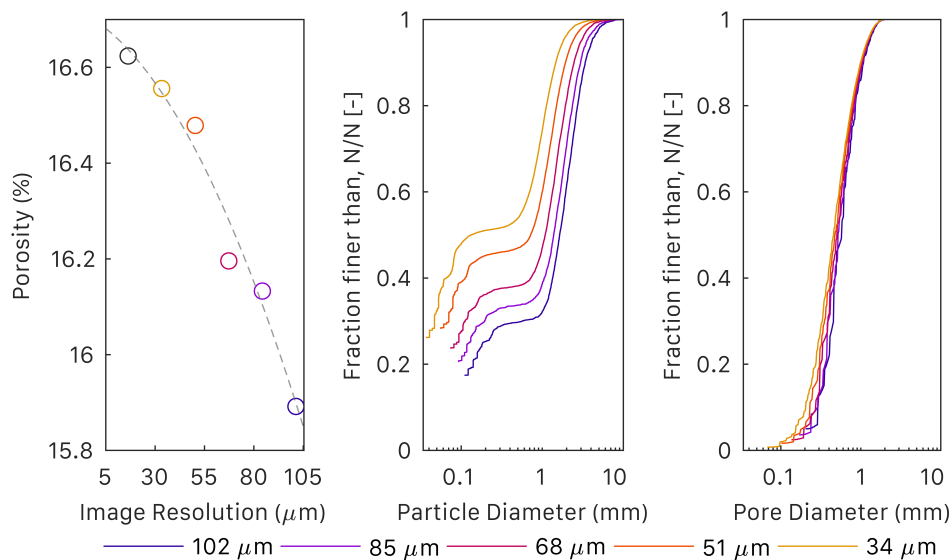
Figure 6.22 The effects of image resolution on XMT substrate property characterisation

Significantly greater differences arise in particle size distributions compared to porosity values. The most obvious difference with changing resolution is the diameter of the smallest identifiable particle (**Figure 6.22**). There are also large differences in median particle diameter (**Table 6.4**), with increases of >500% when downscaling from 34 to 51 um. However, this change is entirely attributed to differences resulting

from the particle separation algorithm. Inspection of **Figure 6.23** reveals that the separation lines are in different places in each image. Additionally, a one pixel thick separation line will also reduce particle sizes by increasing amounts for decreasing resolutions as it represents a greater proportion of the image. A significantly improved particle separation algorithm would be required to isolate the effects of image resolution on identified particle size, particularly for the irregularly shaped and highly porous particles of green roof substrates.

Table 6.4 The effects of image resolution on XMT-derived median particle and pore diameters.

Image Resolution (microns)	102	86	68	51	34
Median Particle Diameter (mm)	1.64	1.38	1.09	0.72	0.13
Median Pore Diameter (mm)	0.58	0.51	0.51	0.49	0.46

Pore size distributions are affected by image resolution but on a reduced scale compared to particle sized distributions. As for particle size distributions, the image resolution dictates the smallest identifiable pore space (**Figure 6.22**). Median pore diameters increase with reducing image resolution, as the smallest pores are not identified. Downscaling from a 34 to 51 µm resolution results in a 6.5% increase in median pore diameter (**Table 6.4**). Visually, the difference in pore size by resolution are only distinguishable between the 34 and 102 µm images (**Figure 6.23**).

> *The main conclusions from the XMT image resolution exploration are: higher image resolutions are key to the identification of the smallest features of interest; image processing algorithms for separating particles result in very different particle size distributions due to varying division of objects at varying resolutions; porosity and pore size distributions are less affected by image resolution than particle size distributions.*
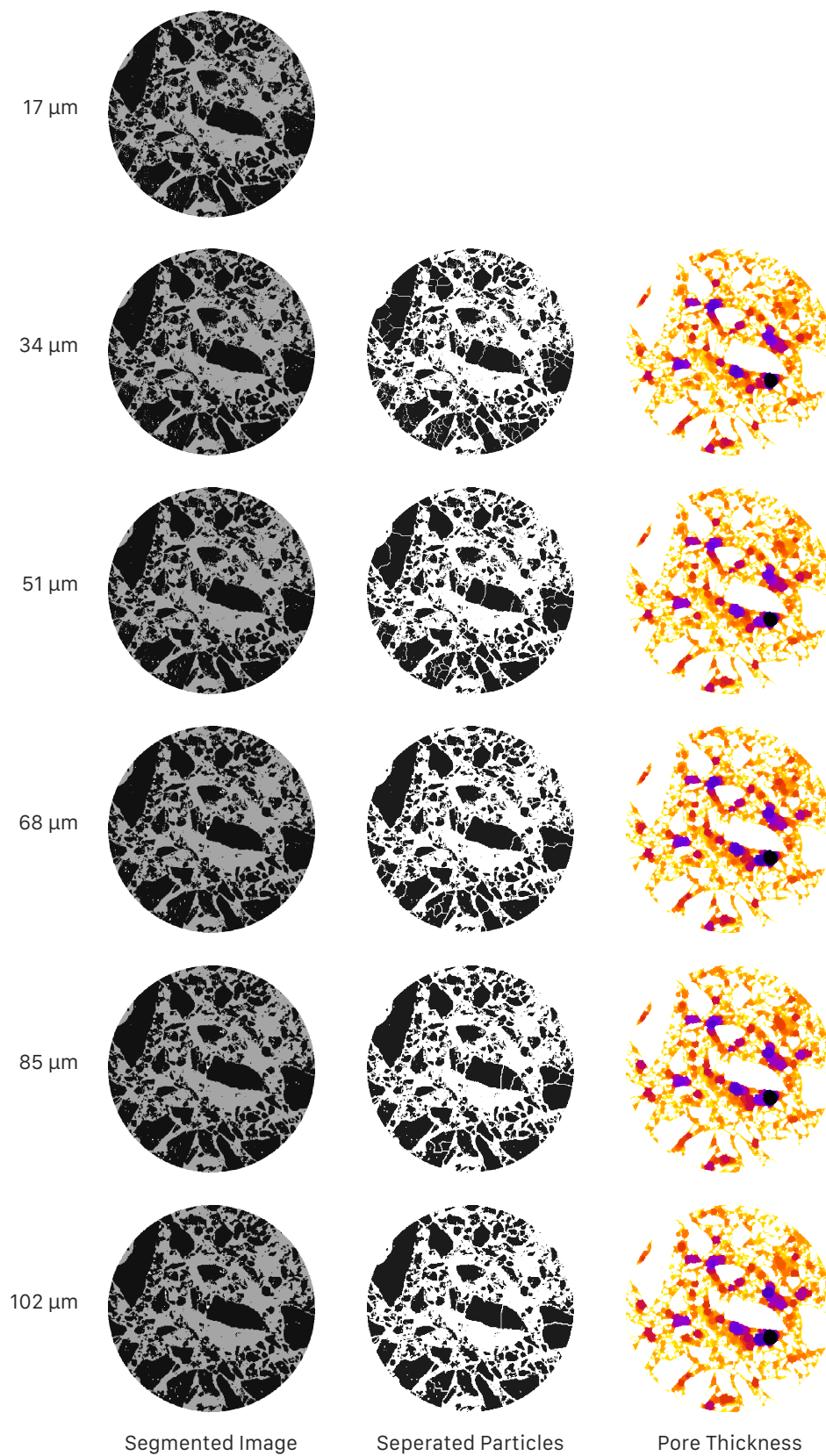
Figure 6.23 Images at varying image resolutions. Note: separated particle and pore thickness images could not be generated for 17 microns due to computer RAM limitations.

6.6 Discussion

6.6.1   Comparison of 50 mm and 150 mm diameter microcosms

A key concern regarding the 50 mm microcosm was whether such small samples, 1/3 the diameter recommended by the FLL (11% of the volume), were a fair representation of typical substrate sample sizes. The characterisation of the smaller 50 mm microcosms alongside a standard 150 mm FLL substrate sample permitted the identification of any negative heterogeneity impacts due to sample size.

At T0 the hydrologically important physical properties (MWHC and K_{sat}) for the 50 and 150 mm microcosms were largely similar, although significant statistical differences were observed in the particle size distributions of the two microcosm sizes for both substrate types. The smaller 50 mm microcosms exhibited a differently graded particle size distribution despite being assembled from the same batches of substrates as the 150 mm microcosms. The exact mechanism by which this alteration of particle sizes arose is unknown. However, this difference also highlights that substrate particle sizes alone are not a good indicator of hydrologically important substrate properties.

The aged microcosms (at T12) exhibit similar differences to those at T0, with significant statistical differences remaining for median particle diameters and the percentage of particles <0.063 mm. All other properties experienced no changes to the statistically significant differences between a 50 and 150 mm microcosm size. This consistency in differences over time suggests there is no impact on ageing processes arising from microcosm size.

6.6.2   Key differences in virgin and aged substrate properties

Statistical tests largely revealed that there was no difference in substrate physical properties over time when characterised by either method. These results indicate that if the aged samples were independent of the initial samples, they could be said to have approximately the same properties. This highlights the relatively large impacts of substrate heterogeneity potentially masking physical property changes over time. By repeatedly characterising the same substrate samples as they age, the effects of this heterogeneity can be mitigated. In the phase 2 tests, the known initial conditions allow for clear indications of the trends identified below in substrate property changes over time.

Physically-derived median particle diameters, in both 50 and 150 mm BBS microcosms, indicate a general decline over time, except the 150 mm Sedum BBS microcosms exhibit a contrasting trend, with a mean increase over time. XMT-derived values are more varied, but final T12 median values indicate similar overall declines in particle size for the 50 mm BBS substrate microcosms. The reductions in median particle diameter are accompanied by increases in the percentage of particles finer than 0.063 mm. Together these findings indicate that there has been some breakdown of BBS particles. LECA microcosms exhibit slight reductions to physically-derived median particle diameters over time. However, XMT-derived values suggest slight increases. This discrepancy is discussed further in section 6.6.3. Physically-derived values of the percentage of particles finer than 0.063 mm have increased with time, further supporting a reduction in median particle sizes with time.

Physically-derived values of MWHC provide some indication of the changes to pore sizes within the substrate. MWHC values correspond to the total pore volume of pores with a dimeter of 50 µm (micropore volume). Observed increases in MWHC for both BBS and LECA microcosms suggest an increase in this micropore volume with time. The XMT-derived pore size characteristics also indicate reductions to median pore sizes over time, suggesting a greater volume of smaller pores. This reduction in pore sizes is also accompanied by an XMT-derived reduction in overall porosity. All this evidence indicates that pore sizes have decreased with increased substrate age. These reductions tally with the increased amounts of fine particles (<0.063 mm), and reduced median particle diameters, as small particles have filled larger pores, reducing overall pore sizes.

The saturated hydraulic conductivity of both substrates has changed over time. XMT-derived estimates of K_{sat} follow the identified trends in pore sizes, with reductions in K_{sat} over time for all substrate types. Physically-derived values of K_{sat} for LECA microcosms also identify a reduction in K_{sat} with age, with similar magnitudes of reduction as for the XMT-derived values. Contrastingly, the physically-derived values of BBS K_{sat} indicate increases with time. The exact mechanism by which this difference arises is unknown, and the clear distinction in trends over time between BBS and LECA substrates is the only occurrence of divergence in the results due to substrate type. The presence of living vegetation may play a role in increasing the values of K_{sat} by a process not identifiable in the XMT methodology. Virahsawmy et al. (2014) identified that the presence of vegetation prevented reductions in bio-filter

media K_{sat} over time. However, the increase in K_{sat} for the unvegetated BBS control microcosms suggests that the difference cannot be solely attributed to the presence of vegetation. The increases in K_{sat} are also contradictory to the pore and particle size findings above. There are significant concerns about the FLL testing procedure for determining hydraulic conductivity, but the systematic increase in K_{sat} is beyond the scope of current criticisms. Hydrological modelling undertaken in chapter 7, provides further exploration of these changes in K_{sat}.

6.6.3 Comparison of physically-derived and XMT-derived properties

The only directly relatable properties from the physical testing programme and the image processing are saturated hydraulic conductivities. Figure 6.24 compares the physically-derived and XMT-derived values of K_{sat} for the 50 mm BBS microcosms, and highlights the underestimation of XMT-derived K_{sat} compared to the physically-derived values. The disparity in K_{sat} values is a result of the substrate's pore size distribution and the inability of the XMT-derived properties to account for pore features smaller than 40 µm. The LBM modelling of fluid flow from the XMT images is therefore only a representation of the substrate's macropore network (pores >50 µm). Given that pore sizes greatly influence the magnitude of K_{sat} (as identified in section 6.3), alignment of the XMT-derived and physically-derived K_{sat} values indicates that substrate hydraulic conductivity is dominated by flow in the macropore network. Where XMT-derived and physically-derived characterisations are different, the substrate's micropore network is responsible for a considerable fraction of water flow.
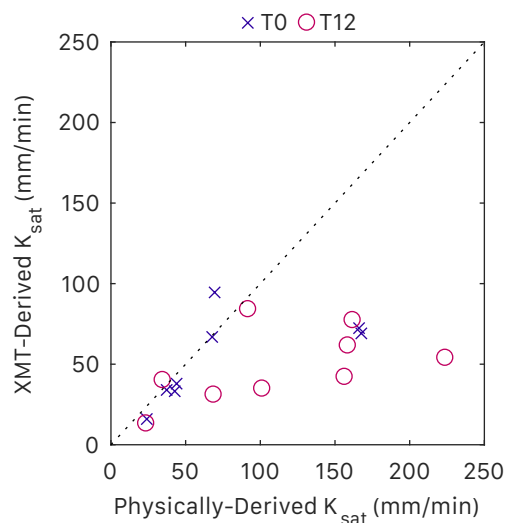
Figure 6.24 Comparison of physically-derived and XMT-derived K_{sat} values.

6.7 Chapter Summary

The repeated characterisation of key physical substrate properties of six green roof microcosm treatment groups revealed that initial (T0) and aged (T12) substrate properties were not the same. Two sizes of green roof microcosm were aged in parallel to determine the effect of microcosm size on ageing processes, and no systematic differences were observed between the T0 and T12 characterisations of the two microcosm sizes. This lack of differences indicates that microcosm size is not a controlling factor for substrate ageing. The changes in physical properties of both substrate types (brick-based and LECA-based) trend toward smaller particle and pore sizes. These reductions lead to increases in substrate micropore volumes which are demonstrated through increased water holding capacities. The impacts that the identified substrate property changes have on hydrological performance is addressed in chapter 7.

X-ray microtomography proved to be a valuable tool for repeatedly characterising the substrates, an approach not achievable with destructive physical measures. The temporal spacing of imaging highlighted that significant structural changes occurred within the first 8 months of ageing, with much smaller changes occurring in the last 4 months. The contrasting root architectures of the Sedum and Meadow Flower vegetation were observed from XMT images, where the growth of Sedum networks over time was seen to be slow. Further characterisation of root networks requires an adjustment of the methodology used for this study to better enhance the contrast between root material and the surrounding substrate matrix.

Similar disparities in physically-derived and XMT-derived properties to those experienced in chapter 5 were observed. An exploration of image resolution on resultant property values identified that significant differences arise from imaging processing techniques as opposed to actual image capture, although image resolution will always dictate the size of the smallest identifiable feature. This adds further weight to the argument that the size of features of interest should be identified before embarking on an XMT imaging programme.

The results and discussion presented here will be brought together with the findings of chapters 4, 5 and 7 to provide an overall synthesis and discussion, which is presented in chapter 8.

7. *Longitudinal Microcosm Study Results & Discussion: Hydrological Performance*

7.1 Chapter Overview

This chapter presents the hydrological performance evolution results of the second phase of X-ray microtomography experiments, which repeatedly characterised green roof microcosm substrate properties. Physically-derived characterisations of substrate properties and hydrological performance undertaken at the start and end of the study are outlined before being supplemented by X-ray imaging data analysis conducted at intervals throughout the year of the study. The performance of two hydrological modelling techniques (reservoir routing and physically-based finite element modelling) is evaluated and accompanied by a discussion of the implications that substrate properties have for long-term hydrological models. The characterisations of hydrological performance presented here have been incorporated into the following conference publication:
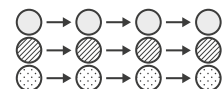
De-Ville, S., Stovin, V., Menon, M., Submitted. 'Hydrological performance evolution of extensive green roof systems'. *14th International Conference on Urban Drainage*.

7.2 Physically-derived Hydrological Performance

The physically-derived MWHC values enable the estimation of maximum potential retention capacities over time (equivalent to PAW). Assuming θ_{PWP} is approximately 6% in BBS and 2% in LECA (Poë, 2016), PAW values for each treatment group at both characterisation dates (T0 and T12) have been evaluated (**Table 7.1**) using equation 3.16. The effects that the changes in PAW have on potential retention performance (PRP) are modelled using a moisture flux model (see section 3.4.8) and are illustrated in **Figure 7.1**. At an ADWP of 0 days all microcosms are modelled as being at field capacity ($\theta = \theta_{FC} = $ MWHC). As the ADWP increases, the PRP increases as the storage within the substrate is recovered through evapotranspiration losses. The rate of recovery (gradient of the lines in **Figure 7.1**) is initially fast as evapotranspiration processes are not substrate moisture limited (θ close to θ_{FC}). At high ADWPs the rate of storage recovery is lower, as reduced moisture levels (θ approaching θ_{PWP}) restrict evapotranspiration losses.

Table 7.1 Physically derived mean PAW values for the 50 mm microcosms, assuming θ_{PWP} is 6% in BBS and 2% in LECA.

Substrate	Vegetation Treatment	Age	MWHC (% v/v)	PAW (% v/v)
BBS	Sedum	T0	31.1	25.1
		T12	36.7	30.7
	Meadow Flower	T0	28.9	22.9
		T12	31.5	25.5
	Control	T0	32.8	26.8
		T12	32.5	26.5
LECA	Sedum	T0	18.4	16.4
		T12	21.2	19.2
	Meadow Flower	T0	19.1	17.1
		T12	19.8	17.8
	Control	T0	18.9	16.9
		T12	16.9	14.9

In response to a 1-in-30-year 1-hour design rainfall event for Sheffield, UK, there is little difference in the PRP for BBS substrates when ADWP is <5 days (all treatment groups and ages PRP approximately 22%, **Figure 7.1**). At a 7-day ADWP, the Sedum BBS microcosms experience the greatest improvement in PRP from T0 to T12 of 3.3%, whilst the BBS control microcosms experience a 0.2% PRP reduction. The differences in T0 and T12 PRP increase as ADWP approaches 28-days. For a 28-day ADWP, Sedum BBS microcosms exhibit a 13.6% improvement in PRP, whilst the BBS control

microcosms exhibit a 0.7% reduction. LECA microcosms exhibit reduced levels of PRP across all vegetation treatments and ages compared to their BBS counterparts. This is a result of the lower MWHC and PAW values for LECA substrates. As for BBS microcosms, there is little difference in PRP of LECA microcosms at ADWPs of 4-days or less (all treatment groups and ages PRP approximately 16%, **Figure 7.1**). For a 7-day ADWP, Sedum LECA microcosms see a similar scale of improvement in PRP as Sedum BBS examples (+3.4% from T0 to T12). The differences in LECA PRP at a 28-day ADWP are also similar to their BBS counterparts, with Sedum microcosms exhibiting a 13.8% improvement. The unvegetated LECA control microcosms are seen to exhibit a reduced PRP at T12 compared to T0, -3.4% at 7-days and -10.3% at 28-days.
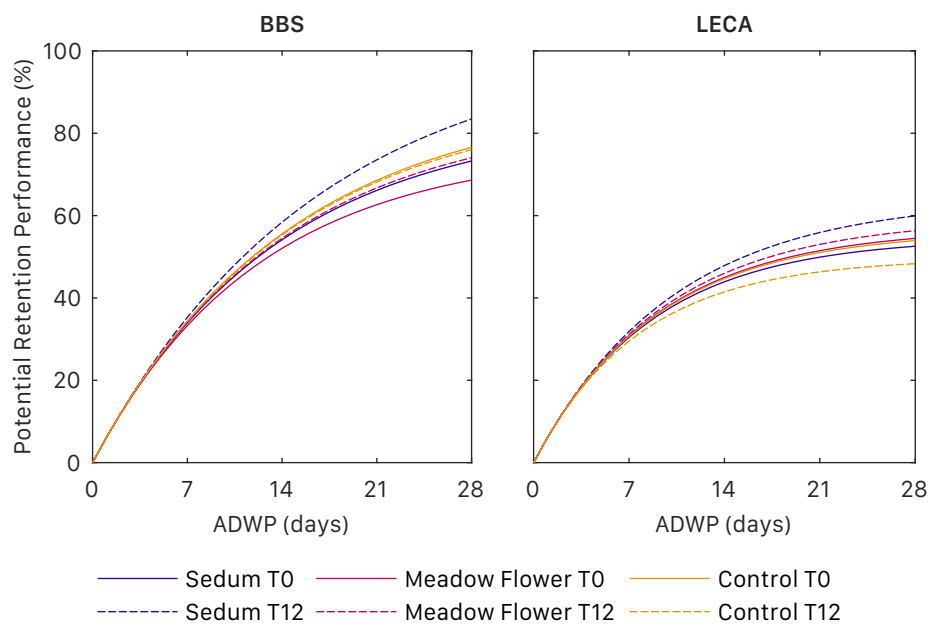
Figure 7.1 Physically-derived estimates of potential retention capacity at varying ADWP for BBS and LECA microcosms under spring conditions for a 1-in-30-year 1-hour design rainfall event.

Detention performance is more difficult to infer from physically-derived properties due to the complex interactions which control unsaturated flow conditions (like those experienced under typical green roof operation). Detention performance was physically assessed from a series of simulated rainfall events undertaken on the 50 mm BBS microcosms at T0 and again at T12. **Figure 7.2** presents a single T0 and T12 rain and runoff profile for each of the 9 BBS microcosms. The detention performance of each microcosm is described through fitted reservoir routing model parameters. The best fit model runoff is also illustrated in in **Figure 7.2**. Model parameters and goodness of fit values are provided in **Table 7.2**.
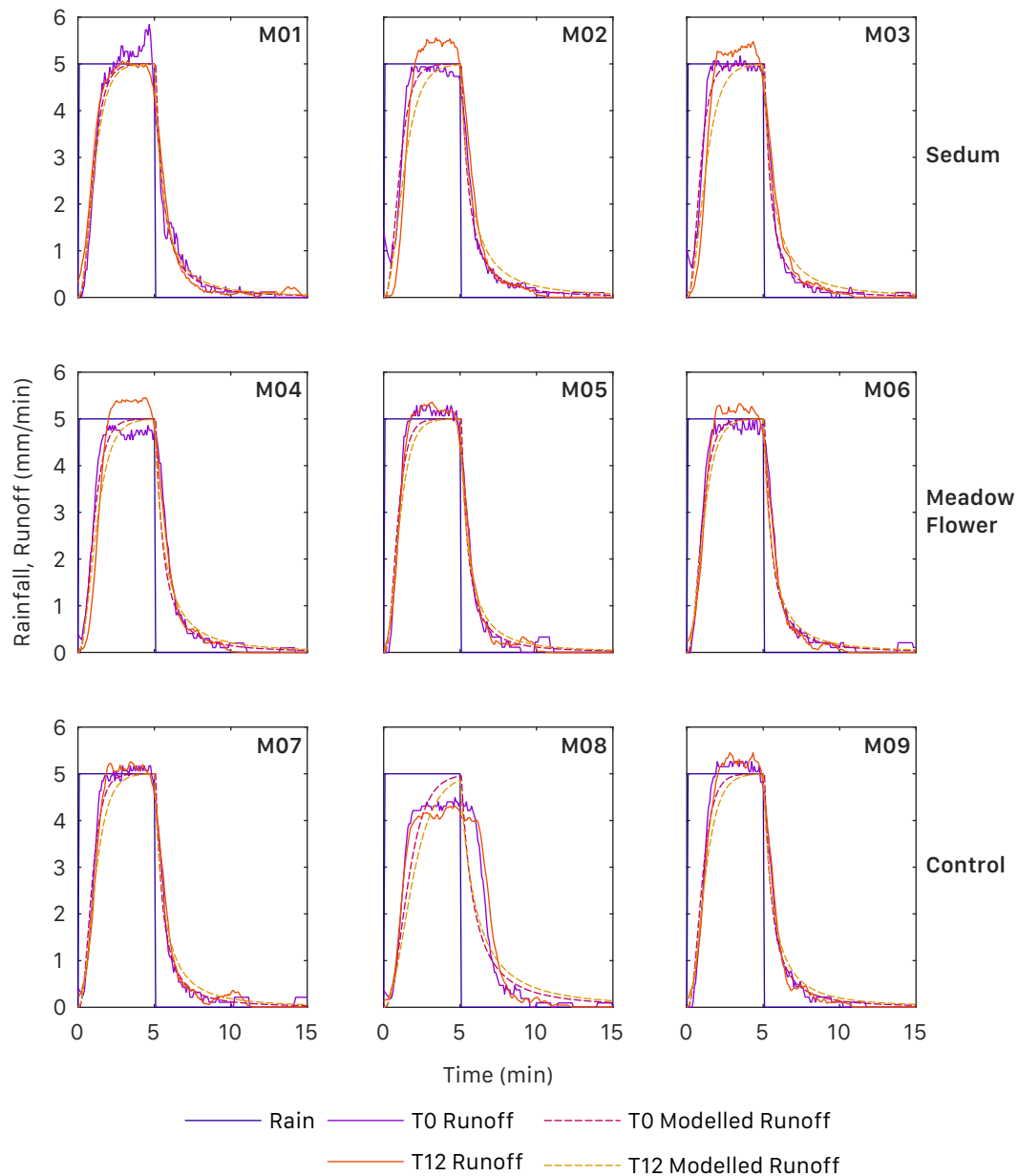
Figure 7.2 Rainfall and runoff from physically-simulated rainfall events on BBS microcosms, including best detention model fit runoff profiles.

Table 7.2 Detention model parameter D_s and R_t^2 goodness of fit values for the modelled runoff profiles of Figure 7.2

Microcosm	M01	M02	M03	M04	M05	M06	M07	M08	M09
D_s at T0	0.0170	0.0159	0.0226	0.0163	0.0219	0.0178	0.0202	0.0062	0.0170
R_t^2 at T0	0.9911	0.9898	0.9934	0.9887	0.9943	0.9937	0.9955	0.9489	0.9933
D_s at T12	0.0145	0.0085	0.0106	0.0099	0.0154	0.0132	0.0129	0.0043	0.0118
R_t^2 at T12	0.9901	0.9830	0.9868	0.9865	0.9920	0.9908	0.9913	0.9365	0.9900

Vegetated BBS microcosms exhibit statistically significant reductions in the detention model parameter (D_s) from T0 to T12 (**Figure 7.3**). The mean value of D_s for the control microcosms also exhibits a reduction but this difference is not statistically significant. The reduced values of D_s indicate an improvement to detention performance, which is also identifiable in **Figure 7.2** where the T12 runoff frequently occurs after the T0 runoff. The reported values of D_s also have an associated model fit, **Figure 7.3** illustrates that there is no reduction in model fit from T0 to T12 so the identified changes in D_s can be attributed to changes within the substrate. The values of D_s identified here are an order of magnitude greater than those identified in section 4.4.1 for the monitored green roof test beds as the microcosms do not include the filter sheet and drainage layer components, thus permitting faster runoff.
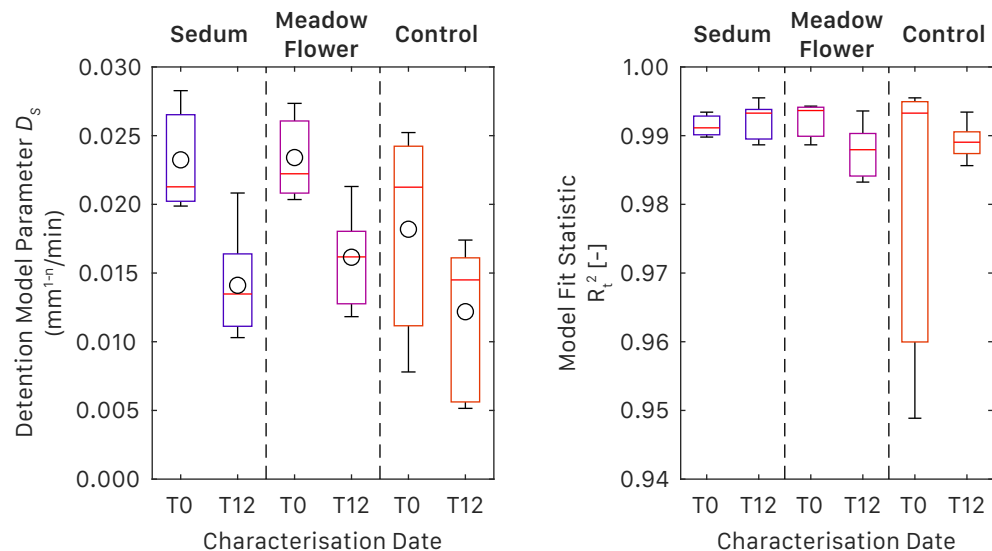
Figure 7.3 Left: Optimised detention parameter D_s for BBS 50 mm substrate microcosms at T0 and T12. **Right**: Corresponding R_t^2 values for detention parameter D_s.

Combining the above retention and detention observations facilitates the prediction of the complete hydrological response of the substrate microcosms for a range of rainfall input types. The combined hydrological response of the BBS microcosms to a 1-in-30-year 1-hour summer design rainfall event for Sheffield, UK, is presented in **Figure 7.4**. Combined predictions for LECA microcosms are not made due to the absence of LECA detention model parameters. Three ADWPs are shown to highlight the influence of retention performance on the overall hydrological response. The

detention only 0-day ADWP results illustrate the differences observed in the detention model parameter D_S, with the largest difference in runoff profiles occurring for the Sedum vegetated microcosms, resulting in a 56% peak attenuation improvement. The unvegetated control microcosms exhibit the highest levels of detention performance due to the low values of D_S identified from the detention testing. However, the improvement in peak attenuation from T0 to T12 is only 30%.
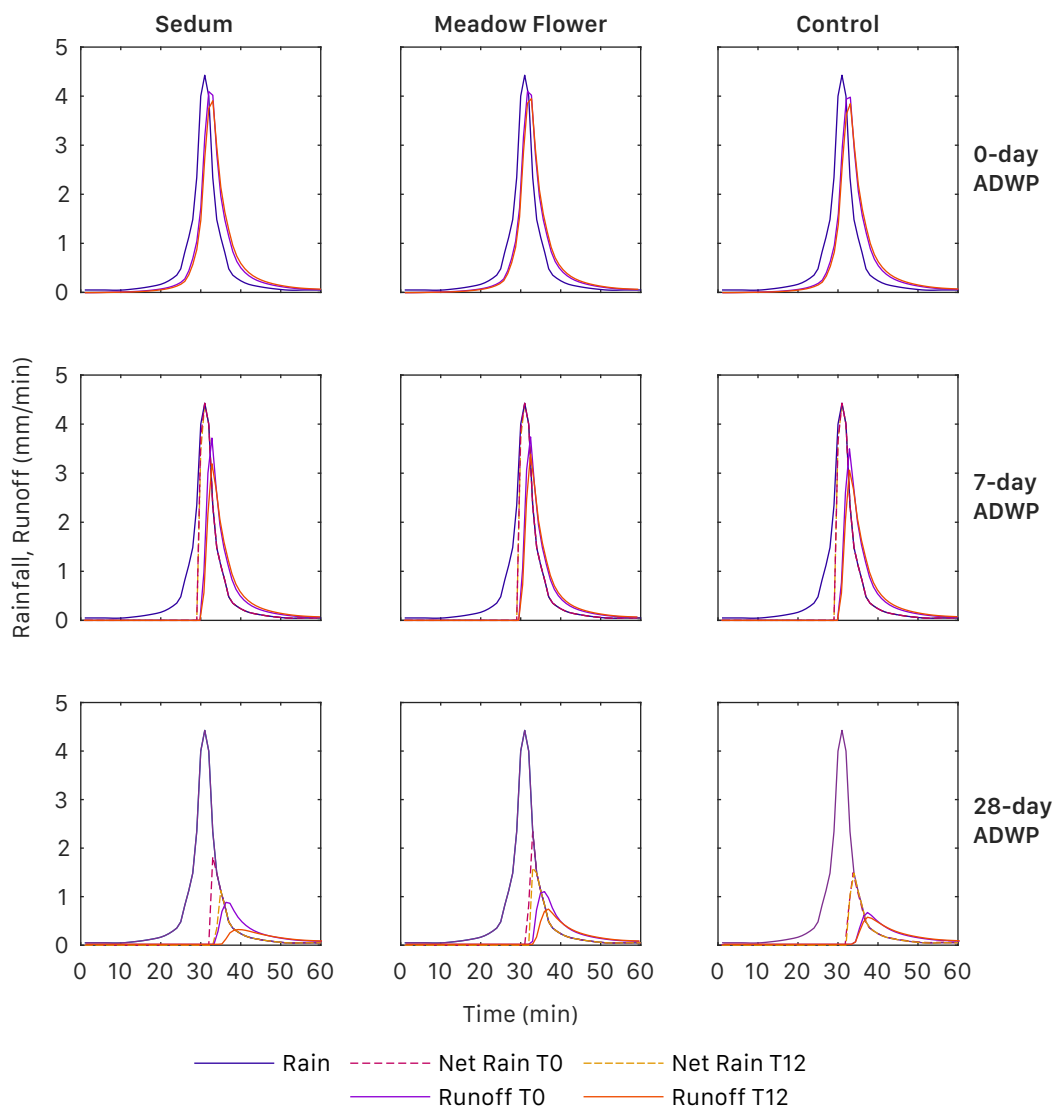
Figure 7.4 Combined hydrological response of the BBS microcosms to a 1-in-30-year 1-hour summer design rainfall event for Sheffield, UK, with varying ADWP.

At 7 and 28-day ADWPs the effects of retention become apparent (**Figure 7.4**), with the net rainfall profiles reflecting the initial losses caused by retention processes in the ADWP. For the 7-day ADWP scenario there is little difference in the net rainfall profiles of T0 and T12, reflecting the small differences observed in PRP (**Figure 7.1**). The reduced volumes of rainfall becoming runoff lead to significant reductions in the levels of peak runoff. Compared with the 0-day ADWP period, peak attenuation has increased by 115% in the 7-day ADWP scenario for the T0 Sedum microcosm. The improvements in detention performance, from T0 to T12, for the 7-day ADWP scenario are higher than those observed in the 0-day ADWP scenario. Peak attenuation improvement for the Sedum vegetated microcosms is 74%, whilst the unvegetated controls exhibit a 47% improvement. At a 28-day ADWP the differences in net rainfall profiles are more distinct, particularly for the Sedum microcosms, reflecting the larger differences in PRP (**Figure 7.1**). The further reductions in rainfall volumes for the 28-day ADWP scenario lead to an 1076% increase in peak attenuation for the T0 Sedum microcosm. Peak attenuation improvements from T0 to T12 are reduced further in the 28-day ADWP scenario compared to a 7-day ADWP, with Sedum vegetated microcosms increasing by 16%, whilst the unvegetated controls exhibit a 3% improvement.

> *The main conclusions from the physically-based hydrological performance predictions are: increased levels of MWHC in aged vegetated microcosms facilitate increased retention capacities, but at common ADWP durations (<7 days) the differences are marginal; detention performance is observed to increase with age for all substrates and vegetation types; combining retention and detention processes highlights the dominating effects of retention processes on the overall hydrological response.*

7.3 XMT-derived Hydrological Performance

The 40 µm resolution of the XMT images prevents a companion prediction of hydrological performance to that presented for physically-derived substrate characteristics. The majority of pore spaces that control retention performance are smaller than the 40 µm lower limit of the data. Therefore, a reliable prediction of retention performance is not possible. However, the XMT-derived values of K_{sat} can be utilised in the physically-based Bayton-model for predicting detention responses. The Bayton-model requires van Genuchten parameters which could not be determined for the LECA substrate, as such the following exploration of hydrological performance is based on the 50 mm BBS microcosms only.

Figure 7.5 presents the runoff response of all BBS microcosms to the same 5-minute constant intensity rainfall event used in the laboratory identification of detention performance. The small changes in XMT-derived K_{sat} result in corresponding small changes in runoff response. In the modelling scenario, as for the laboratory detention tests, moisture levels within the substrate are near to field capacity. At these moisture levels, hydraulic conductivity is greatly reduced from the K_{sat} value due to the $K(\theta)$ relationship (**Figure 2.7**). This reduction further reduces the differences in runoff response from T0 to T12, and in several cases, results in imperceptible visual differences (M02, M06, M07, M08 **Figure 7.5**). Where differences in runoff response can be identified there is a trend toward improved detention performance for reduced values of K_{sat}.

The runoff response of the XMT-derived T0 and T12 median K_{sat} values for a 1-in-30-year 1-hour design rainfall event for Sheffield, UK, is presented in **Figure 7.6**. Intermediate runoff responses at T8 and T10 are not included to improve clarity. The sedum vegetated microcosms exhibit the strongest T0 peak attenuation at 12%. A 23% improvement in peak attenuation is observed for the Sedum test beds from T0 to T12, whilst the smallest improvement of 12% is observed for the unvegetated control microcosms. These peak attenuation improvements are considerably smaller than those identified from physical testing, and the previous observation of strongest detention performance in unvegetated microcosms is not repeated. These discrepancies will be discussed further in the following section.
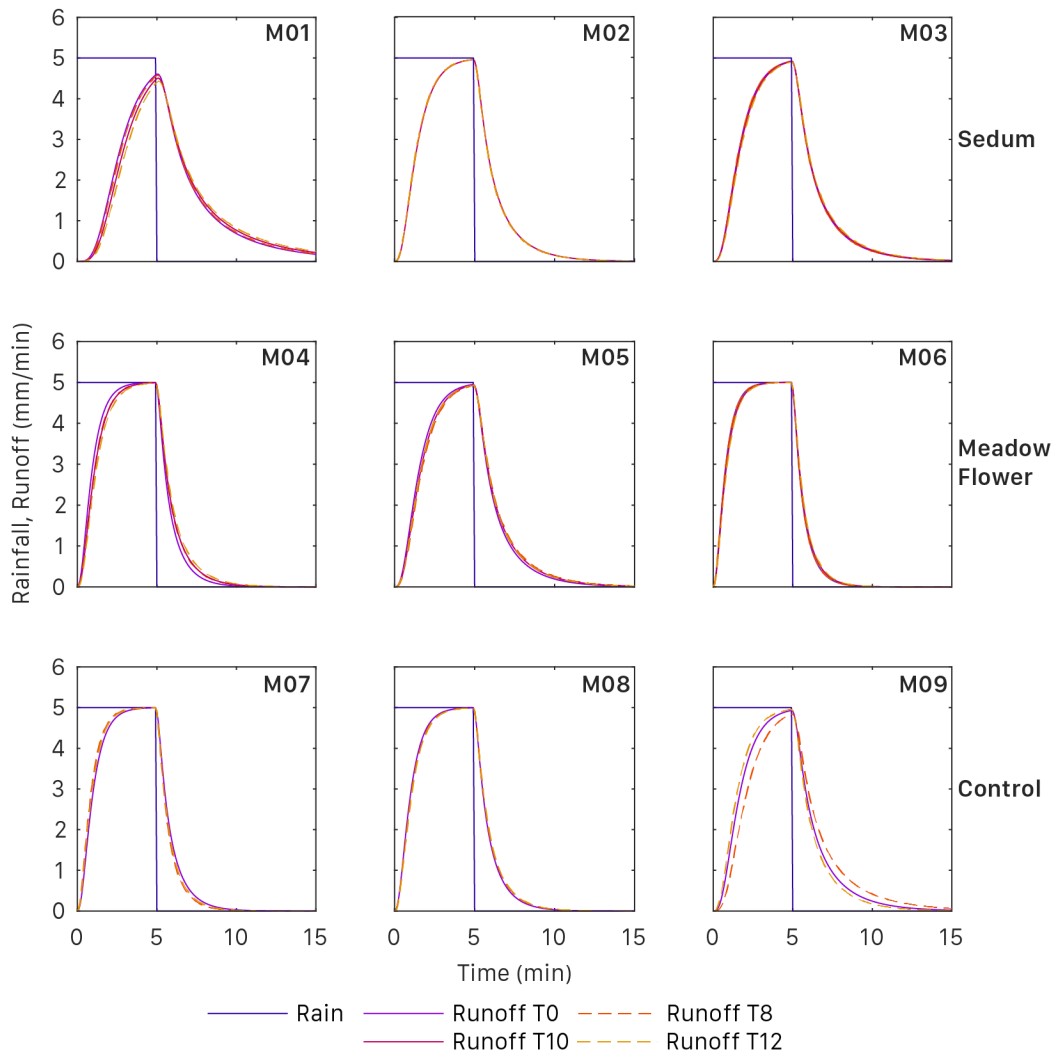
Figure 7.5 Bayton-model runoff from XMT-derived K_{sat} values in response to a modelled 5-minute 5 mm/min constant intensity rainfall event.
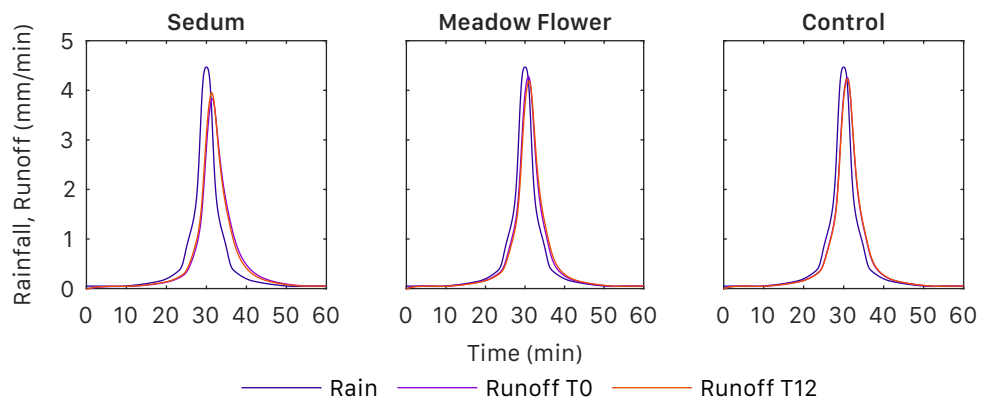
Figure 7.6 Rainfall and Bayton-model runoff from XMT-derived K_{sat} values for a 1-in-30-year 1-hour summer design rainfall event for Sheffield, UK. Equivalent to 0-day ADWP of **Figure 7.4**.

7.4 Comparison of conceptual and mechanistic modelling approaches

The laboratory detention tests provide a dataset which can be used to validate the mechanistic Bayton-model runoff predictions. Inspection of **Figure 7.2** and **Figure 7.5** reveals that there is a difference between the observed and mechanistic model runoff responses. **Figure 7.7** and **Figure 7.8** present direct comparisons of the observed runoff response with the conceptual reservoir routing response, the XMT-derived K_{sat} Bayton-model response, and Bayton-model responses based on physically-derived values of K_{sat} at T0 and T12 respectively.
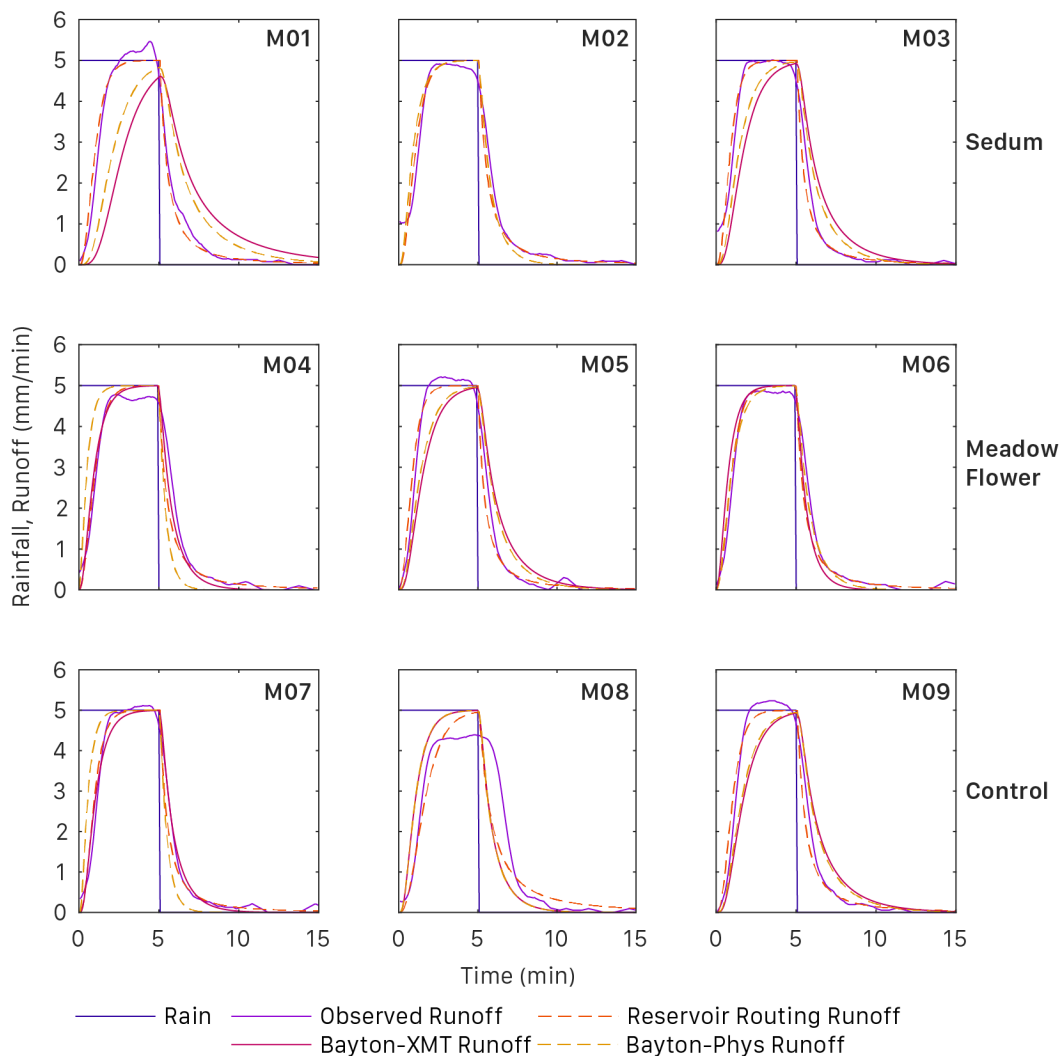
Figure 7.7 Rainfall and modelled rainfall of the three detention modelling approaches at T0.

Inspection of the T0 runoff profiles (**Figure 7.7**) indicates that generally the physically-derived K_{sat} values result in a better fit to the observed runoff data. The XMT-derived responses typically exhibit greater levels of detention performance than the observed data with runoff occurring after the predicted reservoir routing and physically-derived K_{sat} responses (M01). However, whilst there are some significant discrepancies in the predicted runoff responses of the three modelling approaches, all models result in R_t^2 model fits in excess of 0.92 suggesting a good degree of prediction (**Figure 7.9**). The predicted reservoir routing response always exhibits the strongest model fit, which is to be expected as parameters were fitted to the runoff data. XMT-derived responses have the lowest levels of model fit, this is attributed to the underestimation of K_{sat} by XMT compared to physical methods (see section 6.6.3).
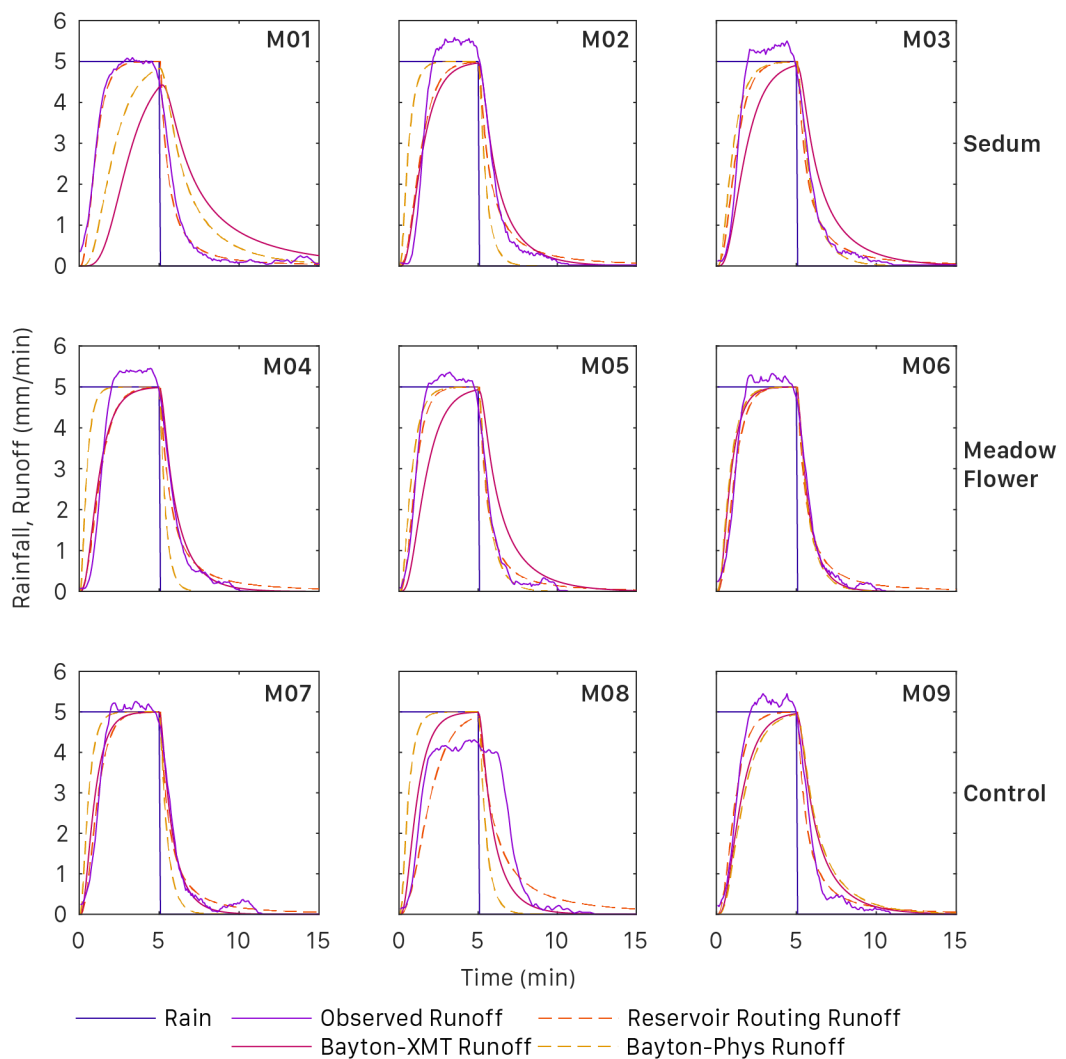
Figure 7.8 Rainfall and modelled rainfall of the three detention modelling approaches at T12.
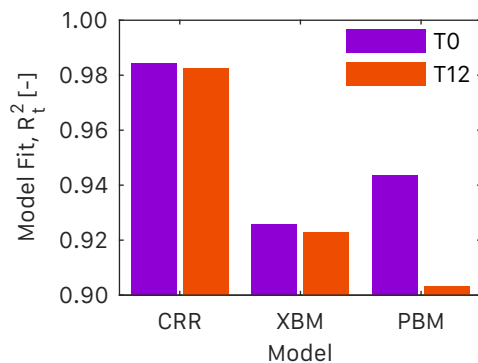
Figure 7.9 Mean model fit across all 9 BBS microcosms at T0 and T12. **CRR:** Conceptual reservoir routing model. **XBM:** XMT-derived K_{sat} Bayton-model. **PBM:** Physically derived K_{sat} Bayton-model.

At T12 the differences between the XMT-derived and physically-derived Bayton-model runoff responses are increased. This is due to the conflicting trends in K_{sat} over time identified via XMT and physical methods, with XMT-derived values decreasing over time, and physically-derived values increasing. The trend to a lower K_{sat}, and so a higher detention performance, in the XMT-derived runoff responses is the same as that of the observed detention tests. Whilst the Physically-derived K_{sat} values trend toward increased values over time (reduced detention performance). The exact mechanism by which this occurs remains unknown. The observed increases in physically-derived K_{sat} values at T12 result in overall model fit falling by 3.5% compared to at T0 (**Figure 7.9**). Assuming that the physically-derived K_{sat} values are realistic characterisations of substrate properties, the reduction in model fit indicates that the originally identified van Genuchten parameters are no longer valid. This suggests that significant changes have occurred in substrate properties, providing further evidence of substrate evolution.

Microcosm M06 exhibits very similar runoff responses for all 3 modelling approaches at T0 and T12. The generic van Genuchten parameters are therefore considered to be a fair estimate of actual substrate properties. Comparing the physically- and XMT-derived K_{sat} and model fit at T0 and T12 reveals that for a 36% difference in K_{sat} values, model fit differs by just 1%. Yet, at T12 where there is a 9% difference in physically- and XMT-derived K_{sat} model fit differs by 0.5%. **Figure 7.10** (**Left**) presents the relationship between model fit and K_{sat}, when comparing M06 T0 modelled runoff to the observed runoff responses of the detention tests. Only K_{sat} was varied, all other model parameters were constant. The steep gradient of the ascending limb indicates a greater sensitivity to low values of K_{sat}, compared to the shallow descending limb at

higher K$_{sat}$ values. This apparent lack of model sensitivity to the high values of K$_{sat}$ arises from the K(θ) relationship. **Figure 7.10** (**Right**) identifies that for stepped increases in K$_{sat}$ (30 mm/min in this example) the difference in K(θ) relationship from the lower value of K$_{sat}$ is reduced over the previous difference. As hydraulic conductivity is much lower than K$_{sat}$ at operational substrate moisture content levels, this difference is further reduced and so the difference in overall runoff response is small. A similar sensitivity relationship was also observed for values of the detention parameter D_S (section 3.3.4), suggesting that the conceptual model may be improved by making D_S a function of moisture content (or effective saturation).

> *The main conclusions from the comparison of conceptual and mechanistic modelling approaches are: the conceptual model has the strongest model fit as parameters are optimised to monitored data, thus limiting the generic application of the model; the mechanistic model yields good model fit results, but using constant van Genuchten parameters over time does not accurately reflect the observed changes in hydrological performance attributed to ageing.*
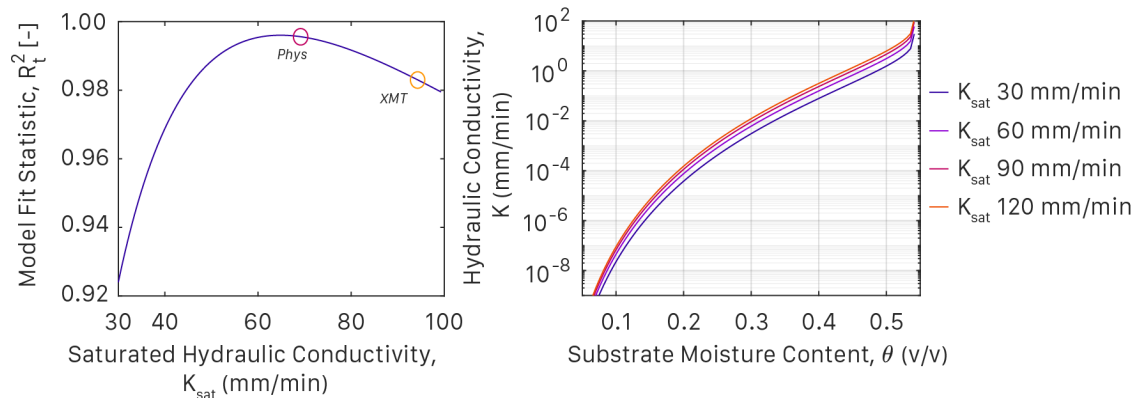
Figure 7.10 Left: Model fit statistic for varying K$_{sat}$, comparing microcosm M06 modelled runoff to observed runoff from detention tests at time T0. Physically-derived and XMT-derived values of K$_{sat}$ are indicated for reference. **Right:** K(θ) relationship for varying K$_{sat}$.

7.5 Discussion

7.5.1   Implications of substrate property changes on hydrological performance

Retention performance

The forecasted improvements in potential retention performance are relatively large given the short 1-year study duration. The determined values of potential retention performance are maximum levels and will only be reached if there are sufficient losses from evapotranspiration. Both the BBS and LECA substrates exhibited similar magnitudes of improvement for vegetated microcosms (+13% for Sedum treatment), although BBS values of PRP are consistently higher than LECA due to a greater MWHC. The largest improvements in PRP require an ADWP of significant length (28-days), such ADWP durations are rarely seen in monitoring study records and so the operational benefits are likely to be below those presented here.

PRP was determined by assuming that the substrate's PWP has not changed over time. As outlined in section 5.5.3, this assumption may not be valid. Hydrological modelling of the microcosms identified that to best represent observed runoff responses in aged substrates, significant changes need to have occurred within the substrates pore matrix over time. More reliable predictions of PRP could be obtained with additional characterisation of PWP, although an alternative method to the pressure plate tests is required to preserve incumbent vegetation and permit long-term re-characterisation.

Detention Performance

The fitting of a conceptual reservoir routing detention model to the observed runoff profiles from T0 and T12 indicates that detention performance is increased in aged BBS substrates (as identified from lower D_S values), irrespective of vegetation treatment. Unsuccessful characterisation of K_{sat} and determination of a water release relationship prohibited exploration of changes to performance in LECA substrates, despite K_{sat} characterisation via XMT-LBM.

The improvements to detention performance are relatively large for the 1-year study period, with peak attenuation improving by up to 56% for a design rainfall event with 0-day ADWP (Sedum microcosms). Retention losses contribute to the largest changes in peak attenuation performance; from a 0-day ADWP to a 28-day ADWP, peak attenuation improves by >1000% for an unaged substrate. In operation, the effects of retention will dominate over any subtle changes to detention performance resulting from substrate age.

7.5.2   Magnitude of identified conceptual model parameters

The identified detention parameter D_S values are comparable to values presented in Yio et al. (2013) for similar brick-based substrate compositions, depths, and conceptual reservoir routing model architectures. This adds confidence in the optimised D_S values but counters the hypothesis that D_S is influenced by rainfall intensity (Yio et al., 2013), as simulated rainfall intensifies of this study are an order of magnitude higher than those previously trialled.

Compared with D_S values determined for the vegetated brick-based test beds of chapter 4, those identified in the detention tests are an order of magnitude higher. This difference is attributable to the lack of filter sheet, drainage layer, and guttering of the microcosms compared with the test beds which will aid in the overall detention response of the green roof. Unvegetated test beds exhibit similar values to those identified in the detention tests. From this, it can be suggested that the additional drainage components of the test beds replicate the detention effect of the additional 20 mm of substrate depth in the microcosms.

7.5.3   Performance of conceptual and mechanistic hydrological models

The conceptual routing model provides the best fit to observed runoff responses. This is to be expected as the parameters are optimised to observed runoff. Due to this, the identified parameters are not a direct indicator of substrate physical properties and remain configuration specific.

Physically-derived and XMT-derived values of K_{sat} led to strong levels of model fit to the observed virgin substrate runoff response, when used as a parameter in a mechanistic model alongside generic brick-based virgin substrate van Genuchten parameters. This highlights the similarity of the BBS substrate used here and the brick-based substrate from which the van Genuchten parameters were derived. However, the opposing trends in K_{sat} over time for the physically-derived and XMT-derived data of the BBS microcosms led to a greater disparity in model fit to observed aged substrate runoff response, when used as parameters in a mechanistic model alongside generic brick-based virgin substrate van Genuchten parameters. The identified van Genuchten parameters are no longer a true reflection of aged substrate physical properties. Where modelled runoff predictions were poor, modelled runoff responses using physically-derived values of K_{sat} typically under-predicted detention performance in aged microcosms, whilst XMT-derived values over-predicted detention performance.

7.5.4 Future methods of water release characteristics determination

Optimisation of van Genuchten parameters can be undertaken to better improve the prediction of the mechanistic-model responses. However, with insufficient observed data points, the quality of prediction may be poor. The acquisition of a water release relationship can be difficult and time-consuming (Poë, 2016). Adaptation of the XMT–LBM modelling approach may prove to be useful in determining a series of data points to define a $K(\theta)$ relationship between field capacity and saturation. This $K(\theta)$ relationship can be supplemented by simple physical tests for identifying moisture contents at field capacity and saturation, to derive a $\theta(\psi)$ relationship. Using these relationships, pore size distributions, retention characteristics and detention responses may be determined.

7.6 Chapter Summary

The hydrological performance implications of observed substrate property changes were identified through the application of suitable hydrological models for retention and detention performance. Observed increases in MWHC for all vegetated microcosms led to increased levels of PRP with age. PRP was found to be consistently elevated in BBS compared with LECA due to higher values of MWHC. For significant improvements in PRP to be realised in operational conditions, the duration of ADWP needs to be larger than 5 days. Maximum benefits to PRP are achieved at a 28-day ADWP, an uncommon phenomenon in the UK with its temperate climate and frontal rainfall patterns.

Detention performance also improved slightly with age. At a 0-day ADWP, where detention provides the only hydrological benefit of a green roof, improvements in aged substrate peak attenuation were approximately 56%. As ADWPs increase in duration, the effects of retention performance on detention metrics become apparent, with peak attenuation improving by over 1000% from a 0-day ADWP to a 28-day ADWP. These dominant effects of retention processes on detention metrics highlight the need for an independent quantification of detention performance.

The results and discussion presented here will be brought together with the findings of chapters 4, 5 and 6 to provide an overall synthesis and discussion, which is presented in chapter 8.

8. *Synthesis & Discussion*

8.1 Chapter Overview

This chapters brings together the key findings of the long-term monitoring study, cored microcosm study, and longitudinal microcosm study to identify overall trends in substrate property and hydrological performance evolution. A consensus on the evolution of hydrologically important substrate properties is first established before the implications on hydrological performance are outlined. Suggestions of how the methodology employed here could be enhanced are also presented, alongside a discussion of research questions arising from the findings of this study.

8.2 Evolution of Substrate Properties

Substrate properties have been evaluated via physical investigation, non-invasive X-ray imaging, and inference from hydrological model parameters at several temporal scales. All methods of determination indicate that substrate properties are not constant through time. As green roof systems age many substrate properties are altered via numerous processes, including substrate consolidation, vegetation root growth, organic matter turnover, weathering, atmospheric deposition, and wash-out. Three properties have been identified as being critical for determining substrate hydrological performance with time, these properties are discussed below.

8.2.1   Pore Size Distribution

A substrate's pore size distribution is a controlling factor of many other substrate properties, particularly those important for hydrological performance. The volume of pores with a diameter of less than 50 μm dictates the maximum water holding capacity of the substrate, whilst pore sizes limit the velocity of flow through the substrate matrix. Pore size distributions of the brick-based and LECA substrates were not evaluated as part of the monitoring study. However, MWHC was determined, and this parameter provides an estimate of total pore volume < 50 μm in size. The core and microcosm studies derived pore size distributions from non-invasive X-ray microtomography and image processing techniques.

All methods of characterisation indicated an increase in the fraction of small pores with increased age in both types of substrate. In the cored microcosm study, BBS substrates exhibited a 58.4% reduction in median pore diameter whilst LECA underwent a 32.3% reduction over a 5-year period. For the longitudinal microcosm study BBS substrates exhibited a 1.1% reduction in median particle size within 1-year, whilst LECA substrates underwent a 22.7% reduction. The differences in the changes between the two studies may be a facet of study length, suggesting that LECA pore size reductions are initially rapid with the majority of changes occurring within the first year, whilst BBS reductions are initially slow. However, the MWHC data of the monitoring study suggests that the majority of changes to pore sizes occur within the first 1-2 years. This is in line with the observations of LECA pore sizes, with 70% of the 5-year change observed in the 1-year longitudinal microcosm study. The BBS substrate had undergone only 1.9% of the 5-year change in median pore sizes during the 1-year longitudinal microcosm study. This small change highlights a limitation of the cored microcosm study, where independent virgin and aged samples of substrate

were characterised as opposed to assessing the same substrate sample over time. This limitation means that the 32.3% reduction in median pore sizes observed for the BBS substrate over 5-years may actually be a result of the separate samples methodology. As the longitudinal microcosm study involved the repeated characterisation of the same microcosms over time there is a high level of confidence in the 1.1% reduction in median pore diameter over time.

There are limited findings in the literature that assess changes to pore sizes with increasing green roof system age. Getter et al. (2007), Köhler and Poll (2010) and Jelinkova et al. (2016) all present changes in pore volumes, but do not elaborate with further pore size metrics. Jelinkova et al. (2016) used a non-invasive XMT technique to quantify pore networks, and observed a reduced in the total macropore volume near the surface of the substrate. This reduction in macropore volumes is similar to the findings of this study, where reducing pore sizes led to reductions in overall porosity of the microcosms. Conversely, both Getter et al. (2007) and Köhler and Poll (2010), identified large increase in total pore volumes, although the exact methodologies for these determinations are not provided. The influence that these changes in pore size distribution have on MWHC and K_{sat} are outlined below.

8.2.2 Maximum Water Holding Capacity

Maximum water holding capacity, equivalent to field capacity, is a controlling factor of green roof retention performance as, in conjunction with the permanent wilting point, it dictates the maximum retention potential of the green roof. Values of MWHC were identified from the long-term monitoring study via substrate moisture data. In the cored and longitudinal microcosm study, MWHC was assessed via physical laboratory testing in accordance with FLL guidelines. Initial values of MWHC for the brick-based substrates (SCS, HLS and BBS) are similar in value, ranging from approximately 30 to 45%. LECA substrates in all 3 methods of assessment also had similar initial values of MWHC, ranging between approximately 20 and 30%.

The long-term monitoring study and both microcosm studies identified increases in MWHC with time. MWHC assessed via the monitoring study over the course of a 5-year period increased by a maximum of 3.9% for a vegetated brick-based substrate. The aged brick-based substrate of the cored microcosm study exhibited a 21.9% increase in MWHC over an equivalent virgin sample. Aged brick based substrates of the longitudinal microcosm study experienced a 9.8% mean increase in MWHC over the course of a single year. For LECA substrates there were more mixed findings, with the

monitoring study identifying 3% increases in MWHC at deeper substrate levels, but reductions of 1.5% near the surface. The LECA substrate in the cored microcosm study exhibited increases to MWHC with age of 34.4%, whilst in the longitudinal microcosm study a mean increase of 23.9% was observed.

It was hypothesised that the shorter duration longitudinal microcosm study was expected to reveal similar trends to the cored microcosm study, but identify smaller magnitudes of change due to the reduced age of the aged microcosms (1 vs 5-years). For both brick-based and LECA substrates this hypothesis was proved to be true. The rate of evolution in MWHC appears to be non-linear. For the brick-based substrate 44% of the 5-year change in MWHC had already occurred in 1-year, whilst in LECA substrates 60% of the 5-year change occurred within the 1-year of the longitudinal microcosm study. The MWHC results of the monitoring study, whilst indicating a considerably reduced level of change over time, did suggest that MWHC evolution occurred only in the first 1-2 years of monitoring (by means of statistically significant differences). Therefore, the large changes in the 1-year longitudinal monitoring study could represent this rapid initial evolution before property values stabilise in years 2–3 onwards.

8.2.3 Saturated Hydraulic Conductivity

Saturated hydraulic conductivity, K_{sat}, and hydraulic conductivity in general, is an important substrate property when determining detention performance as it governs the rate of runoff from the substrate. K_{sat} was determined for the two microcosm studies via XMT-LBM and also physically in the longitudinal microcosm study. Values of K_{sat} derived in the cored microcosm study were largely in line with other reported values in the literature, <40 mm/min for BBS and >40 mm/min for LECA. In the longitudinal microcosm study, values of K_{sat} were considerably higher, with an observed mean of 93 mm/min for BBS and 374 mm/min for LECA (where successfully characterised). LECA characterisations were particularly difficult to undertake as LECA particles are buoyant, causing substrate matrix disassociation under saturation, resulting in unreliable estimates of K_{sat}.

Although there are disparities in the initial values of K_{sat} between the two microcosm studies, the XMT-derived values of K_{sat} in both cases trend toward reduced values with increased substrate age. In the longitudinal microcosm study, LECA samples also exhibited a reduction in physically-derived K_{sat} whilst for BBS microcosms the opposite trend of increasing K_{sat} with age was identified. The exact mechanism by

which this difference arises is unknown, and the clear distinction in trends over time between BBS and LECA substrates is the only occurrence of divergence in substrate evolution trends due to substrate type. The implications of these contrasting findings are discussed in more detail as part of section 8.3.2.

Substrate Evolution Summary

The aim of this research was in part to observe and quantify changes to substrate properties over time. The observation of similar trends in substrate properties across three methods of investigation provides confidence that the results of this study are more widely applicable. Substrate properties trend toward smaller pore and particle sizes with time. The above observations are focused around properties that are hydrologically important, the identified changes in substrate properties may also affect other green roof benefits. The repeated non-invasive characterisation through time of this study may provide data for exploration of changes in additional green roof benefits over time.

8.3 Evolution of Hydrological Performance

8.3.1   Retention

Retention processes provide a green roof's stormwater quantity control, being able to infer potential retention performance from substrate properties is crucial to evaluating the overall effectiveness of a green roof system for a given climate. Estimates of PRP were generated for all three aspects of the study from observed changes in MWHC, and an assumption that PWP is constant through time. The limitations of this observation are discussed in detail in section 5.5.3. PRP is intrinsically linked to estimates of PAW, the rate of losses via ET, and the duration of the ADWP. PRP values have been explored for a variety of ADWPs and at two contrasting rates of PET.

The 6-year monitoring study dataset identified small increases to retention performance (approximately 3%), but identified much greater variation in seasonal trends with increased potential retention performance in winter (up to 10% increase). Whilst winter conditions may permit the highest potential retention performance due to increases in storage capacity, lower PET and shorter ADWPs in winter months will prevent recovery of this enlarged storage capacity. Reduced storage capacities in summer months presents problems for ensuring vegetation health without irrigation.

Potential retention performance was forecast to increase by 7% over 5 years at a 28-day ADWP in the cored microcosm study. As seasonal influences were identified as being an influencing factor on PRP, two different rates of PET were investigated to explore storage recovery under spring and summer conditions. Whilst both seasonal values of PET resulted in similar differences in PRP for the virgin and aged substrates at a 28-day ADWP, there were stark contrasts in performance at lower ADWPs more typical of operational conditions. Summer conditions led to a 10 x greater increases in PRP compared to the increases attributed to ageing at a 7-day ADWP. This observation, and evidence from the monitoring study, suggests that an understanding of significant seasonal variations in green roof retention performance is more critical than the modest evolution of performance with time.

Having identified the impacts of seasonal variations, the longitudinal microcosm study only explored differences in PRP under spring conditions, where vegetated test beds identified up to a 14% increase at a 28-day ADWP. These increased levels of improvement in the longitudinal microcosms compared to the cored microcosms are attributed to substrate depth. The additional 20 mm of substrate provides additional

pore space for the storage of water. At long duration ADWPs, vegetation can use this additional moisture that would not have been present in a shallower substrate and so further retention capacity can be recovered. These observations highlight the increased retention performances of deeper substrates, provided that the increased retention capacity can be recovered via ET losses.

All methods of investigation suggest increases over time to the potential retention capacity of the green roof system. Whether this increase in PRP is evident in actual retention performance is difficult to predict, given the controlling effects of climate and rainfall patterns on retention performance. The small scales of maximum improvement seen here make it easier to accept a lack of significant statistical differences in runoff volumes from roofs of different ages and configurations, as identified by Mentens et al. (2006).

8.3.2 Detention

Detention processes provide the temporal control of stormwater within a green roof system. Coupling predictions of retention performance with suitably identified detention processes permits the generation of a complete hydrological response to rainfall events. Detention performance was identified via all three aspects of this research through the application of two hydrological models. Where there was a lack of physical characterisation (i.e. the monitoring study), parameters from a conceptual reservoir routing model were used to identify detention performance. The extensive characterisation of the two microcosm studies facilitated the application of a physically-based model to explore detention performance.

The long-term monitoring study identified reasonably consistent levels of detention performance in vegetated green roof test beds, with no observed statistically significant differences in the detention model parameter D_S. Unvegetated test beds experienced a consistent annual increase in the value of D_S, indicating a move toward reduced detention performance with increased system age. Detention tests undertaken on the longitudinal microcosms exhibited the opposite trend, with the value of D_S reducing over time irrespective of vegetation treatment, suggesting enhanced detention performance.

Physically-based hydrological models using XMT-derived input parameters, from both microcosm studies, also suggested a reduction in detention performance over time. A constant set of substrate parameters was used for indications of both un-aged

and aged detention performance. Given the above observations of substrate property changes, this assumption of a constant substrate is not correct. The resulting assessments of 'detention performance' for XMT-derived values are therefore more of a sensitivity analysis for a varying K_{sat}. A similar physically-based modelling approach using the physically derived values of K_{sat} identified a worsening of detention performance, similar to that outlined for the long-term microcosm study. Again, the modelling was performed using the same substrate parameters at time T0 and T12. From these investigations, reduced values of k_{sat} lead to improved levels of detention performance, provided all other substrate properties are constant. To better identify the impacts of a changing k_{sat} an accompanying set of water release characteristics are required for the aged substrate.

There is a lack of agreement on the overall trend in observed detention performance with time. However, there is a consensus that for a typical green roof construction (sedum vegetation and brick-based substrate), detention performance has not deteriorated with increased system age. Where improvements to detention performance are identified, their small magnitude means that the dominant effects of retention performance on common detention metrics may mask any observable differences during typical green roof operation.

8.3.3   Hydrological Performance Evolution Summary

The long-term monitoring study provides evidence that small improvements to retention performance and a stable detention performance are achievable for typical green roof configurations with increasing system age. Microcosm studies also suggest improvements to potential retention performance, whilst detention evolution is less certain. However, due to the controlling effects of retention on observable detention performance, the improvements to retention will likely dominate any subtle changes in detention performance.

8.4 Methodology Adaptations

8.4.1 Physical Investigation Methodologies

Whilst largely complete, and in line with the basic requirements of the FLL guidelines, the physical investigation of substrate properties and hydrological performance would benefit from some slight adaptations. Additional characterisation of permanent wilting points would have proved useful for identifying potential retention performance, and could have acted as a surrogate indicator of fine scale pore volume changes.

The methodology of the longitudinal microcosm tests could have been altered to facilitate a higher frequency of data collection. The methodology employed here saturated substrate samples prior to detention testing to ensure they were at field capacity at the onset of simulated rainfall. Concerns surrounding vegetation viability after periods of immersion in water prohibited repeated testing during the duration of the study. An adapted methodology could have applied an intense simulated rainfall prior to detention testing to ensure the substrate was at field capacity, such an approach would have prevented substrate saturation and may have preserved vegetation health. The increased temporal frequency of observed runoff responses would have provided critical evidence to support the currently conflicting trends in detention performance with age.

The physical investigation methodologies of this study have facilitated the primary objective of observing and quantifying substrate and hydrological performance evolution in extensive green roof substrate. With the above additional data, greater confidence and insight may have been attained.

8.4.2 X-ray Microtomography Methodologies

The XMT imaging methodology used as part of this study has provided a wealth of data about substrate matrices over time. Only a fraction of the attainable information has been extracted from the raw images that were obtained. With sufficient adaptations to the image processing methodology, it may be possible to extract further insight from the images relating to rooting architecture and the influence of roots on local substrate properties.

The methodology employed for this study enhanced image contrast to better identify pore spaces and particles from the substrate matrix. In doing so the finer levels of contrast between particle density were largely lost. To better characterise roots and

their interactions with the substrates the contrast needs to be adjusted to enhance the differences between root networks and the surrounding substrate matrix. The enhanced contrast can be achieved by returning to the captured 16-bit greyscale images, as opposed to the 8-bit image used for this study. This enhanced contrast should facilitate an easier identification of root systems. A limitation of the 16-bit images, and the reason for the 8-bit conversion, is a significant increase in computational requirements. These requirements could be mitigated by combining an identified root network with image outputs of this study to infer local substrate properties.

The XMT image resolution cannot be increased for those images already captured. But, the greater understanding of the sizes of features of hydrological interest (i.e. pore sizes) developed as part of this research suggest that the highest resolution attainable should always be acquired. There are limitations on the physical size of samples and the image resolution that can be achieved with current XMT equipment. However, as technology advances it is anticipated that higher resolutions images will be attainable for larger samples. These higher resolution images will again lead to greater computational requirements, but similar technological advancements in computing are likely to accommodate these increases.

Conversely, by decreasing image resolution processing times can be heavily reduced with little reduction to observed property values. The only drawback to this approach is the scale of the smallest identifiable feature. Multiple resolution analysis techniques could be used where there is a reduced need for the highest resolution. For example, to evaluate retention performance, pore sizes of between 0.2 and 50 μm need to be identified. However, LBM modelling of macropore flows only requires pores >50 μm to be identified. Using a downscaled image set for the LBM modelling will heavily reduce computational requirements modelling of a full scale high resolution image set.

Overall the non-invasive imaging technique has proved to be invaluable in the repeated characterisation of functional green roof microcosms. With the above suggested adaptations and other potential refinements, XMT is likely to prove extremely useful in exploring the ageing of other green infrastructure in addition to green roofs.

8.5 Chapter Summary

The findings of all three aspects of this study complement each other to provide an overall assessment of the changes in substrate properties due to system age. The novel identification of a positive trend in the maximum water holding capacity of a substrate over time from monitored moisture data provides evidence that reducing pore sizes with age increase the total volume of micropores. This micropore volume is critical for moisture retention within the substrate, and is the controlling factor for determining the potential retention performance of a green roof system. The application of extensive non-invasive X-ray microtomography to explore the internal structures of green roof substrates for the first time also identified reductions in pore diameters.

The identified reduction in pore sizes has led to an increase in substrate maximum water holding capacity over time. Such increases forecast an improvement in the potential retention performance of vegetated green roof systems. The reorganisation of the pore space within the substrate is also responsible for small improvements in detention performance over time. Whilst these improvements were only noticeable in a controlled microcosm study, the long-term data record indicates there is no reduction in detention performance over time for vegetated green roof systems.

The coupling of positive trends in retention performance and the absence of negative trends in detention performance suggest that whilst substrate property changes do occur as a result of ageing they are unlikely to result in detrimental impacts on overall system hydrological performance. Observations of the effects of climate during the monitoring study identified far greater variations in green roof hydrological performance seasonally than annually. There remains a need for a more thorough investigation of the drivers of seasonal changes in hydrological performance beyond those focused on climatic variables and plant water usage.

9. *Conclusions*

9.1 Chapter Overview

This chapter concludes the thesis by relating summarised findings to the initial primary objectives and overall study aim. The key findings are presented along with some additional important points. Future research questions highlighted by this study are discussed. The chapter ends with the presentation of research questions that have risen during the course of this study.

9.2 Summary of Conclusions

New substrate ageing insight has been developed through the creation of two new substrate evolution datasets, combined with an extended long-term green roof hydrological monitoring programme. With increasing rates of green roof adoption to complement existing urban drainage structures, it was important to identify any negative changes in hydrological performance due to increasing system age. Characterisation of substrate properties, as undertaken physically and via non-invasive X-ray microtomography, indicate that substrate properties responsible for hydrological performance are not constant through time. The magnitude of these changes is determined by the initial substrate composition and the developing vegetation treatment.

The bulk of substrate changes occur within the initial 1-2 years of a green roof system's lifespan. During this period, anticipated substrate consolidation occurs alongside substrate root development, with both processes leading to a reduction of pore sizes within the substrate matrix. This reduction in pore sizes leads to increases in the substrate's maximum water holding capacity, and subsequently the potential retention performance of the green roof system. A series of complex interacting changes in pore diameters, tortuosity and saturated hydraulic conductivity lead to improvements in detention performance. Overall hydrological performance is improved due to the combination of these improvements to retention and detention performance. However, the scale of these improvements is dwarfed by seasonal variations in retention performance, due to differences in potential evapotranspiration, and its subsequent impact on detention performance.

Hydrological models that utilise parameters derived from unaged substrate characterisation cannot reliably predict the runoff response of an aged green roof system. With the above increases in hydrological performance over time, modelled runoff responses based on unaged substrate properties will under-predict hydrological performance. Whilst this under-prediction reduces model accuracy it has the positive effect of incorporating a design safety factor into predicted runoff responses. The knowledge that for a common green roof configuration, of a crushed-brick based substrate and Sedum vegetation, performance does not decline in the immediate years after installation and that modelled runoff responses under – rather than over – predict performance is important for the continued adoption of green roofs.

9.3 Summary Findings

9.3.1 Monitoring Study

Climate and Rainfall

1) Climate data revealed that the study period experienced wetter summers and drier autumns than long term climate averages.

2) 503 individual rainfall events, where rainfall was ≥2 mm and ADWP ≥6 hrs, were identified for the 6-year monitoring study. These events represented 90.5% of all rainfall in the study period.

3) Most identified rainfall events had a return period of <1-year. Only 4 rainfall events had a return period >2-years.

Retention Performance

4) Median per event retention performance for the whole study period was approximately 100% due to the bias toward smaller rainfall events.

5) Green roof test beds with a LECA substrate exhibited reduced levels of median per-event retention performance compared to brick-based configurations.

6) Green roof test beds installed with Sedum vegetation exhibited the highest levels of overall median per-event retention performance.

7) Retention performance from year-to-year cannot be compared due to the controlling effects of climate and rainfall characteristics. Two rainfall events (and their ADWPs) would have to be identical within the 6-year monitoring period, which did not occur.

8) Monitored substrate moisture content data can be used to estimate the maximum water holding capacity of the substrate over time.

9) A vertical moisture gradient is present with the substrate, with greater levels of substrate moisture at depth.

10) All green roof test beds that were monitored for substrate moisture content indicated an increase in maximum water holding capacity over time. The greatest increase was for a brick-based substrate installed with Sedum vegetation (+3% over 5 years).

11) Increases in maximum water holding content only occurred within the first 2–years of the monitoring study. Subsequent changes in MWHC were not statistically significant.

12) There were large changes in MWHC by season, with higher levels in winter and reduced levels in summer. These differences are larger than the differences in potential evapotranspiration rates.

Detention Performance

13) Conventional detention metrics indicate very little difference as a function of roof configuration due to the controlling effects of retention performance.

14) Fitting of appropriate hydrological models to identify detention processes allows model parameters to act as descriptor of detention performance.

15) Green roof test beds with a LECA substrate exhibit the poorest levels of detention performance.

16) Identified model parameters indicate that vegetated brick-based green roof configurations have a consistent level of detention performance over time.

   o Greater variation in detention was observed for test beds with Meadow Flower vegetation due to differing annual vegetation covers.

   o Sedum vegetation installed in a 'sedum carpet' brick-based substrate yields the most consistent level of performance.

17) As system age increased, LECA test beds exhibited reduced levels of detention performance.

18) Unvegetated green roof test beds experienced reductions in detention performance with increasing system age.

19) Overall model fit was improved when using annual median values of hydrological model parameters compared to overall study median. This suggests that time-varying model parameters are required for long term hydrological modelling.

20) Detention performance is strongly affected by season, the worst levels of performance are experienced in summer, whilst the best are in winter.

21) Seasonal influences are reduced in non-vegetated configurations suggesting a partial link to vegetative processes.

9.3.2 Cored Microcosm Study

Substrate Property Characterisation
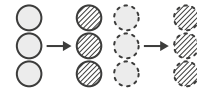
1) Physical characterisation of two contrasting virgin and aged (5-year) green roof substrates indicated reductions to particle sizes and dry density with increased age.

2) Maximum water holding capacity was found to be increased in aged samples of brick-based and LECA substrates compared to virgin samples.

3) X-ray microtomography was successfully used to image the internal matrix of the brick-based and LECA substrates.

4) The non-invasive XMT techniques was used to quantify particle and pore size distributions, and tortuosity.

5) Lattice Boltzmann methods were successfully used to estimate saturated hydraulic conductivity for the virgin and aged substrates.

6) Brick-based substrate matrices were identified to be more dense due to tighter packing of angular aggregates compared with the open matrix of rounded particles for LECA substrates.

7) The LECA substrate was found to be more porous than its brick-based counterpart, with significant volumes of internal particle pore space.

8) A relationship between reduced median pore sizes for increased substrate depth was not observed:

    o This does not support the hypothesis of pore sizes being responsible for the generation of a vertical moisture content gradient.

    o The smallest identifiable pore size was 30 µm, whilst the majority of pores responsible for moisture retention are smaller than this limit. XMT images may not have captured the pores responsible for the establishment of a vertical moisture profile.

9) XMT-derived characterisations of substrate properties identified similar trends as physically-derived values, with reducing particle and pore sizes over time.

Hydrological Performance

10) Potential retention performance was forecast to increase by up to 7% for aged substrates over their virgin counterparts.

11) The effects of seasonal climate on potential evapotranspiration resulted in differences between spring and summer potential retention performance being 10x bigger than differences observed due to ageing.

12) Detention performance was observed to increase with age.

   o Detention performance was determined through the application of generic brick-based substrate van Genuchten parameters, XMT-derived values of K_{sat} and a physically based model.

   o Overall improvements to detention performance were seen to be small for monitored rainfall events.

Evaluation of X-ray Microtomography

13) The resolution of the XMT-images is critical as it defines the size of the smallest identifiable feature within the image.

14) Image resolution should be maximised by reducing sample size, although samples should have a diameter at least twice that of the largest particle size.

9.3.3 Longitudinal Microcosm Study
Physical Substrate Property Characterisations
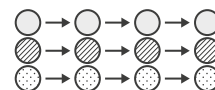
1) Substrate heterogeneity was found to be similar in 50 and 150 mm diameter substrate microcosms.

2) Statistically significant differences in structural substrate properties did not result in corresponding differences in hydrological substrate properties.

3) For brick-based substrates, observed reductions in median particle sizes over time corresponded to increases in the percentage of fine particles. Increases in MWHC and K_{sat} were also identified in aged samples.

4) LECA substrates experienced reductions to median particle diameters, increases to the percentage of fine particles and MWHC, but a reduction in K_{sat}.

5) There were no changes to the significant statistical differences in properties between the 50 and 150 mm diameter microcosms. Indicating that microcosm size does not influence substrate ageing

XMT Substrate Property Characterisation

6) XMT was successfully employed for the repeated characterisation of substrate properties over the course of a vegetation growth cycle (1-year).

7) Median particle diameters were observed to reduce with age for all vegetation treatments of brick-based substrates, whilst they increased for all LECA configurations.

8) Median pore diameters were reduced in aged vegetated brick-based and all LECA microcosms, but increased for unvegetated brick-based configurations.

9) Total porosity was identified to be lower in aged substrates of all configurations.

10) Tortuosity was reduced in aged vegetated brick-based microcosms, suggesting a decrease in flow path length, whilst increased tortuosity of the unvegetated configurations suggests an increase in flow path lengths.

11) Tortuosity increases with age for all LECA configurations, indicating increases to flow path lengths.

12) Saturated hydraulic conductivity is reduced in all aged vegetated microcosms for both brick-based and LECA substrates.

13) Saturated hydraulic conductivity increased in the aged unvegetated microcosms of both substrate types.

14) The majority of XMT-derived substrate property changes occurred prior to 8 months of age; no statistically significant differences are experienced in the changes across the remaining 4 months of the study.

15) Due to substrate heterogeneity, there are no significant statistical differences in substrate properties identified at the start and end of the study.

16) The rooting architecture of Sedum vegetation was identified to be fibrous and shallow, whilst Meadow Flower root networks extend throughout the substrate but are less dense.

17) Sedum root development over time is slow, increasing in depth by 7 mm in 4 months.

Hydrological Performance

18) Potential retention performance was forecast to improve with age in both the brick-based and LECA substrates.

   o Greatest improvements are for extended ADWP durations, +14% for Sedum vegetated brick-based substrates over 28 days ADWP.

   o The potential retention performance of LECA is consistently reduced compared to the brick-based substrate due to a lower MWHC.

19) Detention performance was seen to improve with age from the fitting of a conceptual reservoir routing detention model to observed runoff responses of brick-based microcosms.

20) XMT-derived values of K_{sat} utilised in a mechanistic hydrological model identified increases in detention performance for aged vegetated brick-based microcosms, but reductions in unvegetated configurations.

21) A conceptual model always offered the best fit to observed runoff responses as parameters were optimised to fit the observations.

22) Mechanistic model predictions of runoff response using a set of generic brick-based substrate van Genuchten parameters resulted in strong model fit to observed runoff responses for unaged substrates.

23) Mechanistic model fit was reduced for aged substrates indicating the generic parameters are no longer valid.

   o This indicates that a set of constant van Genuchten parameters are not suitable for modelling long-term hydrological performance of a green roof.

9.4 Future Work

In undertaking the research presented here several new research questions have emerged. These questions, their importance and how they may be answered are discussed below.

1) It was observed that seasonal variations in monitored field capacity and detention performance were considerably larger than those identified year-on-year. It was hypothesised that this variation is due to differences in the wetting and drying responses of the substrates due to varying substrate hydrophobicity across the year. The significantly seasonal variation may be of more concern to stormwater managers than the year-on-year consistencies in performance due to a requirement to mitigate the effects of high intensity summer rainfall events. Further investigation of this phenomenon and the underlying causes is required to better inform stormwater practitioners.

2) The identified detention parameter D_S of the long-term monitoring study currently describes the detention response of the whole green roof system including drainage layer and guttering setups. To increase the comparability of changes in D_S with the microcosm studies, re-characterisation of D_S could be undertaken as part of a two-stage reservoir routing setup. This would allow the evolving substrate and constant drainage components to be characterised separately.

3) Predictions of potential retention performance presented are based on MWHC values derived during each component of the study, but with PWP values determined in similar substrates by other authors. To increase the confidence in the predicted values of PRP, determination of PWP over time should be undertaken. Repeated determination of PWP whilst maintaining substrate structure and vegetation viability may require the development of a new methodology.

4) A set of generic brick-based van Genuchten model parameters are used in this study as the input into a mechanistic model. Specific parameters for the substrates used here were not identified due to prohibitively difficult, time-consuming, and destructive testing methods. The coupled XMT-LBM mehod for exploring hydraulic conductivity could be adapted to derive a K(θ) relationship,

from which a θ(ψ) relationship and an 'equivalent pore size distribution' can be determined.

5)   Whilst the crushed brick-based substrates of this study are representative of several commercial substrate mixes, the evolution of substrate properties in other compositions may be different. Application of the methodology presented here to other substrate compositions will generate additional knowledge of substrate evolution for varying substrate compositions.

9.5 Key Findings

The important findings of this thesis are presented below. For a more discursive interpretation and summary of these findings see Chapter 8. The three key findings of this research are:

1)   Substrate physical properties important for hydrological performance are not constant over time. The magnitude of changes in substrate properties is determined by substrate composition and vegetation treatment. These changes in substrate properties over time can significantly alter green roof hydrological performance.

2)   Identification of substrate property evolution suggests the largest changes are within the first 1-2 years of operation. After this time, the magnitude of substrate property changes are insufficient to result in further improvements to hydrological performance for vegetated roof configurations.

3)   Hydrological modelling parameters determined from virgin substrates are not representative of aged in-situ substrates, and under-predict the hydrological performance of green roof systems. However, practitioners may view this under-prediction as a form of design safety factor.

References

Alfredo, K., Montalto, F., Goldstein, A., 2010. Observed and Modeled Performances of Prototype Green Roof Test Plots Subjected to Simulated Low- and High-Intensity Precipitations in a Laboratory Experiment. J. Hydrol. Eng. 15, 444–457. doi:10.1061/(ASCE)HE.1943-5584.0000135

Allen, R., Pereira, L., Raes, D., Smith, M., 1998. Crop evapotranspiration-Guidelines for computing crop water requirements-FAO Irrigation and drainage paper 56. FAO, Rome 1–15.

Anderson, B., 2006. Conventions for U-value calculations: BR443. Bracknell, UK.

Arias, L., Grimard, J., Bertrand-Krajewski, J., 2016. First results of hydrological performances of three different green roofs. 9th Int. Conf. Novatech.

ASTM. 2011a. Standard practice for determination of dead loads and live loads associated with green roof systems. E2397-11, ASTM, West Conchohocken, PA.

ASTM. 2011b. Standard test method for maximum media density for dead load analysis of green roof systems. E2399-11, ASTM, West Conchohocken, PA.

Bayton, S., 2013. Hydraulic Performance of a Green Roof Substrate (MEng Dissertation). University of Sheffield, Sheffield, UK.

Beattie, D., Berghage, R., 2004. Understanding the Importance of Growing Media Green Roof Media Characteristics : The Basics, in: 2nd North American Green Roof Conference: Greening Rooftops for Sustainable Communities. The Cardinal Group, Portland, OR.

Beck, D.A., Johnson, G.R., Spolek, G.A., 2011. Amending greenroof soil with biochar to affect runoff water quantity and quality. Environ. Pollut. 159, 2111–8. doi:10.1016/j.envpol.2011.01.022

Beck, D., Lenhart, J.H., Spolek, G., 2014. Measured Water Detention Performance of Enhanced Green Roof Tray Systems, in: World Environmental and Water Resources Congress 2014. American Society of Civil Engineers, Reston, VA, pp. 186–196. doi:10.1061/9780784413548.021

Bengough, A.G., 2012. Water Dynamics of the Root Zone: Rhizosphere Biophysics and Its Control on Soil Hydrology. Vadose Zo. J. 11. doi:10.2136/vzj2011.0111

Benvenuti, S., 2014. Wildflower green roofs for urban landscaping, ecological sustainability and biodiversity. Landsc. Urban Plan. 124, 151–161. doi:10.1016/j.landurbplan.2014.01.004

Berghage, R., Miller, C., Bass, B., Moseley, D., Weeks, K., 2010. Stormwater runoff from a large commercial roof in Chicago, in: CitiesAlive!: Eighth Annual Green Roof and Wall Conf. pp. 1–13.

Berghage, R., Wolf, A., Miller, C., 2008. Testing green roof media for nutrient content, in: Greening Rooftops for Sustainable Communities. Minneapolis, MN, May 30–June 2.

Berkompas, B., Marx, K., Wachter, H., Beyerlein, D., Spencer, B., 2008. A study of green roof hydrologic performance in the cascadia region. 2008 Int. Low Impact Dev. Conf. 1–10. doi:10.1061/41009(333)8

Berndtsson, J.C., 2010. Green roof performance towards management of runoff water quantity and quality: A review. Ecol. Eng. 36, 351–360. doi:10.1016/j.ecoleng.2009.12.014

Berndtsson, J.C., Bengtsson, L., Jinno, K., 2009. Runoff water quality from intensive and extensive vegetated roofs. Ecol. Eng. 35, 369–380. doi:10.1016/j.ecoleng.2008.09.020

Berretta, C., Poë, S., Stovin, V., 2014. Moisture content behaviour in extensive green roofs during dry periods: The influence of vegetation and substrate characteristics. J. Hydrol. 511, 374–386. doi:10.1016/j.jhydrol.2014.01.036

Bliss, D.J., Neufeld, R.D., Ries, R.J., 2009. Storm Water Runoff Mitigation Using a Green Roof. Environ. Eng. Sci. 26, 407–418. doi:10.1089/ees.2007.0186

Boivin, M.-A., Lamy, M.-P., Gosselin, A., Dansereau, B., 2001. Effect of Artificial Substrate Depth on Freezing Injury of Six Herbaceous Perennials Grown in a Green Roof System. Horttechnology 11, 409–412.

Bouzouidja, R., Rousseau, G., Galzin, V., Claverie, R., Lacroix, D., Séré, G., 2016. Green roof ageing or Isolatic Technosol's pedogenesis? J. Soils Sediments. doi:10.1007/s11368-016-1513-3

Bruand, A., Cousin, I., Nicoullaud, B., Duval, O., Begon, J.C., 1996. Backscattered Electron Scanning Images of Soil Porosity for Analyzing Soil Compaction around Roots. Soil Sci. Soiciety Am. J. 60, 895–901.

Buccola, N., Spolek, G., 2011. A Pilot-Scale Evaluation of Greenroof Runoff Retention, Detention, and Quality. Water, Air, Soil Pollut. 216, 83–92. doi:10.1007/s11270-010-0516-8

Burszta-Adamiak, E., 2012. Analysis of the retention capacity of green roofs. J. Water L. Dev. 16. doi:10.2478/v10025-012-0018-8

Burszta-Adamiak, E., Mrowiec, M., 2013. Modelling of green roofs' hydrologic performance using EPA's SWMM. Water Sci. Technol. 68, 36–42. doi:10.2166/wst.2013.219

Butler, D., Davies, J., 2010. Urban Drainage, 3rd ed. Spon Press, London.

Cao, C.T.N., Farrell, C., Kristiansen, P.E., Rayner, J.P., 2014. Biochar makes green roof substrates lighter and improves water supply to plants. Ecol. Eng. 71, 368–374. doi:10.1016/j.ecoleng.2014.06.017

Carpenter, C.M.G., Todorov, D., Driscoll, C.T., Montesdeoca, M., 2016. Water quantity and quality response of a green roof to storm events: Experimental and monitoring observations. Environ. Pollut. 218, 664–672. doi:10.1016/j.envpol.2016.07.056

Carpenter, D.D., Kaluvakolanu, P., 2011. Effect of Roof Surface Type on Storm-Water Runoff from Full-Scale Roofs in a Temperate Climate. J. Irrig. Drain. Eng. 137, 161–169. doi:10.1061/(ASCE)IR.1943-4774.0000185

Carson, T.B., Marasco, D.E., Culligan, P.J., McGillis, W.R., 2013. Hydrological performance of extensive green roofs in New York City: observations and multi-year modeling of three full-scale systems. Environ. Res. Lett. 8, 24036. doi:10.1088/1748-9326/8/2/024036

Carter, M.R., 1993. Soil Sampling and Methods of Analysis. Lewis Publishers, CRC Press.

Carter, T.L., Rasmussen, T.C., 2006. Hydrologic behavior of vegetated roofs. JAWRA J. Am. Water Resour. Assoc. 42, 1261–1274. doi:10.1111/j.1752-1688.2006.tb05611.x

Castleton, H.F., Stovin, V., Beck, S.B.M., Davison, J.B., 2010. Green roofs; building energy savings and the potential for retrofit. Energy Build. 42, 1582–1591. doi:10.1016/j.enbuild.2010.05.004

Chen, C.-F., 2013. Performance evaluation and development strategies for green roofs in Taiwan: A review. Ecol. Eng. 52, 51–58. doi:10.1016/j.ecoleng.2012.12.083

Cipolla, S.S., Maglionico, M., Stojkov, I., 2016. A long-term hydrological modelling of an extensive green roof by means of SWMM. Ecol. Eng. 95, 876–887. doi:10.1016/j.ecoleng.2016.07.009

CIRIA, 2013. C723 Water Sensitive Urban Design in the UK: Ideas for built environment practitioners. CIRIA, London.

Clark, O.R., 1940. Interception of rainfall by prairie grasses, weeds, and certain crop plants. Ecol. Monogr. 10, 243–277.

Clark, O.R., 1937. Interception of rainfall by herbaceous vegetation. Science (80-.). 86, 591–592.

Connelly, M., Liu, K., Schaub, J., 2006. BCIT green roof research program, phase 1 summary of data analysis :: NH18-1-2/11-2006E-PDF - Government of Canada Publications. Vancouver.

Costanza-Robinson, M.S., Estabrook, B.D., Fouhey, D.F., 2011. Representative elementary volume estimation for porosity, moisture saturation, and air-water interfacial areas in unsaturated porous media: Data quality implications. Water Resour. Res. 47, 1–12. doi:10.1029/2010WR009655

Denardo, J.C., Jarrett, A.R., Manbeck, H.B., Beattie, D.J., Berghage, R.D., 2005. Stormwater mitigation and surface temperature reduction by green roofs. Trans. ASAE 48, 1491–1496.

Dexter, A.R., 1987. Compression of soil around roots. Plant Soil 97, 401–406. doi:10.1007/BF02383230

Digman, C., AShley, R., Balmforth, D., Balmforth, D., Stovin, V.R., Glerum, J., 2012. C713 Retrofitting for Surface Water Management. CIRIA, London.

Doube, M., Kłosowski, M.M., Arganda-Carreras, I., Cordelières, F.P., Dougherty, R.P., Jackson, J.S., Schmid, B., Hutchinson, J.R., Shefelbine, S.J., 2010. BoneJ: Free and extensible bone image analysis in ImageJ. Bone 47, 1076–1079. doi:10.1016/j.bone.2010.08.023

Dunnett, N., Kingsbury, N., 2004. Planting Green Roofs and Living Walls. Timber Press.

Dvorak, B., Volder, A., 2010. Green roof vegetation for North American ecoregions: A literature review. Landsc. Urban Plan. 96, 197–213. doi:10.1016/j.landurbplan.2010.04.009

Ekşi, M., 2013. A field study to evaluate the runoff quantity and stormwater retention of a typical extensive green roof in bahçeköy, istanbul. Environ. Prot. Eng. 39, 79–89. doi:10.5277/epe130407

Elliott, R.M., Gibson, R.A., Carson, T.B., Marasco, D.E., Culligan, P.J., McGillis, W.R., 2016. Green roof seasonal variation: comparison of the hydrologic behavior of a thick and a thin extensive system in New York City. Environ. Res. Lett. 11, 74020. doi:10.1088/1748-9326/11/7/074020

Emilsson, T., Rolf, K., 2005. Comparison of establishment methods for extensive green roofs in southern Sweden. Urban For. Urban Green. 3, 103–111. doi:10.1016/j.ufug.2004.07.001

Farrell, C., Ang, X.Q., Rayner, J.P., 2013. Water-retention additives increase plant available water in green roof substrates. Ecol. Eng. 52, 112–118. doi:10.1016/j.ecoleng.2012.12.098

Fassman-Beck, E., Voyde, E., Simcock, R., Hong, Y.S., 2013. 4 Living roofs in 3 locations: Does configuration affect runoff mitigation? J. Hydrol. 490, 11–20. doi:10.1016/j.jhydrol.2013.03.004

Fassman, E., Simcock, R., 2012. Moisture Measurements as Performance Criteria for Extensive Living Roof Substrates. J. Environ. Eng. 138, 841–851. doi:10.1061/(ASCE)EE.1943-7870.0000532

Fassman, E., Simcock, R., 2008. Development and Implementation of a Locally-Sourced Extensive Green Roof Substrate in New Zealand., in: World Green Roof Congress. London, 16-17 September 2008.

FEI, 2015. Aviso user's guide [WWW Document] URL http://www.vsg3d.com/sites/default/files/AvizoUsersGuide.pdf (accessed 6.12.15).

Fioretti, R., Palla, a., Lanza, L.G., Principi, P., 2010. Green roof energy and water related performance in the Mediterranean climate. Build. Environ. 45, 1890–1904. doi:10.1016/j.buildenv.2010.03.001

FLL, 2008. Guidelines for the Planning , Construction and Maintenance of Green Roofing - Green Roofing Guideline 119.

Franzaring, J., Steffan, L., Ansel, W., Walker, R., Fangmeier, A., 2016. Water retention, wash-out, substrate and surface temperatures of extensive green roof mesocosms???Results from a two year study in SW-Germany. Ecol. Eng. 94, 503–515. doi:10.1016/j.ecoleng.2016.06.021

Gaches, W., Lea-Cox, J., Cohan, S., Ristvey, A., Sullivan, J., Davis, A., 2013. Substrate particle size distribution of mature mid-Atlantic green roofs, in: International Low Impact Development Symposium.

Getter, K.L., Rowe, D.B., 2006. The Role of Extensive Green Roofs in Sustainable Development 41, 1276–1285.

Getter, K.L., Rowe, D.B., Andresen, J. a., 2007. Quantifying the effect of slope on extensive green roof stormwater retention. Ecol. Eng. 31, 225–231. doi:10.1016/j.ecoleng.2007.06.004

Getter, K.L., Rowe, D.B., Robertson, G.P., Cregg, B.M., Andresen, J. a, 2009. Carbon sequestration potential of extensive green roofs. Environ. Sci. Technol. 43, 7564–70.

Graceson, A., Hare, M., Monaghan, J., Hall, N., 2013. The water retention capabilities of growing media for green roofs. Ecol. Eng. 61, 328–334. doi:10.1016/j.ecoleng.2013.09.030

Gray, H.F., 1940. Sewerage in Ancient and Mediaeval Times. Sewage Work. J. 12, 939–946. doi:10.2307/25029094

Gregoire, B.G., Clausen, J.C., 2011. Effect of a modular extensive green roof on stormwater runoff and water quality. Ecol. Eng. 37, 963–969. doi:10.1016/j.ecoleng.2011.02.004

Hakimdavar, R., Culligan, P.J., Finazzi, M., Barontini, S., Ranzi, R., 2014. Scale dynamics of extensive green roofs: Quantifying the effect of drainage area and rainfall characteristics on observed and modeled green roof hydrologic performance. Ecol. Eng. 73, 494–508. doi:10.1016/j.ecoleng.2014.09.080

Hallett, P.D., Gordon, D.C., Bengough, A.G., 2003. Plant influence on rhizosphere hydraulic properties: direct measurements using a miniaturized infiltrometer. New Phytol. 157, 597–603. doi:10.1046/j.1469-8137.2003.00690.x

Hargreaves, G., Allen, R., 2003. History and evaluation of Hargreaves evapotranspiration equation. J. Irrig. Drain. … 53–63.

Harper, G.E., Limmer, M.A., Showalter, W.E., Burken, J.G., 2015. Nine-month evaluation of runoff quality and quantity from an experiential green roof in Missouri, USA. Ecol. Eng. 78, 127–133. doi:10.1016/j.ecoleng.2014.06.004

Hashemi, S.S.G., Mahmud, H. Bin, Ashraf, M.A., 2015. Performance of green roofs with respect to water quality and reduction of energy consumption in tropics: A review. Renew. Sustain. Energy Rev. 52, 669–679. doi:10.1016/j.rser.2015.07.163

Hill, J., Drake, J., Sleep, B., 2016. Comparisons of extensive green roof media in Southern Ontario. Ecol. Eng. 94, 418–426. doi:10.1016/j.ecoleng.2016.05.045

Hillel, D., 2004. Introduction to environmental soil physics. Elsevier Academic Press.

Hilten, R.N., Lawrence, T.M., Tollner, E.W., 2008. Modeling stormwater runoff from green roofs with HYDRUS-1D. J. Hydrol. 358, 288–293. doi:10.1016/j.jhydrol.2008.06.010

Hodge, A.T., 2002. Roman Aqueducts & Water Supply, Duckworth Archaeology Series. Duckworth.

Hutchinson, D., Abrams, P., Retzlaff, R., Liptan, T., 2003. Stormwater monitoring two ecoroofs in Portland, Oregon, USA. Green. Rooftops Sustain. Communities 1–18.

Ichihara, K., Cohen, J.P., 2010. New York City property values: what is the impact of green roofs on rental pricing? Lett. Spat. Resour. Sci. 4, 21–30. doi:10.1007/s12076-010-0046-4

Jarrett, A.R., Berghage, R.D., 2008. Annual and individual green roofs storm water response models, in: 6th Greening Rooftops for Sustainable Communities Conference. Baltimore, MD, USA.

Jassogne, L., McNeill, A., Chittleborough, D., 2007. 3D-visualization and analysis of macro- and meso-porosity of the upper horizons of a sodic, texture-contrast soil. Eur. J. Soil Sci. 58, 589–598. doi:10.1111/j.1365-2389.2006.00849.x

Jelinkova, V., Dohnal, M., Sacha, J., 2016. Thermal and water regime studied in a thin soil layer of green roof systems at early stage of pedogenesis. J. Soils Sediments 16, 2568–2579. doi:10.1007/s11368-016-1457-7

Jenkins, G.J., Murphy, J.M., Sexton, D.M.H., Lowe, J.A., Jones, P., Kilsby, C.G., 2009. UK Climate Projections: Briefing report. Exeter, UK.

Jha, P., Biswas, A.K., Lakaria, B.L., Subba Rao, A., 2010. Biochar in agriculture - prospects and related implications. Curr. Sci.

Kasmin, H., Stovin, V.R., Hathway, E. a, 2010. Towards a generic rainfall-runoff model for green roofs. Water Sci. Technol. 62, 898–905. doi:10.2166/wst.2010.352

Koehler, M., Schmidt, M., 2008. Benefits for sustainable water management – green roof technology, in: World Green Roof Congress, 17–18 September, London.

Köhler, M., Poll, P.H., 2010. Long-term performance of selected old Berlin greenroofs in comparison to younger extensive greenroofs in Berlin. Ecol. Eng. 36, 722–729. doi:10.1016/j.ecoleng.2009.12.019

Köhler, M., Schmidt, M., Grimme, F.W., Laar, M., Paiva, V.L.D.A., Tavares, S., 2002. Green roofs in temperate climates and in the hot-humid tropics – far beyond the aesthetics. Environ. Manag. Heal. 13, 382–391. doi:10.1108/09566160210439297

Krebs, G., Kuoppamäki, K., Kokkonen, T., Koivusalo, H., 2016. Simulation of green roof test bed runoff. Hydrol. Process. 30, 250–262. doi:10.1002/hyp.10605

Kurtz, T., 2009. Flow monitoring of three ecoroofs in Portland, Oregon. Low Impact Dev. Urban Ecosyst. Habitat Prot. doi:10.1061/41009(333)10

Lado, M., Paz, A., Ben-Hur, M., 2004. Organic Matter and Aggregate Size Interactions in Infiltration, Seal Formation, and Soil Loss. Soil Sci. Soc. Am. J. 68, 935. doi:10.2136/sssaj2004.9350

Li, J., Wai, O.W.H., Li, Y.S., Zhan, J., Ho, Y.A., Li, J., Lam, E., 2010. Effect of green roof on ambient CO2 concentration. Build. Environ. 45, 2644–2651. doi:10.1016/j.buildenv.2010.05.025

Li, Y., Babcock, R.W., 2014. Green roof hydrologic performance and modeling: A review. Water Sci. Technol. 69, 727–738. doi:10.2166/wst.2013.770

Licht, J., Lundholm, J., 2006. Native coastal plants for northeastern extensive and semi-extensive green roof trays: substrates, fabrics, and plant selection, in: Annual Greening Rooftops for Sustainable Communities Conference. Boston, MA, USA.

Liu, K., 2004. Engineering performance of rooftop gardens through field evaluation. Interface 4–12.

Liu, K.K.Y., Minor, J., 2005. Performance Evaluation of an Extensive Green Roof. Green. Rooftops Sustain.

Communities 1–11. doi:10.1109/ICEOE.2011.6013104

Liu, R., Fassman-Beck, E., 2017. Hydrologic response of engineered media in living roofs and bioretention to large rainfalls: experiments and modeling. Hydrol. Process. 31, 556–572. doi:10.1002/hyp.11044

Locatelli, L., Mark, O., Mikkelsen, P.S., Arnbjerg-Nielsen, K., Bergen Jensen, M., Binning, P.J., 2014. Modelling of green roof hydrological performance for urban drainage applications. J. Hydrol. 519, 3237–3248. doi:10.1016/j.jhydrol.2014.10.030

Lu, J., Yuan, J., Yang, J., Yang, Z., 2014. Responses of morphology and drought tolerance of Sedum lineare to watering regime in green roof system: A root perspective. Urban For. Urban Green. 13, 682–688. doi:10.1016/j.ufug.2014.08.003

Lundholm, J., Macivor, J.S., Macdougall, Z., Ranalli, M., 2010. Plant species and functional group combinations affect green roof ecosystem functions. PLoS One 5, e9677. doi:10.1371/journal.pone.0009677

MacIvor, J.S., Lundholm, J., 2011. Performance evaluation of native plants suited to extensive green roof conditions in a maritime climate. Ecol. Eng. 37, 407–417. doi:10.1016/j.ecoleng.2010.10.004

Maire, E., Withers, P.J., 2014. Quantitative X-ray tomography. Int. Mater. Rev. 59, 1–43. doi:10.1179/1743280413Y.0000000023

Mairhofer, S., Zappala, S., Tracy, S.R., Sturrock, C., Bennett, M., Mooney, S.J., Pridmore, T., 2012. RooTrak: Automated Recovery of Three-Dimensional Plant Root Architecture in Soil from X-Ray Microcomputed Tomography Images Using Visual Tracking. Plant Physiol. 158, 561–569. doi:10.1104/pp.111.186221

Manning, J., 1987. Applied Principles of Hydrology. Merrill Publishing, Ohio, USA.

Marasco, D.E., Hunter, B.N., Culligan, P.J., Gaffin, S.R., McGillis, W.R., 2014. Quantifying Evapotranspiration from Urban Green Roofs: A Comparison of Chamber Measurements with Commonly Used Predictive Methods. Environ. Sci. Technol. 48, 10273–10281. doi:10.1021/es501699h

Marsh, T., Hannaford, J., 2007. The summer 2007 floods in England & Wales – a hydrological appraisal.

Materechera, S.A., Dexter, A.R., Alston, A.M., 1992. Formation of aggregates by plant roots in homogenised soils. Plant Soil 142, 69–79. doi:10.1007/BF00010176

Mawdsley, J.A., Ali, M.F., 1985. Estimating Nonpotential Evapotranspiration by Means of the Equilibrium Evaporation Concept. Water Resour. Res. 21, 383–391. doi:10.1029/WR021i003p00383

Menon, M., Jia, X., Lair, G.J., Faraj, P.H., Blaud, A., 2015. Analysing the impact of compaction of soil aggregates using X-ray microtomography and water flow simulations. Soil Tillage Res. 150, 147–157. doi:10.1016/j.still.2015.02.004

Menon, M., Yuan, Q., Jia, X., Dougill, a. J., Hoon, S.R., Thomas, a. D., Williams, R. a., 2011. Assessment of

physical and hydrological properties of biological soil crusts using X-ray microtomography and modeling. J. Hydrol. 397, 47–54. doi:10.1016/j.jhydrol.2010.11.021

Mentens, J., Raes, D., Hermy, M., 2006. Green roofs as a tool for solving the rainwater runoff problem in the urbanized 21st century? Landsc. Urban Plan. 77, 217–226. doi:10.1016/j.landurbplan.2005.02.010

MET Office, 2014. The Recent Storms and Floods in the UK. London, UK.

Miller, C., 2003. Moisture management in green roofs, in: Greening Rooftops for Sustainable Communities. Chicago, USA.

Miller, J.D., Kjeldsen, T.R., Hannaford, J., Morris, D.G., 2013. A hydrological assessment of the November 2009 floods in Cumbria, UK. Hydrol. Res. 44, 180. doi:10.2166/nh.2012.076

Molineux, C.J., Fentiman, C.H., Gange, A.C., 2009. Characterising alternative recycled waste materials for use as green roof growing media in the U.K. Ecol. Eng. 35, 1507–1513. doi:10.1016/j.ecoleng.2009.06.010

Monteith, J.., 1965. Evaporation and Environment.

Monterusso, M.A., Rowe, D.B., Rugh, C.L., 2005. Establishment and Persistence of Sedum spp. and Native Taxa for Green Roof Applications. HortScience 40, 391–396.

Moran, A., Hunt, B., Jennings, G., 2003. A North Carolina Field Study to Evaluate Greenroof Runoff Quantity, Runoff Quality, and Plant Growth. World Water Environ. Resour. Congr. 2003 1–10. doi:10.1061/40685(2003)335

Morbidelli, R., Corradini, C., Saltalippi, C., Flammini, A., Rossi, E., 2011. Infiltration-soil moisture redistribution under natural conditions: experimental evidence as a guideline for realizing simulation models. Hydrol. Earth Syst. Sci 15, 2937–2945. doi:10.5194/hess-15-2937-2011

Morbidelli, R., Saltalippi, C., Flammini, A., Rossi, E., Corradini, C., 2014. Soil water content vertical profiles under natural conditions: matching of experiments and simulations by a conceptual model. Hydrol. Process. 28, 4732–4742. doi:10.1002/hyp.9973

Morgan, S., Celik, S., Retzlaff, W., 2013. Green Roof Storm-Water Runoff Quantity and Quality. J. Environ. Eng. 139, 471–478. doi:10.1061/(ASCE)EE.1943-7870.0000589

Murphy, J.M., Sexton, D.M.H., Jenkins, G.J., Boorman, P.M., Booth, B.B.B., Brown, C.C., Clark, R.T., Collins, M., Harris, G.R., Kendon, E.J., Betts, R.A., Brown, S.J., Howard, T.P., Humphrey, K.A., McCarthy, M.P., McDonald, R.E., Stephens, A., Wallace, C., Warren, R., Wilby, R., Wood, R.A., 2009. UK Climate Projections Science Report: Climate change projections. Exeter, UK.

Nagase, A., Dunnett, N., 2012. Amount of water runoff from different vegetation types on extensive green roofs: Effects of plant species, diversity and plant structure. Landsc. Urban Plan. 104, 356–363. doi:10.1016/j.landurbplan.2011.11.001

Nawaz, R., McDonald, A., Postoyko, S., 2015. Hydrological performance of a full-scale extensive green roof located in a temperate climate. Ecol. Eng. 82, 66–80. doi:10.1016/j.ecoleng.2014.11.061

NERC, 2000. The 2000/01 Floods — a Hydrological Appraisal [WWW Document]. URL http://www.nerc-wallingford.ac.uk/ih/nrfa/yb/yb2000/flood2000/2000FloodIndex.html (accessed 6.23.14).

NERC, 1999. Flood Estimation Handbook (FEH) CD.

Noble, A.G., 2007. Traditional Buildings: A Global Survey of Structural Forms and Cultural Functions. I.B.Tauris.

Oberndorfer, E., Lundholm, J., Bass, B., Coffman, R.R., Doshi, H., Dunnett, N., Gaffin, S., Köhler, M., Liu, K.K.Y., Rowe, B., 2007. Green Roofs as Urban Ecosystems: Ecological Structures, Functions, and Services. Bioscience 57, 823. doi:10.1641/B571005

ONS, 2013. 2011 Census Analysis - Comparing Rural and Urban Areas of England and Wales.

Osmundson, T., 1999. Roof Gardens: History, Design, and Construction. W.W. Norton.

Palla, A., Gnecco, I., Lanza, L.G., 2012. Compared performance of a conceptual and a mechanistic hydrologic models of a green roof. Hydrol. Process. 26, 73–84. doi:10.1002/hyp.8112

Palla, A., Sansalone, J.J., Gnecco, I., Lanza, L.G., 2011. Storm water infiltration in a monitored green roof for hydrologic restoration. Water Sci. Technol. 64, 766. doi:10.2166/wst.2011.171

Palla, A., Sansalone, J.J., Gnecco, I., Lanza, L.G., 2010. Storm water infiltration in a monitored green roof for hydrologic restoration L ' infiltration des eaux pluviales dans une toiture végétalisée instrumentée pour la restauration du cycle hydrologique naturel 1–10.

Palomo Del Barrio, E., 1998. Analysis of the green roofs cooling potential in buildings. Energy Build. 27, 179–193. doi:10.1016/S0378-7788(97)00029-7

Penman, H., 1948. Natural evaporation from open water, bare soil and grass. Proc. R. Soc. … 193, 120–145.

Poë, S., 2016. The influence of a green roof configuration's moisture balance on hydrological performance.

Poë, S., Stovin, V., 2012. Advocating a physically-based hydrological model for green roofs : Evapotranspiration during the drying cycle, in: World Green Roof Congress. Copenhagen, 19-20 September 2012.

Poë, S., Stovin, V., Berretta, C., 2015. Parameters influencing the regeneration of a green roof's retention capacity via evapotranspiration. J. Hydrol. 523, 356–367. doi:10.1016/j.jhydrol.2015.02.002

Poë, S., Stovin, V., Dunsiger, Z., 2011. The Impact of Green Roof Configuration on Hydrological Performance, in: 12th International Conference on Urban Drainage. Porto Alegre, Brazil, 11-16 September 2011.

Porsche, U., Köhler, M., 2003. LIFE CYCLE COSTS OF GREEN ROOFS - A Comparison of Germany, USA, and

Brazil, in: RIO 3 - World Climate & Energy Event. Rio de Janeiro, Brazil, 1-5 December 2003, pp. 1–5.

Priestley, C.H.B., Taylor, R.J., 1972. On the Assessment of Surface Heat Flux and Evaporation Using Large-Scale Parameters. Mon. Weather Rev. 100, 81–92. doi:10.1175/1520-0493(1972)100<0081:OTAOSH>2.3.CO;2

Rab, M.A., Haling, R.E., Aarons, S.R., Hannah, M., Young, I.M., Gibson, D., 2014. Evaluation of X-ray computed tomography for quantifying macroporosity of loamy pasture soils. Geoderma 213, 460–470. http://dx.doi.org/10.1016/ j.geoderma.2013.08.037.

Razzaghmanesh, M., Beecham, S., 2014. The hydrological behaviour of extensive and intensive green roofs in a dry climate. Sci. Total Environ. 499, 284–296. doi:10.1016/j.scitotenv.2014.08.046

Rezaei, F., Jarrett, A.., 2006. Measure and predict evapotranspiration rate from green roof plant species, in: Penn State College of Engineering Research Symposium, Penn State University.

Ristvey, A.G., Solano, L., Wharton, K., Cohan, S.M., Lea-Cox, J.D., 2010. Effects of Crumb Rubber Amendments on the Porosity, Water Holding Capacity, and Bulk Density of Three Green Roof Substrates, in: Low Impact Development. ASCE Press, Reston, VA, pp. 889–896.

Rizwan, A.M., Dennis, L.Y.C., Liu, C., 2008. A review on the generation, determination and mitigation of Urban Heat Island. J. Environ. Sci. 20, 120–128. doi:10.1016/S1001-0742(08)60019-4

Roehr, D., Laurenz, J., 2008. Green living envelopes for food and energy production in cities., in: The Sustainable City V: Proceedings of the 5th International Conference on Urban Regeneration and Sustainability. Skiathos, Greece, 24-26th September 2008, pp. 663–671.

Rowe, D.B., 2011. Green roofs as a means of pollution abatement. Environ. Pollut. 159, 2100–10. doi:10.1016/j.envpol.2010.10.029

Rowell, D.L., 1994. Soil science: methods and applications. Longman Scientific & Technical.

Rumble, H., Gange, A.C., 2013. Soil microarthropod community dynamics in extensive green roofs. Ecol. Eng. 57, 197–204. doi:10.1016/j.ecoleng.2013.04.012

Salvucci, G.D., Gentine, P., 2013. Emergent relation between surface vapor conductance and relative humidity profiles yields evaporation rates from weather data. Proc. Natl. Acad. Sci. U. S. A. 110, 6287–91. doi:10.1073/pnas.1215844110

Sayed, O.H., 2001. Crassulacean Acid Metabolism 1975–2000, a Check List. Photosynthetica 39, 339–352. doi:10.1023/A:1020292623960

Schanz, T., 2007. Experimental Unsaturated Soil Mechanics. Springer-Verlag, Berlin and Heidelberg GmbH & Co., Berlin.

Schneider, C.A., Rasband, W.S., Eliceiri, K.W., 2012. NIH image to ImageJ: 25 years of image analysis. Nat. Methods 9, 671–675. http://dx.doi.org/10.1038/ nmeth.2089.

Schwen, A., Bodner, G., Scholl, P., Buchan, G.D., Loiskandl, W., 2011. Temporal dynamics of soil hydraulic

properties and the water-conducting porosity under different tillage. Soil Tillage Res. 113, 89–98. http://dx.doi.org/10.1016/j. still.2011.02.005.

She, N., Pang, J., 2010. Physically Based Green Roof Model. J. Hydrol. Eng. 15, 458–464. doi:10.1061/(ASCE)HE.1943-5584.0000138

Sims, A.W., Robinson, C.E., Smart, C.C., Voogt, J.A., Hay, G.J., Lundholm, J.T., Powers, B., O'Carroll, D.M., 2016. Retention performance of green roofs in three different climate regions. J. Hydrol. 542, 115–124. doi:10.1016/j.jhydrol.2016.08.055

Šimůnek, J., van Genuchten, M.T., Šejna, M., 2008. Development and Applications of the HYDRUS and STANMOD Software Packages and Related Codes. Vadose Zo. J. 7, 587. doi:10.2136/vzj2007.0077

Snodgrass, E.C., McIntyre, L., 2010. The green roof manual : a professional guide to design, installation, and maintenance.

Snodgrass, E.C., Snodgrass, L.L., 2006. Green roof plants : a resource and planting guide. Timber Press.

Speak, A.F., Rothwell, J.J., Lindley, S.J., Smith, C.L., 2013. Rainwater runoff retention on an aged intensive green roof. Sci. Total Environ. 461–462, 28–38. doi:10.1016/j.scitotenv.2013.04.085

Spolek, G., 2008. Performance monitoring of three ecoroofs in Portland, Oregon. Urban Ecosyst. 11, 349–359. doi:10.1007/s11252-008-0061-z

Starry, O., Lea-Cox, J., Ristvey, A., Cohan, S., 2016. Parameterizing a Water-Balance Model for Predicting Stormwater Runoff from Green Roofs. J. Hydrol. Eng. 21, 4016046. doi:10.1061/(ASCE)HE.1943-5584.0001443

Stephenson, V., D'Ayala, D., 2014. A new approach to flood vulnerability assessment for historic buildings in England. Nat. Hazards Earth Syst. Sci. 14, 1035–1048. doi:10.5194/nhess-14-1035-2014

Stovin, V., 2010. The potential of green roofs to manage Urban Stormwater. Water Environ. J. 24, 192–199. doi:10.1111/j.1747-6593.2009.00174.x

Stovin, V., Poë, S., Berretta, C., 2013. A modelling study of long term green roof retention performance. J. Environ. Manage. 131, 206–15. doi:10.1016/j.jenvman.2013.09.026

Stovin, V., Poë, S., De-Ville, S., Berretta, C., 2015a. The influence of substrate and vegetation configuration on green roof hydrological performance. Ecol. Eng. 85. doi:10.1016/j.ecoleng.2015.09.076

Stovin, V., Vesuviano, G., De-Ville, S., 2015b. Defining green roof detention performance. Urban Water J. doi:10.1080/1573062X.2015.1049279

Stovin, V., Vesuviano, G., Kasmin, H., 2012. The hydrological performance of a green roof test bed under UK climatic conditions. J. Hydrol. 414–415, 148–161. doi:10.1016/j.jhydrol.2011.10.022

Succi, S., 2001. The Lattice Boltzmann Equation for Fluid Dynamics and Beyond. Clarendon Press, Oxford, UK. doi:10.1016/S0997-7546(02)00005-5

Taina, I.A., Heck, R.J., Elliot, T.R., 2008. Application of X-ray computed tomography to soil science: A literature review. Can. J. Soil Sci. 88, 1–19. doi:10.4141/CJSS06027

Takebayashi, H., Moriyama, M., 2007. Surface heat budget on green roof and high reflection roof for mitigation of urban heat island. Build. Environ. 42, 2971–2979. doi:10.1016/j.buildenv.2006.06.017

Teemusk, A., Mander, Ü., 2007. Rainwater runoff quantity and quality performance from a greenroof: The effects of short-term events. Ecol. Eng. 30, 271–277. doi:10.1016/j.ecoleng.2007.01.009

Theodosiou, T., 2009. Green Roofs in Buildings: Thermal and Environmental Behaviour. Adv. Build. Energy Res. 3, 271–288. doi:10.3763/aber.2009.0311

Thuring, C.E., Dunnett, N., 2014. Vegetation composition of old extensive green roofs (from 1980s Germany). Ecol. Process. 3, 11. doi:10.1186/2192-1709-3-4

TRCA, 2006. Evaluation of an Extensive Greenroof 167.

Uhl, M., Schiedt, L., 2008. Green Roof Storm Water Retention –Monitoring Results, in: 11th International Conference on Urban Drainage. Edinburgh, Scotland, UK.

UK METOffice, 2016. Sheffield Cdl climate information - Met Office [WWW Document]. URL http://www.metoffice.gov.uk/public/weather/climate/gcqzwq04e (accessed 3.30.17).

UN, 2010. Population Situation Analysis: A Conceptual and Methodological Guide. United Nations Population Fund (UNFPA), New York.

van Genuchten, M.T., 1980. A Closed-form Equation for Predicting the Hydraulic Conductivity of Unsaturated Soils1. Soil Sci. Soc. Am. J. doi:10.2136/sssaj1980.03615995004400050002x

van Genuchten, M.T., Leij, F.J., Yates, S.R., 1991. The RETC Code for Quantifying the Hydraulic Functions of Unsaturated Soils. United States Environ. Reseach Lab. 93. doi:10.1002/9781118616871

Van Renterghem, T., Botteldooren, D., 2008. Numerical evaluation of sound propagating over green roofs. J. Sound Vib. 317, 781–799. doi:10.1016/j.jsv.2008.03.025

VanWoert, N.D., Rowe, D.B., Andresen, J.A., Rugh, C.L., Fernandez, R.T., Xiao, L., 2005a. Green Roof Stormwater Retention. J. Environ. Qual. 34, 1036. doi:10.2134/jeq2004.0364

VanWoert, N.D., Rowe, D.B., Andresen, J.A., Rugh, C.L., Xiao, L., 2005b. Watering regime and green roof substrate design affect Sedum plant growth. HortScience 40, 659–664. doi:10.2134/jeq2004.0364

Vervoort, R.W., Cattle, S.R., 2003. Linking hydraulic conductivity and tortuosity parameters to pore space geometry and pore-size distribution. J. Hydrol. 272, 36–49. doi:10.1016/S0022-1694(02)00253-6

Vesuviano, G., Sonnenwald, F., Stovin, V., 2014. A two-stage storage routing model for green roof runoff detention. Water Sci. Technol. 69, 1191–7. doi:10.2166/wst.2013.808

Vesuviano, G., Stovin, V., 2013. A generic hydrological model for a green roof drainage layer. Water Sci. Technol. 68, 769–75. doi:10.2166/wst.2013.294

Villarreal, E.L., 2007. Runoff detention effect of a sedum green-roof. Hydrol. Res. 38.

Villarreal, E.L., Bengtsson, L., 2005. Response of a Sedum green-roof to individual rain events. Ecol. Eng. 25, 1–7. doi:10.1016/j.ecoleng.2004.11.008

Virahsawmy, H., Stewardson, M., Vietz, G., Tim, D., 2013. Factors that affect the hydraulic performance of raingardens : Implications for design and maintenance Facteurs influençant la performance hydraulique des jardins de pluie : implications pour la conception et l ' entretien 1–10.

Voyde, E., Fassman, E., Simcock, R., 2010. Hydrology of an extensive living roof under sub-tropical climate conditions in Auckland, New Zealand. J. Hydrol. 394, 384–395. doi:10.1016/j.jhydrol.2010.09.013

Werthmann, C., 2007. Green Roof-A Case Study: Michael Van Valkeenburgh Associates' Design for the Headquarters of the American Society of Landscape Architects. Princeton Architectural Press.

Western, A.W., Seyfried, M.S., 2005. A calibration and temperature correction procedure for the water-content reflectometer. Hydrol. Process. 19, 3785–3793. doi:10.1002/hyp.6069

Whittinghill, L.J., Rowe, D.B., Cregg, B.M., 2013. Evaluation of Vegetable Production on Extensive Green Roofs. Agroecol. Sustain. Food Syst. 37, 465–484. doi:10.1080/21683565.2012.756847

Whittinghill, L.J., Rowe, D.B., Ngouajio, M., Cregg, B.M., 2016. Evaluation of nutrient management and mulching strategies for vegetable production on an extensive green roof. Agroecol. Sustain. Food Syst. 40, 297–318. doi:10.1080/21683565.2015.1129011

Wolf, D., Lundholm, J.T., 2008. Water uptake in green roof microcosms: Effects of plant species and water availability. Ecol. Eng. 33, 179–186. doi:10.1016/j.ecoleng.2008.02.008

Wong, G.K.L., Jim, C.Y., 2014. Quantitative hydrologic performance of extensive green roof under humid-tropical rainfall regime. Ecol. Eng. 70, 366–378. doi:10.1016/j.ecoleng.2014.06.025

Woods-Ballard, B., Kellagher, R., Martin, P., Bray, R., Jefferies, C., Shaffer, P., 2007. C697 The SUDS manual. CIRIA, London.

Woods-Ballard, B., Wilson, S., Udale-Clarke, H., Illman, S., Scott, T., Ashley, R., Kellagher, R., 2015. The SUDS manual, Ciria C753. CIRIA, London. doi:London C697

Yio, M.H.N., Stovin, V., Werdin, J., Vesuviano, G., 2013. Experimental analysis of green roof substrate detention characteristics. Water Sci. Technol. 68, 1477–86. doi:10.2166/wst.2013.381

Young, I.., Crawford, J.., Rappoldt, C., 2001. New methods and models for characterising structural heterogeneity of soil. Soil Tillage Res. 61, 33–45. doi:10.1016/S0167-1987(01)00188-X

Young, P., Jakeman, A., McMurtrie, R., 1980. An instrumental variable method for model order identification. Automatica 16, 281–294. doi:10.1016/0005-1098(80)90037-0

Youssef, S., Rosenberg, E., Gland, N.F., Kenter, J.A., Skalinski, M., Vizika, O., 2007. High Resolution CT And Pore-Network Models To Assess Petrophysical Properties Of Homogeneous And Heterogeneous Carbonates. SPE/EAGE Reserv. Charact. Simul. Conf. doi:10.2118/111427-MS

Zhao, L., Xia, J., Xu, C., Wang, Z., Sobkowiak, L., Long, C., 2013. Evapotranspiration estimation methods in hydrological models. J. Geogr. Sci. 23, 359–369. doi:10.1007/s11442-013-1015-9